UNITED NATIONS EDUCATIONAL, SCIENTIFIC AND CULTURAL ORGANIZATION
INTERNATIONAL CENTRE FOR THEORETICAL PHYSICS
I.C.T.P., P.O. BOX 586, 34100 TRIESTE, ITALY. CABLE: CENTRATOM TRIESTE

H4.SMR/782-5

Second Workshop on
Three-Dimensional Modelling of Seismic Waves
Generation, Propagation and their Inversion

7 - 18 November 1994

Seismic Response of Topographies and Alluvial Basins

F.J. Sánchez-Sesma

Universidad Nacional Autonoma de Mexico
Instituto de Ingenieria
Coyoacan, Mexico

Site effects on strong ground motion

FRANCISO J. SÁNCHEZ-SESMA

Instituto de Ingenieria, Universidad Nacional Autònoma de México, Cd. Universitaria, Apdo. 70-472, Coyoacán 04510, Mexico, D.F. Mexico

A review of some of the available methods to study the effects of site conditions on strong ground motion is presented. The need of unified treatment of source, path and side effects in the assessment of seismic risk is pointed out.

Key Words: strong ground motion, site effects

INTRODUCTION

It has long been recognized that site effects can significantly affect the nature of strong ground motion. In some situations, ground motion amplification can adequately be inferred using simple one-dimensional models. However, due to lateral variations, the problem must be dealt with as a spatial phenomenon.

Local conditions can generate large amplifications and important spatial variations of seismic ground motion. These effects are of particular significance in the assessment of seismic risk, in studies of microzonation, in planning and in the seismic design of important facilties (Esteva, 1977; Ruiz, 1977). In particular, local irregularities can be relevant in calculating the seismic response of long structures (see Fig. 1) like dams, bridges or life-line systems (e.g., Esquivel and Sánchez-Sesma, 1980; Ruiz and Esteva, 1981).

The effect of soil conditions in ground motion has been observed in well-documented earthquakes (Sozen *et al.*, 1968; Jennings, 1971) and in regression analyses of strong motion data. For instance, there is significant evidence that subsurface topography, i.e., lateral heterogeneities; are related to localized damage distribution in the Skopje, Yugoslavia earthquake of July 26, 1963 (Poceski, 1069). It has been suggested that focusing of the wave energy, by irregular interfaces, generated large motion amplification in limited zones of the city (Jackson, 1971). The same can be said of the recent destructive Michoacán earthquake of September 19, 1985. In this case the combination of site effects with a continuous flux of energy from a distant source was of disastrous consequences in Mexico City. The phenomenon of local amplification in sedimentary basins has been related to the formation of caustics Rial, 1984). Damage statisitics of buried utility pipes in the Miyagiken-Oki, Japan earthquake of June 12, 1978 have shown spectacular increase in the number of occurred failures near the cut-and-fill boundary of a newly developed area (Kubo and Isoyama, 1980). Such damage has been associated with failures of the ground (Irikura, personal communication).

Topographical effects have been invoked to explain the high acceleration recorded at the Pacoima Dam (1.25 g) during the San Fernando, California earthquake of February 9, 1971 (Trifunac and Hudson, 1971; Boore, 1973). For the aftershocks of the same earthquake, Davis and West (1973) in a series of observations have found significative local amplifications due to topographical relief. In a field study in the Appalachian Mountains using distant mine blasts as sources, average amplitude ratios between mountain top and valley sites were determined (Griffiths and Bollinger, 1979). These average ratios showed that the seismic wave amplitudes at the crests were amplified by factors from 1.7 to 3.4. In Fig. 2 three seismograms for the same event in the Powell Mountain area are shown. The positions of recording sites are also displayed in the figure. Dealing with destructive earthquakes, evidence shows that damaging effects tend to increase where steep relief or complicated topography

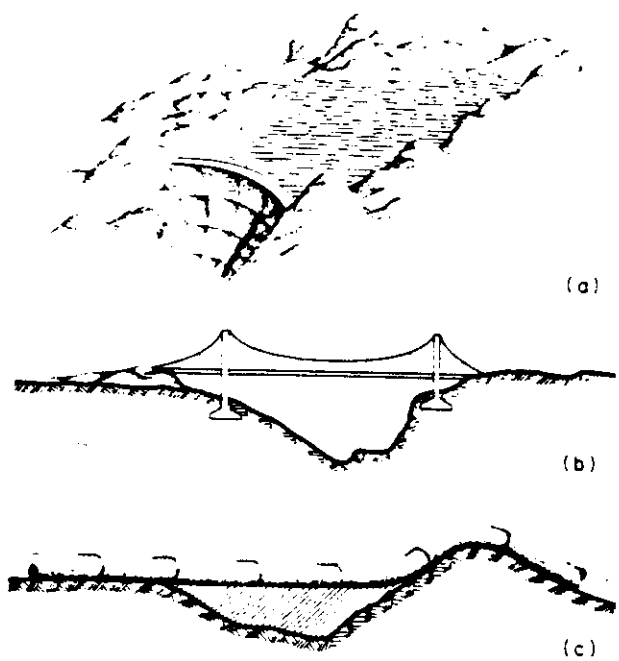

Fig. 1. Long structures at irregular sites: (a) dam; (b) bridge; and (c) a lift-line system

Accepted February 1986. Discussion closes June 1987.

0267-7261/87/010124-0952.00

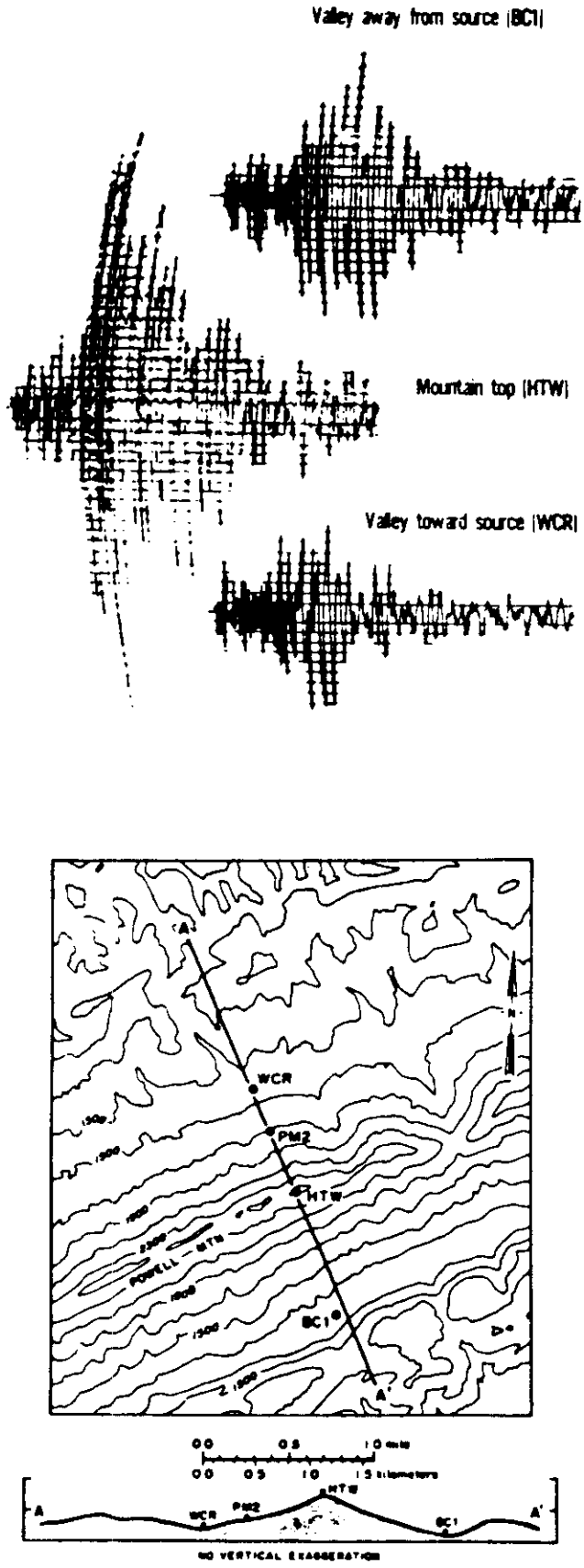

Fig. 2. Seismograms at three stations at the Powell Mountain area and location of the recording sites. Epicentral distance was about 30 km. Topographic contour interval is 200 ft (61 m) (After Griffiths and Bollinger, 1979)

is present. Recent case histories were offered by the November 23, 1980 Southern Italy earthquake, where topography related increments of up to 2 degrees in the MSK intensity scale have been observed (Siro, 1982).

As pointed out by Trifunac (1980), the strong earthquake shaking of interest in earthquake engineering falls in the frequency range from about 0.1 Hz to about 20 Hz and since the seismic wave velocities near the earth's surface lie in the range from about 0.1 km/s to about 3 km/s, it can be seen that the corresponding wave lengths are from tens of meters to tens of kilometers. Thus, the topographical and geological irregularities of dimensions near to this range will have considerable influence on the corresponding waves. It follows that the extent and detail of local conditions required to study their effects should be considered in terms of the wave lengths associated with the periods of motion which are more important for a particular analysis. For a tall building, a dam or a bridge, for example, these local site dimensions might be of several kilometers. On the other hand, for stiff structures or small buildings, these dimensions can be from tens to hundreds of meters.

Although recent work has emphasized the physical understanding of site effects so that quantitative predictions can be made (Boore, 1983a), there is still lack of criteria for dealing with the problem taking into account source, path and local conditions. Active research is needed to predict more accurately the local effects, given the source parameters. Indeed, it is encouraging the recent progress on strong motion prediction using mathematical modelling techniques (Aki, 1982). Much of the research is concentrated on the understanding of fault mechanics and wave propagation in the Earth. It is generally accepted that high frequency radiation, which controls accelerations, comes from very localized parts of the fault. A powerful asymptotic theory of high frequency radiation has been recently developed (Madariaga, 1983). Applications of the theory are coming (e.g., Bernard and Madariaga, 1984). However, it should be noted that the foci of future earthquakes are not known; their location, mechanism and amount of released energy can only be speculated in terms of regional seismicity models (Esteva, 1976). On the other hand, the knowledge of geological details is generally small to justify the use of very refined models of wave propagation, particularly for the high frequencies. It is then clear, in view of the mentioned uncertainties, that the problem of seismic risk assessment must be dealt within a probabilistic framework. A promising approach seems to be the use of integral measures of intensity such as Arias' (1970) combined with stochastic descriptions of the input (Boore, 1983b) and simplified models of the local irregularities (Sánchez-Sesma *et al.*, 1986).

The aim of this work is to review the problem of calculating the effects of topographical and geological irregularities on ground motion given some knid of seismic waves as input. For this purpose the current formulation of the problem, the known analytical solutions and some of the available numerical methods are briefly discussed. It is hoped that this work could serve to stimulate discussion and interest on the problem.

FORMULATION OF THE PROBLEM

There is no doubt that the source mechanism governs the

Fig. 3. Half-space with irregular surface and incident elastic waves

way in which the released seismic energy is radiated in space and time. However, seismic waves, once emitted by the source, are dependent on the mechanical properties of earth materials and the heterogeneities encountered in their path. This is also true dealing with irregular local conditions. Moderate changes in mechanical impedances or irregularities with size comparable to incident wave lengths can generate significant amplifications and spatial variations of ground motion (Boore, 1972b).

Plane waves are reflected back and refracted forward as they arrive at a plane interface. The amounts of reflected and transmitted energy depend on the mechanical properties of the media involved. Reflection and refraction in elastic wave propagation can well be described by geometrical means. Let us call diffraction to every change in the waves' path that can not be described as reflection or refraction. To study diffraction of elastic waves it is necessary to solve a boundary value problem for the governing equations of linear elasticity (e.g. Achenbach, 1973; Aki and Richards, 1980).

To fix ideas, consider an elastic, homogeneous and isotropic half-space with an irregular surface as shown in Fig. 3. Under incidence of elastic waves the irregularity will difrract the incident waves (diffraction is frequently called scattering). Diffracted waves must satisfy, together with incident waves, the governing equations (Navier equations) and the boundary conditions. Moreover, the diffracted fields must satisfy the Sommerfeld (1949) radiation condition at infinity, which means that the diffracted fields must scatter to infinity; i.e., no energy may be radiated from infinity into the irregular region. The Sommerfeld radiation condition has been extended to elastic wave fields by Kupradze (1965).

ANALYTICAL SOLUTIONS

The simplest problems in elastic wave diffraction are the two-dimensional *SH*-wave problems because they can be analyzed separately from other body waves. The governing equation for this case is the scalar wave equation. Then, analytical solutions can be obtained for geometries of the scatterer which allow separation of variables (Mow and Pao, 1971). Using this method, exact solutions have been obtained for the diffraction of *SH*-waves by canyons and alluvial valleys with semi-circular (Trifunac, 1971, 1973) or semi-elliptical shapes (Wong and Trifunac, 1947a,b). Even with these simple models of local irregularities, complicated interference patterns were found and the calculated surface displacement fields varied strongly in space (see Fig. 4). Results are very sensitive to incidence angle and frequency. Results for alluvial valleys show the importance of the two-dimensional behaviour gives much larger amplifications than those obtained from unidimensional calculations. These analytical solutions have shown the importance of the problem and they provide a check for numerical procedures.

A very simple result can also be obtained for two-dimensional wedges of any angle under incidence of plane or cylindrical of *SH*-waves. Using a representation of the solution given by Macdonald (1902) it is possible to show that the amplification (or reduction) coefficient at the vertex is given by 2ν, where $\nu\pi$ = internal angle of the wedge (Sánchez-Sesma, 1985). Suprisingly, amplifications larger than 2ν were found in other regions of the surface.

For the more difficult cases pf *P*- or *SV*-incident waves the orthogonal wave functions developed in classical physics are not separable for the half-space surface due to the coupling of boundary conditions. Lee (1982) overcame this difficulty for a semi-spherical canyon by expanding the spherical wave functions into a power series which matched all the boundary conditions successfully. However, this approach limited to small frequencies.

Under additional simplifying assumptions other analytical solutions have been obtained using orthongonal wave functions. For an acoustic medium exact expressions for the scattered fields generated by incidence of *P*-waves on canyons of semi-circular and semi-spherical shapes have been obtained (Singh and Sabina, 1977). The results however, are of small utility because the acoustic assumption can hardly be met in real cases. The problem of vertically incident *P*-waves upon a semi-ellipsoidal three-dimensional scatterer has been solved exactly for an elastic medium in which horizontal displacements are restricted. Results for vertical displacement are in reasonable agreement with those from more reliable computations for a truly elastic medium (see e.g. Sánchez-Sesma, 1983). This is illustrated in Fig. 5.

Under the assumption of small-slope irregularities a perturbation solution has been obtained for the elastic scattered field by two-dimensional geometries (Gilbert and Knopoff, 1960). The approximation is based on replacing the irregularity by an equivalent stress distribution. An application of this method by Hudson

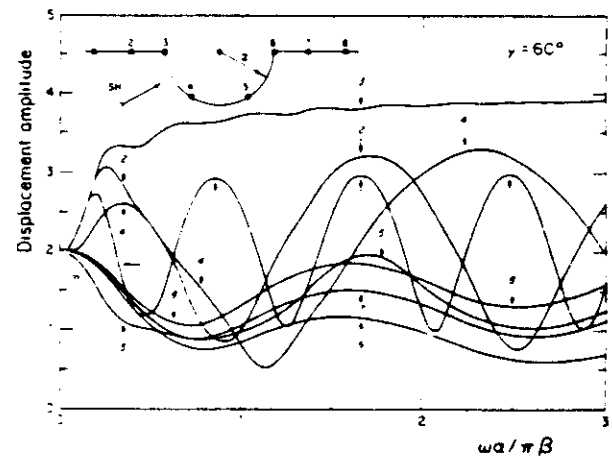

Fig. 4. Displacement amplitudes at points in the surface of a semi-circular canyon. Incidence of harmonic plane SH waves (After Trifunac, 1973)

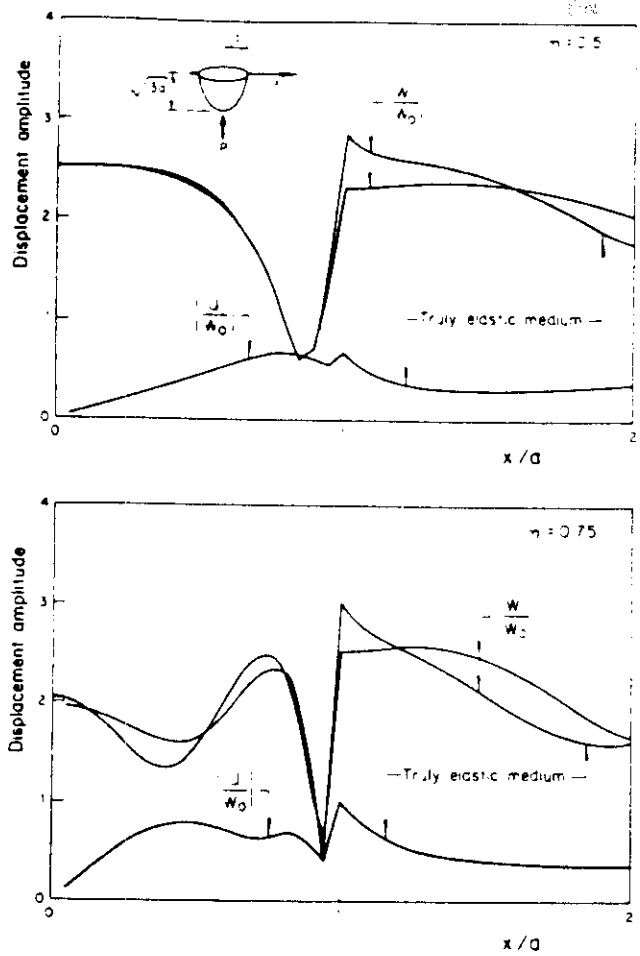

Fig. 5. Displacement amplitudes in a semi-ellipsoidal surface cavity under vertical incidence of P waves. Vertical displacements are computed for a simplified elastic medium in which horizontal motion is restricted. Comparison is provided with computations for a truly elastic medium

(1967) deals with small-slope three-dimensional scatters. With this approach reasonable estimates have been obtained of the scattered Rayleigh waves as compared with observations even in cases in which slope angles are as large as 25° or 30° (Hudson and Boore, 1980).

The method of matched asymptotic expansions has no restrictions on the slope of the irregularity. It is based in matching the first terms of an outer expansion of the near field with those of an inner expansion of the far field (Sabina and Willis, 1975, 1977). Although the method is limited to very small frequencies, results are in qualitative agreement with observations.

NUMERICAL METHODS

A powerful technique has been developed by Aki and Larner (1970) to treat scattering of *SH*-waves by irregular interfaces. In the Aki-Larner method, it is assumed incidence of a plane single-frequency. The diffracted field is represented by superposition of plane waves of unknown complex amplitudes propagating in many directions. Inhomogeneous plane waves are allowed. The method is restricted to small-slope irregularities for numerical reason only because it does not include explicitly upgoing waves. Then, even if the representation in terms of plane waves is complete, convergence to the true solution can be very slow. The total motion is obtained from integration over horizontal wave number. Under the assumption of horizontal periodicity of the irregularity, the integral is replaced by an infinite sum. Truncation of this sum and application of the interface conditions of continuity of stress and displacement in the wavenumber domain lead to a system of linear equations for the complex scattering coefficients. This method has been applied by Bouchon (1973) to study the effects of two-dimensional irregular topographies on ground motion for incidence of *SH*, *SV* and *P* waves. Figure 6 shows some results. An extension of the method has been advanced by Bouchon and Aki (1977a,b) to represent with this discrete-wave-number technique near source seismic fields in a layered medium with irregular interfaces. Another extension, now to time domain calculations, has been developed to study the seismic response of alluvial valleys (Bard and Bouchon, 1980a,b) under incidence of *SH*, *P* and *SV* waves. The Aki-Larner technique has been used by Bard (1982) to analyze the effects of two-dimensional elevated topography on ground motion. An additional extension of the method is due to Bouchon (1985) in which upgoing waves are explicitly included in the analysis, thus eliminating the restriction of small-slopes. Calculations for irregular layered media show a very good performance of the extended method (Campillo and Bouchon, 1985). The method has been used to model the fields generated by real faults (Bouchon, 1979; Campillo, 1983). It can be

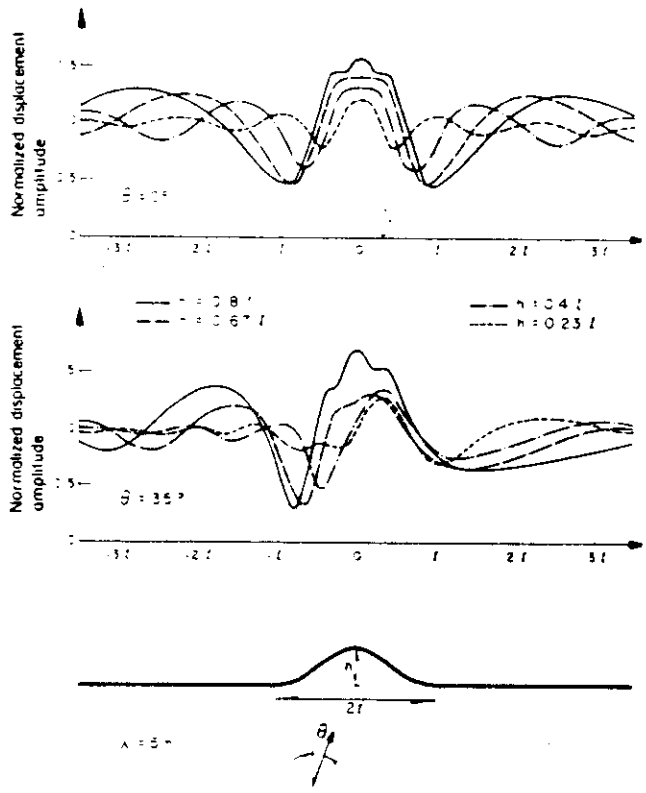

Fig. 6. Normalized displacement amplitudes in the surface of a ridge under incident SH waves. (After Bouchon, 1973)

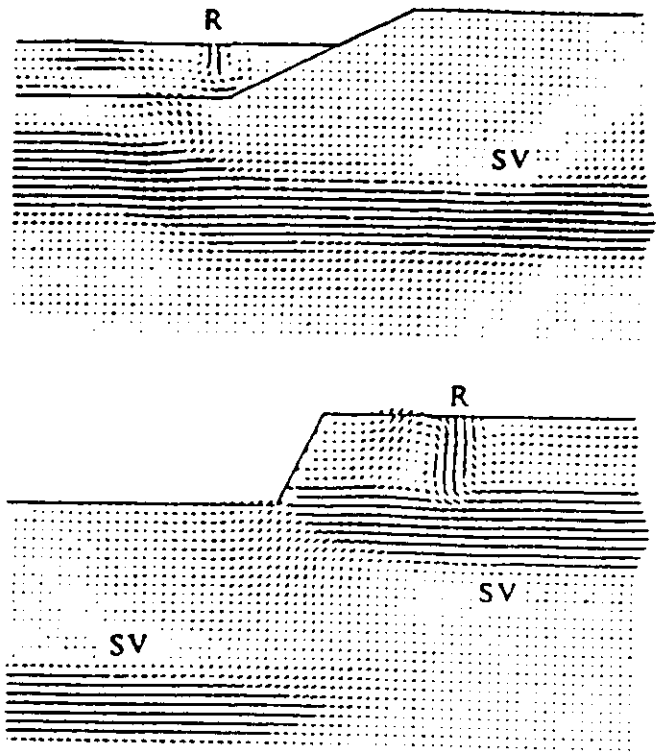

Fig. 7. Generation of surface Rayleigh waves by surface irregularities. In both cases the incident field consists of SV waves. (After Ohtsuki, et al., 1984)

used to model ground motion considering together the effects of source, path and local conditions. However, the numerical computations involved may become very expensive for many real cases.

The finite difference method is also a powerful tool in elastic wave propagation studies (Alterman and Karal, 1968; Boore, 1972a). It has been applied to model two-dimensional irregular interfaces (Boore *et al.*, 1971) and ridges (Boore, 1972b) in the *SH* case and also for incident *P* and *SV*-waves upon a sedimentary basin (Harmsen and Harding, 1981) and a step-like topography (Boore *et al.*, 1981). Interesting results have been found concerning the significant generation of Rayleigh surface waves by lateral irregularities. Recent work by Ohtsuki and coworkers (Ohtsuki and Harumi, 1983; Ohtsuki *et al.*, 1984a; 1984b) confirm this fact. They have used a combination of finite differences and finite elements. Figure 7 displays some results which slow this important effect. For incidence of *P* waves upon a surface slot the computations by Ilan and Bond (1981) give good agreement with experiments. It is found that the amplitude of the scattered Rayleigh wave is, as expected, dependent on incidence angle. A finite difference analysis of axisymmetric topographical irregularities has been presented to study the effects of vertically incident shear waves (Liao *et al.*, 1980). Spectral ratios were obtained and comparison with observations gives reasonable agreement. The finite difference method is theoretically unlimited to model details and nonlinear behaviour of materials, but the size of the problem can easily exceed the capacity of major computing facilities.

The finite element method also allows a detailed description of site topography and layering. With this method it is possible to calculate the response of two-dimensional soil configurations with truly nonlinear stress-strain relations (Streeter *et al.*, 1974; Joyner and Chen, 1975; Joyner, 1975). The major disadvantage of the method is its low-frequency limit and high cost. Usually, real time analysis must be shortened to avoid the reflections from the artificial boundaries. The use of different transmitting techniques can reduce the spurious waves to some extent (e.g., Smith, 1974, 1975; Ayala and Aranda, 1977; Clayton and Engquist, 1977; Castellani *et al.*, 1981; Liao and Wong, 1981). Successful criteria have been developed for damping out the unwanted reflections by means of nonuniform element size (Day, 1977) or by combining finite elements with a boundary integral representation of the conditions at the edges of the studied domain (Franssens and Langasse, 1984). Finite elements have been used to treat problems of irregular layering (Lysmer and Drake, 1972; Drake, 1972; Ayala and Aranda, 1977) and two-dimensional topographical irregularities (Castellani *et al.*, 1982) under idealized conditions. Nevertheless, a realistic wave analysis can be very costly.

Ray methods have also been used to study the ground motion in sediment filled basins with irregular interfaces (e.g., Jackson, 1971; Hong and Helmberger, 1977; Lee and Langston, 1983; Rial, 1984) or dipping layers (Ziegler and Pao, 1984).

An extension of ray theory based on a paraxial approximation of the elastic solution has been recently used to study many problems of wave propagation in inhomogeneous media (e.g., Nowack and Aki, 1984; Madriaga, 1984). These solutions are called Gaussian beams because of the Gaussian shape of the wave amplitude around a central ray. The high frequency character of Gaussian beams place them as a very promising tool to study site effects on strong ground motion.

Experimental techniques can be very useful in describing topographical or layering site effects. Using polyurethane foam models King and Brune (1981) were able to obtain results for sedimentary basins. Excellent agreement was found with analytical solutions.

In recent years boundary methods have gained increasing popularity. This fact is mainly due to the availability of high speed computers. Boundary methods are well suited to deal with wave propagation problems because they avoid the introduction of fictitious boundaries and reduce by one the dimensionality of the problem. These facts yield numerical advantages. Moreover, boundary methods can be used together with the finite element method (Zienkiewics *et al.*, 1977). Then, the region modelled with finite elements can be smaller (e.g., Ayala and Gomez, 1979; Shah *et al.*, 1982).

There are two main approaches to the formulation of boundary methods; one is based on the use of boundary integral equations (Cruse and Rizzo, 1968a,b; Brebbia, 1978; Cole *et al.*, 1978; Alarcon *et al.*, 1979), and the other, on the use of complete systems of solutions (Herrera and Sabina, 1978; Herrera, 1980a). The scattering of incident *SH*-waves from two-dimensional irregular topographies has been formulated with integral equations by Wong and Jennings (1975) for arbitrarily shaped canyon-like profiles and by Sills (1978) for ridges and mixed shapes. This method has been applied with success to calculate the effects of a dipping layer of alluvium on the displacement field due to a *SH*-wave source on the surface

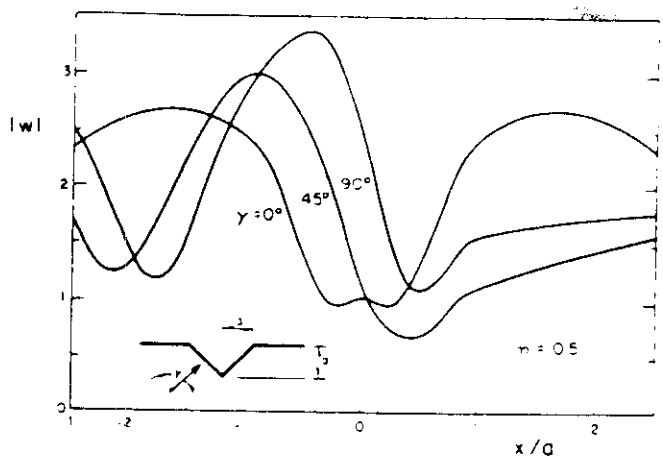

Fig. 8. Displacement amplitudes on the surface of a triangular canyon with 45° slopes for different incidence angles and normalized frequency $\eta = 0.5$, incidence of SH waves

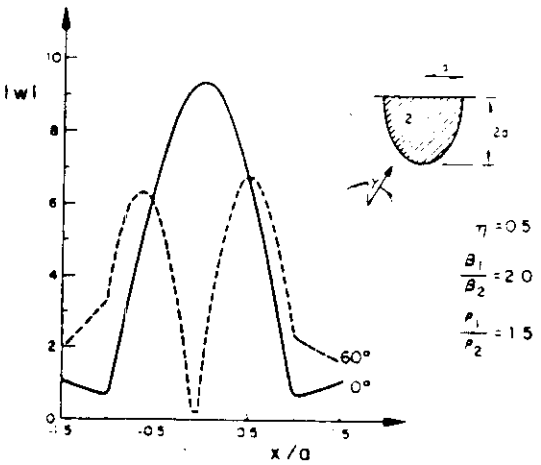

Fig. 9. Displacement amplitudes at the free-surface. Semi-elliptical alluvial valley. Incidence of SH waves with angles 0 and 60 degrees. Normalized frequency $\eta = 0.5$

(Wong *et al.*, 1977). Results compare favourably with observations during a full-scale low-amplitude propagation test. A powerful approach which combines the boundary integral equation method with finite differences in time has been presented (Cole *et al.*, 1978) for elastodynamic problems. The performance of the method was found to be good in a simple numerical problem. A boundary method has been developed and applied to solve two-dimensional scattering of harmonic elastic waves by canyons (Sánchez-Sesma, 1978, 1981; Sabina *et al.*, 1979; Sánchez-Sesma and Rosenblueth, 1979; Wong, 1979, 1982; England *et al.*, 1980; Sánchez-Sesma *et al.*, 1982a; 1985), alluvial deposits (Sánchez-Sesma and Esquivel, 1979; Ize *et al.*, 1981; Dravinski, 1982a,b, 1983) and ridges (Sánchez-Sesma and Esquivel, 1980; Sánchez-Sesma *et al.*, 1982b) for different types of waves and shapes of the scatterers. The method consists of constructing the scattered fields with linear combinations of members of a complete family of wave functions (Herrera and Sabina, 1978; Herrera, 1984). These families of functions, which are solutions of the governing equations of the problem, can be constructed in a very general way, with single or multipolar sources having their singularities outside the region of interest. Coefficients of the linear forms thus constructed are obtained from a least-squares matching of boundary conditions. As pointed out by Wong (1982), the method can be considered as a generalized inverse one. He suggested a procedure which improves the solution numerically. A general framework for the method is given by a recent algebraic theory of boundary value problems (Herrera, 1979, 1980a,b; 1984). Figures 8, 9 and 10 illustrate typical results for incidence of *SH*-waves. Figure 11 shows the amplitudes of vertical and horizontal displacements in the surface of a semicircular canyon for incidence of Rayleigh waves. Results are displayed for three different frequencies $\eta = 2a/\lambda$, where λ = wavelength of the incoming waves.

The approach has been extended to three-dimensional problems (Sánchez-Sesma, 1983; Sánchez-Sesma *et al.*, 1984). The case of incident elastic *P*, *SV* and Rayleigh waves upon axisymmetric irregularities on the surface of an elastic half-space was formulated using an azimuthal decomposition. The diffracted fields were constructed with multipolar solutions of the reduced Navier equations in spherical coordinates (Takeuchi and Saito, 1972; Aki and Richards, 1980). For a semi-spherical alluvial deposit and vertical incidence of *P*-waves a very large amplification was found as compared with the flat layer problem. In Figs 12 and 13 the amplitudes of displacements are shown for two three-dimensional problems. In both cases incidence of *P* waves is assumed with normalized frequency $\eta_k = \omega a/\pi\beta = 1$. Figure 12 present the case of a semi-spherical canyon. Finally, an example for a ridge appears in Fig. 13. The shape of the ridge is given by $z = -h(1 + 2\xi^3 - 3\xi^2)$, where $\xi^2 = (x^2 + y^2)/a^2 < 1$.

CONCLUDING REMARKS

The influence of topographic and geological irregularities on seismic ground motion has been briefly discussed and some of the available methods to deal with the problem

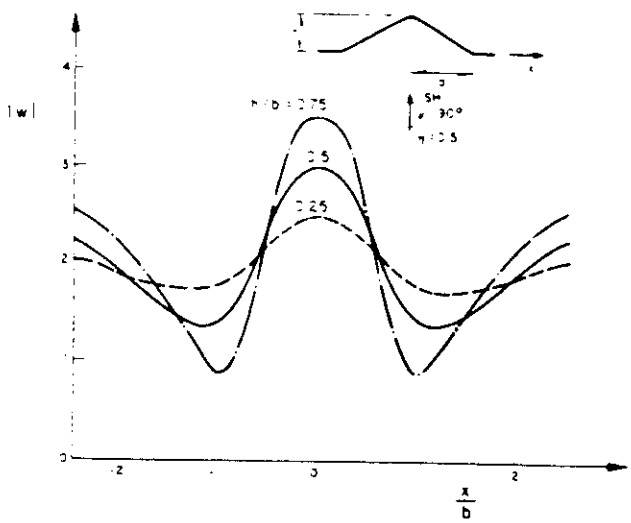

Fig. 10. Displacement amplitudes at the free-surface. Ridges with different aspect ratio h/b. Vertical incidence of SH waves with normalized frequency $\eta = 0.5$

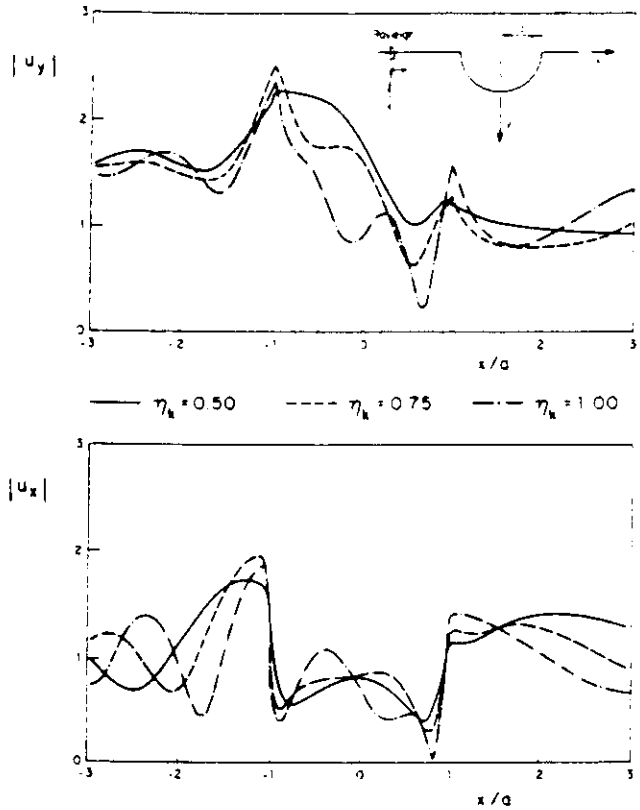

Fig. 11. Amplitudes of vertical and horizontal displacements at the free-surface. Semicircular canyon. Incidence of Rayleigh waves with normalized frequencies $\eta_k = 0.5, 0.75, 1.0$ (Poisson ratio 0.33)

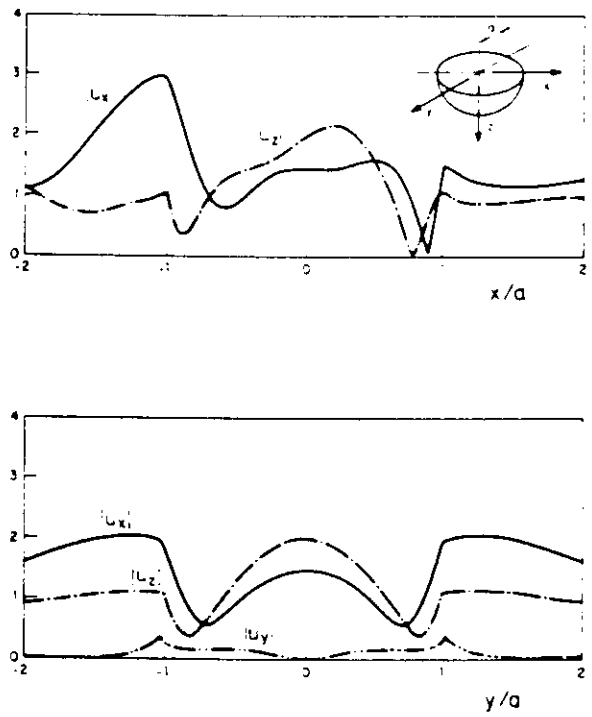

Fig. 12. Surface displacement amplitudes. Semi-spherical canyon under incidence of P waves with incidence angle of 60° and normalized frequency $\eta_k = 1.0$ (Poisson ratio 0.25)

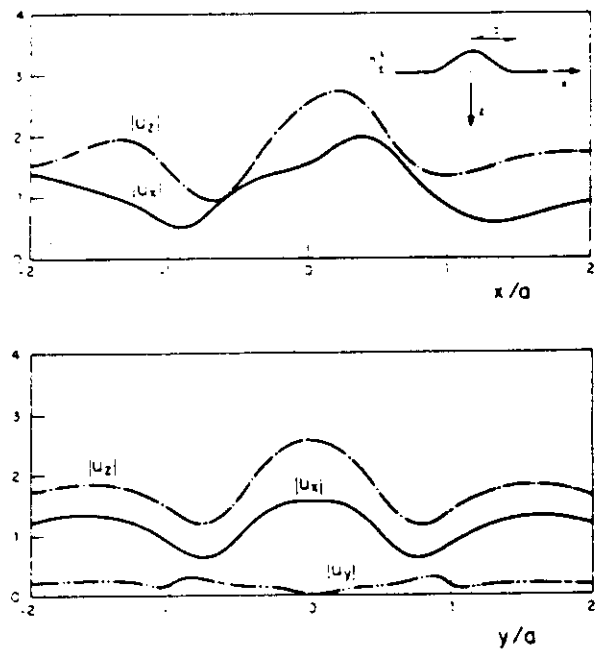

Fig. 13. Surface displacement amplitudes. Axisymmetri ridge with h/a = 0.5. Incidence of P waves with incidenc angle of 30° and normalized frequency $\eta_k = 1.0$ (Poisso ratio 0.25)

were reviewed. They have been used to study variou aspects of local effects. Discrete wave number and finit differences allow the modelling of various types o irregularities and provide physical understanding of sit effects as they are aimed to produce time signals of th response. With the advent of supercomputers thei capabilities are being extended both in the complexity o the problems and in the possibility of dealing with hig frequency signals. Ray methods including the use o Gaussian beams seem to be powerful tools to deal wit high frequencies. On the other hand, boundary methods which allow the study of three-dimensional local features are still in the development stage. It is hoped that a comparative study among the various methods will defin in a clear way the advantages and limitations of each one

There is no doubt that local conditions play ar important role in the spatial variation of ground shakin and should be explicitly considered in the design of som important facilties, as well as in microzoning. However seismic hazard involves also the effects of source mechanism and path of seismic waves. Thus, a complete description of the problem is needed.

ACKNOWLEDGEMENTS

Thanks are given to K. Aki, K. Irikura, M. A. Bravo and F. J. Chávez-Garcia for the critical reading of the manuscript and for helpful discussions. This review was done while the author was on leave from the National University of Mexico as a visiting professor at the Department of Geological Sciences, University of Southern California, Los Angeles, California, USA. This work was partially supported by the National Science Foundation under Grant CEE-8408227.

REFERENCES

Achenbach, J. D. *Wave propagation in elastic solids*. North-Holland Publishing Co., Amsterdam, 1973

Aki, K. Strong motion prediction using mathematical modeling techniques. *Bull. Seism. Soc. Am.* 1982, **72**, S29–S41

Aki, K. and Larner, K. L. Surface motion of a layered medium having an irregular interface due to incident plane SH waves. *J. Geophys. Res.* 1970, **70**, 933–954

Aki, K. and Richards, P. G. *Quantitative seismology, theory and methods*. W. H. Freeman and Co., San Francisco, 1980

Alarcon, E., Martin, A. and Paris, F. Boundary elements in potential and elasticity theory. *J. Computers and Structures* 1979, **10**, 351–362

Alterman, Z. S. and Karal, F. C., Jr Propagation of elastic waves in layered media by finite difference methods. *Bull. Seism. Soc. Am.* 1968, **58**, 367–398

Arias, A. A measure of earthquake intensity in *Seismic design for nuclear power plants*. (Ed. R. J. Hansen), MIT Press, Cambridge, Massachusetts, 1970

Ayala, G. A. and Aranda, G. R. Boundary conditions in soil amplification studies. *Proc. World Conf. Earthquake Eng., 6th*, New Delhi, 1977

Ayala, G. A. and Gomez, R. A. A general procedure for solving three dimensional elasticity problems in geomechanics in *Numerical methods in geomechanics*, (Ed. W. Wittke), Aachen, A. A. Balkema, Rotterdam, 1979

Bard, P. Y. Diffracted waves and displacement field over two-dimensional elevated topographies. *Geophys. J. R. Astr. Soc.* 1982, **71**, 731–760

Bard, P. Y. and Bouchon, M. The seismic response of sediment-filled valleys, Part 1. The case of incident SH waves. *Bull. Seism. Soc. Am.* 1980a, **70**, 1263–1286

Bard, P. Y. and Bouchon, M. The seismic response of sediment-filled valleys, Part 2. The case of incident P and SV waves. *Bull. Sism. Soc. Am.* 1980b, **70**, 1921–1941

Bernard, P. and Madariaga, R. High-frequency seismic radiation from a buried circular fault. *Geophys. J. R. Astr. Soc.* 1984, **78**, 1–17

Boore, D. M. Finite difference methods for seismic wave propagation in heterogeneous materials in *Methods in computational physics* 11, (Ed. B. A. Bolt), Academic Press, New York, 1972a

Boore, D. M. A note on the effect of simple topography on seismic SH waves. *Bull. Seism. Soc. Am.* 1972b, **62**, 275–284

Boore, D. M. The effect of simple topography on seismic waves: implications for accelerations recorded at Pacoima Dam, San Fernando Valley, California. *Bull. Seism. Soc. Am.* 1973, **63**, 1603–1609

Boore, D. M. Strong-Motion Seismology – 1979 through 1982. *Reviews of Geophysics and Space Physcis* 1983a, **21**, 1308–1318

Boore, D. M. Stochastic simulation of high-frequency ground motions based in seismological models of the radiated spectra. *Bull. Seism. Soc. Am.* 1983b, **73**, 1865–1894

Boore, D. M., Larner, K. L. and Aki, K. Comparison of two independent methods for the solution of wave scattering problems: response of a sedimentary basin to incident SH waves. *J. Geophys. Res.* 1971, **76**, 558–569

Boore, D. M., Harmsen, S. C. and Harding, S. T. Wave scattering from a steep change in surface topography. *Bull. Seism. Soc. Am.* 1981, **71**, 117–125

Bouchon, M. Effect of topography on surface motion. *Bull. Seism. Soc. Am.* 1973, **63**, 615–632

Bouchon, M. Predictability of ground displacement and velocity near an earthquake fault. An example: the Parkfield earthquake of 1966. *J. Geophys. Res.* 1979, **84**, 6149–6156

Bouchon, M. A simple, complete numerical solution to the problem of diffraction of SH waves by an irregular surface. *J. Acoust Soc. Am.* 1985, **77**, 1–5

Bouchon, M. and Aki, K. Discrete wave number representation of seismic source wave fields. *Bull. Seism. Soc. Am.* 1977a, **67**, 259–277

Bouchon, M. and Aki, K. Near-field of seismic source in a layered medium with irregular interfaces. *Geophys. J. R. Astr. Soc.* 1977b, **50**, 669–684

Brebbia, C. A. *The boundary element method for engineers*. Pentech Press, London, 1978

Campillo, M. Numerical evaluation of the near field high-frequency radiation from quasi-dynamic circular faults. *Bull. Seism. Soc. Am* 1983, **73**, 723–734

Campillo, M. and Bouchon, M. Synthetic SH-seismograms in a laterally varying medium by the discrete wavenumber method. *Geophys. J. R. Astr. Soc.* in press

Castellani, A., Chesi, C. and Mitsopoulou, E. An earthquake engineering wave propagation model. *Meccanica*, Journal of the Italian Association of Theoretical and Applied Mechanics, March 1981, 33–41

Castellani, A., Peano, A. and Sardella, L. On analytical and numerical techniques for seismic analysis of topographic irregularities. *Proc. European Conf Earthquake Eng. 7th*, Athens, Greece, 1982, **2**, 415–423

Clayton, R. and Engquist, B. Absorbing boundary conditions for acoustic and elastic wave equations. *Bull. Seism. Soc. Am.* 1977, **67**, 1529–1540

Cole, D. M., Kosloff, D. D. and Minster, Bernard J. A numerical boundary integral equation for elastodynamics. I. *Bull. Seism. Soc. Am.* 1978, **68**, 1331–1357

Cruse, T. A. and Rizzo, F. J. A direct formulation and numerical solution of the general transient elastodynamic problem. I. *J. Math. Anal. Appl.* 1968a, **22**, 244–259

Cruse, T. A. and Rizzo, F. J. A direct formulation and numerical solution of the general transient elastodynamic problem. II. *J. Math. Anal. Appl.* 1968b, **22**, 341–355

Davis, L. L. and West, L. R. Observed effects of topography on ground motion. *Bull. Seism. Soc. Am.* 1973, **63**, 283–298

Day, S. M. Finite element analysis of seismic scattering problems. PhD Thesis, University of California, San Diego, California, 1977, 149 pp.

Drake, L. A. Love and Rayleigh waves in non-horizontal layered media. *Bull. Seism. Soc. Am.* 1972, **62**, 1241–1258

Dravinski, M. Scattering of SH waves by subsurface topography. *J. Eng. Mech. Div., Proc. ASCE* 1982a, **108**, 1–17

Dravinski, M. Influence of interface depth upon strong ground motion. *Bull. Seism. Soc. Am.* 1982b, **72**, 597–614

Dravinski, M. Amplification of P, SV and Rayleigh waves by two alluvial valleys. *Soil Dynamics and Earthquake Eng.* 1983, **2**, 66–77

England, R., Sabina, F. J. and Herrera, I. Scattering of SH waves by surface cavities of arbitrary shape using boundary methods. *Phys. Earth Planet. Ints.* 1980, **21**, 148–157

Esquivel, J. A. and Sanchez-Sesma, F. J. Effects of canyon topography on dynamic soil-bridge interaction for incident plane SH waves. *Proc. World Conf. Earthquake Eng., 7th*, Instanbul, 1980, **2**, 153–160

Esteva, L. Seismicity in *Seismic risk and engineering decisions*, (Eds C. Lomnitz and E. Rosenblueth), Elsevier Scientific Pub. Co., Amsterdam, 1976

Esteva, L. Microzoning: models and reality. *Proc. World Conf. Earthquake Eng., 6th*, New Delhi, 1977

Franssens, G. R. and Lagasse, P. E. Scattering of elastic waves by a cylindrical obstacle embedded in a multilayered medium. *J. Acoust. Soc. Am.* 1984, **76**, 1535–1542

Gilbert, F. and Knopoff, L. Seismic scattering from topographic irregularities. *J. Geophys. Res.* 1960, **65**, 3437–3444

Griffiths, D. W. and Bollinger, G. A. The effect of the Appalachian Moutain topography on seismic waves. *Bull. Seism. Soc. Am.* 1979, **69**, 1081–1105

Harmsen, S. C. and Harding, S. T. Surface motion over a sedimentary valley for incident plane P and SV waves. *Bull. Seism. Soc. Am.* 1981, **72**, 655–670

Herrera, I. Theory of connectivity: a systematic formulation of boundary element methods. *Applied Math. Modelling* 1979, **3**, 151–156

Herrera, I. Variational principles for problems with linear constraints, prescribed jumps and continuation type restrictions. *J. Inst. Maths and Applics.* 1980a, **25**, 67–96

Herrera, I. Boundary methods. A criterion for completeness. *Proc. Nat'l. Acad. Sci., USA* 1980b, **77**, 4395–4398

Herrera, I. *Boundary methods: an algebraic theory*. Pitman Adv Publishing Program, Boston, 1984

Herrera, I. and Sabina, F. J. Connectivity as an alternative to boundary integral equations. Construction of bases. *Proc. Nat'l. Acad. Sci. USA* 1978, **75**, 2059–2063

Hong, T. L. and Helmberger, D. V. Glorified optics and wave propagation in non planar structures. *Bull. Seism. Soc. Am.* 1977, **68**, 1313–1330

Hudson, J. A. Scattered surface waves from a surface obstacle. *Geophys. J. R. Astr. Soc.* 1967, **13**, 441–458

Hudson, J. A. and Boore, D. M. Comments on 'Scattered surface waves from a surface obstacle'. *Geophys. J. R. Astr. Soc.* 1980, **60**, 123–127

Ilan, A. and Bond, L. J. Interaction of a compressional impulse with a slot normal to the surface of an elastic half space – II. *Geophys. J. R. Astr. Soc.* 1981, **65**, 75–90

Ize, J. R., England, R. and Sabina, F. J. Theoretical and numerical study of diffraction of waves by inhomogeneous obstacles. Comunicaciones internas, 291, IIMAS-UNAM, Mexico, 1981

Jackson, P. S. The focusing of earthquakes. *Bull. Seism. Soc. Am.* 1971, **61**, 685–695

Jennings, P. C. (editor) San Fernando earthquake of February 9, 1971.

Earthquake Eng. Res. Lab., EERL 71-02, Calif. Inst. of Tech., Pasedena, California, 1971
Joyner, W. B. A method for calculating nonlinear seismic response in two dimensions. *Bull. Seism. Soc. Am.* 1975, **65**, 1337–1357
Joyner, W. B. and Chen, A. T. F. Calculation of nonlinear ground response in earthquakes. *Bull. Seism. Soc. Am.* 1975, **65**, 1315–1336
King, J. L. and Brune, J. N. Modeling the seismic response of sedimentary basins. *Bull. Seism. Soc. Am.* 1981, **72**, 1469–1487
Kubo, K. and Isoyama, R. Damage to buried utility pipes in the 1978 Miyagiken-Oki earthquake. *Proc. World Conf. Earthquake Eng., 7th*, Istanbul, 1980, **8**, 225–232
Kupradze, V. D. Potential methods in the theory of elasticity. Israel Program for Scientific Translations, Jerusalem, 1965
Lee, J. J. and Langston, C. A. Wave propagation in a three-dimensional circular basin. *Bull. Seism. Soc. Am.* 1983, **73**, 1637–1655
Lee, V. W. A note on the scattering of elastic plane waves by a hemispherical canyon. *Soil Dynamics and Earthquake Engineering* 1982, **1**, 122–129
Liao, Z. P. Baipo, Y. and Yifan, Y. Effect of three-dimensional topography on earthquake ground motion. *Proc. World Conf. Earthquake Eng., 7th*, Istanbul, 1980, **2**, 161–168
Liao, Z. P. and Wong, H. L. A transmitting boundary for discrete methods. *Proc. 4th, ASCE-EMD Specialty Conf.*, Purdue University, 1981
Lysmer, J. and Drake, L. A. A finite element method for seismology in *Methods of Computational Physics, II*. (Ed. B. A. Bolt), Academic Press, New York, 1972
Macdonald, H. M. *Electric Waves*. Cambridge University Press, Cambridge, England, 1902
Madariaga, R. High frequency radiation from dynamic earthquake fault models. *Ann. Geophysical* 1983, **1**, 17–23
Madariaga, R. Gaussian beam synthetic seismograms in a vertically varying medium. *Geophys. J. R. Astr. Soc.* 1984, **79**
Mow, C. C. and Pao, Y. H. The diffraction of elastic waves and dynamic stress concentrations. Report R-482-PR, The Rand Corporation, Santa Monica, California, 1971
Nowack, R. and Aki, K. The two-dimensional Gaussian beam synthetic method: testing and applications. *J. Geophys. Res.* 1984, **89**, 7797–7819
Ohtsuki, A. and Harumi, K. Effect of topography and subsurface inhomogeneities on seismic SV waves. *Int. J. Earthquake Engrg. Struct. Dyn.* 1983, **11**, 441–462
Ohtsuki, A., Yamahara, H. and Harumi, K. Effect of topography and subsurface inhomogeneity on seismic Rayleigh waves. *Int. J. Earthquake Engr. Struct. Dyn.* 1984a, **12**, 37–58
Ohtsuki, A., Yamahara, H. and Tazoh, T. Effect of lateral inhomogeneity on seismic waves. II Observations and analyses. *Int. J. Earthquake Engrg. Struct. Dyn.* 1984b, **12**, 795–816
Poceski, A. The ground effect of the Skopje July 26, 1963 earthquake. *Bull. Siesm. Soc. Am.* 1969, **59**, 1–29
Rial, J. A. Caustics and focusing produced by sedimentary basins. Application of catastrophe theory to earthquake seismology. *Geophys. J. R. Astr. Soc.* 1984, **79**, 923–938
Ruiz, S. E. Influencia de las condiciones locales en las caracteristicas de los sismos. Instituto de Ingenieria, UNAM, 1977, **387**, pp. 65
Ruiz, S. E. and Esteva, L. Probabilistic response of multi-support structures on non uniform soil conditions. *Int. Conf. on Recent Advances in Geotechnical Earthquake Engineering and Soil Dynamics*, St. Louis, Missouri, 1981, **1**, 351–354
Sabina, F. J. and Willis, J. R. Scattering of SH waves by a rough half-space of arbitrary slope. *Geophys. J. R. Astr. Soc.* 1975, **42**, 685–703
Sabina, F. J. and Willis, J. R. Scattering of Rayleigh waves by a ridge. *J. Geophys.* 1977, **43**, 401–419
Sabina, F. J., England, R. and Herrera, I. Theory of connectivity: Applications to scattering of seismic waves. I. SH wave motion. *Proc. 2nd International Conf. on Microzonation*, San Francisco, California, 1979, **2**, 813–824
Sánchez-Sesma, F. J. Ground motion amplification due to canyons of arbitrary shape. *Proc. Int. Conf. on Microzonation, 2nd*, San Francisco, California, 1978, **2**, 729–738
Sánchez-Sesma, F. J. A boundary method applied to elastic scattering problems. *Arch. Mech.* 1981, **33**, 167–179
Sanchez-Sesma, F. J. Diffraction of elastic waves by three-dimensional surface irregularities. *Bull. Seism. Soc. Am.* 1983, **73**, 1621–1636
Sánchez-Sesma, F. J. Diffraction of elastic SH waves by wedges. *Bull. Seism. Soc. Am* 1985, **75**, 1435–1446
Sánchez-Sesma, F. J. and Rosenblueth, E. Ground motion at canyons of arbitrary shape under incident SH waves. *Int. J. Earthquake Eng. Struct. Dyn.* 1979, **7**, 441–450
Sanchez-Sesma, F. J. and Esquivel, J. A. Ground motion on alluvia valleys under incident plane SH waves. *Bull. Seism. Soc. Am.* 1979, **69**, 1107–1120
Sanchez-Sesma, F. J. and Esquivel, J. A. Ground motion on ridges under incident SH waves. *Proc. World Conf. Earthquake Eng. 7th* Istanbul, 1980, **1**, 33–40
Sanchez-Sesma, F. J., Herrera, I. and Bravo, M. A. Diffracion de ondas P, SV y de Rayleigh en un semiespacio elastico. Instituto de Ingenieria UNAM, Mexico, 1982a
Sanchez-Sesma, F. J., Herrera, I. and Aviles, J. A boundary method for elastic wave diffraction. Application to scattering of SH waves by surface irregularities. *Bull. Seism. Soc. Am.* 1982b, **72**, 473–490
Sanchez-Sesma, F. J., Chavez-Perez, S. and Aviles, J. Scattering of elastic waves by three-dimensional topographies. *Proc. World Conf. Earthquake Engrg 8th*, San Francisco, California, 1984, **2**, 639–646
Sanchez-Sesma, F. J., Bravo, M. A. and Herrera, I. Surface motion of topographical irregularities for incident P, SV and Rayleigh waves. *Bull Seism. Soc. Am.* 1985, **75**, 263–269
Sanchez-Sesma, F. J., Faccioli, E. and Fregonese, R. An index for measuring the effects of topography on seismic ground motions intensity. *Int. J. Earthquake Engrg. Struct. Dyn.* 1986, in press
Shah, A. H., Wong, K. C. and Datta, S. K. Diffraction of plane SH waves in a half-space. *Int. J. Earthquake Eng.rg. Struct. Dyn.* 1982, **10**, 519–528
Sills, L. B. Scattering of horizontally polarized shear waves by surface irregularities. *Geophys. J. R. Astr. Soc.* 1978, **54**, 319–348
Siro, L. Emergency microzonations by Italian Geodynamics Project after November 23, 1980 earthquake: a short technical report. *Proc. Int. Conf. Microzonation, 3rd*, Seattle, Washington, 1982, **3**, 1417–1427
Singh, S. K. and Sabina, F. J. Ground motion amplification by topographic depressions for incident P waves under acoustic approximation. *Bull. Seism. Soc. Am.* 1977, **67**, 345–352
Smith, W. D. A nonreflecting boundary for wave propagation problems. *J. Computational Phys.* 1974, **15**, 492–503
Smith, W. D. The application of finite element analysis to body wave propagation problems. *Geophys. J. R. Astr. Soc.* 1975, **42**, 747–768
Sommerfeld, A. *Partial differential equations in physics*, Academic Press, Inc., New York, 1949
Sozen, M. A., Jennings, P. C., Mattiesen, R. B., Housner, G. W. and Newmark, N. M. Engineering Report of the Caracas Earthquake of July 29, 1967, National Acedemy of Sciences, Washington DC, 1968
Streeter, V. L., Wylie, E. B. and Richard, F. E., Jr Soil motion computations by characteristics method. *Proc. Am. Soc. Civil Eng., J Geotech Eng. Div.* 1974, **100**, 247–263
Takeuchi, H. and Saito, M. Seismic surface waves in *Methods in Computational Physics*. (Ed. B. A. Bolt), Academic Press, New York, 1972, **11**
Trifunac, M. D. Surface motion of a semi-cylindrical alluvial valley for incident plane SH waves. *Bull. Seism. Soc. Am.* 1971, **61**, 1755–1770
Trifunac, M. D. Scattering of plane SH waves by a semi-cylindrical canyon. *Intl J. Earthquake Eng. Struct. Dyn.* 1973, **1**, 267–281
Trifunac, M. D. Effects of site geology on amplitudes of strong motion. *Proc. World Conf. Earthquake Eng., 7th*, Instanbul, 1980, **2**, 145–152
Trifunac, M. D. and Hudson, D. E. Analysis of the Pacoima Dam accelerogram – San Fernando, California, earthquake of 1971. *Bull. Seism. Soc. Am.* 1971, **61**, 1393–1411
Wong, H. L. Diffraction of P, SV and Rayleigh waves by surface topographies, Report CE 79-05, Department of Civil Engineering, University of Southern California, Los Angeles, California, 1979
Wong, H. L. Effect of surface topography on the diffraction of P, SV and Rayleigh waves. *Bull. Seism. Soc. Am.* 1982, **72**, 1167–1183
Wong, H. L. and Trifunac, M. D. Scattering of plane SH wave by a semi-elliptical canyon. *Int. J. Earthquake Eng. Struct. Dyn.* 1974a, **3**, 157–169
Wong, W. L. and Trifunac, M. D. Surface motion of a semi-elliptical alluvial valley for incident plane SH wave. *Bull. Seism. Soc. Am.* 1974b, **64**, 1389–1408
Wong, H. L. and Jennings, P. C. Effect of canyon topography on strong ground motion. *Bull. Seism. Soc. Am.* 1975, **65**, 1239–1257
Wong, H. L., Trifunac, M. D. and Westermo, B. Effects of surface and subsurface irregularities on the amplitude of monochromatic waves. *Bull. Seism. Soc. Am.* 1977, **67**, 353–368
Ziegler, F. and Pao, Y.-H. Transient elastic waves in a wedge-shaped layer. *Acta Mechanica* 1984, **52**, 133–163
Zienkiewicz, O. C., Kelly, D. W. and Bettess, P. The coupling of the finite element and boundary solution procedures. *Int. J. Num. Meth. Eng.* 1977, **11**, 355–377

$$\sigma_{ij} = c_{ijkl} \frac{\partial u_k}{\partial x_l}$$

$$\frac{\partial \sigma_{ij}}{\partial x_j} + f_i + \rho \omega^2 u_i = 0$$

$$c_{ijkl} \frac{\partial^2 u_k}{\partial x_j \partial x_l} + \rho \omega^2 u_i = -f_i$$

Soit

$$f_i = \boxed{e_m}\, \delta_{im}\, \delta(x-\xi)$$

$$u_i = G_{im} \quad \boxed{e_m} \quad = \quad G_{im}(x/\xi)$$

$$c_{ijkl} \frac{\partial^2 G_{km}}{\partial x_j \partial x_l} + \rho \omega^2 G_{im} = -\delta(x-\xi)\, \delta_{im}$$

$$c_{ijkl} \frac{\partial^2 u_k}{\partial x_j \partial x_l} G_{im} + \rho \omega^2 u_i G_{im} = -f_i G_{im}$$

$$c_{ijkl} \frac{\partial^2 G_{km}}{\partial x_j \partial x_l} u_i + \rho \omega^2 u_i G_{im} = -\delta(x-\xi)\, u_i \delta_{im}$$

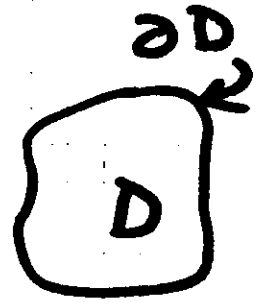

$$c_{ijkl} \frac{\partial^2 u_k}{\partial x_j \partial x_l} G_{im} - c_{ijkl} \frac{\partial^2 G_{km}}{\partial x_j \partial x_l} u_i = -f_i G_{im} + \delta(x-\xi)\, u_m$$

$$\frac{\partial}{\partial x_j}\left[c_{ijkl} \frac{\partial u_k}{\partial x_l} G_{im} - c_{ijkl} \frac{\partial G_{km}}{\partial x_l} u_i \right] = c_{ijkl} \frac{\partial^2 u_k}{\partial x_j \partial x_l} G_{im} - c_{ijkl} \frac{\partial^2 G_{km}}{\partial x_j \partial x_l} u_i +$$

$$\underbrace{\sigma_{ij}(\partial_j G_{im}) - (\partial_j u_i) \Sigma_{ijm}}_{\equiv 0} \longleftarrow \left\{ + c_{ijkl} \left(\frac{\partial u_k}{\partial x_l} \frac{\partial G_{im}}{\partial x_j} - \frac{\partial G_{km}}{\partial x_l} \frac{\partial u_i}{\partial x_j} \right) \right.$$

$$\int_{\partial D} \left\{ n_j\, c_{ijkl} \frac{\partial u_k}{\partial x_l} G_{im} - n_j c_{ijkl} \frac{\partial G_{km}}{\partial x_l} u_i \right\} dS = -\int_D f_i G_{im}\, dV + u_m(\xi)$$

$$\uparrow$$

$$\delta_{im} u_i$$

$$\left.\begin{matrix}1\\ \frac{1}{2}\\ 0\end{matrix}\right\} \delta_{im}\, u_i(\xi) = \int_{\partial D} \left\{ G_{im}^{(x/\xi)}\, t_i^{(x)} - T_{im}^{(x/\xi)}\, u_i^{(x)} \right\} dS_x + \int_D f_i^{(x)}\, G_{im}^{(x/\xi)}\, dV_x$$

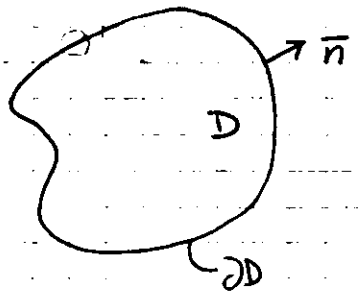

l'equation integral est alors pour $x_\xi \in \partial D$

$$\frac{1}{2}\delta_{im}\, u_i(\xi) = \int_{\partial D} \left[G_{im}(x/\xi)\, t_i(x) - T_{im}(x/\xi)\, u_i(x) \right] dS + \int_D f_i(y) G_{im}$$

Soit $\hat{u}_i(x)$ une solution du probleme exterieur (avec $\hat{t}_i(x)$)

on a dans ce cas

$$\frac{1}{2}\delta_{im}\, \hat{u}_i(\xi) = -\int_{\partial D} \left[G_{im}(x/\xi)\, \hat{t}_i(x) - T_{im}(x/\xi)\, \hat{u}_i(x) \right] dS$$

si $\hat{u}_i(\xi) = u_i(\xi)$

$$\delta_{im}\, u_i(\xi) = \int_{\partial D} \left(t_i(x) - \hat{t}_i(x) \right) G_{im}(x/\xi)\, dS + \int_D f_i(y) G_{im}(y/\xi)\, dV$$

si $t_i(x) - \hat{t}_i(x) = \phi_i(x)$

$$u_m(\xi) = \int_{\partial D} \phi_i(x) G_{im}(x/\xi)\, dS + \int_D f_i(y)\, G_{im}(y/\xi)\, dV$$

pour $\xi \in \partial D$

si $\xi \in D$ (point interieur) on a $u_m(\xi) = \int \left[G_{im}(x/\xi)\, t_i(x) - T_{im}(x/\xi)\, u_i(x) \right] dS$

et $0 = -\int \left[G_{im}(x/\xi)\, \hat{t}_i(x) - T_{im}(x/\xi)\, \hat{u}_i(x) \right] dS + \int_D f_i(y) G_{im}$

$$\boxed{u_m(\xi) = \int_{\partial D} \phi_i(x)\, G_{im}(x/\xi)\, dS + \int_D f_i(y)\, G_{im}(y/\xi)\, dV}$$

$\Rightarrow$ l'expression est valable pour $\xi \in D \cup \partial D$

D'autre part comme $G_{im}(x|\xi) = G_{mi}(x|\xi) = G_{mi}(\xi|x)$

on peut ecrire

$$u_i(x) = \int_{\partial D} \phi_j(\xi)\, G_{ij}(x|\xi)\, dS_\xi + \int_D f_j(\xi)\, G_{ij}(x|\xi)\, dV_\xi$$

Dont ϕ_j est clairement une distribution de sources à la frontière

$$\sigma_{ij} = c_{ijkl} \frac{\partial u_k}{\partial x_l} \qquad t_i = \sigma_{ij}\, n_j$$

$$t_i^{n(x)}(x) = \int_{\partial D} \phi_m(\xi)\; c_{ijkl} \frac{\partial G_{km}(x|\xi)}{\partial x_l} n_j(x)\, dS_\xi + \int_D f_m(\xi)\, c_{ijkl} \frac{\partial G_{km}}{\partial x_l} n_j\, dV$$

pour $x \in D$

$$t_i(x) = \int_{\partial D} \phi_m(\xi) \underbrace{c_{ijkl} \frac{\partial G_{km}(x|\xi)}{\partial x_l} n_j(x)}_{T_{im}(x|\xi)} dS_\xi + \int_D f_m(\xi)\, T_{im}(x|\xi)\, dV$$

$x \in D$

$$t_i(x) = \int_{\partial D} \phi_m(\xi)\, T_{im}(x|\xi)\, dS_\xi + \int_D f_m(\xi)\, T_{im}(x|\xi)\, dV_\xi$$

$x \in \partial D$

terme libre

$$t_i(x) = \pm\frac{1}{2}\phi_i(x) + \int_{\partial D} \phi_m(\xi)\, T_{im}(x|\xi)\, dS_\xi + \int_D f_m(\xi)\, T_{im}\, dV_\xi$$

Bulletin of the Seismological Society of America, Vol. 81, No. 6, pp. 2234–2253, December 1991

DIFFRACTION OF *P*, *SV*, AND RAYLEIGH WAVES BY TOPOGRAPHIC FEATURES: A BOUNDARY INTEGRAL FORMULATION

By Francisco J. Sánchez-Sesma and Michel Campillo

Abstract

A method is presented to compute the diffraction of *P*, *SV*, and Rayleigh waves by an irregular topographic feature in an elastic half-space. It is based on an integral representation of the diffracted elastic fields in terms of single-layer boundary sources that is derived from Somigliana's identity. Introduction of boundary conditions leads to a Fredholm integral equation of the second kind for boundary sources. A discretization scheme based on the numerical and analytical integration of exact Green's functions for displacements and tractions is employed. Calculations are performed in the frequency domain and synthetic seismograms are obtained using the fast Fourier transform.

In order to give perspective on the range of effects caused by topographic anomalies, various examples that cover extreme cases are presented. It is found that topography may cause significant effects both of amplification and of deamplification at the irregular feature itself and its neighborhood, but the absolute level of amplification is generally lower than about four times the amplitude of incoming waves. Such facts must be taken into account when the spectral ratio technique is used to characterize topographical effects.

Introduction

Site effects can generate large ground motion amplification during earthquakes. This fact is well known (see, e.g., Sánchez-Sesma, 1987, and Aki, 1988, for recent reviews). However, quantitative procedures to account for topographical amplification in practical instances are less well known. According to Geli *et al.* (1988), observed amplification values in the field are systematically larger than theoretical predictions based on scalar two-dimensional models. They have pointed out the need to study the effects that the propagation of *P*, *SV*, and Rayleigh waves may produce at and near irregular two- and three-dimensional configurations in order to better explain the observations.

The problem is not new. Significant progress has been achieved since the pioneering work of Aki and Larner (1970), who introduced a numerical method based on a discrete superposition of plane waves. At the same time, Trifunac (1971, 1973) found the analytical solutions for the response of semi-circular alluvial valleys and canyons under incident *SH* waves. For arbitrary geometries, a formulation based on an integral representation was used by Wong and Jennings (1975). On the other hand, Bouchon (1973) and later Bard (1982) and Geli *et al.* (1988) used the Aki-Larner technique to study the response of irregular topographies. This method, however, cannot deal with large slope features because of the numerical difficulties to correctly simulate locally upgoing waves (see Sánchez-Sesma *et al.*, 1989, for a discussion). In practice, this problem has been removed by using the combination of boundary integral representations with the discrete wavenumber method. Bouchon (1985), Campillo and Bouchon (1985), Campillo (1987), Gaffet and Bouchon (1989), Bouchon *et al.* (1989), and Campillo *et al.* (1990) used direct source distributions on the boundaries, whereas Kawase (1988) and Kawase and Aki (1989) used Somigliana representation (see, e.g., Aki and Richards, 1980).

Another type of boundary method has been used to deal with this class of problems (see, e.g., Sánchez-Sesma, 1978; Sánchez-Sesma and Rosenblueth, 1979; Sánchez-Sesma and Esquivel, 1979; Wong, 1979, 1982; Dravinski, 1982; Dravinski and Mossessian, 1987; Sánchez-Sesma *et al.*, 1985; Bravo *et al.*, 1988; Eshraghi and Dravinski, 1989; Khair *et al.*, 1989; Bouden *et al.*, 1990; Luco *et al.*, 1990). In its many variants, including in some cases three-dimensional problems and layered media, the technique is based upon the superposition of solutions for sources with their singularities placed *outside* the region of interest. Boundary conditions are satisfied in a least-squares sense (Wong, 1982, considered the problem as one of generalized inversion). This leads to a system of linear equations for the sources' strengths. In some applications, however, the location of sources requires particular care and the trial and error process needed is difficult to apply. This is particularly true when many frequencies are to be computed.

In this work, we use a single-layer boundary integral representation for diffracted waves. In this respect, this approach is similar to the *source* method just mentioned above, except for the fact that now we put the sources at the boundary and directly solve the linear system that arise from the discretization. In this way, the uncertainty about the location of sources is eliminated. This approach was motivated by the success achieved using the combination of boundary integral formulations and the discrete wave number method (e.g., Bouchon, 1985; Campillo and Bouchon, 1985; Campillo, 1987; Kawase, 1988; Kawase and Aki, 1989). Such a combination is particularly attractive as the singularities of Green's functions are not present in each one of the terms of the discrete wave number expansion. The integration along the boundary effectively makes the singularities vanish and improves convergence as well. However, such procedures require considerable amount of computer resources. For many applications, an alternative approach may be welcomed. Indeed, when the Green's functions are explicit, its singularities are integrable as it is done in numerous BIEM applications (see, e.g., Brebbia, 1978; Banerjee and Butterfield, 1981). In fact, our direct approach retains the physical insight of the source method, with all the benefits of analytical integration of *exact* Green's functions. We represent diffracted fields with the superposition of the radiation from boundary line sources computed using the exact expressions of the two-dimensional Green's functions in an unbounded elastic space.

In what follows, we show that a direct single-layer boundary integral representation stems from that of Somigliana, and we apply it to study the surface motion at various topographic features for incident *P*, *SV*, and Rayleigh waves. This plane strain case can be regarded as the simplest of a class of vector problems of seismological interest.

In order to test our method, we compared results with those obtained by Wong (1982), Sánchez-Sesma *et al.* (1985), and Kawase (1988) for the diffraction of *P*, *SV*, and Rayleigh waves by a semicircular canyon on a half-space. We found excellent agreement with these results. Various examples that cover extreme profiles are presented. Thus, giving perspective on the range of effects caused by topography, we show that relatively simple topographies may induce significant variations of ground-motion at and around the irregularity. We believe that this fact explains the large relative amplifications reported in the literature (see,

e.g., Geli *et al.*, 1988). Our examples show that, even though relative amplification due to the topography is sometimes quite big, the absolute level of amplification is generally lower than about four times the amplitude of incoming waves. Such facts must be taken into account when the spectral ratio technique is used to characterize topographical effects.

Integral Representation Using Boundary Sources

Consider the domain V and its boundary S. If an elastic material occupies such a region, the displacement field under harmonic excitation can be written by means of the Somigliana representation theorem for an interior problem (see, e.g., Achenbach, 1973; Aki and Richards, 1980; Banerjee and Butterfield, 1981)

$$cu_m(\xi) = \int_S \left[G_{im}(\mathbf{x}, \xi) t_i(\mathbf{x}) - T_{im}(\mathbf{x}, \xi) u_i(\mathbf{x}) \right] dS_x + \int_V f_i(\mathbf{y}) G_{im}(\mathbf{y}, \xi)\, dV_y, \tag{1}$$

where u_m = mth component of displacement; t_i = ith component of traction at the boundary; $G_{im}(\mathbf{x}, \xi)$ = Green function, i.e., the displacement in the direction i at point $\mathbf{x}$ due to the application of a unit force in the direction m at point ξ; $T_{im}(\mathbf{x}, \xi)$ = traction Green function, i.e., the traction in the direction i at point $\mathbf{x}$ on the boundary with normal $\mathbf{n}(\mathbf{x})$ (assumed to be specified) due to the application of a unit force in the direction m applied at ξ; and f_i = components of body force distribution. The constant c takes the values 1 or 0 if the point ξ is inside or outside V, respectively, and is equal to 0.5 when ξ is located on the smooth boundary. The subscripts in the differentials indicate the space variable over which the integration is performed. This representation theorem is the departure of various integral formulations and seismological applications (see, e.g., Aki and Richards, 1980).

Assume now that $u'_i(\mathbf{x})$ is a solution of the exterior problem with boundary traction $t'_i(\mathbf{x})$. Assume also that the material that occupies the exterior region is the same. Therefore, both interior and exterior regions share Green's functions. Neglecting body forces we can write

$$c' u'_m(\xi) = -\int_S \left[G_{im}(\mathbf{x}, \xi) t'_i(\mathbf{x}) - T_{im}(\mathbf{x}, \xi) u'_i(\mathbf{x}) \right] dS_x, \tag{2}$$

where c' is a constant with values 0, 0.5, or 1 if the point ξ is inside V, at S, or outside V, respectively. In writing equation (2), the radiation conditions at infinity of the displacement fields have been taken into account.

Summing up equations (1) and (2), we have

$$cu_m + c' u'_m = \int_S \left[(t_i - t'_i) G_{im} - (u_i - u'_i) T_{im} \right] dS_x + \int_V f_i G_{im}\, dV_y. \tag{3}$$

If we impose that at the boundary $u_i = u'_i$ and if $t_i - t'_i = \phi_i$, we can write

$$u_m(\xi) = \int_S \phi_i(\mathbf{x}) G_{im}(\mathbf{x}, \xi)\, dS_x + \int_V f_i(\mathbf{y}) G_{im}(\mathbf{y}, \xi)\, dV_y, \tag{4}$$

which is a representation valid in region V and its boundary S. On the other hand, the Green function satisfies

$$G_{im}(\mathbf{x}, \xi) = G_{mi}(\mathbf{x}, \xi) = G_{mi}(\xi, \mathbf{x}); \tag{5}$$

therefore, we can write

$$u_i(\mathbf{x}) = \int_S \phi_j(\xi) G_{ij}(\mathbf{x}, \xi)\, dS_\xi + \int_V f_j(\xi) G_{ij}(\mathbf{x}, \xi)\, dV_\xi, \tag{6}$$

where $\phi_j dS_\xi$ is clearly a force distribution at the boundary. This *single layer* integral representation has been studied by Kupradze (1963). He showed that the displacement field is continuous across S if $\phi_i(\xi)$ is continuous on S. This is in agreement with our choice for $u_i = u'_i$. Other choices are possible. If for example $t'_i = t_i$, then $u_i - u'_i$ would be unknown and the displacement field would be expressed in terms of the *traction* Green's function. (This is an usual approach in dealing with certain crack problems; see, e.g., Bonnet, 1989; Coutant, 1989). With our derivation, that closely follows that of Bonnet (1986a), we have shown that this *single layer* integral representation stems from Somigliana's one. In its scalar version (*SH* waves), it is called the Kirchhoff-Helmholtz representation (see, e.g., Kouoh-Bille *et al.*, 1991).

This integral representation allows computation of stresses and tractions by direct application of Hooke's law. However, when $\mathbf{x} = \xi$ on the boundary, this requires particular care. From a limiting process based on equilibrium considerations around an internal neighborhood of the boundary, we can write, for $\mathbf{x}$ on S that

$$t_i(\mathbf{x}) = \frac{1}{2}\phi_i(\mathbf{x}) + \int_S \phi_j(\xi) T_{ij}(\mathbf{x}, \xi)\, dS_\xi + \int_V f_j(\xi) T_{ij}(\mathbf{x}, \xi)\, dV_\xi. \tag{7}$$

The first term of the right hand side must be dropped if $\mathbf{x}$ is inside V. This result has also been found by Kupradze (1963). He used a formal technique of singularity extraction that is now used to deal with the hypersingular integral equations of dynamic elasticity (see, e.g., Bonnet, 1986b, 1989).

Equations (6) and (7) are the basis of our approach. They allow direct interpretation of all physical quantities involved.

Two-Dimensional Green's Functions in Unbounded Space

In a homogeneous isotropic elastic unbounded medium, the Green functions for harmonic time dependence $e^{i\omega t}$, where $i^2 = -1$, ω = circular frequency, and

t = time, can be expressed in the following compact form:

$$G_{22} = \frac{1}{i4\rho} \frac{H_0^{(2)}(kr)}{\beta^2},$$

$$G_{ij} = \frac{1}{i8\rho} \left[\delta_{ij} A - (2\gamma_i\gamma_j - \delta_{ij}) B\right] \quad i, j = 1, 3, \tag{8}$$

$$T_{22} = \frac{i}{4r} D(kr)\gamma_k n_k,$$

$$T_{ij} = \frac{i\mu}{2\rho r} \left\{ \left[B + \frac{\lambda D(qr)}{2\mu\alpha^2} \right] \gamma_i n_j + \left[B + \frac{D(kr)}{2\beta^2} \right] \times \left[\gamma_i n_j + \gamma_k n_k \delta_{ij} \right] + (C - 4B)\gamma_i\gamma_j\gamma_k n_k \right\},$$

where

$$A = \frac{H_0^{(2)}(qr)}{\alpha^2} + \frac{H_0^{(2)}(kr)}{\beta^2},$$

$$B = \frac{H_2^{(2)}(qr)}{\alpha^2} - \frac{H_2^{(2)}(kr)}{\beta^2}, \tag{9}$$

$$C = \frac{D(qr)}{\alpha^2} - \frac{D(kr)}{\beta^2},$$

$$D(p) = pH_1^{(2)}(p),$$

ρ = mass density, $k = \omega/\beta = S$ wavenumber, $q = \omega/\alpha = P$ wavenumber, $\alpha = \sqrt{(\lambda + 2\mu)/\rho} = P$-wave velocity, $\beta = \sqrt{\mu/\rho} = S$-wave velocity, λ, μ = Lamé's constants, δ_{ij} = Kronecker's delta, $\gamma_i = (x_i - \xi_i)/r$, n_i = unit normal vector, $r = \sqrt{(x_1 - \xi_1)^2 + (x_3 - \xi_3)^2}$, and $H_m^{(2)}(\cdot)$ = Hankel function of the second kind and order m.

In the previous expressions, the usual summation convention for subscripts is assumed and it is restricted to 1 and 3 because of the two-dimensional nature of the problem considered herein, i.e., there is no dependence to x_2. We may use in what follows the usual correspondence for axis' names: $x_1 = x$, $x_2 = y$, and $x_3 = z$, respectively. Also: $u_1 = u_x = u$ and $u_3 = u_z = w$. The terms G_{22} and T_{22} correspond to a *SH antiplane* unit line force, whereas G_{ij} and T_{ij}, where i, $j = 1, 3$, are associated to an *inplane* unit line force with direction j. Terms G_{2j}, G_{j2}, T_{2j}, and T_{j2} are null for $j = 1, 3$. Similar expressions for the in-plane Green's functions have been presented by Kummer *et al.* (1987).

Equations (8) and (9) allow a direct view of their singularities at the point of application of the line force. The singularity of displacements is logarithmic. This can be seen from the behavior of Hankel functions for small arguments (see, e.g., Abramowitz and Stegun, 1972). Regarding the tractions, the singularity is explicitly of the form r^{-1} because for zero arguments we have the constant limiting forms: $D = 2i/\pi$ and $C = 2B = 2i(\alpha^{-2} - \beta^{-2})/\pi$. In particular, when frequency tends to zero, equations (8) lead to their static counterparts

(see, e.g., Love, 1944). These properties are invoked below in connection with our discretization scheme.

Diffraction of Elastic Waves by a Topographic Feature

Consider an elastic half space with a localized topographic relief as depicted in Figure 1. The ground motion in this irregular configuration comes from the interferences of incoming waves with reflected and diffracted ones. It is also usual to say that the total motion is the superposition of the so called *diffracted* waves and the free-field:

$$u_i = u_i^{(0)} + u_i^{(d)}, \tag{10}$$

where $u_i^{(0)}$ = free-field displacement, i.e., the solution in the absence of the irregularity. In this application, the displacement free-field is that produced by incident plane waves and is analytically extended to the parts of topography that are not included in the reference half-space. This means that incoming and reflected waves are assumed to exist for $z < 0$ fulfilling the *same* analytical expressions that they satisfy for $z \geq 0$. Therefore, the free-field is continuous everywhere.

According to our previous discussion, the diffracted field is given by equation (6), which, in the absence of body forces, can be written as

$$u_i^{(d)}(\mathbf{x}) = \int_S \phi_j(\xi) G_{ij}(\mathbf{x}, \xi)\, dS_\xi. \tag{11}$$

The traction-free boundary condition implies that $t_i^{(0)} + t_i^{(d)} = 0$. Then, from equation (7) such condition can be expressed by means of

$$\frac{1}{2}\delta_{ij}\phi_j(\mathbf{x}) + \int_S \phi_j(\xi) T_{ij}(\mathbf{x}, \xi)\, dS_\xi = -t_i^{(0)}(\mathbf{x}), \tag{12}$$

which is a singular Fredholm integral equation of the second kind for the boundary sources, i.e., those producing the diffracted field. This expression is discretized along a finite portion of the boundary S that includes the topography and the lateral flat parts. We have used values of $3L$ to $5L$, where

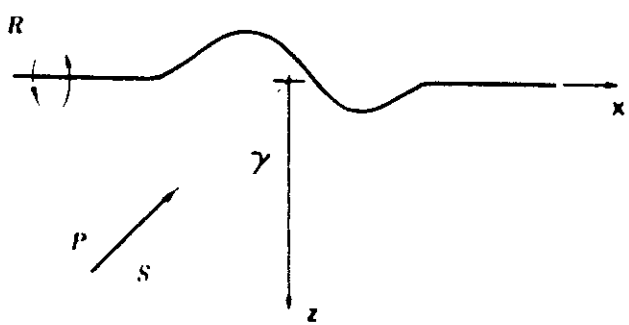

Fig. 1. Irregular half space and incidence of plane *P*, *SV*, and Rayleigh waves.

L = surface length of the surface anomaly. Assuming $\phi_j(\xi)$ constant over each of the N boundary segments with equal length ΔS leads to the system of linear equations

$$\sum_{j=1}^{N} \phi_j(\xi_j) t_{ij}(\mathbf{x}_n, \xi_j) = -t_i^{(0)}(\mathbf{x}_n), \quad n = 1, N, \tag{13}$$

where

$$t_{ij}(\mathbf{x}_n, \xi_j) = \frac{1}{2}\delta_{ij}\delta_{nj} + \int_{\xi_j - \frac{\Delta S}{2}}^{\xi_j + \frac{\Delta S}{2}} T_{ij}(\mathbf{x}_n, \xi)\, dS_\xi. \tag{14}$$

These integrals are computed numerically using Gaussian integration except when $n = j$. In this case, we have

$$t_{ij}(\mathbf{x}_n, \xi_n) = \frac{1}{2}\delta_{ij}, \tag{15}$$

because the integral in equation (14) for $n = j$ is null as long as the discretization segment is a straight line, which is the case assumed here. From equations (8), it can be verified that, under this circumstance, the integrand is a singular *odd* function on the segment. Therefore, its Cauchy's principal value is zero. The value for t_{ij} in equation (15) can be interpreted as half of the applied unit line force and means that the force is distributed symmetrically for any two half spaces containing the line of application of the load, regardless of its direction. In fact, this result also corresponds to the static solution.

Once the values of $\phi_j(\xi_j)$ are known, the diffracted field is computed by means of

$$u_i^{(d)}(\mathbf{x}) = \sum_{j=1}^{N} \phi_j(\xi_j) g_{ij}(\mathbf{x}, \xi_j), \tag{16}$$

where

$$g_{ij}(\mathbf{x}, \xi_j) = \int_{\xi_j - \frac{\Delta S}{2}}^{\xi_j + \frac{\Delta S}{2}} G_{ij}(\mathbf{x}, \xi)\, dS_\xi. \tag{17}$$

These integrals are also computed numerically with Gaussian integration, except in the case when $\mathbf{x}$ is in the neighborhood of ξ_j, for which we obtained analytical expressions from the ascending series for Bessel functions (see, e.g., Abramowitz and Stegun, 1972). For example, the integral of the Hankel function

$$\int_{-\Delta S/2}^{\Delta S/2} H_0^{(2)}(k\,|\,s\,|)\, ds$$

can be written as $\Delta S[1 + i2/\pi(1 - \gamma - \log k\Delta S/4)]$, where γ = Euler constant, if only the leading terms of the series are taken. We considered up to quadratic terms, which is enough if the number of segments per wavelength is larger than about 6.

For the elevated portions of the relief, the analytical extension of the free-field provides the boundary excitation. In the case of incident Rayleigh waves or for SV waves with incidence angle larger than the critical one, the analytical extension gives exponential growth of the extended field (incident plane SV waves with an incident angle of 45°, having no mode conversion and unit reflection coefficient, do not present this effect). This difficulty, when it appears, can be solved by means of an adaptative integration scheme, but it implies heavy computation. One way to remove this problem is to define an auxiliary region limited by the irregular topography and a fictitious boundary completely embedded in the half-space. The corresponding integral equation and the conditions of continuity of displacements and tractions may lead to the solution (see, e.g., Kawase and Aki, 1990). Obviously, in that case there is no need of the analytical extension. However, as we desire to keep only one region, we choose to produce Rayleigh waves by loading our irregular half-space with a vertical force. Then, the excitation comes from imposing vertical tractions in a small region of the flat part of the free surface. This is an *ad hoc* solution to the problem and illustrates well the wide potential applications of our method. In fact, the surface load problem is well known (Lamb, 1904). In this case, more of two thirds of the total energy is radiated as Rayleigh waves (Woods, 1968). Regarding our application, at the surface the relative amount of Rayleigh waves is much larger.

Testing of the Method and Discussion

The accuracy of this approach has been gauged by comparing results with those obtained by Wong (1979, 1982), Sánchez-Sesma *et al.* (1985), and Kawase (1988). The diffraction of P, SV, and Rayleigh waves by a semi-circular canyon has been studied by Wong (1979, 1982) for a half-space with Poisson ratio of 1/3 and no attenuation using a boundary method.

Wong's results (1982) were verified by Sánchez-Sesma *et al.* (1985) and Dravinski and Mossessian (1987) for a normalized frequency $\eta = \omega a/\pi\beta = 0.5$, where a is the radius of the canyon. Generally excellent agreement was found for incident P and SV waves.

For a larger normalized frequency $\eta = 2$, results by Wong (1982) and Kawase (1988) are available for P and SV waves with 0 and 30 degrees of incidence angle each. Kawase (1988) used a boundary integral representation combined with the discrete wavenumber method. Figures 2 and 3 display our results for both horizontal and vertical displacement amplitudes with solid and dashed lines, respectively. We considered a total discretization length of $5L$, where $L = \pi a$ and 15 segments per S wavelength. The solution is stable even when such parameters are reduced to $3L$ and to 6, respectively. Wong's and Kawase's results are shown by symbols. Excellent agreement is found for both horizontal and vertical components. However, small differences can be seen among these results. For instance, both Wong (1982) and Kawase (1988) predict amplitudes at the "incidence" rim of the canyon that are somewhat larger than our results for SV incidence with 30° (Fig. 3b). Generally, our results (see also Figs. 2 and 3) are closer to those of Kawase. However, in some cases they approach those of Wong. For some locations, both inside and outside the canyon our results are in between.

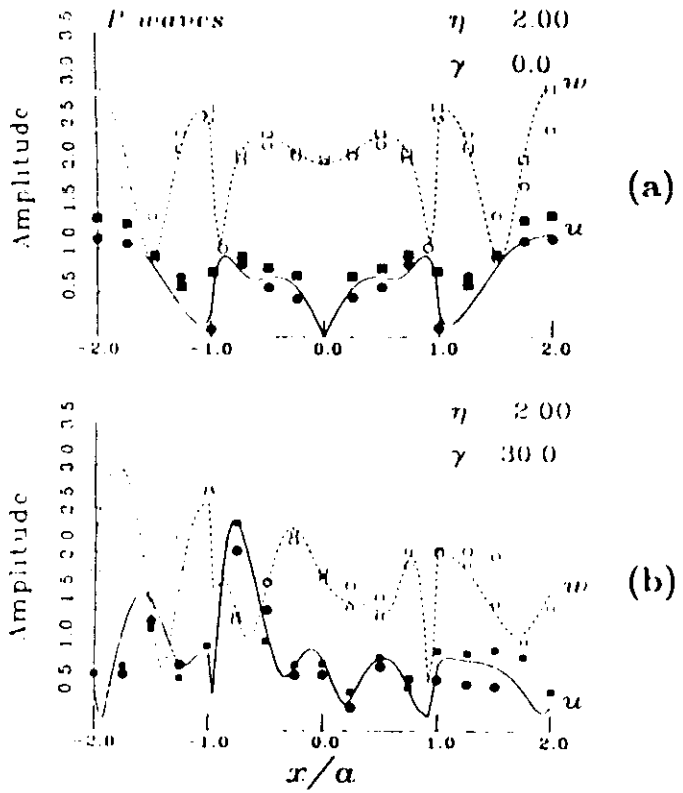

FIG. 2. Amplitudes of horizontal and vertical displacements for incidence of harmonic P waves upon a semicircular canyon, (a) vertical incidence, (b) 30° incidence. Poisson ratio is 1/3 and the normalized frequency $\eta = 2$. Solid and dashed lines correspond to horizontal (u) and vertical (w) components obtained in the present study, while solid and open symbols correspond to previous works. The results by Wong (1982) and those by Kawase (1988) are represented by circles and squares, respectively.

These three methods are approximate. The only way to assess their accuracy is through comparisons of results among them and with other procedures and by comparing the assumptions and the characteristics of each one as well.

Both Wong (1982) and Kawase (1988) considered as departure Lamb's (1904) integrals for the half-space. Working directly in frequency domain, Wong (1982) computed such integrals with "4 digits of accuracy." He considered such solutions for compressional and shear line sources as trial functions with the singularities "removed from the domain of interest," i.e., *outside* the irregular half space, inside the region left by the canyon. He satisfied boundary conditions using a generalized inversion scheme, which guarantees good results in a global sense. On the other hand, Kawase (1988) integrated analytically along the boundary the terms of the discrete wavenumber expansion for which he assumed a horizontal periodicity of 10 times the diameter of the canyon, then by careful monitoring he computed the appropriate summations to get the coefficients of the linear system of equations. He used an imaginary frequency to damp out the effect of the spurious sources introduced by the periodicity assumption. In order to obtain reliable results in the frequency domain, Kawase first got time series, then corrected with an exponentially increasing time window, which compensates for the effect of the imaginary frequency. Spectral ratios were then computed from the Fourier transforms of both the response and the input waveforms.

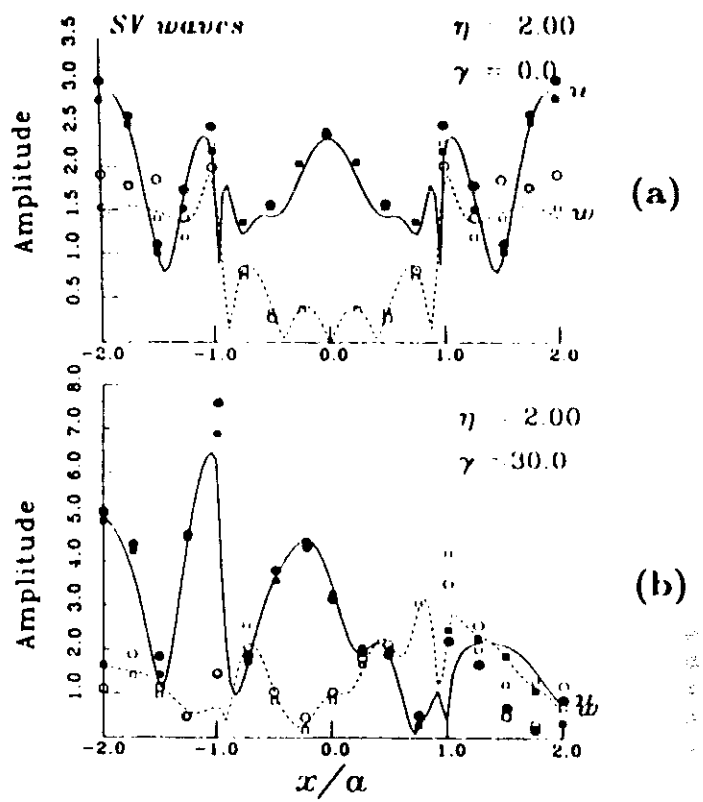

FIG. 3. Amplitudes of horizontal and vertical displacements for incidence of harmonic SV waves upon a semicircular canyon; (a) vertical incidence, (b) 30° incidence. The interpretation of the figure and parameters is the same as in Figure 2.

In contrast, we work directly in frequency domain and used the exact Green's function for the whole-space. Our approach is aimed to obtain diffracted waves, i.e., those produced both at the irregular boundary and at the free surface by means of the direct distribution of boundary sources for which we obtained either exact or analytical values at singularities. Hence, this formulation can be seen as an approximate numerical realization of Huygens' principle. For the numerical integration, we used Gaussian integration of three points per segment (which would produce exact results for a polynomial integrand of fifth degree; considering a typical value of six segments per S wavelength, our

numerical integrations can well be regarded as exact). To examine edge effects due to the finite size of the discretized boundary, we performed several tests and found that, for the range of frequencies studied, it suffices to discretize a total length of $3L$, where L = surface length of the topographic feature. The comparisons presented here have been computed for total discretization lengths of $3L$ and $5L$ and the results are virtually the same. It shows that edge effects have little or no influence in our computations and that, apart from the discretization of part of the free boundary, there is no need for fictitious or absorbing boundaries. We consider this fact a significant advantage of our approach. In order to qualitatively verify the validity of this interpretation, we computed the phase of diffracted waves and observed that for both components the phase variation with space shows slopes consistent with the expected outgoing nature of such waves. Figure 4 displays the phase of diffracted waves from the semi-circular canyon studied for incident P, SV (both with incidence angle of 30 degrees) and Rayleigh waves, respectively. It was assumed a normalized frequency of $\eta = 2$. Note that the slopes of the plots are negative (positive) for the positive (negative) portion of the flat boundary displayed. Therefore, our boundary sources correctly produce diffracted waves and their essentially *outgoing* characteristics.

Examples

In order to give some perspective on the range of effects caused by topography, various examples that cover extreme geometries are presented. We chose from a big set of results a sample that, being of reasonable dimension, allows one to describe the salient characteristics of such effects. Our results are displayed in both frequency and time domains for various canyons and mountains under incident, P, SV, and Rayleigh waves. A Poisson coefficient of 0.25 was selected and no attenuation was assumed. We considered four topographies: (1) a triangular canyon with a maximum depth of $\sqrt{3}a$ (dipping angles of 60°); (2) a semi-elliptical canyon with a maximum depth of three times the half width ($h = 3a$); (3) a triangular mountain with dipping angles of 45°; and (4) a semi-elliptical mountain with maximum height of $2a$. The discretization is extended over a total length of only 3 times the surface length of the topographic feature. The relatively small size of the discretized region is an advantage of the direct formulation. In the following examples, we used 15 segments per S wavelength.

For these topographies, we considered various cases of incidence of elastic waves. The incidence angles selected for P and SV waves were 30°, with respect to the vertical. For the canyons, the incident Rayleigh wave is a plane wave, whereas for the mountains such a pulse is generated with a vertical load of 12.5 force units applied over a length of $0.25a$ centered at $x = -4.5a$ for the semi-elliptical mountain and $x = -2.5a$ for the triangular one. These results are displayed on six figures (from Fig. 5 to Fig. 10). Each figure contains four plots: synthetic seismograms for horizontal and vertical components, respectively, frequency response for selected receivers, and spatial variation at a given frequency.

Computations were performed in the frequency domain and synthetic seismograms where computed using the FFT algorithm for a Ricker wavelet with central frequency $\omega_p = 1.5\pi\beta/a$ for 101 receivers equally spaced between $x = -4a$ and $x = 4a$ for the semi-elliptical profiles and between $x = -2a$ and

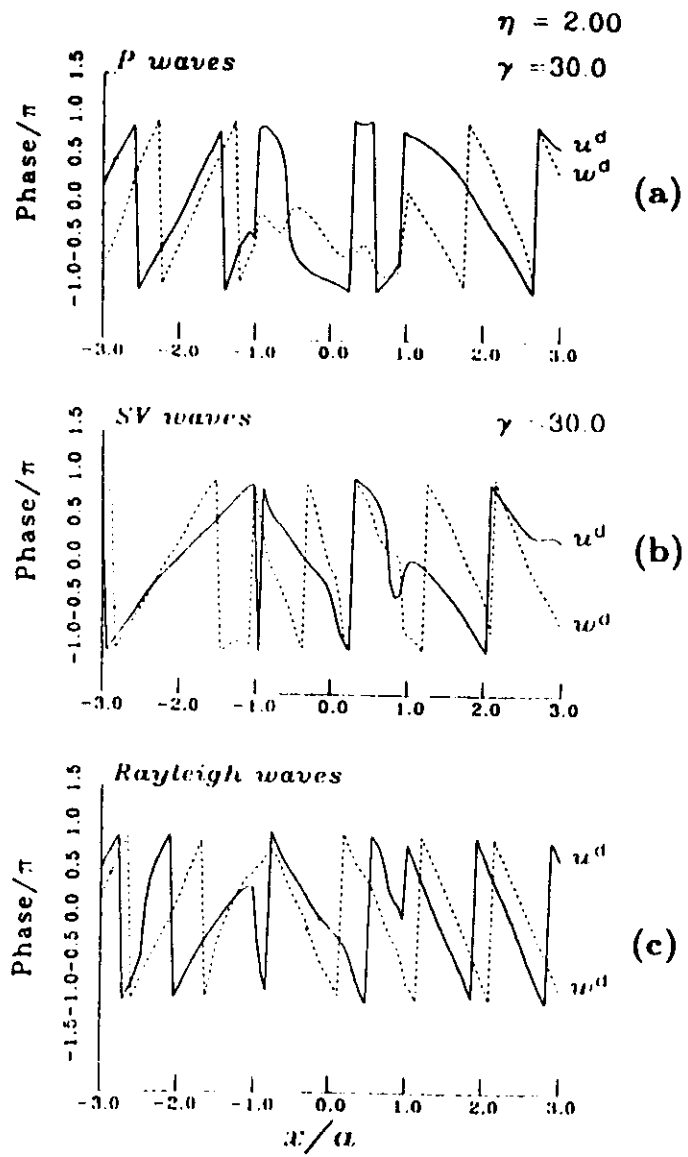

Fig. 4. Phases of horizontal and vertical diffracted displacements for incidence of harmonic waves upon a semicircular canyon; (a) P waves at 30° incidence, (b) SV waves at 30° incidence, and (c) Rayleigh waves. Solid and dashed lines correspond to horizontal ($u^{(d)}$) and vertical ($w^{(d)}$) components obtained in the present study. The parameters are the same as in Figure 2.

$x = 2a$ for the triangular ones. It was assumed that $2a/\beta = 1$ sec in order to define the time scale. For example, if $2a/\beta$ has another value, say 0.5, for $a = 0.5$ km and $\beta = 2$ km/sec, the time range will be half of the one used here; the actual time scale is then $\beta t/2a$.

Results in frequency domain are presented against $\omega a/\pi\beta$ and correspond to nine equally spaced surface receivers (out of the 101 for which we computed the synthetics). Our purpose is to give a view of the range of amplification and of its large variability rather than to present the individual response curves. In any case, we displayed also the amplitude of both horizontal and vertical displacements as a function of the receiver location for the frequency corresponding to the central one of the Ricker pulse.

For elevated topographies, the cases labeled "Rayleigh wave" correspond to the vertical load discussed above, and the frequency spectra clearly show the logarithmic singularity for the vertical displacement at small frequencies. In this case, the vertical displacement for a static load is also logarithmic in r (Love, 1944) and can have an arbitrary additive constant. Therefore, for the purpose of plotting the frequency dependence of displacement amplitude, the zero frequency values correspond to $\omega a/\pi\beta = 0.005$. However, both the synthetics and the results in the frequency domain, for $\omega a/\pi\beta > 1$ correctly describe the effects of topography upon incidence of Rayleigh waves. In fact, this can be seen on the synthetics, which show the appropriate amplitude of the incident Rayleigh wave.

Figure 5 displays the response of the triangular canyon for incident SV waves with incidence angle of 30°. Reflected P waves and diffracted Rayleigh waves can be identified on the synthetics for left and right parts of the

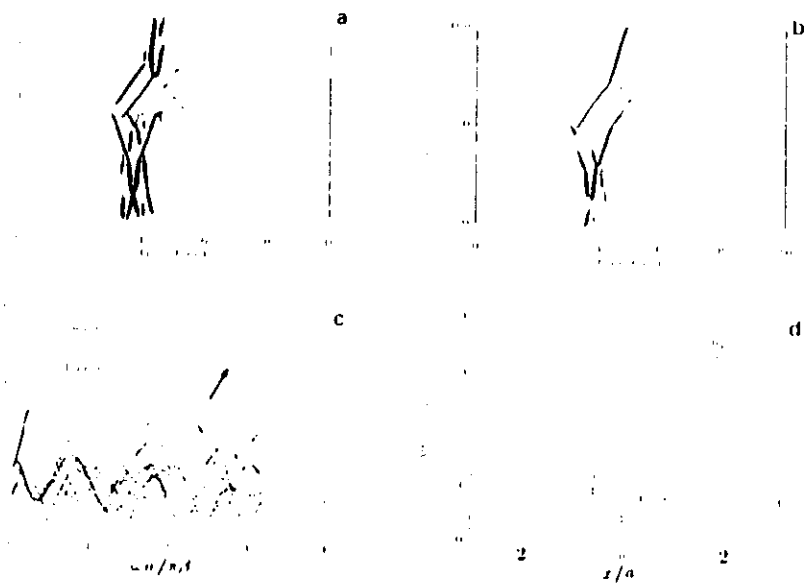

FIG. 5. Incidence of a plane SV wave with incidence angle of 30°. Synthetic seismograms and frequency response for surface receivers equally spaced between $x = -2a$ and $x = 2a$ at the surface of a triangular canyon with dipping angles of 60° (a) and (b) horizontal and vertical components, u_x and u_y, respectively. The incident time signal is a Ricker wavelet with central frequency $\omega_0 = 1.5\pi\beta/a$. Amplitudes of horizontal (continuous line) and vertical (dotted line) surface displacements (c) for nine receivers against normalized frequency and (d) for the central frequency of the Ricker wavelet for all the receivers against their horizontal location.

irregularity resulting in a criss-cross pattern and a significant increase of duration. The frequency domain results show large variations. For the horizontal component and for a wide range of frequencies, relative amplifications or deamplifications are larger than 20. However, maximum amplification is of about 4 times the amplitude of incoming wave in the horizontal component at the left rim. Note that frequency response for this point oscillates around the expected amplification (3.46 and 2 for horizontal and vertical motion, respectively) for an infinite wedge with internal angle of 120° and this incidence of SV waves (Sánchez-Sesma, 1990). Synthetic seismograms display this effect in the early response of left rim.

Figures 6 and 7 illustrate the surface motion of the deep semi-elliptical canyon for incident plane P and Rayleigh waves, respectively. Again, large variability emerges as a consequence of the superposition of incoming and reflected-diffracted energy. In the synthetics, the first arrivals at the right flat port clearly show both a delay and a reduction of amplitude that indicates a shadow zone and, thus, diffraction. In Figure 6, the reflected P wave is clearly seen along the left canyon's wall. This wave precedes both reflected S and diffracted *creeping* Rayleigh waves that propagate along the canyon's surface. The creeping waves are produced at the corners and bounce back and forth between them. Early and late emissions of diffracted Rayleigh phases are clearly seen also in the flat part of the model.

Figure 7 shows that a deep canyon effectively acts as a barrier for surface waves. In this case, good agreement is found with the theoretical prediction of Fujii *et al.* (1984) for the amplitude of the reflected and transmitted Rayleigh waves at the corner of a quarter space. Such values are of about 30 and 68%,

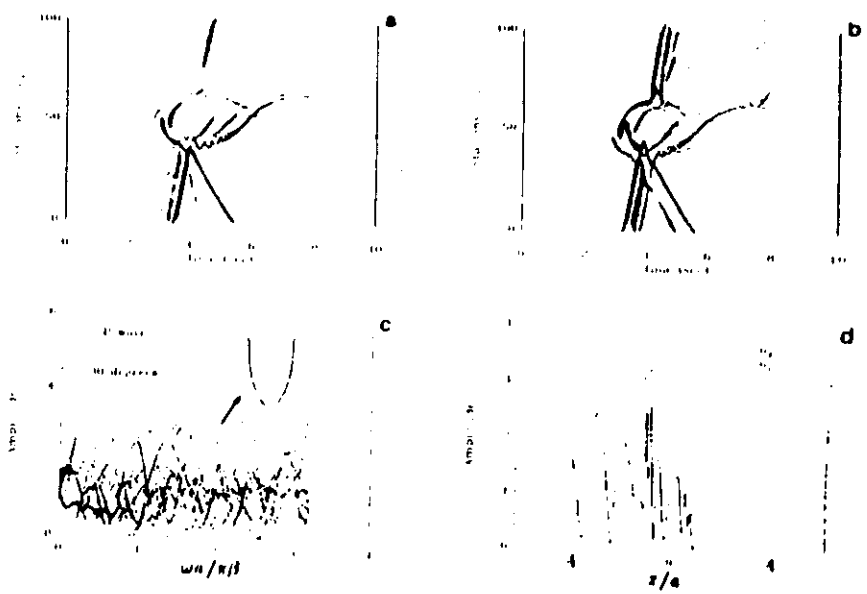

FIG. 6. Incidence of a plane P wave with incidence angle of 30°. Synthetic seismograms and frequency response for surface receivers equally spaced between $x = -4a$ and $x = 4a$ at the surface of a semi-elliptical canyon with maximum depth of $3a$. (a-d) Same as Figure 5.

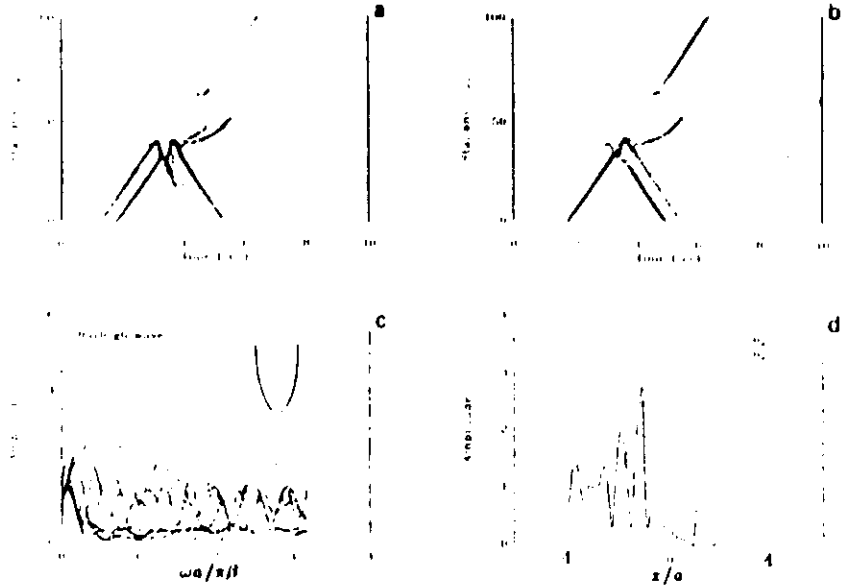

FIG. 7. Incidence of a plane Rayleigh wave. Synthetic seismograms and frequency response for surface receivers equally spaced between $x = -4a$ and $x = 4a$ at the surface of a semi-elliptical canyon with maximum depth of $3a$. (a–d) Same as Figure 6.

respectively. Amplification at the canyon's left rim are of about 2.5 for both components. Significant effects can be seen for the response of the left flat part.

The responses of the deep elliptical canyon to the two different types of incident waves show a common phenomenon, namely the appearance of creeping Rayleigh waves that produce the identical patterns on Figures 6 and 7.

Figure 8 corresponds to SV waves incident on a mountain with unit slopes. Top amplification in frequency domain reaches 4. However, maximum amplification for the other stations does not exceed the level of two times the amplitude of incident wave. Forward scattering of SV to Rayleigh waves is the salient characteristics of the synthetics.

In Figures 9 and 10, we present the surface motion of the semi-elliptical mountain for incident plane P and Rayleigh waves. This topographic feature is an extreme model that shows the wide potential applications of this approach. Great variability of amplifications in frequency domain is again present: at some receivers amplifications reach values of about 4 for the P wave. Time-domain results show significant interference patterns of creeping waves along the curved part of the free surface and late emission of Rayleigh waves.

CONCLUSIONS

We presented a method to compute the diffraction of P, SV, and Rayleigh waves by an irregular topographic feature in an elastic half-space. It is based on a direct integral representation of the diffracted elastic fields in terms of single layer boundary sources. A discretization scheme based on the numerical and analytical integration of exact Green's functions for displacements and tractions

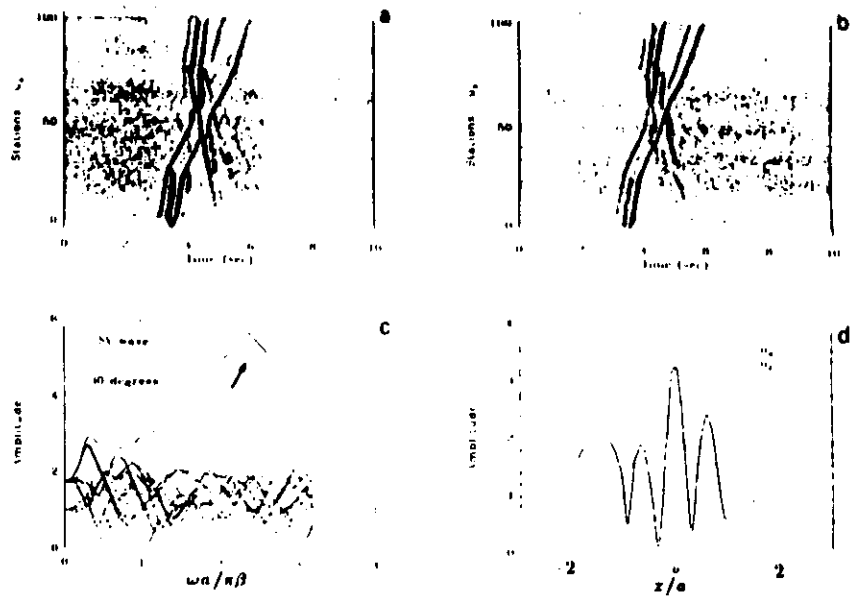

FIG. 8. Incidence of a plane SV wave with incidence angle of 30°. Synthetic seismograms and frequency response for surface receivers equally spaced between $x = -2a$ and $x = 2a$ at the surface of a triangular mountain with unit slopes. (a–d) Same as Figure 5.

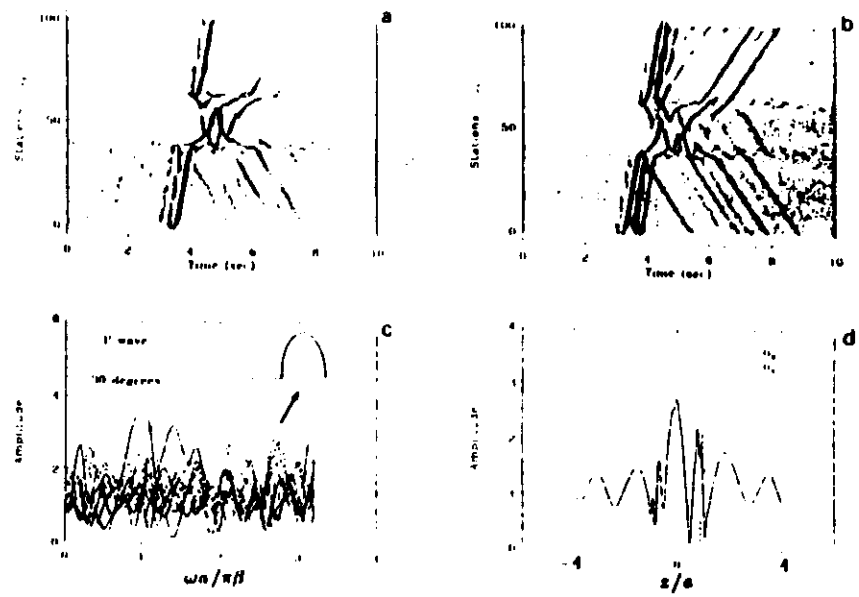

FIG. 9. Incidence of a plane P wave with incidence angle of 30°. Synthetic seismograms and frequency response for surface receivers equally spaced between $x = -4a$ and $x = 4a$ at the surface of a semi-elliptical mountain with maximum height of $2a$. (a–d) Same as Figure 6.

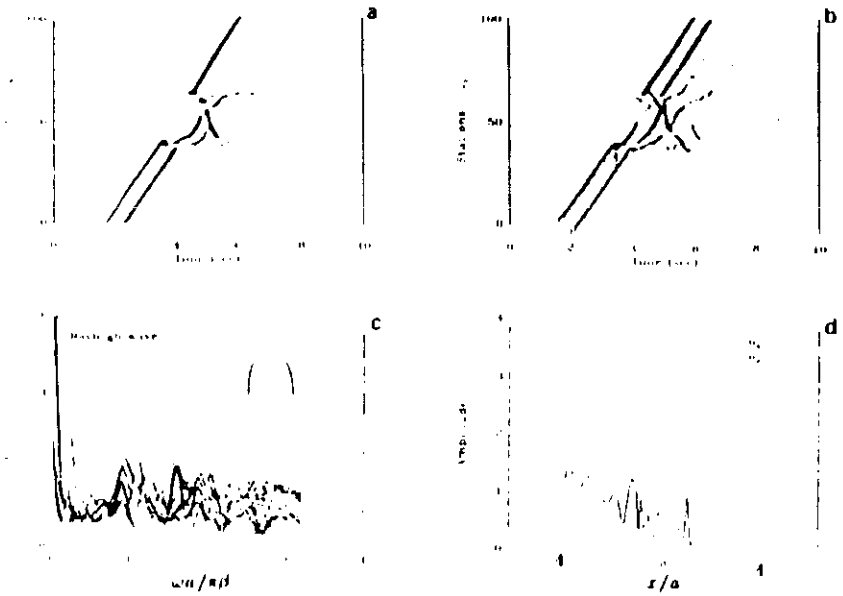

FIG. 10. Response to a nearby vertical load. Except at low frequencies, results correctly describe the effects of an incoming Rayleigh wave. Synthetic seismograms and frequency response for surface receivers equally spaced between $x = -4a$ and $x = 4a$ at the surface of a semi-elliptical mountain with maximum height of $2a$. (a–d) Same as Figure 5.

is employed. Our formulation can be seen as a numerical realization of Huygens' principle, i.e., the diffracted waves are constructed at the boundary from which they are radiated. Therefore, an advantage of the single-layer representation is that absorbing boundaries are not required. In addition to the physical insight gained with this method, it appears to be accurate and fast.

These results correspond to a relatively simple set of conditions, namely: (1) the incidence of a plane wave (or the application of a vertical load in the neighborhood), (2) the assumption of an elastic half-space with Poisson ratio of 1/4, and (3) symmetrical shape for the irregularity. Nevertheless, they display significant aspects of the response on topographic features. One of these is the spectacular amplitude of creeping waves and, as its counterpart, the large increase of duration of the motion on the irregular topography.

It is of interest to consider the plots of the frequency response at selected receivers. It has been commonplace in the literature on site effects to say, for instance, that results show large variability with respect to frequency, incidence angle, and location of receivers. Our results confirm that indeed such is the case. They show that variability is not restricted to the topographic feature. Its presence strongly affects nearby locations. This is more dramatic for elevated topographies in which a large duration coda may arise. They also show that the interaction of elastic waves produce complex amplification and deamplification patterns. We believe that, despite the relative simplicity of the models studied, our results give a glimpse of the effects that the real topographic feature may induce. They present very large relative amplifications values that can be in many cases larger than 10.

A direct look at the frequency response at various locations shows why the spectral ratio technique cannot account for the seismic behavior of topographies. In fact, the large variability of the spectral content of ground motion in both frequency and spatial domains may explain why the search for a simple "topographic factor" remains so far futile. In order to interpret the data, we cannot rule out the need of a quantitative model and careful assessment of the type of incoming waves as well. In any event, our results show that the absolute level of amplification is generally lower than about four times the amplitude of incoming waves.

Acknowledgments

Thanks are given to M. Bonnet for his comments and suggestions and to F. J. Chávez-García and V. Farra for the critical reading of the manuscript. K. Aki, P.-Y. Bard, M. Bouchon, V. Farra, G. Jobert, M. Koller, R. Madariaga, A. Tarantola, J. E. Vidale, and A. Wirgin made valuable suggestions. The critical comments from an unknown reviewer helped to improve this paper. This research was done while one of us (F.J.S.-S.) was on leave from the National University of Mexico and the Centro de Investigación Sísmica A. C., México, at the Université Joseph Fourier of Grenoble, France, and at the Laboratoire de Sismologie of the Institute de Physique du Globe of Paris, France, as a Visiting Professor. Some computations were performed at Centre de Calcul Vectoriel pour la Recherche. This work was partially supported by the Pole Grenoblois de Recherche sur les Risques Naturels, by University of Paris VI, France, and by the Departamento del Distrito Federal, México.

References

Abramowitz, M. and I. A. Stegun (1972). *Handbook of Mathematical Functions*, Dover, New York.

Achenbach, J. D. (1973). *Wave Propagation in Elastic Solids*, North-Holland, Amsterdam.

Aki, K. (1988). Local site effects on strong ground motion, in *Earthquake Engineering and Soil Dynamics II: Recent Advances in Ground Motion Evaluation*, J. L. Von Thun (Editor), Geotechnical Special Publication No. 20, Am. Soc. Civil Engr., New York, 103–155.

Aki, K. and K. L. Larner (1970). Surface motion of a layered medium having an irregular interface due to incident plane *SH* waves, *J. Geophys. Res.* **75**, 1921–1941.

Aki, K. and P. G. Richards (1980). *Quantitative Seismology*, W. H. Freeman, San Francisco.

Banerjee, P. K. and R. Butterfield (1981). *Boundary Element Methods in Engineering Science*, McGraw Hill, London.

Bard, P.-Y. (1982). Diffracted waves and displacement field over two-dimensional elevated topographies, *Geophys. J. R. Ast. Soc.* **71**, 731–760.

Bonnet, G. (1986a). *Méthode des Équations Intégrales Appliquée à la mécanique*, Université Joseph Fourier, Grenoble.

Bonnet, M. (1986b). Méthode des équations intégrales régularisées en élastodynamique, *Doctorate Thesis*, École Nationale des Ponts et Chaussées, Paris.

Bonnet, M. (1989). Regular boundary integral equations for three-dimensional finite or infinite bodies with and without curved cracks in elastodynamics, in *Boundary Element Techniques: Applications in Engineering*, C. A. Brebbia and N. G. Zamani (Editors), Computational Mechanics Publications, Southampton.

Bouchon, M. (1973). Effect of topography on surface motion, *Bull. Seism. Soc. Am.* **63**, 615–632.

Bouchon, M. (1985). A simple, complete numerical solution to the problem of diffraction of *SH* waves by an irregular surface, *J. Acoust. Soc. Am.* **77**, 1–5.

Bouchon, M., M. Campillo, and S. Gaffet (1989). A boundary integral equation-discrete wavenumber representation method to study wave propagation in multilayered media having irregular interfaces, *Geophysics* **54**, 1134–1140.

Bouden, M., K. R. Khair, and S. K. Datta (1990). Ground motion amplification by cylindrical valleys embedded in a layered medium, *Int. J. Earthq. Eng. Struct. Dyn.* **19**, 497–512.

Bravo, M. A., F. J. Sánchez-Sesma, and F. J. Chávez García (1988). Ground motion on stratified alluvial deposits for incident *SH* waves, *Bull. Seism. Soc. Am.* **78**, 436–450.

Brebbia, C. A. (1978). *The boundary Element Method for Engineers*, Pentech Press, London.

Campillo, M. (1987). Modeling of *SH* wave propagation in an irregularly layered medium: application to seismic profiles near a dome, *Geophys. Prospect.* **35**, 236–249.

Campillo, M. and M. Bouchon (1985). Synthetic *SH* seismograms in a laterally varying medium by the discrete wavenumber method, *Geophys. J. R. Ast. Soc.* **83**, 307–317.

Campillo, M., F. J. Sánchez-Sesma, and K. Aki (1990). Influence of small lateral variations of a soft surficial layer on seismic ground motion, *Int. J. Soil Dyn. Earthquake Eng.* **9**, 284–287.

Coutant, O. (1989). Numerical study of the diffraction of elastic waves by fluid-filled cracks, *J. Geophys. Res.* **94**, 17805–17818.

Dravinski, M. (1982). Influence of interface depth upon strong ground motion, *Bull. Seism. Soc. Am.* **72**, 597–614.

Dravinski, M. and T. K. Mossessian (1987). Scattering of plane harmonic *P*, *SV*, and Rayleigh waves by dipping layers of arbitrary shape, *Bull. Seism. Soc. Am.* **77**, 212–235.

Eshraghi, H. and M. Dravinski (1989). Scattering of elastic waves by nonaxisymmetric three-dimensional dipping layer, *J. Num. Methods Partial Differential Equations* **5**, 327–345.

Fujii, K., S. Takeuchi, Y. Okano, and M. Nakano (1984). Rayleigh wave scattering at various wedge corners, *Bull Seism. Soc. Am.* **74**, 41–60.

Gaffet, S. and M. Bouchon (1989). Effects of two-dimensional topographies: using the discrete wavenumber-boundary integral equation method in *P-SV* cases, *J. Acoust. Soc. Am.* **85**, 2277–2283.

Geli, L., P.-Y. Bard, and B. Jullien (1988). The effect of topography on earthquake ground motion: a review and new results, *Bull. Seism. Soc. Am.* **78**, 42–63.

Kawase, H. (1988). Time-domain response of a semicircular canyon for incident *SV*, *P*, and Rayleigh waves calculated by the discrete wavenumber boundary element method, *Bull. Seism. Soc. Am.* **78**, 1415–1437.

Kawase, H. and K. Aki (1989). A study on the response of a soft basin for incident *S*, *P*, and Rayleigh waves with special reference to the long duration observed in Mexico City, *Bull. Seism. Soc. Am.* **79**, 1361–1382.

Kawase, H. and K. Aki (1990). Topography effect at the critical *SV*-wave incidence: possible explanation of damage pattern by the Whittier Narrows, California, earthquake of 1 October 1987, *Bull. Seism. Soc. Am.* **80**, 1–22.

Khair, K. R., S. K. Datta, and A. H. Shah (1989). Amplification of obliquely incident seismic waves by cylindrical alluvial valleys of arbitrary cross-sectional shape. Part I. Incident *P* and *SV* waves, *Bull. Seism. Soc. Am.* **79**, 610–630.

Kouah Bille, L., F. J. Sánchez-Sesma, and A. Wirgin (1991). Réponse resonante d'une montagne cylindrique a une onde sismique *SH*, *C. R. Acad. Sci. Paris* **312**, Série II, 849–854.

Kummer, B., A. Behle, and F. Dorau (1987). Hybrid modeling of elastic wave propagation in two-dimensional laterally inhomogeneous media, *Geophysics* **52**, 765–771.

Kupradze, V. D. (1963). *Dynamical Problems in Elasticity*, in *Progress in Solid Mechanics*, vol. 3, I. N. Sneddon and R. Hill (Editors), North Holland, Amsterdam.

Lamb, H. (1904). On the propagation of tremors over the surface of an elastic solid, *Philos. Trans. Roy. Soc. Lond. Ser. A.* **203**, 1–42.

Love, A. E. H. (1944), *A Treatise on the Mathematical Theory of Elasticity*, Dover, New York.

Luco, J. E., H. L. Wong, and F. C. P. De Barros (1990). Three-dimensional response of a cylindrical canyon in a layered half-space, *Intl. J. Earthq. Eng. Struct. Dyn.* **19**, 799–817.

Sánchez-Sesma, F. J. (1978). Ground motion amplification due to canyon of arbitrary shape, *Proc. 2nd Intl. Conf. Microzonation*, **2**, 729–742.

Sánchez-Sesma, F. J. (1987). Site effects on strong ground motion, *Intl. J. Soil Dyn. Earthquake Eng.* **6**, 124–132.

Sánchez-Sesma, F. J. (1990). Elementary solutions for the response of a wedge-shaped medium to incident *SH* and *SV* waves, *Bull. Seism. Soc. Am.* **80**, 737–742.

Sánchez-Sesma, F. J., M. A. Bravo, and I. Herrera (1985). Surface motion of topographical irregularities for incident *P*, *SV*, and Rayleigh waves, *Bull. Seism. Soc. Am.* **75**, 263–269.

Sánchez-Sesma, F. J., M. Campillo, and K. Irikura (1989). A note on the Rayleigh hypothesis and the Aki-Larner method, *Bull. Seism. Soc. Am.* **79**, 1996–1999.

Sánchez-Sesma, F. J. and J. Esquivel (1979). Ground motion on alluvial valleys under incident plane *SH* waves, *Bull. Seism. Soc. Am.* **69**, 1107–1120.

Sánchez-Sesma, F. J. and E. Rosenblueth (1979). Ground motion at canyons of arbitrary shape under incident *SH* waves, *Intl. J. Earthq. Eng. Struct. Dyn.* **7**, 441–4450.

Trifunac, M. D. (1971). Surface motion of a semi-cylindrical alluvial valley for incident plane *SH* waves, *Bull. Seism. Soc. Am.* **61**, 1755–1770.

Trifunac, M. D. (1973), Scattering of plane *SH* waves by a semi-cylindrical canyon, *Intl. J. Earthquake Eng. Struct. Dyn.* **1**, 267–281.

Wong, H. L. (1979). Diffraction of *P*, *SV* and Rayleigh waves by surface topographies, Report CE 79-05, Dept. of Civil Engineering, University of Southern California, Los Angeles.

Wong, H. L. (1982). Effect of surface topography on the diffraction of *P*, *SV*; and Rayleigh waves, *Bull. Seism. Soc. Am.* **72**, 1167–1183.

Wong, H. L. and P. C. Jennings (1975). Effect of canyon topographies on strong ground motion, *Bull. Seism. Soc. Am.* **65**, 1239–1257.

Woods, R. D. (1968). Screening of surface waves in soils, *J. Soil Mech.*, Found Div. Am. Soc. Civil Engrs., **94**, 951–979.

INSTITUTO DE INGENIERÍA, UNAM
CIUDAD UNIVERSITARIA, APTDO. 70-472
COYOACÁN 04510, MÉXICO, D.F.
MÉXICO
(F.J.S.-S.)

CENTRO DE INVESTIGACIÓN SÍSMICA, A.C.
FUNDACIÓN J. BARROS SIERRA
CARR. AL AJUSCO 203, COL. H. DE PADIERNA
TLALPÁN 14200, MÉXICO D.F.
MÉXICO
(F.J.S.-S.)

OBSERVATOIRE DE GRENOBLE
UNIVERSITÉ JOSEPH FOURIER
L.G.I.T.-I.R.I.G.M.
B.P. 53X
38041 GRENOBLE CEDEX
FRANCE
(M.C.)

Manuscript received 13 June 1990

Tectonophysics, 218 (1993) 113–125
Elsevier Science Publishers B.V., Amsterdam

Topographic effects for incident P, SV and Rayleigh waves

Francisco J. Sánchez-Sesma [a,b] and Michel Campillo [c]

[a] *Instituto de Ingeniería, UNAM Cd. Universitaria, Apdo. 70-472, Coyoacán 04510, México D.F., Mexico*
[b] *Centro de Investigación Sísmica, A.C. Carr. al Ajusco 203, Col. H. de Padierna, Tlalpan 14200, México D.F., Mexico*
[c] *Observatoire de Grenoble, Université Joseph Fourier, LGIT-IRIGM, BP 53X, 38041 Grenoble Cedex, France*

(Received June 4, 1991; revised version accepted January 10, 1992)

ABSTRACT

Sánchez-Sesma, F.J. and Campillo, M., 1993. Topographic effects for incident P, SV and Rayleigh waves. In: F. Lund (Editor), New Horizons in Strong Motion: Seismic Studies and Engineering Practice. *Tectonophysics*, 218: 113–125.

The topographical effects for incident P, SV and Rayleigh waves in an elastic half-space were studied using an integral representation of the diffracted elastic waves in terms of single-layer boundary sources. The free-boundary condition leads to a Fredholm integral equation of the second kind for boundary sources. We used a discretization scheme based on the numerical and analytical integration of exact Green's functions. This approach is called indirect BEM in the literature. However, it provides far more insight on the physics of diffraction problems than the direct approaches. This is because diffracted waves are constructed at the boundaries from which they are radiated. Therefore, this method can be regarded as a numerical realization of Huygens' principle. Various examples that cover extreme cases are presented. It is found that topography may cause significant effects both of amplification and of deamplification at the irregular feature itself and its neighborhood but the absolute level of amplification is generally lower than about 4 times the amplitude of incoming waves. These facts must be taken into account when the spectral ratio technique is used to study topographical response.

Introduction

The effects of local site conditions may produce large ground motion amplification during earthquakes and concentrated damage (see Sánchez-Sesma (1987) and Aki (1988) for reviews). During the last two decades significant progress has been achieved both in the observation and in the evaluation of such effects. In particular, the effects of topography on surface ground motion have been observed and studied from field experiments. Trifunac and Hudson (1971), Davis and West (1973), Griffiths and Bollinger (1979) and Tucker et al. (1984), among others, discovered significant effects. However, as pointed out by Bard and Tucker (1985) and Geli et al. (1988), the observed amplifications in the field are systematically larger than the values predicted using theoretical models (e.g., Bard, 1982). They suggested that the models should incorporate layering, variations in wave velocities and even irregular two- and three-dimensional configurations in order to explain the observations more precisely. Bard and Tucker (1985) have tested several such models and improved the predictions but still showed amplifications smaller than the observed ones.

Theoretical studies aimed at predicting site effects are numerous. It is worth mentioning the work by Trifunac (1971; 1973), who found analytical solutions for the response of semi-circular alluvial valleys and canyons under incident SH waves. Other analytical solutions have been recently obtained for shallow circular geometries (e.g. Lee and Cao, 1989; Todorovska and Lee, 1992a,b). An exact solution for the incidence of plane SH and SV waves upon an infinite, moun-

Correspondence to: F.J. Sánchez-Sesma, Instituto de Ingeniería, UNAM Cd. Universitaria, Apdo. 70-472, Coyoacán 04510, Mexico D.F., Mexico.

tain-like wedge has been obtained for certain angles by geometrical means (Sánchez-Sesma, 1990). For arbitrary geometries analytical solutions are no longer valid. Therefore, numerical techniques have to be developed. A recent compilation of works on the numerical modeling of seismic wave propagation in realistic media (Kelly and Marfurt, 1990) gives a good account of the state-of-the-art of the so-called domain methods.

Boundary methods have gained increasing popularity. The boundary integral equation (BIE) and their discretizations into boundary element methods (BEM) have been useful in the study of dynamic elasticity problems. Among the advantages over domain approaches are the dimensionality reduction and the simple fulfillment of radiation conditions at infinity. Excellent surveys of the available literature on BEM in elastodynamics are those of Kobayashi (1987) and Manolis and Beskos (1988). The most popular BEM approaches are the so-called *direct*, because in their formulation the unknowns are the sought values of displacements and tractions. They arise from the discretization of integral representation theorems. It is worth noting that Wong and Jennings (1975) used a direct formulation based on an integral representation to study the seismic response of arbitrary canyon geometries. A similar approach was used by Zhang and Chopra (1991) to consider the three-dimensional response of canyons.

In contrast, the *indirect* BEM, which formulates the problem in terms of force or moment boundary densities, is not as popular. This is despite the fact that such densities can give a deep physical insight into the nature of diffracted waves. Moreover, the indirect BEM has a longer history than the direct BEM and is closely related to classical work on integral equations (see, for example, Manolis and Beskos, 1988).

On the other hand, the combination of discrete wavenumber expansions for Green's functions (Bouchon and Aki, 1977; Bouchon, 1979) with boundary integral representations has been successful in various studies of elastic wave propagation. Bouchon (1985), Campillo and Bouchon (1985), Campillo (1987), Gaffet and Bouchon (1989), Bouchon et al. (1989) and Campillo et al. (1990) used source distributions on the boundaries, whereas Kawase (1988) and Kawase and Aki (1989) used Somigliana representation theorem. These two approaches are discrete wavenumber versions of indirect BEM and direct BEM, respectively. However, such procedures require a considerable amount of computer resources. An alternative approach may be welcomed for many applications.

In this work we study the surface motion at various topographic features for incident P, SV and Rayleigh waves. This plane strain case can be regarded as the simplest of a class of vector problems of seismological interest. We use a single-layer boundary integral representation of diffracted waves. Therefore, our method can be classified as an indirect BEM. In this approach, diffracted waves are constructed at the boundaries from which they are radiated. Therefore, it can be regarded as a numerical realization of Huygens' principle (this is true for any indirect method). This approach is, in fact, an improvement over the boundary method, which has been used to deal with various problems of the diffraction of elastic waves (see, for example, Sánchez-Sesma and Esquivel, 1979; Sánchez-Sesma and Rosenblueth, 1979; Dravinski, 1982; Wong, 1982; Dravinski and Mossessian, 1987; Luco et al., 1990). In its many variants, such a technique is based upon the superposition of solutions for sources with their singularities placed outside the region of interest. However, this requires particular care and the trial and error process needed is difficult to apply, particularly when many frequencies are to be computed.

As the singularities of Green's functions are integrable (e.g., Kobayashi, 1987; Manolis and Beskos, 1988) we can put the sources at the boundary and properly consider their effects. In this way, the uncertainty about the location of sources is eliminated and the linear system of equations that arises from the discretization can be directly solved. Therefore, our indirect BEM approach retains the physical insight of the sources method, with all the benefits of the analytical integration of exact Green's functions. In the applications reported here, we represent diffracted fields with the superposition of the

radiation from boundary sources using exact expressions of the two-dimensional Green's functions in an unbounded elastic space.

In order to test the method, we compared results with those obtained by Wong (1982), Sánchez-Sesma et al. (1985) and Kawase (1988) for the incidence of P, SV and Rayleigh waves upon a semi-circular canyon on a half-space. We found excellent agreement with those results. Moreover, we present various examples that cover extreme profiles. We show that relatively simple topographies may induce significant variations in the ground motion at and around the irregularity. We believe that this fact partially explains the large relative amplifications reported in the literature (e.g., Geli et al., 1988). Our examples show that, even though relative amplification due to the topography is sometimes quite big, the absolute level of amplification is generally lower than about 4 times the amplitude of incoming waves. Such facts must be taken into account when the spectral ratio technique is used to characterize topographic effects.

Integral representation using boundary sources

Consider the domain, V and its boundary, S. If an elastic material occupies such a region, the displacement field under harmonic excitation can be written (neglecting body forces) by means of the single layer boundary integral:

$$u_i(x) = \int_S \phi(\xi) G_{ij}(x,\xi) \mathrm{d}S_\xi \qquad (1)$$

where $u_i(x) = i$th component of displacement at x; $G_{ij}(x,\xi) =$ Green function, that is, the displacement in the direction i at point x, due to the application of a unit force in the direction j at point ξ; $\phi_j(\xi) =$ force density in the direction j. Therefore, $\phi_j(\xi)\mathrm{d}S$ is clearly a force distribution at the boundary. The subscripts in the differentials indicate the space variable over which the integration is performed.

This single layer integral, which can be related to Somigliana identity (Sánchez-Sesma and Campillo, 1991), has been studied by Kupradze (1963). He showed that the displacement field is continuous across S if $\phi_j(\xi)$ is continuous along S.

This integral representation allows computation of stresses and tractions by direct application of Hooke's law, except at boundary singularities, that is, when $x = \xi$ on the boundary. By a limiting process based on equilibrium considerations around an internal neighborhood of the boundary, it is possible to write, for x on S that:

$$t_i(x) = \tfrac{1}{2}\phi_i(x) + \int_S \phi_j(x) T_{ij}(x,\xi) \mathrm{d}S_\xi \qquad (2)$$

where $t_i = i$th component of traction at the boundary; $T_{ij}(x,\xi) =$ traction Green function, that is, the traction in the direction i at point x on the boundary with normal, $\mathrm{n}(x)$ (assumed to be specified) due to the application of a unit force in the direction j applied at ξ. The first term of the right hand side must be dropped if x is at V. This result was also found by Kupradze (1963). He used a formal technique of singularity extraction, which is now used to deal with the hypersingular integral equations of dynamic elasticity (e.g., Bonnet, 1986; 1989).

Equations (1) and (2) are the basis of our approach. Although *indirect*, it allows direct interpretation of the physical quantities involved. Expressions for Green's functions can be found in the literature (e.g., Kobayashi, 1987; Sánchez-Sesma and Campillo, 1991). It suffices to say here that the singularity of displacements is either logarithmic or $1/r$ for two-dimensional or three-dimensional problems, respectively. Regarding the tractions, such singularities are explicitly of the form $1/r$ or $1/r^2$, respectively. In particular, when the frequency tends to zero, Green's functions lead to their static counterparts. These properties are invoked below in connection with our discretization scheme.

Diffraction of elastic waves by topography

Consider an elastic half space with a localized topographic relief as shown in Figure 1. The ground motion in this irregular configuration comes from the interferences of incoming waves with reflected and diffracted ones. It is also usual to say that the total motion is the superposition of the so-called *diffracted* waves and the free-field:

$$u_i = u_i^{(0)} + u_i^{(d)} \qquad (3)$$

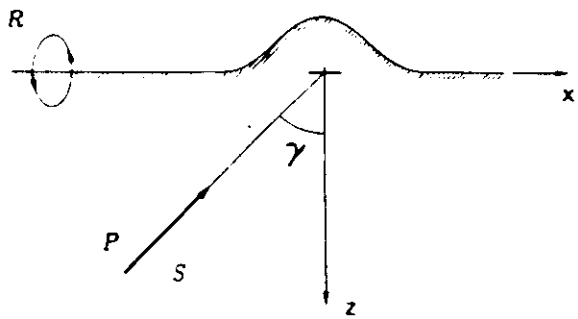

Fig. 1. Irregular half-space and incidence of P, SV and Rayleigh waves.

where $u_i^{(0)}$ = free-field displacement; that is, the solution in the absence of the irregularity.

In this application the displacement free-field is that produced by incident plane waves and is analytically extended to the parts of the topography that are not included in the reference half-space. This means that incoming and reflected waves are assumed to exist for $z < 0$, fulfilling the same analytical expressions (Navier equations) they satisfy for $z \geqslant 0$. Therefore, the free-field is continuous everywhere.

According to our previous discussion, the diffracted field is given by eqn. (1), which can be written as:

$$u_i^{(d)}(x) = \int_S \phi_j(\xi) G_{ij}(x,\xi) \mathrm{d}S_\xi \tag{4}$$

The traction-free boundary condition implies that:

$$t_i^{(0)} + t_i^{(d)} = 0 \tag{5}$$

then, from eqn. (2), such conditions can be expressed by means of:

$$\tfrac{1}{2}\phi_i(x) + \int_S \phi_j(\xi) T_{ij}(x,\xi) \mathrm{d}S = -t_i^{(0)} \tag{6}$$

which is a Fredholm integral equation of the second kind for the boundary tractions; that is, those producing the diffracted field. This expression is discretized along a finite portion of the boundary, S, which includes the topography and the lateral flat parts. We have used values of $3L$–$5L$ (where L = surface length of the surface anomaly). Assuming $\phi_j(\xi)$ is constant over each of the N boundary segments with equal length ΔS, leads to the system of linear equations:

$$\sum_{l=1}^{N} \phi_j(\xi_l) t_{ij}(x_n,\xi_l) = -t_i^{(0)} \quad n = 1,N \tag{7}$$

where:

$$t_{ij}(x_n,\xi_1) = \tfrac{1}{2}\delta_{ij}\delta_{nl} + \int_{\xi_l - \Delta S/2}^{\xi_l + \Delta S/2} T_{ij}(x_n,\xi) \mathrm{d}S_\xi \tag{8}$$

These integrals are computed numerically using Gaussian integration except when $n = l$. In this case we have:

$$t_{ij}(x_n,\xi_n) = \tfrac{1}{2}\delta_{ij} \tag{9}$$

because the integral in eqn. (8) for $n = l$ is zero as long as the discretization segment is a straight line, which is the case assumed here. It can be verified that, under this circumstance, the integrand is a singular odd function on the segment. Therefore, its Cauchy's principal value is zero. The value for t_{ij} in eqn. (9) can be interpreted as half of the applied unit line force and means that the force is distributed symmetrically for any two half-spaces containing the line of application of the load, regardless of its direction. This result also corresponds to the static solution. Once the values of $\phi_j(\xi_l)$ are known, the diffracted field is computed by means of:

$$u_i^{(d)} = \sum_{l=1}^{N} \phi_j(\xi_l) g_{ij}(x,\xi_l) \tag{10}$$

where:

$$g_{ij}(x,\xi_l) = \int_{\xi_l - \Delta S/2}^{\xi_l + \Delta S/2} G_{ij}(x,\xi) \mathrm{d}S_\xi \tag{11}$$

These integrals are also computed numerically with Gaussian integration, except in the case when x is in the neighborhood of ξ_l, for which we obtained analytical expressions from the ascending series for Bessel functions (e.g., Abramowitz and Stegun, 1972). Sánchez-Sesma and Campillo (1991) presented an example for such expressions when only the leading terms of the series are retained. We considered up to quadratic terms, which is enough if the number of segment per wavelength is larger than about 6. For the elevated portions of the relief the analytical extension of the free-field provides the boundary excitation. In the case of incident Rayleigh waves, or for SV waves with an incidence angle larger than the critical one, the analytical extension gives exponential growth of the extended field (the incident plane SV waves, with an incident angle

of 45°, having no mode conversion and unit reflection coefficient, do not present this effect). To avoid this difficulty we choose to produce Rayleigh waves by loading our irregular half-space with a vertical force (e.g., Sánchez-Sesma and Campillo, 1991). In this case, the excitation comes from imposing vertical tractions in a small region of the flat part of the free surface. This illustrates well the wide potential applications of our method. The surface load problem is well known (Lamb, 1904). In this case, more than two-thirds of the total energy is radiated as Rayleigh waves (Woods, 1968). At the surface the relative amount of Rayleigh waves is much larger.

Testing of the method and discussion

The accuracy of this approach has been gauged by comparing results with those obtained by Wong (1979; 1982), Sánchez-Sesma et al. (1985) and Kawase (1988). The diffraction of P, SV and Rayleigh waves by a semicircular canyon has been studied by Wong (1979; 1982) for a half-space with Poisson ratio of 1/3 and no attenuation using a boundary method. Wong's (1982) results were verified by Sánchez-Sesma et al. (1985) and Dravinski and Mossessian (1987), for a normalized frequency $\eta = 0.5$, where $\eta = \omega a/\pi\beta$ and a = radius of canyon. In general, excellent agreement was found for incident P and SV waves. The larger difference occurs for Rayleigh waves in the horizontal motion at the top of the rim of the canyon: Wong (1982) predicted an amplification of about 2.5 there, whereas Sánchez-Sesma et al. (1985) gave a value of about 2. Figure 2 shows their results, together with our solution.

For a larger normalized frequency, $\eta = 2$ results by Wong (1982) and Kawase (1988) are available for Rayleigh waves and for P and SV waves with an angle of incidence of 0°. Kawase (1988) used a boundary integral representation combined with the discrete wavenumber method. Sánchez-Sesma and Campillo (1991) compared results for incident P and SV waves. Here we restrict our comparisons to Rayleigh waves. Figure 3 shows our results for both horizontal and vertical displacement amplitudes. We considered a total discretization length of $5L$, where $L = \pi a$,

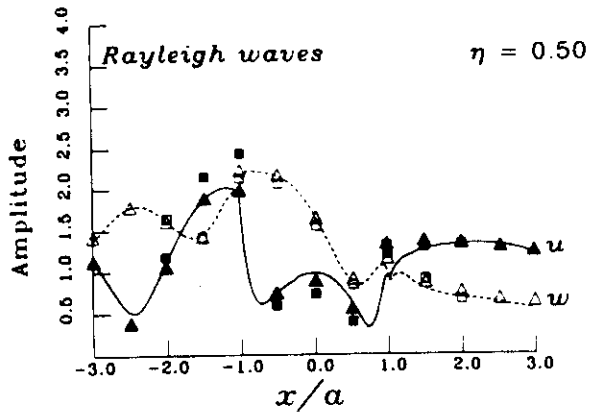

Fig. 2. Amplitudes of horizontal and vertical displacements for incidence of harmonic Rayleigh waves upon a semi-circular canyon. Poisson ratio is 1/3 and the normalized frequency $\eta = 0.5$. Solid and dashed lines = horizontal, u, and vertical, w, components obtained in this study: squares = results of Wong (1982); triangles = results of Sánchez-Sesma et al. (1985).

and 15 segments per S wavelength. The solution is stable, even when such parameters are reduced to $3L$ and to 6, respectively. Wong's and Kawase's results are also shown. Excellent agreement is found for both horizontal and vertical components. However, small differences can be seen. For instance, both Wong (1982) and Kawase (1988) predict amplitudes at the "incidence" rim

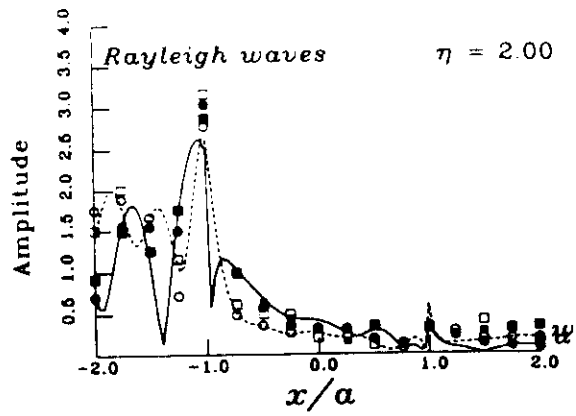

Fig. 3. Amplitudes of horizontal and vertical displacements for incidence of harmonic Rayleigh waves upon a semi-circular canyon. Poisson ratio is 1/3 and the normalized frequency $\eta = 2$. Solid and dashed lines correspond to horizontal, u, and vertical, w, components obtained in this study; circles = results of Wong (1982); squares = results of Kawase (1988).

of the canyon that are somewhat larger than our results. Generally, our results (see also Sánchez-Sesma and Campillo, 1991) are closer to Kawase's. However, in some cases they approach those of Wong. For some locations, both inside and outside the canyon, our results are between the other two results.

These methods are approximate. The only way to assess on their performance is through comparisons of results and with other procedures and by comparing the assumptions and the characteristics of each one. Sánchez-Sesma and Campillo (1991) discussed these issues in detail. Here we will give a brief account.

Both Wong (1982) and Kawase (1988) took as their departure point Lamb's (1904) integrals for the half-space in frequency domain. Wong (1982) computed such integrals for compressional and shear line sources and used them as trial functions with the singularities "removed from the region of interest"; that is, outside the irregular half-space, inside the region left by the canyon. He satisfied boundary conditions using a generalized inversion scheme, which guarantees good results in a global sense. In contrast, Kawase (1988) integrated analytically along the boundary the expressions of the discrete wavenumber expansion, for which he assumed a horizontal periodicity of ten times the diameter of the canyon. In order to obtain reliable results in the frequency domain, Kawase first got time series and then computed the frequency response. These two methods have the shortcoming of the time-consuming evaluation of Lamb's integrals. Wong

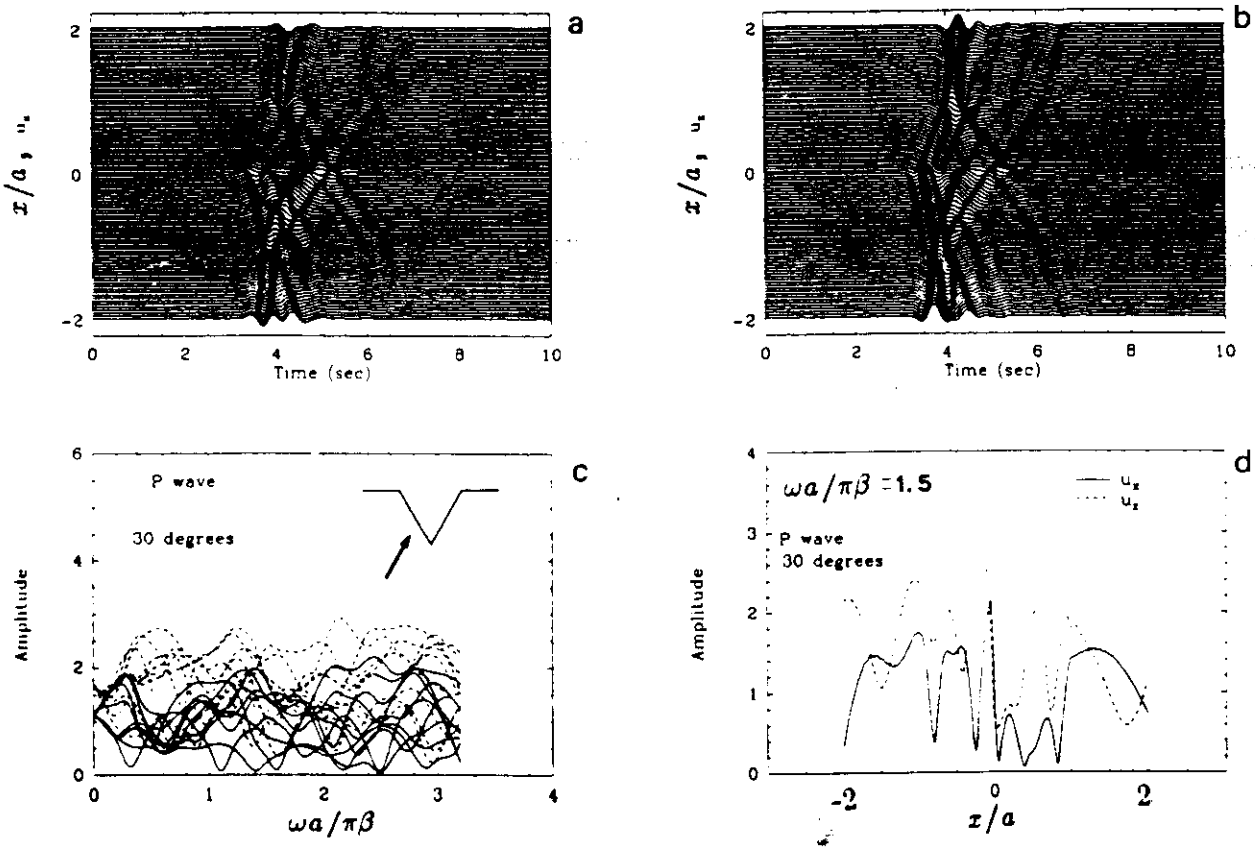

Fig. 4. Incidence of a plane P wave with incidence angle of 30°. Synthetic seismograms and frequency response for surface receivers equally spaced between $x = -2a$ and $x = 2a$ at the surface of a triangular canyon with a angle of dip of 60°. (a) Horizontal component, ux, and (b) vertical component, uz. The incident time signal is a Ricker wavelet with central frequency $\omega_p = 1.5\pi\beta/a$. Amplitudes of horizontal (continuous line) and vertical (dotted line) surface displacements (c) for nine receivers against normalized frequency and (d) for the central frequency of the Ricker wavelet for all the receivers against their horizontal location.

(1982), as well as Sánchez-Sesma and Rosenblueth (1979) for instance, had to accept a certain uncertainty about the optimum location and number of sources.

In contrast, we had less sources of error. We used the exact Green's function for the whole space, which can be computed in a fast manner. Our approach is aimed at obtaining only diffracted waves; that is, those produced both at the irregular boundary and at the free surface, by means of boundary force densities, for which we obtained either exact or analytical values at singularities. Hence, this formulation can be seen as an approximate numerical realization of Huygens' principle (this is true for any indirect formulation). For the numerical integration we used Gaussian integration of three points per segment.

To examine edge effects due to the finite size of the discretized boundary we performed several tests and found that, for the range of frequencies studied, it suffices to discretize a total length of $3L$, where L is the surface length of the topographic feature. The comparisons presented here have been computed for total discretization lengths of $3L$ and $5L$ and the results are virtually the same. This implies that edge effects have little or no influence in our computations and shows that only the discretization of a relatively small part of the free boundary is needed. We consider this fact to be a significant advantage of our approach. Sánchez-Sesma and Campillo (1991) verified this interpretation. They computed the phase of diffracted waves and observed that, for both components, the phase variation with space shows slopes consistent with the expected outgoing nature of such waves.

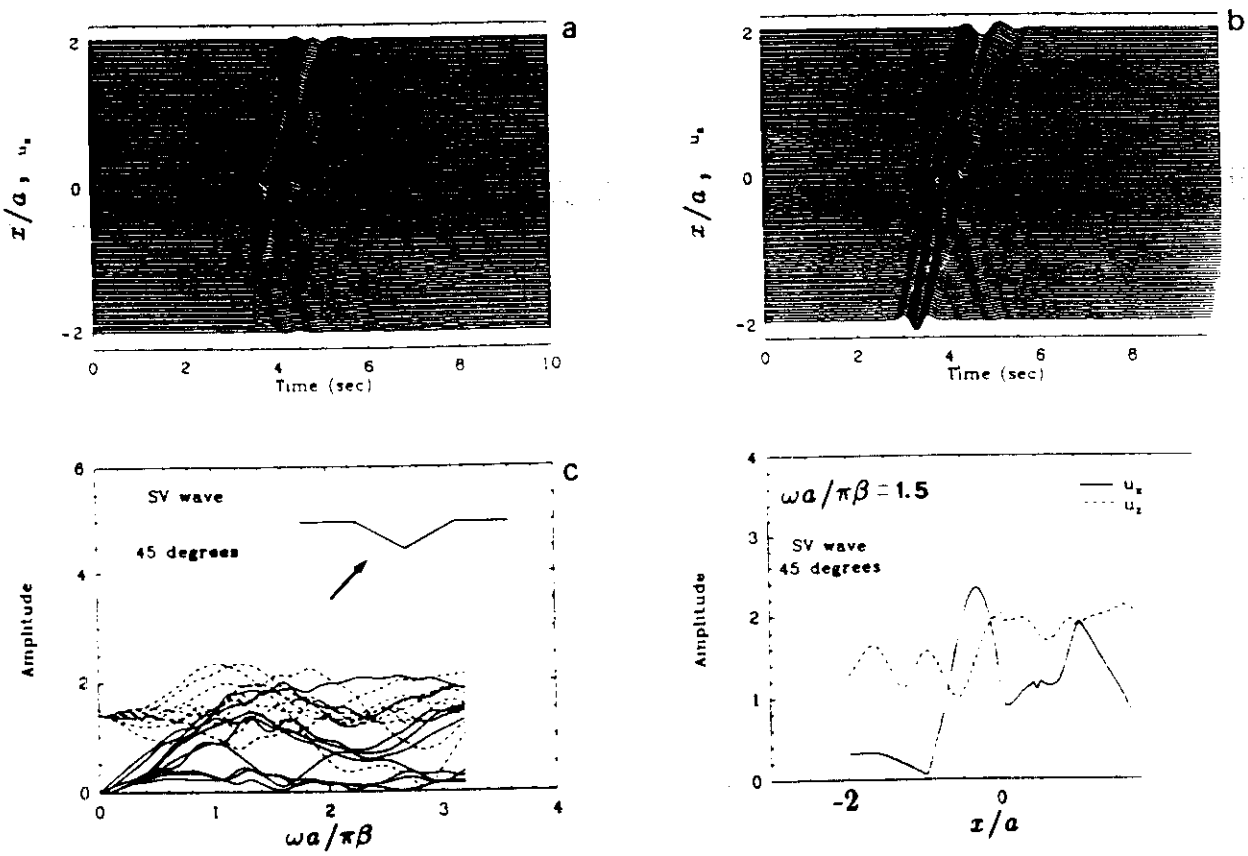

Fig. 5. Incidence of a plane SV wave with incidence angle of 45°. Synthetic seismograms and frequency response receivers equally spaced between $x = -2a$ and $x = 2a$ at the surface of a triangular canyon with an angle of dip of 3 in Fig. 4.

Examples

In order to show the range of effects caused by topography, we present various examples that cover extreme geometries. We choose from a big set of results a sample that, being of reasonable dimension, allows the salient characteristics of such effects to be described. Other examples can be seen in Sánchez-Sesma and Campillo (1991). Our results are displayed in both frequency and time domains for various canyons and mountains under incident P, SV and Rayleigh waves. A Poisson coefficient of 1/4 was selected and no attenuation was assumed. We present five examples:

(1) A triangular canyon with $h = 1.732\ a$, where a = surface half-width (angle of dip 60°) under incident P waves with an angle of incidence of 30° (Fig. 4).

(2) A triangular canyon with $h = 0.577\ a$, where a = surface half-width (angle of dip 30°) under incident SV waves with an angle of incidence of 45° (Fig. 5).

(3) A semi-elliptical canyon with a maximum depth of 3 times the half width ($h = 3a$) under incident SV waves with an angle of incidence of 45° (Fig. 6).

(4) A triangular mountain with an angles of dip of 45° for incident Rayleigh waves (Fig. 7).

(5) A semi-elliptical mountain with a maximum height of $2a$ under incident SV waves with an angle of incidence of 30° (Fig. 8).

For these examples the discretization was carried out over a total length of $3L$, where L = surface length of the topographic feature. The relatively small size of the discretized region is an advantage of our formulation. We used 15 segments per S wavelength.

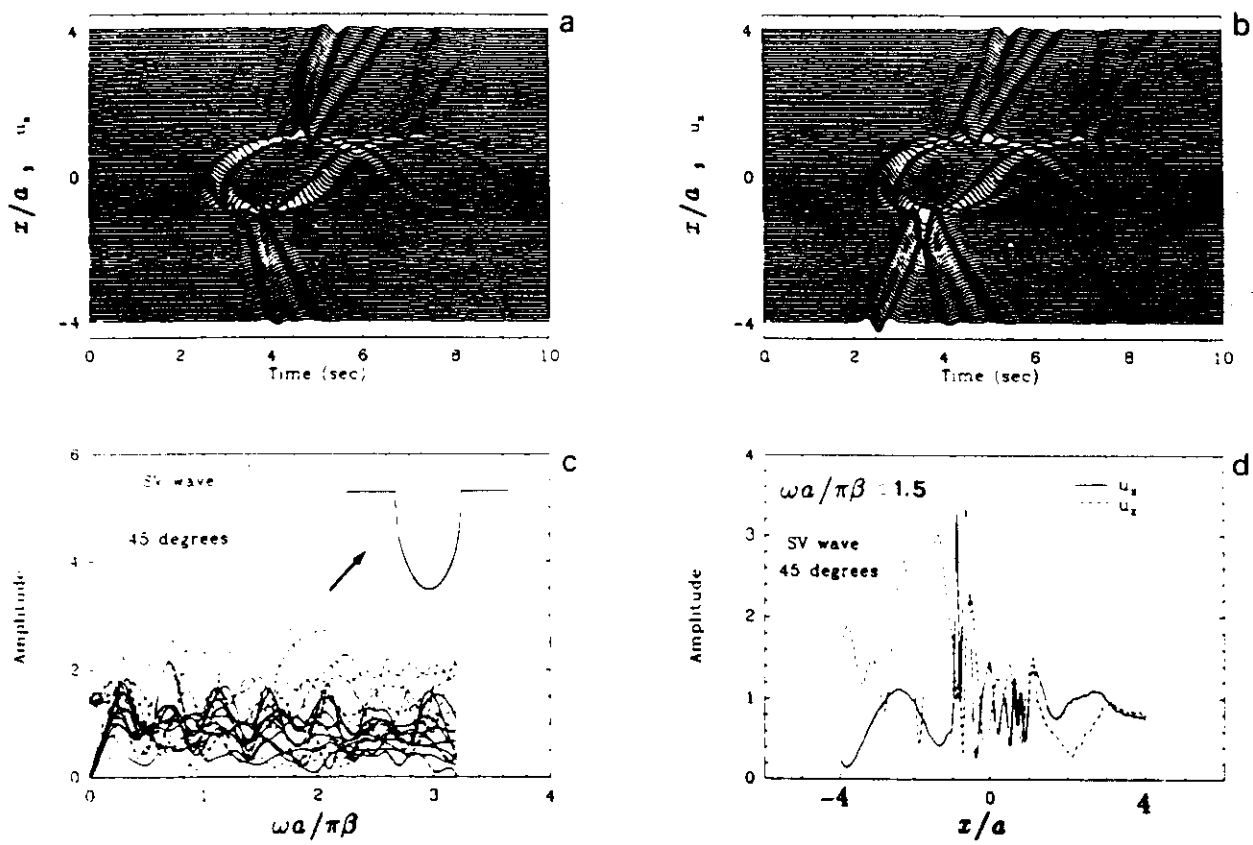

Fig. 6. Incidence of a plane SV wave with incidence angle of 45°. Synthetic seismograms and frequency response for surface receivers equally spaced between $x = -4a$ and $x = 4a$ at the surface of a semi-elliptical canyon with maximum depth of $3a$. (a)–(d) as in Fig. 4.

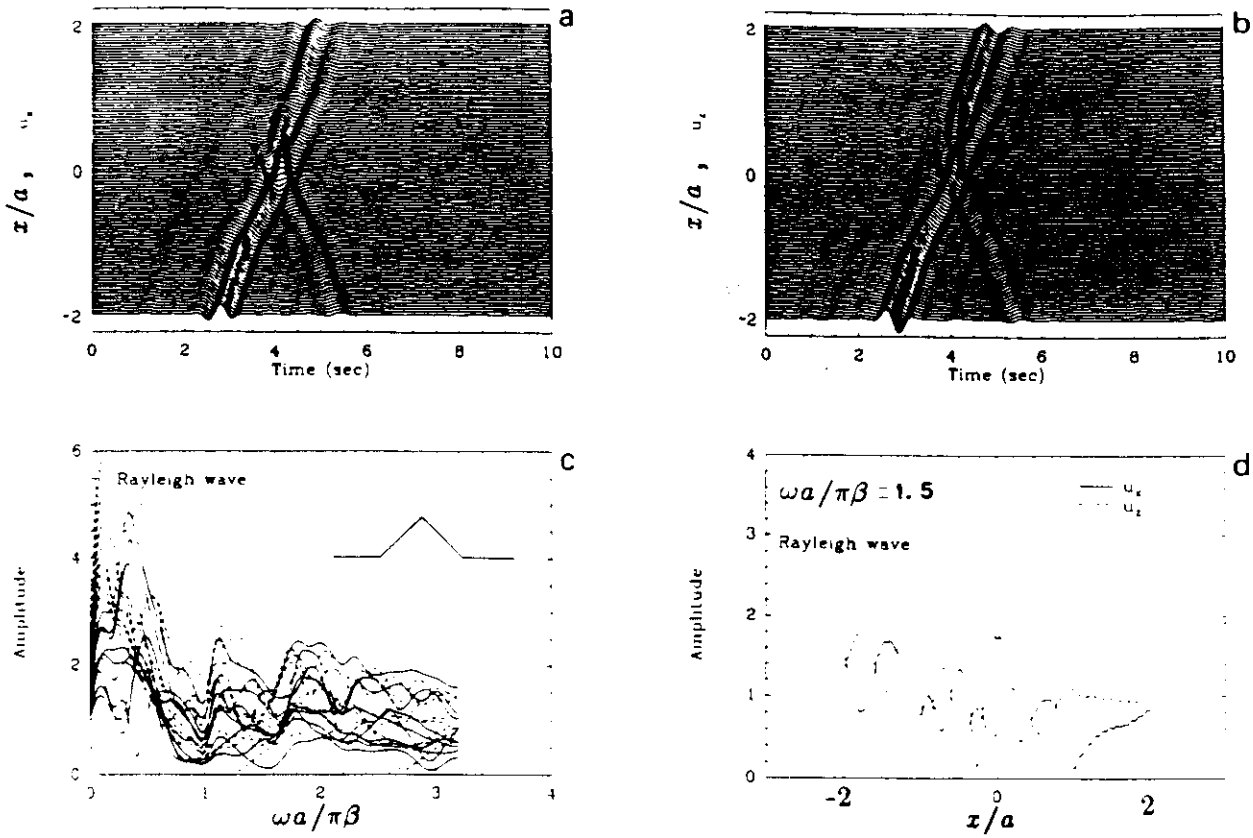

Fig. 8. Incidence of a plane SV wave with incidence angle of 30°. Synthetic seismograms and frequency response for surface receivers equally spaced between $x = -4a$ and $x = 4a$ at the surface of a semi-elliptical mountain with maximum height of $2a$. (a)–(d) as in Fig. 4.

Results are displayed in Figures 4–8. Each figure contains four plots: synthetic seismograms for horizontal and vertical components, frequency response for selected receivers and spatial variation at a given frequency. Computations were performed in the frequency domain and synthetic seismograms where computed using the FFT algorithm for a Ricker wavelet with central frequency $\omega_p = 1.5\pi\beta/a$ for 101 receivers equally spaced between $x = -4a$ and $x = 4a$ for the semi-elliptical profiles and between $x = -2a$ and $x = 2a$ for the triangular ones. It was assumed that $2a/\beta = 1$ s in order to define the time scale. The actual scale is $\beta t/2a$. The results in the frequency domain are presented against $\omega a/\pi\beta$ and correspond to nine equally spaced surface receivers (out of the 101 for which we computed the synthetics). For the frequency corresponding to the central one of the Ricker pulse, we displayed the amplitude of both horizontal and vertical displacements against space.

For the triangular mountain the incident Rayleigh wave is generated with a uniform vertical load applied over a length of $0.25a$ centered at $x = -2.5a$. The frequency spectra clearly show the logarithmic singularity at small frequencies. The vertical displacement for a static load is, in fact, logarithmic in r (Love, 1944) and can have an arbitrary additive constant. Therefore, for the purpose of plotting the frequency dependance of displacement amplitude, the zero frequency values correspond to $\omega a/\pi\beta = 0.005$. However, both synthetics and results in the frequency domain, for $\omega a/\pi\beta > 1$ correctly describe the effects of topography upon the incidence of Rayleigh waves. This can be seen on the synthetics which show the appropriate amplitude of the incident wave.

Figures 4 and 5 display the responses of the

deep and shallow triangular canyons for incident P and SV waves with incidence angles of 30° and 45°, respectively. For the deep canyon large variations in both space and frequency plots can be seen. The synthetics show diffracted Rayleigh waves with a criss-cross pattern. For the shallow canyon the synthetics show minor effects. In fact, a small-amplitude Rayleigh wave is produced at the left rim. Frequency domain results also show large variations. In both cases, and for a wide range of frequencies, relative amplifications or de-amplifications are larger than 20. However, maximum amplification is of about 2.5 times the amplitude of the incoming wave. Sánchez-Sesma and Campillo (1991) studied other incidences and found that the absolute maximum of response is generally lower than about 4.

Figure 6 illustrates the surface motion of the deep semi-elliptical canyon for incident SV waves. Again, a great variability emerges as a consequence of the superposition of incoming and reflected–diffracted energy. In the synthetics, the first arrivals at the right flat part clearly show both a delay and a reduction of amplitude that indicates a shadow zone and, thus, diffraction. In the figure the reflected SV wave is clearly seen along the left canyon's wall. This wave precedes diffracted creeping Rayleigh waves that propagate along the canyon's surface. These waves are produced at the corners and bounce back and forth between them. Early and late emissions of diffracted Rayleigh phases are also clearly seen in the flat part of the model. Results near the left rim seem to confirm the theoretical prediction of null motion at the vertex of a quarter space under the incidence of a plane SV wave propagating

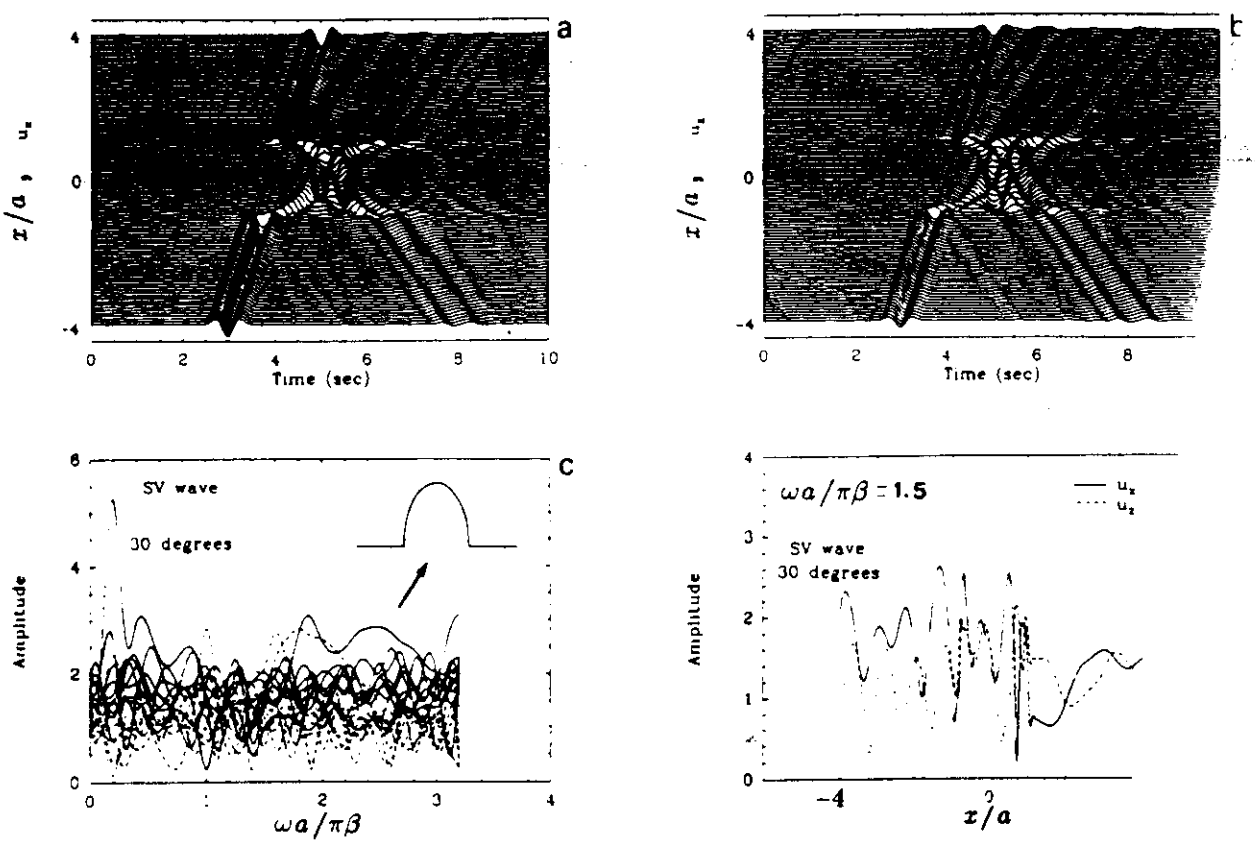

Fig. 7. Response to a nearby vertical load. Except at low frequencies, results correctly describe the effects of an incor wave. Synthetic seismograms and frequency response for surface receivers equally spaced between $x = -2a$ and surface of a triangular mountain with unit slopes. (a)–(d) as in Fig. 4.

along the bisector angle (Sánchez-Sesma, 1990). The responses of the deep elliptical canyon to various types of incident waves show the appearance of creeping Rayleigh waves (see Sánchez-Sesma and Campillo, 1991).

Figure 7 shows a mountain with unit slopes under incident Rayleigh waves. Maximum amplifications do not exceed the level of 2 times the horizontal amplitude of the incident wave. As shown in the figure, the diffraction of Rayleigh waves mainly produces a backward-propagating phase of the same type. Figure 7c shows that the effect of the near-source terms of the applied load dominates at low frequencies.

In Figure 8 the surface motion of the semi-elliptical mountain for incident plane SV waves and 30° is illustrated. This is an extreme model that shows the wide potential applications of this approach. A great variability in the amplifications in the frequency domain is again present. At one receiver amplifications reach more than 5 times the amplitude of incident waves but the absolute level of amplification is, for this example, generally lower than about 3 times the amplitude of incoming waves. Time domain results show significant interference patterns, due to creeping waves along the curved part of the surface and the late emission of Rayleigh waves.

Conclusions

A method for computing the diffraction of P, SV and Rayleigh waves by an irregular topographic feature in an elastic half-space has been presented. It is based on a direct integral representation of the diffracted elastic fields in terms of single-layer boundary sources. A discretization scheme based on the numerical and analytical integration of exact Green's functions for displacements and tractions is employed. Our formulation can be seen as a numerical realization of Huygens' principle; that is, the diffracted waves are constructed at the boundary from which they are radiated. In addition to the physical insight gained with this method, it appears to be accurate and fast.

The results correspond to a relatively simple set of conditions, namely:

(1) the incidence of a plane wave (or the application of a vertical load in the neighborhood);

(2) the assumption of an elastic half-space with a Poisson ratio of $\frac{1}{4}$;

(3) a symmetrical shape for the irregularity.

Nevertheless, they display significant aspects of the response of topographic features. One of those is the spectacular amplitude of creeping waves and, as its counterpart, the large increase in the duration of the motion on the irregular topography.

Our results confirm the large variability of site effects, reported in the literature with respect to frequency, incidence angle and location of receivers. They show that variability is not restricted to the topographic feature: its presence strongly affects nearby locations. They also show that the interaction of elastic waves produce complex amplification and de-amplification patterns. For example, Bard and Tucker (1985) observed significant amplifications at some underground sites and concluded that they were due to free surface reflections. We believe that, despite the relative simplicity of our models, our results give a glimpse of the effects that the real topographic feature may induce. They present very large relative amplifications with values that, in many cases, can be larger than 20.

The plots of the frequency response at various locations show why simple spectral ratios cannot account for the seismic behavior of topographies. The large variability in the spectral content of ground motion in both frequency and space suggests that, in order to interpret the data, we cannot rule out the need for a quantitative model and careful assessment of the type of incoming waves as well. Therefore, the selection of reference sites and the windowing of the records are crucial for characterizing topographical effects by means of spectral ratios. For windowing data, a polarization analysis, such as that of Bernard and Zollo (1989), can be useful. In any event, our results (those shown here and in Sánchez-Sesma and Campillo (1991)) show that the absolute level of amplification is generally lower than about 4 times the amplitude of incoming waves.

Acknowledgements

Thanks are given to M. Bonnet for his comments and suggestions, to D.A. Alvarez-Cuevas and J. Ramos-Martínez for the critical reading of the manuscript, and to M. Suarez for her assistance. K. Aki, P.-Y. Bard, M. Bouchon, V. Farra, R. Madariaga and A. Wirgin made valuable suggestions. The critical comments from two anonymous reviewers helped to improve this work. Part of this study was carried out while one of us (F.J.S.-S.) was on leave from the National University of Mexico and the Centro de Investigacion Sísmica A.C., Mexico, at the Université Joseph Fourier of Grenoble, France, and Laboratoire de Sismologie of the Institute de Physique du Globe of Paris, France, as a Visiting Professor. Some computations were performed at Centre de Calcul Vectoriel pour la Recherche. This work was partially supported by Pole Grenoblois de Recherche sur les Risques Naturels, University of Paris VI, France, by Departamento del Distrito Federal, Mexico, and by Consejo Nacional de Ciencia y Tecnología, Mexico, under Grants P127CCOT904892 and P0523-T9109.

References

Abramowitz, M. and Stegun, I.A., 1972. Handbook of Mathematical Functions. Dover, New York.

Aki, K., 1988. Local site effects on strong ground motion. In: J.L. Von Thun (Editor), Earthquake Engineering and Soil Dynamics II—Recent advances in ground motion evaluation. (Geotechnical Spec. Publ. No. 20.) Am. Soc. Civil Eng., New York, pp. 103–155.

Bard, P.-Y., 1982. Diffracted waves and displacement field over two-dimensional elevated topographies. Geophys. J.R. Astron. Soc., 71: 731–760.

Bard, P.-Y. and Tucker, B.E., 1985. Underground and ridge site effects: a comparison of observation and theory. Bull. Seismol. Soc. Am., 75: 905–922.

Bernard, P. and Zollo, A., 1989. Inversion of near-source S polarization for parameters of double-couple point sources. Bull. Seismol. Soc. Am., 79: 1779–1809.

Bonnet, M., 1986. Méthode des equationes integrales regularisees en elastodynamique. PhD Thesis, Ecole Nat. Ponts et Chaussees, Paris.

Bonnet, M., 1989. Regular boundary integral equations for three-dimensional finite or infinite bodies with and without curved cracks in elastodynamics. In: C.A. Brebbia and N.G. Zamani (Editors), Boundary Element Techniques: Applications in Engineering. Computational Mechanics, Southampton.

Bouchon, M., 1973. Effect of topography on surface motion. Bull. Seismol. Soc. Am., 63: 615–632.

Bouchon, M., 1979. Discrete wave number representation of elastic wave fields in three-space dimensions. J. Geophys. Res., 84 (B7): 3609–3614.

Bouchon, M., 1985. A simple, complete numerical solution to the problem of diffraction of SH waves by an irregular surface. J. Acoust. Soc. Am., 77: 1–5.

Bouchon, M. and Aki, K., 1977. Discrete wave-number representation of seismic-source wave fields. Bull. Seismol. Soc. Am., 67: 259–277.

Bouchon, M., Campillo, M. and Gaffet, S., 1989. A boundary integral equation—discrete wavenumber representation method to study wave propagation in multilayered media having irregular interfaces. Geophysics, 54: 1134–1140.

Campillo, M., 1987. Modeling of SH wave propagation in an irregularly layered medium. Application to seismic profiles near a dome. Geophys. Prospect., 35: 236–249.

Campillo, M. and Bouchon, M., 1985. Synthetic SH seismograms in a laterally varying medium by the discrete wavenumber method. Geophys. J.R. Astron. Soc., 83: 307–317.

Campillo, M., Sánchez-Sesma, F.J. and Aki, K., 1990. Influence of small lateral variations of a soft surficial layer on seismic ground motion. Int. J. Soil Dyn. Earthquake Eng., 9: 284–287.

Davis, L.L. and West, L.R., 1973. Observed effects of topography on ground motion. Bull. Seismol. Soc. Am., 63: 283–298.

Dravinski, M., 1982. Influence of interface depth upon strong ground motion. Bull. Seismol. Soc. Am., 72: 597–614.

Dravinski, M. and Mossessian, T.K., 1987. Scattering of plane harmonic P, SV and Rayleigh waves by dipping layers of arbitrary shape. Bull. Seismol. Soc. Am., 77: 212–235.

Gaffet, S. and Bouchon, M., 1989. Effects of two-dimensional topographies using the discrete wavenumber–boundary integral equation method in P-SV cases. J. Acoust. Soc. Am., 85: 2277–2283.

Geli, L., P.-Y. Bard and Jullien, B., 1988. The effect of topography on earthquake ground motion: A review and new results. Bull. Seismol. Soc. Am., 78: 42–63.

Griffiths, D.W. and Bollinger, G.A., 1979. The effect of Appalachian mountain topography on seismic waves. Bull. Seismol. Soc. Am., 69: 1081–1105.

Kawase, H., 1988. Time-domain response of a semicircular canyon for incident SV, P, and Rayleigh waves calculated by the discrete wavenumber boundary element method. Bull. Seismol. Soc. Am., 78: 1415–1437.

Kawase, H. and Aki, K., 1989. A study on the response of a soft basin for incident S, P and Rayleigh waves with special reference to the long duration observed in Mexico City. Bull. Seismol. Soc. Am., 79: 1361–1382.

Kelly, K.R. and Marfurt, K.J., 1990. Numerical modeling of

seismic wave propagation. (Geophysics Reprint Series, No. 13.) Soc. Explor. Geophys., Tulsa, Okla., USA.

Kobayashi, S., 1987. Elastodynamics. In: D.E. Beskos (Editor), Boundary Element Methods in Mechanics. North-Holland, Amsterdam.

Kupradze, V.D., 1963. Dynamical problems in elasticity. In: I.N. Sneddon and R. Hill (Editors), Progress in Solid Mechanics, Vol. III. North-Holland, Amsterdam, pp. 191–255.

Lamb, H., 1904. On the propagation of tremors over the surface of an elastic solid. Philos. Trans. R. Soc. London Ser. A, 203: 1–42.

Lee, V.W. and Cao, H., 1989. Diffraction of SV waves by circular canyons of various depths. J. Eng. Mech. Am. Soc. Civil Eng., 115: 2035–2056.

Love, A.E.H., 1944. A Treatise on the Mathematical Theory of Elasticity. Dover, New York.

Luco, J.E, Wong, H.L. and De Barros, F.C.P., 1990. Three-dimensional response of a cylindrical canyon in a layered half-space. Int. J. Earthquake Eng. Struct. Dyn., 19: 799–817.

Manolis, G.D and Beskos, D.E., 1988. Boundary Element Methods in Elastodynamics. Unwin Hyman, London.

Sánchez-Sesma, F.J., 1987. Site effects on strong ground motion. Int. J. Soil Dyn. Earthquake Eng., 6: 124–132.

Sánchez-Sesma, F.J., 1990. Elementary solutions for the response of a wedge-shaped medium to incident SH and SV waves. Bull. Seismol. Soc. Am., 80: 737–742.

Sánchez-Sesma, F.J. and Campillo, M., 1991. Diffraction of P, SV and Rayleigh waves by topographical features: a boundary integral formulation. Bull. Seismol. Soc. Am., 81: 2234–2253.

Sánchez-Sesma, F.J. and Esquivel, J., 1979. Ground motion on alluvial valleys under incident plane SH waves. Bull. Seismol. Soc. Am., 69: 1107–1120.

Sánchez-Sesma, F.J. and Rosenblueth, E., 1979. Ground motion at canyons of arbitrary shape under incident SH waves. Int. J. Earthquake Eng. Struct. Dyn., 7: 441–450.

Sánchez-Sesma, F.J., Bravo, M.A. and Herrera, I., 1985. Surface motion of topographical irregularities for incident P, SV and Rayleigh waves. Bull. Seismol. Soc. Am., 75: 263–269.

Todorovska, M.I. and Lee, V.W., 1992a. Surface motion of shallow circular alluvial valleys for incident plane SH waves—analytical solution. Int. J. Soil Dyn. Earthquake Eng. (in press).

Todorovska, M.I. and Lee, V.W., 1992b. A note on response of shallow circular valleys to Rayleigh waves—analytical approach. Earthquake Eng. Eng. Vibration (in press).

Trifunac, M.D., 1971. Surface motion of a semi-cylindrical alluvial valley for incident plane SH waves. Bull. Seismol. Soc. Am., 61: 1755–1770.

Trifunac, M.D., 1973. Scattering of plane SH waves by a semi-cylindrical canyon. Int. J. Earthquake Eng. Struct. Dyn., 1: 267–281.

Trifunac, M.D. and Hudson, D.E., 1971. Analysis of the Pacoima Dam accelerogram. San Fernando, California, earthquake of 1971. Bull. Seismol. Soc. Am., 61: 1393–1411.

Tucker, B.E., King, J.L., Hatzfeld, D. and Nersesov, I.L., 1984. Observations of hard-rock site effects. Bull. Seismol. Soc. Am., 74: 121–136.

Wong, H.L., 1979. Diffraction of P, SV and Rayleigh waves by surface topographies. Dep. Civil Eng. Univ. Southern California, Los Angeles, Calif., Rep. CE 79-05.

Wong, H.L., 1982. Effect of surface topography on the diffraction of P, SV and Rayleigh waves. Bull. Seismol. Soc. Am., 72: 1167–1183.

Wong, H.L. and Jennings, P.C., 1975. Effect of canyon topographies on strong ground motion. Bull. Seismol. Soc. Am., 65: 1239–1257.

Woods, R.D., 1968. Screening of surface waves in soils. J. Soil Mech. Found. Div. Am. Soc. Civil Eng., 94: 951–979.

Zhang, L. and Chopra, A.K., 1991. Three-dimensional analysis of spatially varying ground motions around a uniform canyon in a homogeneous half-space. Int. J. Earthquake Eng. Struct. Dyn., 20: 911–926.

EARTHQUAKE ENGINEERING AND STRUCTURAL DYNAMICS, VOL. 22, 279–295 (1993)

AN INDIRECT BOUNDARY ELEMENT METHOD APPLIED TO SIMULATE THE SEISMIC RESPONSE OF ALLUVIAL VALLEYS FOR INCIDENT P, S AND RAYLEIGH WAVES

F. J. SÁNCHEZ-SESMA[1,2], J. RAMOS-MARTÍNEZ[1,3] AND M. CAMPILLO[4]

[1]*Instituto de Ingeniería, U.N.A.M., Cd. Universitaria, Apdo. 70-472, Coyoacán 04510 México D.F., Mexico*
[2]*Centro de Investigación Sísmica, A.C., Carr. al Ajusco 203, Col. H. de Padierna, Tlalpan 14200 México D.F., Mexico*
[3]*Posgrado en Geofísica, Instituto de Geofísica, U.N.A.M., Cd. Universitaria Coyoacán 04510 México D.F., Mexico*
[4]*Observatoire de Grenoble, Université Joseph Fourier, LGIT-IRIGM, B.P. 53X, 38041 Grenoble Cedex, France*

SUMMARY

A boundary integral formulation is presented and applied to model the ground motion on alluvial valleys under incident P, S and Rayleigh waves. It is based on integral representations for the diffracted and the refracted elastic waves using single-layer boundary sources. This approach is called *indirect BEM* in the literature as the sources' strengths should be obtained as an intermediate step. Boundary conditions lead to a system of integral equations for boundary sources. A discretization scheme based on the numerical and analytical integration of exact Green's functions for displacements and tractions is used. Various examples are given for two-dimensional problems of diffraction of elastic waves by soft elastic inclusion models of alluvial deposits in an elastic half-space. Results are displayed in both frequency and time domains. These results show the significant influence of locally generated surface waves in seismic response and suggest approximations of practical interest. For shallow alluvial valleys the response and its resonant frequencies are controlled by a coupling mechanism that involves both the simple one-dimensional shear beam model and the propagation of surface waves.

INTRODUCTION

The effects of local topographic and geological conditions may generate amplification of ground motion and concentrated damage. The last two decades have seen significant progress in the evaluation of such effects (see References 1 and 2 for recent reviews) and dramatic examples of their reality as well (see e.g. References 3–6).

Boundary element methods (BEM) have gained increasing popularity. Recognized advantages over domain approaches are the dimensionality reduction, the relatively easy fulfilment of radiation conditions at infinity and the high accuracy of results. Excellent surveys of the available literature on BEM in elastodynamics are those of Kobayashi[7] and Manolis and Beskos.[8] The most popular BEM approaches are the so-called *direct* ones because in their formulation, the unknowns are the sought values of displacements and tractions. They arise from the discretization of integral representation theorems. In contrast, the *indirect BEM*, which formulates the problem in terms of force or moment boundary densities, is not as popular. This is despite the fact that such densities can give a deep physical insight on the nature of diffracted waves. Moreover, the indirect BEM has a longer history than the direct BEM and is closely related to classical work on integral equations (see e.g. Reference 8).

On the other hand, in a pioneering work, Aki and Larner[9] introduced a numerical method based on a discrete superposition of homogeneous and inhomogeneous plane waves. Using this technique, Bard and Bouchon[10–12] studied alluvial valleys and pointed out the significant role of sediment-induced surface waves in the valleys' response and the resonant characteristics of these configurations as well. The Aki–Larner technique is the departure of discrete wave number approximations. The combination of discrete wave number expansions for Green's functions[13] with boundary integral representations has been successful in

0098-8847/93/040279-17$13·50

Received 3 March 1992
Revised 14 August 1992

various studies of elastic wave propagation. In some of them, source distributions at the boundaries are used (e.g. Reference 14), whereas others make use of the Somigliana representation theorem (e.g. References 15 and 6). These are discrete wave number versions of BEM, indirect and direct, respectively. In a recent work, Papageorgiou and Kim[6] applied the discrete wave number direct BEM to study the propagation and amplification of SH waves in a model of Caracas Valley. Their results correlate well with observations during the 29 July 1967 earthquake and even suggest that amplifications were larger than the previously estimated ones.

The combination of BEM with discrete wave number is particularly attractive: the singularities of Green's functions are not present in each one of the terms of the discrete wave number expansion. The integration along the boundary effectively makes the singularities to vanish and improves convergence as well. However, such procedures require considerable amount of computer resources. An alternative approach may be welcomed for many applications. Such an alternative could be the BEM, either direct or indirect, with analytical Green's functions for the full space. Zhang and Chopra[16] applied a direct BEM to model the ground motion at a three-dimensional (3D) topography.

In this work the indirect BEM is applied to study ground motion on alluvial valleys under incident P, S and Rayleigh waves. It is based upon the integral representation of the diffracted elastic waves in terms of single-layer boundary sources. In our approach, diffracted waves are constructed at the boundaries from which they are radiated. Therefore, it can be regarded as a numerical realization of Huygens' principle. This is, in fact, an improvement over a boundary method that has been used to deal with various problems of diffraction of elastic waves (e.g. References 17 and 18). In its many variants, such technique is based upon the superposition of solutions for *sources* with their singularities placed *outside* the region of interest. However, in the applications, the location of sources requires particular care and the trial-and-error process needed is difficult to apply, particularly when many frequencies are to be computed. In our approach, the uncertainty about the location of sources is eliminated. Therefore, our indirect BEM approach retains the physical insight of the sources method, with all the benefits of analytical integration of *exact* Green's functions. In the applications reported here, we use exact expressions of the two-dimensional (2D) Green's functions in an unbounded elastic space.

The method has been applied by Sánchez-Sesma and Campillo[19] to study the diffraction of P, SV and Rayleigh waves by topographical irregularities in an elastic half-space. Excellent agreement was found with published results. Ramos-Martínez and Sánchez-Sesma[20] applied the method to simulate the response of alluvial valleys and validated their results by comparing them with those obtained by Kawase and Aki.[15] A successful application of this approach to three-dimensional soil–structure dynamic interaction has been recently proposed.[21]

In what follows, the single-layer boundary representation of elastic wave fields is described and applied to compute the response of various models of alluvial deposits for incident elastic waves in a half-space. Comparisons are provided with both the exact[22] and the numerical[23] solutions for a semicircular soft inclusion under incident SH and SV waves, respectively. The response of a semielliptical valley is then studied in frequency and time domains for incident Rayleigh waves. So is done for a shallow soft valley under vertical incidence of SH and SV waves. In this case, transfer functions are given in a frequency–space description which suggests approximations of practical interest. These allowed the identification of a coupling mechanism that controls the response and its resonant frequencies. It involves both the simple one-dimensional (1D) shear beam model and the propagation of surface waves. Time domain results are combined to produce a quasi-3D time response in which locally generated Love and Rayleigh surface waves produce rotating polarization patterns.

INTEGRAL REPRESENTATION USING BOUNDARY SOURCES

Consider the domain V and its boundary S. If an elastic material occupies such a region, the harmonic displacement field can be written, neglecting body forces, by means of the *single-layer* boundary integral

$$u_i(\mathbf{x}) = \int_S \phi_j(\xi) G_{ij}(\mathbf{x}, \xi)\, dS_\xi \tag{1}$$

where $u_i(\mathbf{x})$ is the ith component of displacement at $\mathbf{x}$, $G_{ij}(\mathbf{x}, \xi)$ is Green's tensor, i.e. the displacement in the direction i at point $\mathbf{x}$ due to the application of a unit force in the direction j at point ξ and (ξ) is the unknown force density in the direction j. Therefore, $\phi_j(\xi)\,dS$ is clearly a force distribution at the boundary. The subscripts in the differential element indicate the space variable over which the integration is performed. This single-layer integral, that can be obtained from the Somigliana identity,[18] has been studied by Kupradze[24] from the point of view of potential theory. He showed that the displacement field is continuous across S if $\phi_j(\xi)$ is continuous *along* S. This is clear if we consider that $G_{ij}(\mathbf{x}, \xi)$ has an integrable singularity at $\mathbf{x} = \xi$. In its scalar 2D version (SH waves) this representation is called the Kirchhoff–Helmholtz representation (see Reference 25).

This integral representation allows computation of stresses and tractions by direct application of Hooke's law except at the boundary singularities, i.e. when $\mathbf{x} = \xi$ on the boundary. By a limiting process, based on equilibrium considerations around a neighbourhood of the boundary, it is possible to write, for $\mathbf{x}$ on S, that

$$t_i(\mathbf{x}) = c\phi_i(\mathbf{x}) + \int_S \phi_j(\xi)\, T_{ij}(\mathbf{x}, \xi)\, dS_\xi \tag{2}$$

where t_i is the ith component of traction at the boundary and $c = \pm 0{\cdot}5$ for a smooth boundary. The signs $+$ or $-$ are used if $t_i(\mathbf{x})$ corresponds to the *interior* domain or to the *exterior* one, respectively, relative to S (these interior and exterior domains are clearly defined once the direction of the normal vector on S is specified: it always points towards the exterior region), $T_{ij}(\mathbf{x}, \xi)$ is the traction Green's function, i.e. the traction in the direction i at point $\mathbf{x}$ on the boundary with normal $\mathbf{n}(\mathbf{x})$ (assumed to be specified and pointing outside if $\mathbf{x}$ is at S) due to the application of a unit force in the direction j applied at ξ. The first term on the right-hand side must be dropped if $\mathbf{x}$ is not at S. This result has also been found by Kupradze. In its scalar version, the result appeared first in a paper by Fredholm in 1900 (see Reference 26).

Equations (1) and (2) form the basis of our approach. Although *indirect*, it allows a direct interpretation of the physical quantities involved. Expressions for Green's functions can be found in the literature (e.g. References 7, 27 and 19). It suffices to say here that the singularity of displacements is either logarithmic or $1/r$ for 2D or 3D problems, respectively. Regarding the tractions, such singularities are explicitly of the form $1/r$ or $1/r^2$, respectively. In particular, when frequency tends to zero, Green's tractions lead to their static counterparts. These properties are invoked below in connection with our discretization scheme.

DIFFRACTION OF ELASTIC WAVES BY AN ALLUVIAL VALLEY

Consider the elastic half-space, E, with an alluvial valley, R, as shown in Figure 1 under incidence of elastic waves. The free-surface boundaries of regions E and R are denoted by $\partial_1 E$ and $\partial_1 R$, respectively. The interface $\partial_2 E = \partial_2 R$ is the common boundary between them. The ground motion in this irregular configuration comes from the interferences of incoming waves with reflected, diffracted and refracted ones. It is also usual to say that the total motion in the half-space is the superposition of the so-called *diffracted* waves and the free field:

$$u_i^E = u_i^{(0)} + u_i^{(d)} \tag{3}$$

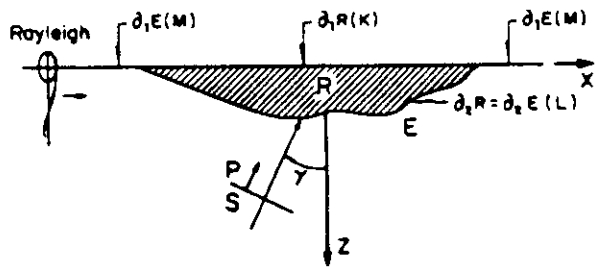

Figure 1. Half-space, E, with an elastic inclusion, R, and incidence of P, S and Rayleigh waves. The discretization along the interface, the free surface of inclusion and portions of the flat surface of the half-space gives L, K and $2M$ segments, respectively.

where $u_i^{(0)}$ = free-field displacement, i.e. the solution in the absence of the irregularity. According to our previous discussion, the diffracted field is given by equation (1) which, with appropriate superscripts to indicate the region of validity, can be written as

$$u_i^{(d)}(\mathbf{x}) = \int_{\partial E} \phi_j^E(\xi) G_{ij}^E(\mathbf{x}, \xi)\, dS_\xi \tag{4}$$

The refracted elastic fields on the inclusion R can be written as

$$u_i^{(r)}(\mathbf{x}) = \int_{\partial R} \phi_j^R(\xi) G_{ij}^R(\mathbf{x}, \xi)\, dS_\xi \tag{5}$$

The traction-free boundary conditions imply that

$$t_i^{(0)} + t_i^{(d)} = 0 \quad \text{on} \quad \partial_1 E \tag{6}$$

and

$$t_i^{(r)} = 0 \quad \text{on} \quad \partial_1 R \tag{7}$$

where $t_i^{(r)}$ = tractions of refracted field. Then, from equation (2) such conditions can be expressed by means of

$$0{\cdot}5\phi_i^E(\mathbf{x}) + \int_{\partial E} \phi_j^E(\xi) T_{ij}^E(\mathbf{x}, \xi)\, dS_\xi = 0 \tag{8}$$

and

$$-0{\cdot}5\phi_i^R(\mathbf{x}) + \int_{\partial R} \phi_j^R(\xi) T_{ij}^R(\mathbf{x}, \xi)\, dS_\xi = 0 \tag{9}$$

On $\partial_{2E} = \partial_{2R}$, continuity of displacements and tractions implies

$$u_i^{(0)} + u_i^{(d)} = u_i^{(r)} \tag{10}$$

$$t_i^{(0)} + t_i^{(d)} = t_i^{(r)} \tag{11}$$

and these conditions can be expressed by

$$\int_{\partial E} \phi_j^E(\xi) G_{ij}^E(\mathbf{x}, \xi)\, dS_\xi - \int_{\partial R} \phi_j^R(\xi) G_{ij}^R(\mathbf{x}, \xi)\, dS_\xi = -u_i^{(0)}(\mathbf{x}) \tag{12}$$

and

$$0{\cdot}5[\phi_i^E(\mathbf{x}) + \phi_i^R(\mathbf{x})] + \int_{\partial E} \phi_j^E(\xi) T_{ij}^E(\mathbf{x}, \xi)\, dS_\xi - \int_{\partial R} \phi_j^R(\xi) T_{ij}^R(\mathbf{x}, \xi)\, dS_\xi = -t_i(\mathbf{x}) \tag{13}$$

Equations (8), (9), (11) and (12) constitute a system of integral equations for boundary sources, i.e. those producing the diffracted and the refracted fields. These expressions are discretized along a finite portion of the boundary ∂E that includes the interface topography and the lateral flat parts and along ∂R, according to the definition of each integral.

DISCRETIZATION

In order to solve the above system of integral equations, we have to discretize them. Let us assume the force densities $\phi_j(\xi)$ constant over each of the boundary segments with equal length ΔS along each appropriate boundary. Assume that $2M$, L and K are the number of segments (elements) along the discretized part of the flat surface on both sides, the irregular interface and the free surface of region R, respectively, as depicted in Figure 1. It becomes clear that the total number of equations is $4M + 4L + 2K$, which is the same as the number of unknowns.

To clarify ideas, let us write the discretized versions of equations (1) and (2) ($N = M + L + M$):

$$u_i(\mathbf{x}) = \sum_{j=1}^{N} \phi_j(\xi_j) g_{ij}(\mathbf{x}, \xi_j) \tag{14}$$

where

$$g_{ij}(\mathbf{x}, \xi_j) = \int_{\xi_j - \Delta S/2}^{\xi_j + \Delta S/2} G_{ij}(\mathbf{x}, \xi)\, dS_\xi \tag{15}$$

and

$$t_i(\mathbf{x}) = \sum_{j=1}^{N} \phi_j(\xi_j) t_{ij}(\mathbf{x}, \xi_j) \tag{16}$$

where, for $\mathbf{x} = \mathbf{x}_n$, we have

$$t_{ij}(\mathbf{x}_n, \xi_j) = c\delta_{ij}\delta_{nj} + \int_{\xi_j - \Delta S/2}^{\xi_j + \Delta S/2} T_{ij}(\mathbf{x}_n, \xi)\, dS_\xi \tag{17}$$

The integrals in equation (15) are computed numerically with Gaussian integration, except in the case when $\mathbf{x}$ is in the neighbourhood of ξ_j, the midpoint of segment, for which we obtained analytical expressions from the ascending series for Bessel functions (see e.g. Reference 28). Sánchez-Sesma and Campillo[19] presented an example for such expressions when only the leading terms of the series are retained. We considered up to quadratic terms, which is enough if the number of segments per wavelength is larger than about six. The integrals in equation (17) are also computed numerically using Gaussian integration except when $\mathbf{x}_n = \xi_j$. In this case, we have

$$t_{ij}(\mathbf{x}_n, \xi_n) = c\delta_{ij}, \tag{18}$$

because the only contribution to the integral in equation (17) for $n = j$ comes from the free term. The contribution from the tractions Green's tensor is null because the discretization segment is a straight line and ξ_j is the midpoint. In fact, it can be verified that, under this circumstance, such part of the integrand is a singular odd function on the segment. Therefore, its Cauchy's principal value is zero. The value for t_{ij} in equation (18) can be interpreted as half of the applied unit line force and means that the force is distributed symmetrically for any two half-spaces containing the line of application of the load, regardless of its direction. This result also holds for the static Green's function.

Equations (8), (9), (11) and (12) are discretized in a similar manner. This leads to a linear system of $4M + 4L + 2K$ equations with the same number of unknowns. The system is solved using Gauss method. Once the values of $\phi_j(\xi_j)$ are known, the diffracted field is computed by means of the appropriate discretization of equations (4) and (5).

TESTING OF THE METHOD

The accuracy of this approach in its application to topographical irregularities has been verified by Sánchez-Sesma and Campillo[19] by comparing results with published solutions[29-31] for the diffraction of P, SV and Rayleigh waves by a semicircular canyon. Excellent agreement was found for both horizontal and vertical components of surface displacements.

Comparisons are provided here with both the exact[22] and the numerical[23] solutions for a semicircular soft inclusion under incident SH and SV waves, respectively. The model response is studied for a normalized frequency $\eta = 1.0$, where $\eta = \omega a/\pi\beta_E$ and a = radius of valley. Material properties are $\rho_R/\rho_E = 2/3$ and $\beta_R/\beta_E = 1/2$ for mass density and shear wave velocity ratios, respectively. Figure 2 displays the surface amplitudes for a horizontal incidence of a plane SH wave. Trifunac's[22] exact solution is given by symbols. The agreement is excellent. Figure 3 shows the horizontal and vertical surface displacement amplitudes for an incident SV wave. Dravinski and Mossessian[23] results are marked with symbols. Some small differences in

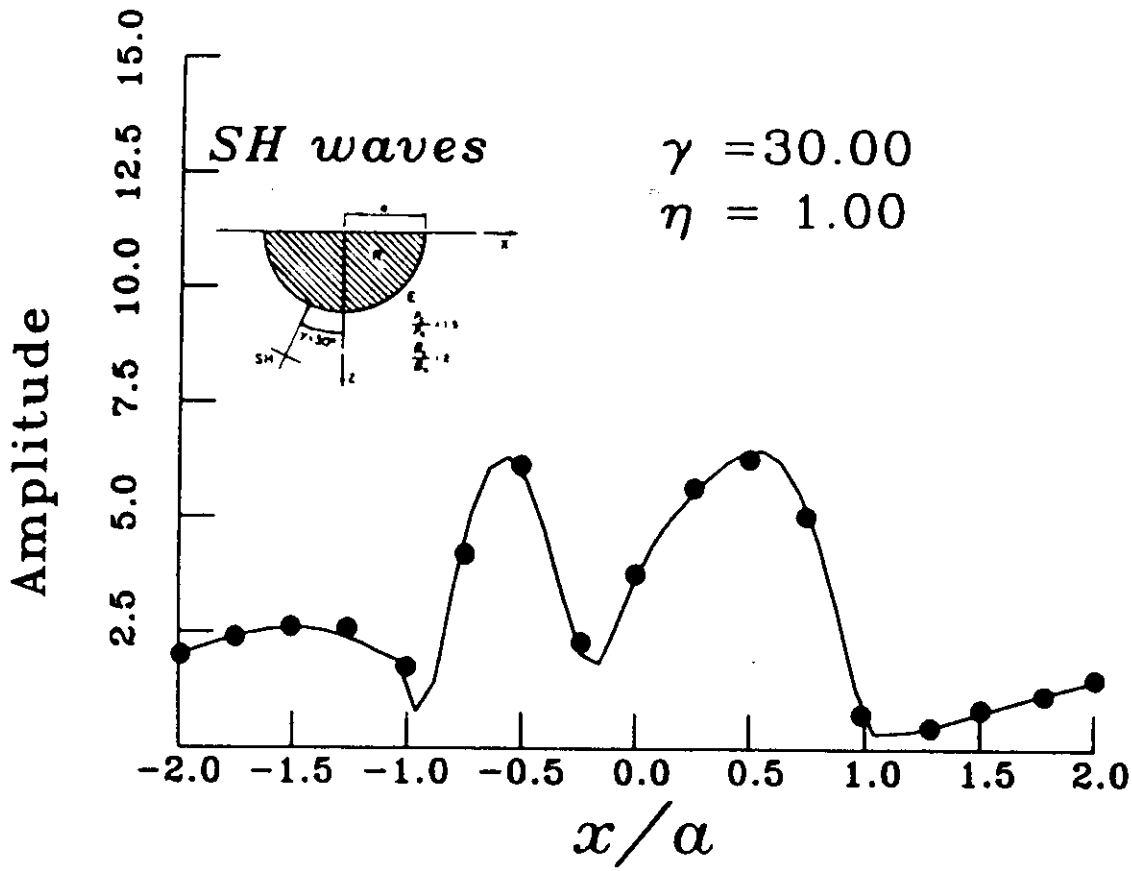

Figure 2. Amplitudes of horizontal antiplane displacement v for oblique incidence ($\gamma = 30°$) of harmonic SH waves upon a semicircular valley. Material properties are $\rho_R/\rho_E = 2.3$ and $\beta_R/\beta_E = 1.2$ for mass density and shear wave velocity ratios, respectively. Normalized frequency $\eta = 1$. Solid line corresponds to results obtained in the present study, while solid symbols correspond to Trifunac's[22] exact solution.

the horizontal component can be seen. Note that in this case both techniques are approximate. In any event, these results show significant differences between the responses of the same model to different types of incident waves.

The results presented here were obtained using a discretization length of $2\pi a$ (two times the perimeter of the interface) for each of the flat parts, and 10 segments per S wavelength. The displacements are virtually the same even when such parameters are reduced to πa and to 6, respectively. This implies that edge effects have little or no influence in our computations and shows that, apart from the discretization of part of the free boundary, there is no need of fictitious or absorbing boundaries. Sánchez-Sesma and Campillo[19] verified this interpretation. They computed the phase of diffracted waves and observed that the phase variation with space shows slopes consistent with the expected *outgoing* nature of such waves.

EXAMPLES

A deep semielliptical soft deposit under incident Rayleigh waves

In order to illustrate a complete set of results, we study the response of a semielliptical valley in both the frequency and time domains for incident Rayleigh waves (Figure 4). The maximum depth is 0·5 times the half-width ($h = 0{\cdot}5a$). Material properties are $\rho_R/\rho_E = 1$ and $\beta_R/\beta_E = 1/2$ for mass density and shear wave

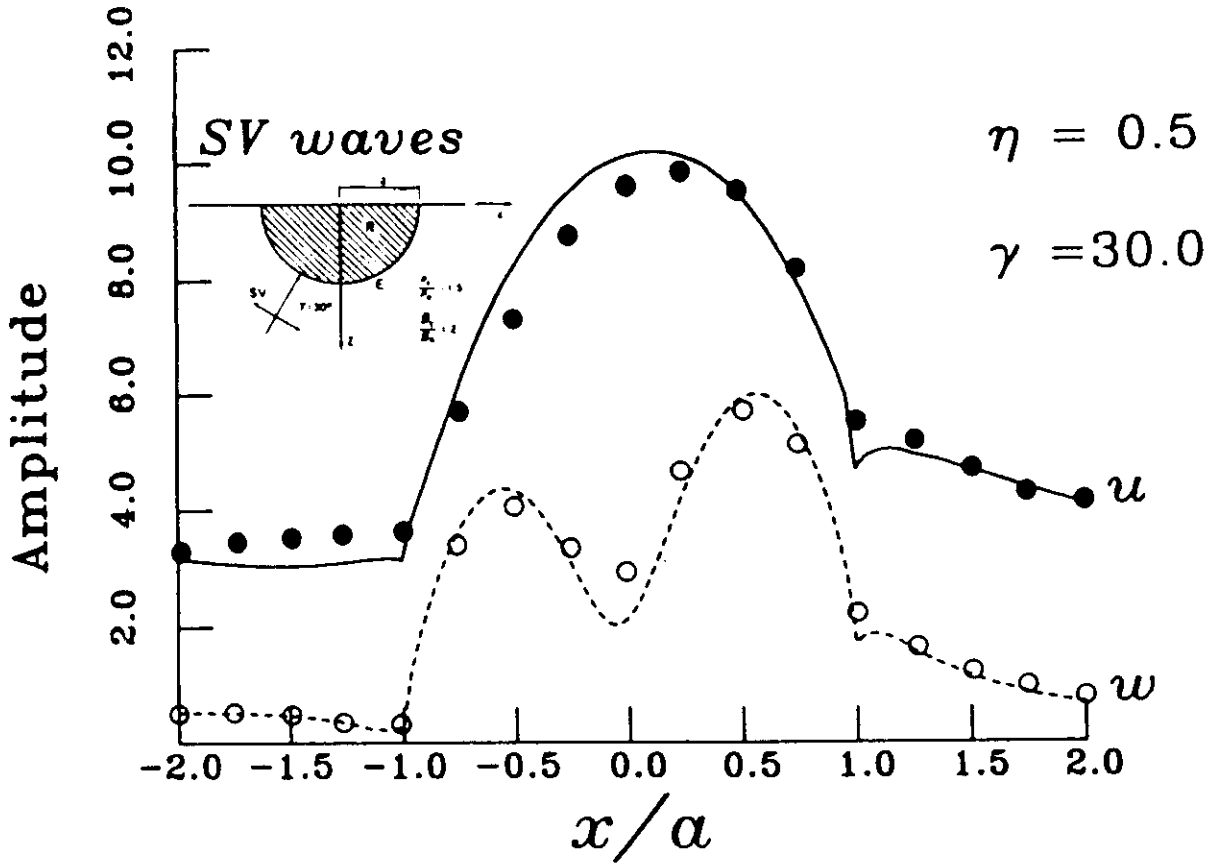

Figure 3. Amplitudes of horizontal and vertical displacements (u, w) for incidence of harmonic Rayleigh waves upon a semicircular valley. Material properties are $\rho_R/\rho_E = 2.3$ and $\beta_R/\beta_E = 1.2$ for mass density and shear wave velocity ratios, respectively. Normalized frequency $\eta = 1$. Solid and dashed lines correspond to results obtained in the present study, while solid and open symbols correspond to the numerical results of Dravinski and Mossessian.[23]

velocity ratios, respectively. Poisson ratios of 1.4 and 1.3 were selected for the half-space and the valley, respectively.

For a normalized frequency $\eta = 1$, Figure 4 shows the amplitude of displacements vs. space. Figure 5 displays the horizontal and the vertical displacement amplitudes for selected receivers along the free surface between $x = -2a$ and $x = 2a$, where a is the half-width of valley. These plots are, in fact, *transfer functions* with respect to the free-field horizontal component and are given against the normalized frequency $\eta = \omega a/\pi\beta E$. Large variability can be seen for the receivers with absolute amplification of about three for both components. However, relative amplifications reach values of about 18 inside the valley, with respect to some external points.

Note that maximum absolute amplifications at the valley's centre appears for a normalized frequency $\eta = 0.9$. This is in good agreement with the Rial's[32] asymptotic theory and Bard and Bouchon[33] results on the resonant eigenfrequencies in sedimentary basins. The predicted value for the fundamental mode of a deep semielliptical valley with the same shape ratio under *in-plane* SV excitation is given approximately by $\eta_1/\eta_0 = 1.8$, where $\eta_0 = 0.5$ is the resonant frequency of the 1D shear model applied at the basin's centre. The amplitude is consistent with the values predicted by Bard and Bouchon.[33]

From frequency domain results, we computed synthetic seismograms using the FFT algorithm for a Ricker wavelet with central frequency $\omega_p = 2\pi\beta_E/3a$; thus, the characteristic period of the Ricker pulse is

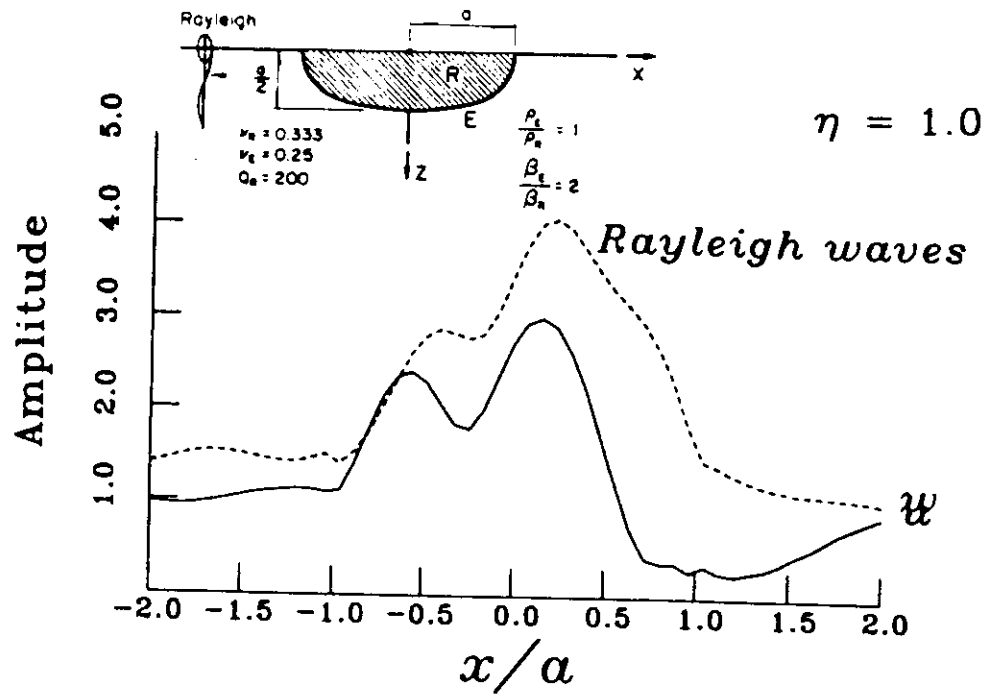

Figure 4. Amplitudes of horizontal (continuous line) and vertical (dotted line) displacements for incidence of Rayleigh waves upon semielliptical alluvial valley. Material properties are $\rho_R/\rho_E = 1$ and $\beta_R/\beta_E = 1.2$ for mass density and shear wave velocity ratios, respectively. Poisson ratios are 1.4 and 1.3 for regions E and R. Normalized frequency $\eta = 1.0$.

$t_p = 3a/\beta_E$. In Figure 6 such time series are plotted for 51 receivers equally spaced between $x = -2a$ and $x = 2a$. It was assumed that $2a/\beta_E = 1$ sec, in order to define the time scale. The actual scale is $\beta_E t/2a$. Figure 7 displays the same results for only 11 receivers in the same range by means of *polarigrams*,[34] which are plots that display displacement vectors shifted along the time scale. In our example, horizontal displacement u goes along with time, whereas vertical displacement $-w$ runs along the stations. These results show that even a relatively mild heterogeneity can generate important variations in both amplitude and polarization of ground motion.

A shallow parabolic soft deposit under incident S waves

In this example, our aim is to present some results for incident S waves, both *antiplane* SH and *inplane* SV ones for a very soft shallow parabolic valley and study the mechanisms of generation of surface waves and the resonant characteristics. The maximum depth is 0·05 times the half-width ($h = a/20$) as shown in Figure 8. Material properties are $\rho_R/\rho_E = 1/2$ and $\beta_R/\beta_E = 1/4$ for mass density and shear wave velocity ratio, respectively. Poisson ratios of 1/3 and 0·49 were selected for the half-space and the valley. The α/β ratios are then 2 and 7·14, respectively.

It is clear that we can consider the incidence of a plane S wave with a given incidence angle γ and arbitrary polarization θ (see Figure 8) by the simple combination of SH ($\theta = 0$) and SV ($\theta = \pi/2$) responses. Each one is be modulated by $\sin\theta$ and $\cos\theta$, respectively. This allows one to study how the propagation of Love and Rayleigh surface waves, which produce the antiplane and inplane components, interact and control the polarization of the horizontal motion.

Computations were again performed in the frequency domain. Horizontal displacement amplitudes u and v are shown in Figure 9 for vertical incident SH and SV waves, respectively. A great variability of amplifications in frequency domain can be seen. It is larger for the SH case. In both cases, the horizontal

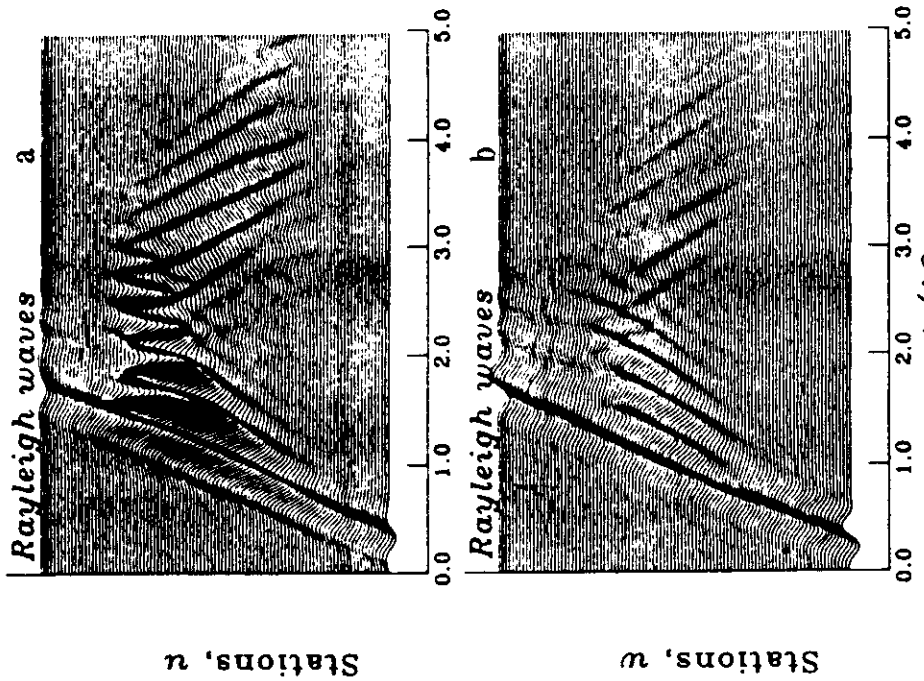

Figure 6. Incidence of a harmonic Rayleigh wave upon a semielliptical valley. Synthetic seismograms for 51 surface receivers equally spaced between $x = -2a$ and $x = 2a$ at the surface: (a) and (b) horizontal and vertical components, u and w, respectively. The incident time signal is a Ricker wavelet with central frequency $\omega_p = 2\pi\beta_2/3a$

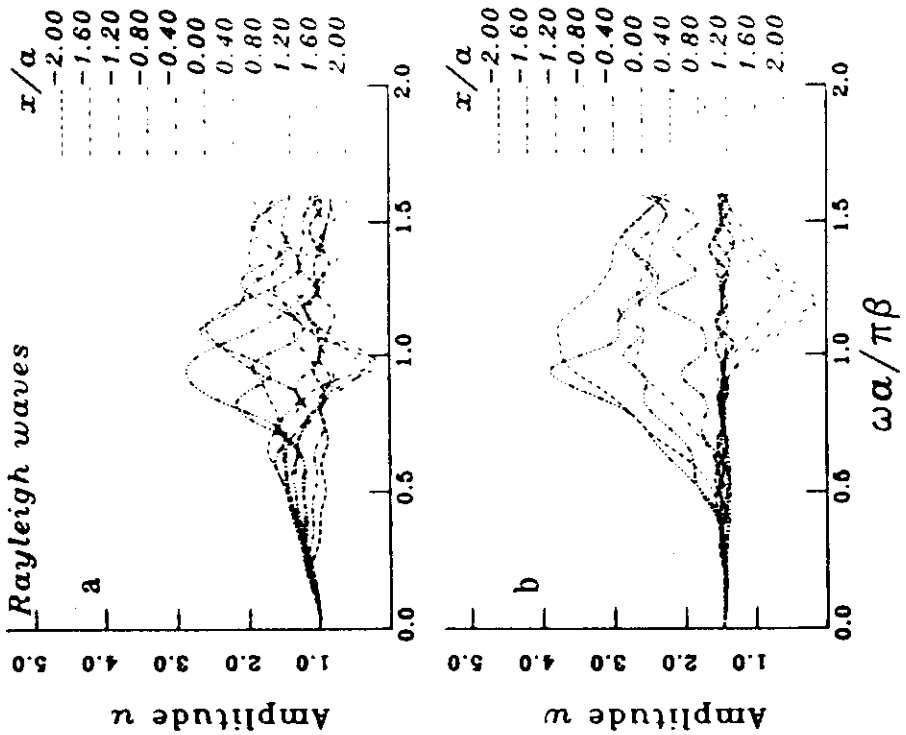

Figure 5. Incidence of a harmonic Rayleigh wave upon a semielliptical valley. Amplitudes of surface displacements for 11 receivers against normalized frequency: (a) horizontal displacement and (b) vertical displacement.

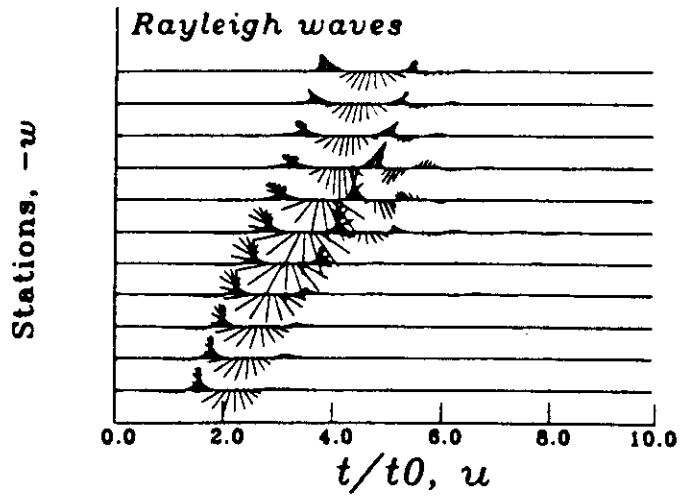

Figure 7. Incidence of a harmonic Rayleigh wave upon a semielliptical valley. Synthetic polarigrams for 11 surface receivers equally spaced between $x = -2a$ and $x = 2a$ at the surface. Horizontal and vertical component, u and $-w$, are plotted along time and stations scales, respectively. The incident time signal is a Ricker wavelet with central frequency $\omega_p = 2\pi\beta_E/3a$.

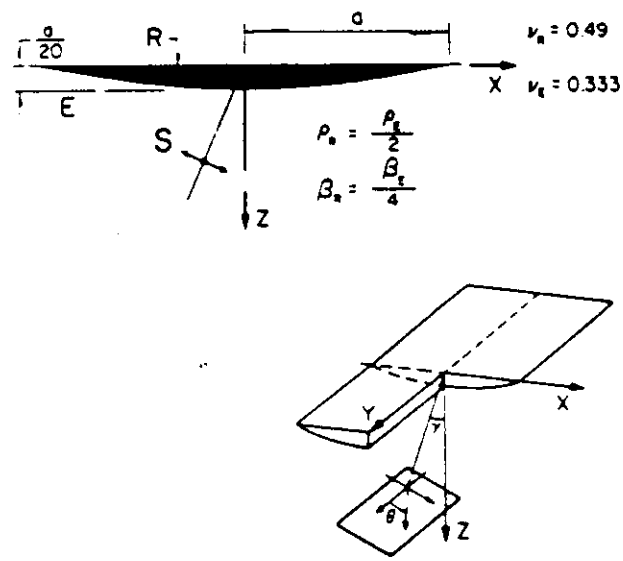

Figure 8. Soft alluvial valley with parabolic interface under incidence of plane S waves. Incidence and polarization angles are represented by γ and θ, respectively. Material properties are $\rho_R/\rho_E = 1.2$ and $\beta_R/\beta_E = 1.4$ for mass density and shear wave velocity ratios, respectively. Poisson ratios are 1/3 and 0·49 for regions E and R.

amplification reached more than 25 times the amplitude of incident waves at some receivers. This happens for frequencies larger than about $\eta = 2$. Note that the 1D shear model predicts a maximum amplification of 16, and, for the centre of the model, that would occur at $\eta = 2{\cdot}5$. However, lateral interferences from surface waves strongly modify that. On the other hand, vertical motion (not shown) is significantly excited for frequencies larger than about $\eta = 2$, giving a value of 10 for $\eta = 3{\cdot}75$. In any event, the horizontal motion dominates the valley's response for the range of frequencies studied.

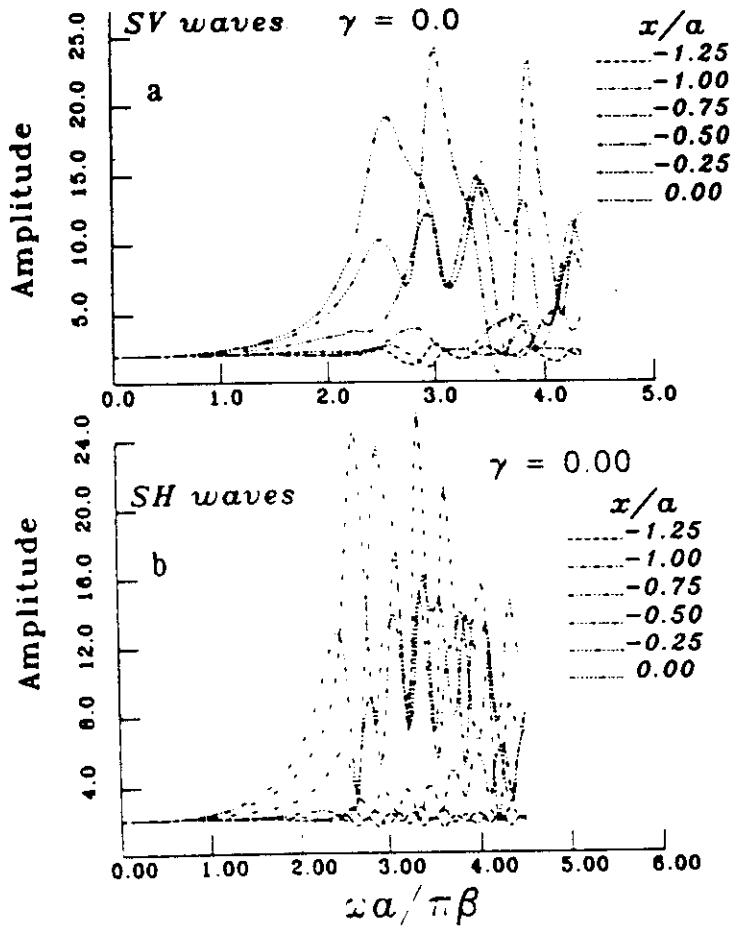

Figure 9. Incidence of a plane S wave with incidence angle of 0°. Frequency response for surface receivers equally spaced between $x = -1{\cdot}25a$ and $x = 0{\cdot}0$ at the surface of a shallow parabolic valley: (a) SV case and (b) SH case.

Apart from the large amplifications, these plots of frequency response suggest a rather chaotic behaviour. However, the corresponding contour maps of transfer functions in the frequency–space domain (f–x) of Figures 10 and 11 reveal a fine structure in which lateral propagation plays a significant role for frequencies higher than the one that controls the 1D response at the centre. Figure 10 shows such a map for vertical incidence of SH waves. The maximum amplifications for normalized frequencies larger than $\eta = 2{\cdot}5$ occur at the borders of a portion that grows with frequency. Indeed, if we consider that a first resonant frequency of an associated 1D shear model with the local thickness $h(x)$ is given by $f_0 = \beta_R/4h(x)$, which, for this model, can be written as

$$\eta_0 = 2{\cdot}5[1 - (x/a)^2]^{-1} \tag{21}$$

therefore, the borders of the excited central portion for a given frequency $\eta > 2{\cdot}5$ occur approximately at $x \cong \pm a(1 - 2{\cdot}5/\eta)^{1/2}$. Outside this region, amplification is moderate. The amplification inside can be very large with a clearly defined resonant behaviour. This is clear from the peaks that appear all along the map. The number of peaks grows with frequency, but for certain frequencies there are few or no peaks at all. One reasonable explanation for such peaks comes from ray theory. Consider that some rays exist that, after many

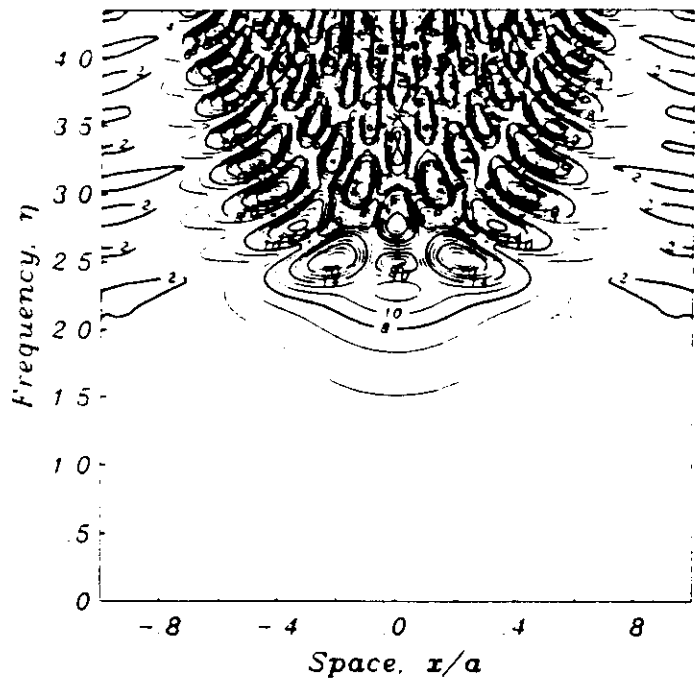

Figure 10. Contour map of transfer function v in the frequency–space domain (f–x) for vertical incidence of SH waves upon a shallow parabolic valley. η = normalized frequency.

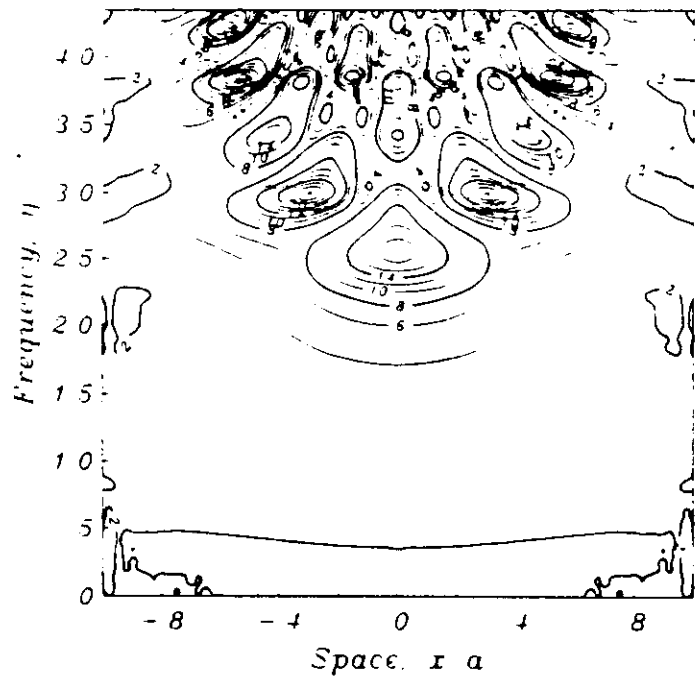

Figure 11. Contour map of transfer function u in the frequency–space domain (f–x) for vertical incidence of SV waves upon a shallow parabolic valley. η = normalized frequency.

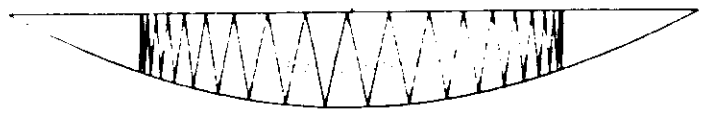

Figure 12. Ray diagram inside the parabolic valley. The vertical scale was enhanced.

bouncings up and down inside the valley, describe a total length ℓ, as shown in Figure 12. In agreement with Rial's[32,35] asymptotic theory, we found that a condition for resonance implies that $2\ell = \lambda(2m + 1)$, where $\lambda = 2\pi\beta_R/\omega$ is the wavelength, and $m = 0, 1, 2, \ldots$ For ℓ fixed, the resonant frequencies are defined. In our study, ℓ is allowed to vary, so the resonant frequencies come accompanied by variations in the size of the resonant region. Amplifications come as *quanta*, with clearly defined jumps. This phenomenon can be explained if we consider that from a given zone of 'local' resonance, wave propagation is *stimulated* towards deeper parts. Then, amplifications are also controlled by surface waves. In fact, it can be shown by means of frequency–wave-number diagrams (f–$\mathbf{k}$, where $\mathbf{k} = \omega/c$ is the wave-number, c is the phase velocity) that the lateral resonant patterns are formed by surface waves.[36,37]

Figure 11 displays these results for the horizontal displacement amplitude u under vertical incidence of SV waves. The response pattern, even with the mode conversions that occur, is similar with fewer maxima than in the SH case. This can be explained considering the different behaviour of dispersion curves of Love and Rayleigh waves in this model (see Figure 13).

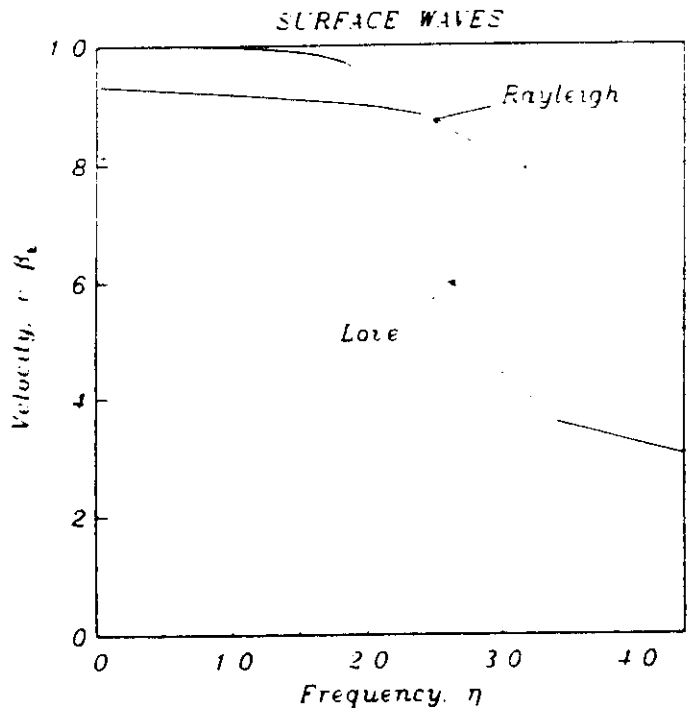

Figure 13. Dispersion curves of surface waves for a 1D model with a depth of 0·05 times the half-width of parabolic deposit and the same physical properties.

Although in these computations we have used a very small material damping ($Q = 500$), the results suggest that practical approximations can be found to describe the response of shallow, soft alluvial deposits in terms of surface waves. In fact, for flat alluvial basins, a simple approximation allows one to deal with 3D configurations, at least for small frequencies.[38]

Finally, we computed synthetic seismograms from frequency domain results by using the FFT algorithm. The time variation of an incoming wavefield is given by a Ricker wavelet with characteristic period $t_p = 0{\cdot}5t_0$, where $t_0 = 2a/\beta_E$. For an incidence angle $\gamma = 0$, Figure 14(a) and (b) shows the synthetics for SH and SV waves, respectively. These results can be combined to produce a quasi-3D response with the horizontal motion given by the inplane u and antiplane v components, respectively. Figure 15 shows the particle motion and polarigrams for sites across the valley when the polarization angle is $\theta = 60°$. The soft layer response produces rotating horizontal polarization patterns.

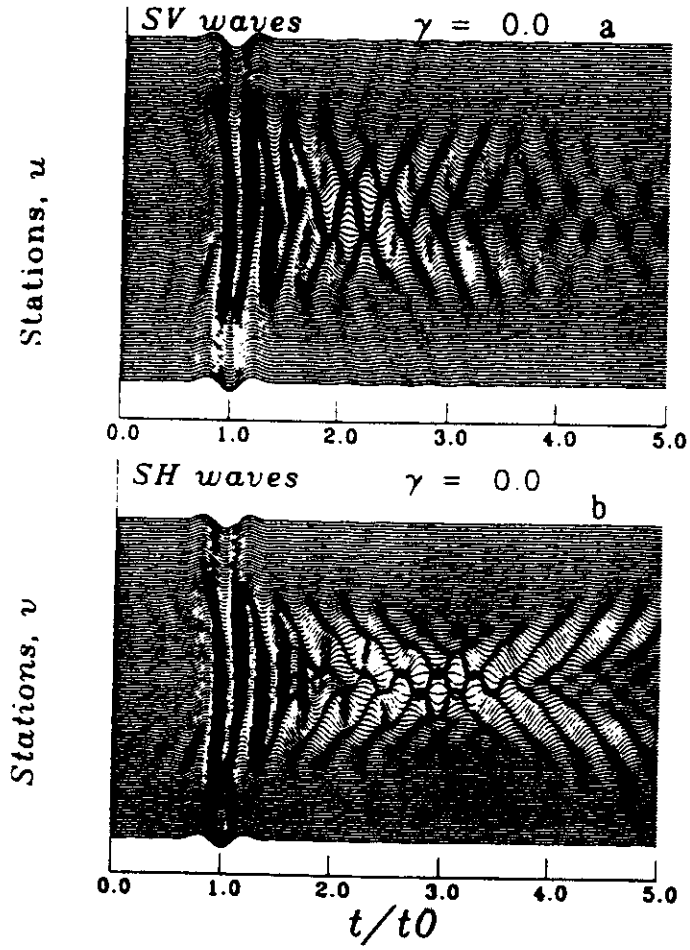

Figure 14. Synthetic seismograms $u(t)$ vs. $v(t)$ for incidence of (a) SV and (b) SH waves, respectively, in 51 stations (from $-1{\cdot}25a$ to $1{\cdot}25a$) across the surface of the 2D shallow parabolic valley. The incident time signal is a Ricker wavelet with central frequency $\omega_p = 2\pi\beta_E/a$.

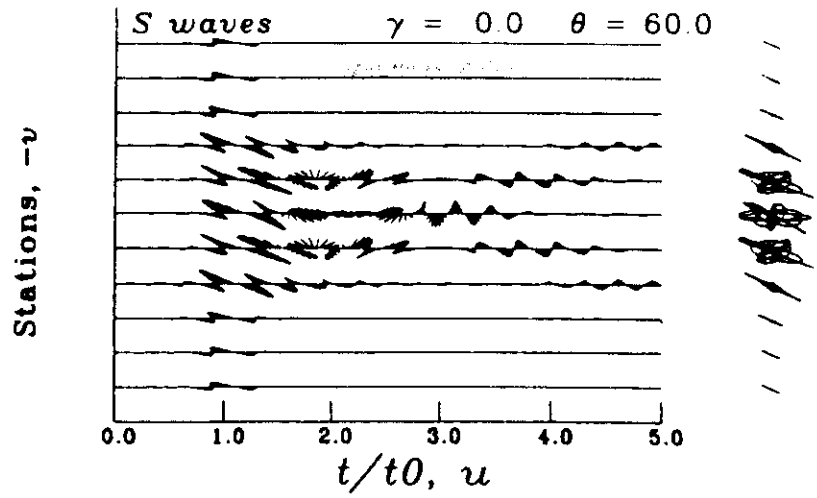

Figure 15. Horizontal polarigrams and particle motion for 11 stations (from $-1{\cdot}25a$ to $1{\cdot}25a$) across the 2D shallow parabolic valley model. Vertical incidence of S waves with polarization angle $\theta = 60°$.

CONCLUSIONS

An indirect boundary integral formulation for dynamic elasticity has been presented. It is based upon the integral representation of the diffracted elastic waves in terms of single-layer boundary sources. Although this approach is called indirect BEM in the literature, it provides far more insight into the physics of diffraction problems than does the direct approaches. This is because diffracted waves are constructed at the boundaries from which they are radiated. Therefore, this method can be regarded as a numerical realization of Huygens' principle. From boundary conditions, a system of integral equations for boundary sources is obtained. A discretization scheme based upon the numerical and analytical integration of *exact* Green's functions for displacements and tractions is used. In addition to the physical insight gained with this method, it appears to be accurate and fast.

Some examples are given for 2D problems of diffraction of elastic waves by soft elastic inclusion models of alluvial deposits in an elastic half-space. A semielliptical soft deposit was studied for incident Rayleigh waves and a complete set of results show that even a relatively mild heterogeneity can generate important variations in both amplitude and polarization of ground motion.

A very soft shallow deposit was analysed for incident SH and SV waves. Very large amplifications were found and the contour maps of transfer functions in the frequency–space domain (f–x) reveal a fine structure in which locally generated surface waves play a significant role for frequencies higher than the one that controls the 1D response at the centre. The maximum amplifications occur at the borders of a portion that grows with frequency. Such a frequency corresponds to the 'local' 1D shear model resonance. As wave propagation is *stimulated* towards deeper parts, amplifications are also controlled by surface waves. These results suggest that practical approximations can be found to describe the response of shallow, soft alluvial deposits in terms of surface waves, Love and Rayleigh for the SH and SV cases, respectively.

Finally, the responses in time domain are combined to produce a quasi-3D motion. As expected, the propagation of Love and Rayleigh surface waves interact and control the polarization of horizontal motion.

ACKNOWLEDGEMENTS

We express our thanks to M. Bonnet and two anonymous reviewers for their comments and suggestions. This work was partially supported by Departamento del Distrito Federal, Mexico, and by Consejo Nacional de Ciencia y Tecnologia, Mexico, under Grant P0523-T9109.

REFERENCES

1. F. J. Sánchez-Sesma, 'Site effects on strong ground motion', *Int. j. soil dyn. earthquake eng.* **6**, 124–132 (1987).
2. K. Aki, 'Local site effects on strong ground motion', in J. L. Von Thun (ed.), *Earthquake Engineering and Soil Dynamics II—Recent advances in ground motion evaluation*, Geotechnical Special Publication No. 20, Am. Soc. Civil Engr., New York, 1988, pp. 103–155.
3. P.-Y. Bard, M. Campillo, F. J. Chávez-García and F. J. Sánchez-Sesma, 'A theoretical investigation of large and small-scale amplification effects in Mexico City valley', *Earthquake spectra* **4**, 609–633, (1988).
4. M. Campillo, J. C. Gariel, K. Aki and F. J. Sánchez-Sesma, 'Destructive strong ground motion in Mexico city: source, path, and site effects during great 1985 Michoacan earthquake', *Bull. seism. soc. Am.* **6**, 1718–1735 (1989).
5. F. J. Sánchez-Sesma, S. Chávez-Perez, M. Suárez, M. A. Bravo and L. E. Pérez-Rocha, 'On the seismic response of the Valley of Mexico', *Earthquake spectra* **4**, 569–589 (1988).
6. A. S. Papageorgiou and J. Kim, 'Study of the propagation and amplification of seismic waves in Caracas Valley with reference to the 29 July 1967 earthquake: SH waves', *Bull. seism. soc. Am.* **81**, 2214–2233 (1991).
7. S. Kobayashi, Elastodynamics, in D. E. Beskos (ed.), *'Boundary Element Methods in Mechanics'*, North-Holland, Amsterdam, 1987.
8. G. D. Manolis and D. E. Beskos, *Boundary Element Methods in Elastodynamics*, Unwin Hyman, London, 1988.
9. K. Aki and K. L. Larner, 'Surface motion of a layered medium having an irregular interface due to incident plane SH waves', *J. geophys. res.* **75**, 1921–1941 (1970).
10. P.-Y. Bard and M. Bouchon, 'The seismic response of sediment-filled valleys. Part 1. The case of incident SH waves', *Bull. seism. soc. Am.* **70**, 1263–1286 (1980).
11. P.-Y. Bard and M. Bouchon, 'The seismic response of sediment-filled valleys. Part 2. The case of incident P and SV waves', *Bull. seism. soc. Am.* **70**, 1921–1941 (1980).
12. P.-Y. Bard and M. Bouchon, 'The two-dimensional resonance of sediment-filled valleys', *Bull. seism. soc. Am.* **75**, 519–554 (1985).
13. M. Bouchon and K. Aki, 'Discrete wave-number representation of seismic-source wave fields', *Bull. seism. soc. Am.* **67**, 259–277 (1977).
14. M. Bouchon, M. Campillo and S. Gaffet, 'A boundary integral equation-discrete wavenumber representation method to study wave propagation in multilayered media having irregular interfaces', *Geophysics* **54**, 1134–1140 (1989).
15. H. Kawase and K. Aki, 'A study on the response of a soft basin for incident S, P and Rayleigh waves with special reference to the long duration observed in Mexico City', *Bull. seism. soc. Am.* **79**, 1361–1382 (1989).
16. L. Zhang and A. K. Chopra, 'Three-dimensional analysis of spatially varying ground motions around a uniform canyon in homogeneous half-space', *Earthquake eng. struct. dyn.* **20**, 911–926 (1991).
17. F. J. Sánchez-Sesma and J.A. Esquivel, 'Ground motion on alluvial valleys under incident plane SH waves', *Bull. seism. soc. Am.* **69**, 1107–1120 (1979).
18. J. E. Luco, H. L. Wong and F. C. P. De Barros, 'Three-dimensional response of a cylindrical canyon in a layered half-space', *Earthquake eng struct. dyn.* **19**, 799–817 (1990).
19. F. J. Sanchez-Sesma and M. Campillo, 'Diffraction of P, SV and Rayleigh waves by topographical features: a boundary integral formulation', *Bull. seism. soc. Am.* **81**, 2234–2253 (1991).
20. J. Ramos-Martinez and F. J. Sanchez-Sesma, 'Respuesta sismica de valles aluviales usando ecuaciones integrales', *Proc. IX Congreso Nacional de Ingenieria Sismica* Manzanillo, Colima, Mexico, October 1991, Vol. 7, pp. 289–298.
21. L. Auersch and G. Schmid, 'A simple boundary element formulation and its application to wavefield excited soil-structure interaction', *Earthquake eng. struct. dyn.* **19**, 931–947 (1990).
22. M. D. Trifunac, 'Surface motion of a semi-cylindrical alluvial valley for incident plane SH waves', *Bull. seism. soc. Am.* **61**, 1755–1770 (1971).
23. M. Dravinski and T. K. Mossessian, 'Scattering of plane harmonic P, SV and Rayleigh waves by dipping layers of arbitrary shape', *Bull. seism. soc. Am.* **77**, 212–235 (1987).
24. V. D. Kupradze, *Dynamical problems in elasticity*, in I. N. Sneddon and R. Hill (eds), *Progress in Solid Mechanics, Vol. III*, North-Holland, Amsterdam, 1963.
25. L. Kouoh-Bille, F. J. Sánchez-Sesma and A. Wirgin, 'Response resonante d'une montagne cylindrique a une onde sismique SH', *C. R. acad. sci. Paris* **312** serie II, 849–854 (1991).
26. A. G. Webster, *Partial Differential Equations in Mathematical Physics*, Dover, New York, 1955.
27. M. Bonnet, 'Méthode des equationes integrales regularisees en elastodynamique', Ph.D. Thesis, Ecole Nationale des Ponts et Chaussees, Paris, 1986.
28. M. Abramowitz and I. A. Stegun, *Handbook of Mathematical Functions*, Dover, New York, 1972.
29. H. L. Wong, 'Effect of surface topography on the diffraction of P, SV and Rayleigh waves', *Bull. seism. soc. Am.* **72**, 1167–1183 (1982).
30. F. J. Sánchez-Sesma, M. A. Bravo and I. Herrera, 'Surface motion of topographical irregularities for incident P, SV and Rayleigh waves', *Bull. seism. soc. Am.* **75**, 263–269 (1985).
31. H. Kawase, 'Time-domain response of a semicircular canyon for incident SV, P, and Rayleigh waves calculated by the discrete wavenumber boundary element method', *Bull. seism. soc. Am.* **78**, 1415–1437 (1988).
32. J. A. Rial, 'Seismic waves resonances in 3-D sedimentary basins', *Geophys. j. int.* **99**, 81–90 (1989).
33. P.-Y. Bard and M. Bouchon, 'The two-dimensional resonance of sediment-filled valleys', *Bull. seism. soc. Am.* **75**, 519–542 (1985).
34. P. Bernard and A. Zollo, 'Inversion of near-source S polarization for parameters of double-couple point sources', *Bull. seism. soc. Am.* **79**, 1779–1809 (1989).

35. H Ling and J A. Rial. 'Computing SH-wave eigenmodes in arbitrary shaped alluvial valleys by approximate Poincare maps'. *Geophys. j. int.* (1992) (submitted).
36. J. Ramos-Martinez, F. J Sánchez-Sesma and L. E. Pérez-Rocha, 'Resonance characteristics of shallow alluvial valleys', *Proc. of int. symp. earthq disast. prev.*, Mexico City, Mexico, 1992.
37. J. Ramos-Martinez, 'Simulación numérica de la respuesta sísmica de valles aluviales', *M. S. Thesis*. Posgrado en Geofísica, Instituto de Geofísica, UNAM, 1992.
38. F. J. Sánchez-Sesma, J. L. Rodriguez-Zuñiga, L. E. Pérez-Rocha, D. A. Álvarez-Cuevas and M. Suarez, 'The seismic response of shallow alluvial valleys using a simplified model', *Proc. of int. symp. earthq. disast. prev.*, Mexico City, Mexico, 1992.

Bulletin of the Seismological Society of America, Vol. 84, No. 4, pp. 1169–1183, August 1994

Three-Dimensional Scattering by Two-Dimensional Topographies

by H. A. Pedersen, F. J. Sánchez-Sesma, and M. Campillo

Abstract Three-dimensional seismic responses of two-dimensional topographies are studied by means of the indirect boundary element method (IBEM). The IBEM yields, in the presented form, very accurate results and has the advantage of low computational cost. In IBEM, diffracted waves are constructed in terms of single-layer boundary sources. The appropriate Green's functions used are those of a harmonic point force moving along the axis of the topography in a full space. Obtained results are compared against those published by other authors. Examples of simulations are presented for different geometries, for different types of incident wave fields, and, in particular, for different arrival angles to the topography to quantitatively study three-dimensional effects of the scattering. The accuracy of the results makes it possible to analyze them in both the time and frequency domains. Frequency-space representations allow identification of diffraction and interference patterns in the seismic response of the topography. Synthetic seismograms are obtained by Fourier analysis. Using time-space domain representations, the nature of each of the scattered waves are identified in terms of, for example, creeping waves and reflected compressional waves.

Introduction

Surface topography has been reported to produce significant site effects (e.g., Davis and West, 1973; Griffiths and Bollinger, 1979; Bard and Tucker, 1985). These effects take the form of a relative amplification of seismic signals recorded at the top of a mountain with respect to a reference station located at the base of the mountain. The relative amplification can be significant over a large frequency interval. Knowledge of these effects is important for the prediction of ground movement close to topographic features.

Two-dimensional topographic effects on wave fields have been numerically modeled by a number of authors. Analytical solutions have been found for simple geometries (Trifunac, 1973; Lee and Cao, 1989; Todorovska and Lee, 1990, 1991). Bouchon (1973), Bard (1982), and Geli *et al.* (1988) have used techniques based on the method proposed by Aki and Larner (1970) to model topographic effects. A large number of simulations have been performed with techniques based on representation theorems. These methods include the direct boundary element method (BEM) (Wong and Jennings, 1975; Zhang and Chopra, 1991), the indirect boundary element method (IBEM) (Sánchez-Sesma and Rosenblueth, 1979; Wong, 1982; Luco *et al.*, 1990; Sánchez-Sesma and Campillo, 1991, 1993), and combinations of integral representations with discrete wavenumber expansions of Green's functions (Bouchon, 1985; Kawase, 1988; Pei and Papageorgiou, 1993a). While BEM directly finds the unknown tractions and displacements, IBEM searches a force distribution for which the radiated field satisfies the boundary conditions. Displacements are obtained by superposition of the radiation from these sources. A more detailed discussion of the use of these methods in site effect simulations can be found in Sánchez-Sesma and Campillo (1993).

While theoretical models predict significant scattering by topographies, they have not yet quantitatively explained observations (e.g., Bard and Tucker, 1985; Geli *et al.*, 1988). Some observations seem to show both higher and more broadband amplification than predicted by numerical simulations. To evaluate whether topographic effects alone can account for the observed amplifications, it is necessary to extend the numerical simulation to geologically more realistic models, taking into account the three-dimensional character of real topographies and the presence in nature of all types of incident wave fields.

Different attempts have been made to extend the simulation of scattering by two-dimensional structures from pure two-dimensional scattering (incident wave field perpendicular to the structure) to three-dimensional scattering (incident wave field with an arbitrary arrival angle to the structure). In particular, to study the diffraction by a canyon, Luco *et al.* (1990) use IBEM and locate

55

sources off the surface of the canyon to displace singularities in the Green's functions from the surface. In this approach, sources must be carefully located to avoid numerical problems and the location off the surface leads to an approximate solution. Pei and Papageorgiou (1993a) simulate the scattered wave field across a canyon by using half-space Green's functions to solve the boundary integral equation on the surface itself. While more accurate, the latter method has a high computational cost as a result of the calculation of half-space Green's functions. Three-dimensional scattering by two-dimensional structures has also been treated in the case of alluvial valleys (Khair *et al.*, 1989; Khair *et al.*, 1991; Liu *et al.*, 1991; Pei and Papageorgiou, 1993b).

In this article we present a method to simulate three-dimensional scattering by ridge and canyon structures of arbitrary shapes. The IBEM, with full space Green's functions, is used to create the scattered wave field. By using compact expressions of Green's functions appropriate to the problem, highly accurate results are produced for a low computational cost. The method, therefore, makes it possible to perform a large number of simulations for the study of how different parameters influence the scattering and for the study of three-dimensional effects due to the obliquely incident waves. It is possible, in particular, to quantitatively model observed site effects on topographies because the arrival angle of the incident waves on the structure can be taken into account.

The article is organized as follows: first, a brief introduction is given to IBEM, and then compact expressions for Green's functions are derived for use in the simulations. The theoretical part is concluded by a discussion of the implementation of the method. Results from applying the method are compared against those from other approaches, and finally, examples are presented of simulations performed for simple geometries.

Integral Representation of Elastic Wave Fields

The IBEM is based on an integral representation of wave fields. Neglecting body forces, the displacement field in a domain V with boundary S occupied by an elastic material can be written (see Sánchez-Sesma and Campillo, 1991)

$$u_i(\mathbf{x}) = \int_s \psi_j(\zeta)\, G_{ij}(\mathbf{x}, \zeta) dS_\zeta, \qquad (1)$$

where $u_i(x)$ is the ith component of displacement at $\mathbf{x}$. The term $G_{ij}(\mathbf{x}, \zeta)$ is the Green's function; i.e., the displacement in direction i at $\mathbf{x}$ due to a point force in direction j applied at the point ζ; $\psi_j(\zeta)$ is the force density in direction j at ζ. The term $\psi_j(\zeta)dS_\zeta$ is therefore a force distribution on S. The integration is performed over the space variable ζ.

Equation (1) shows that if G_{ij} is known, one simply needs to find the force density ψ_j on the surface S to calculate the displacement at any point in V. Furthermore, the displacement field is continuous across S if ψ_j is continuous on S (Kupradze, 1963). When displacements u_i are known, it is possible to calculate stresses and tractions by applying Hooke's law. Special care must be taken at boundary singularities. The contribution of the singularity to the traction equals half the surface force applied, assuming a smooth boundary (e.g., Kupradze, 1963),

$$t_i(\mathbf{x}) = c\psi_i(\mathbf{x}) + \int_s \psi_j(\zeta) T_{ij}(\mathbf{x}, \zeta) dS_\zeta, \qquad (2)$$

where $t_i(\mathbf{x})$ is the ith component of traction at $\mathbf{x}$; c equals 0 if $\mathbf{x}$ is outside S, c equals $1/2$ if $\mathbf{x}$ tends to S from the inside of V, and c equals $-1/2$ if $\mathbf{x}$ tends to S from the outside of V. $T_{ij}(\mathbf{x}, \zeta)$ is the traction Green's function; i.e., the traction in direction i at point $\mathbf{x}$ of a point source in direction j applied at point ζ. The T_{ij} is found by application of Hooke's law to equation (1).

In the following sections, the displacement and traction Green's functions are first derived for use in finding the three-dimensional scattered field for a two-dimensional structure. Then, the procedure used to solve the problem of three-dimensional scattering by a two-dimensional topography is defined.

Green's Functions for Moving Point Sources in an Elastic Medium

The geometry of the problem is shown in Figure 1. A two-dimensional structure that is infinite in the di-

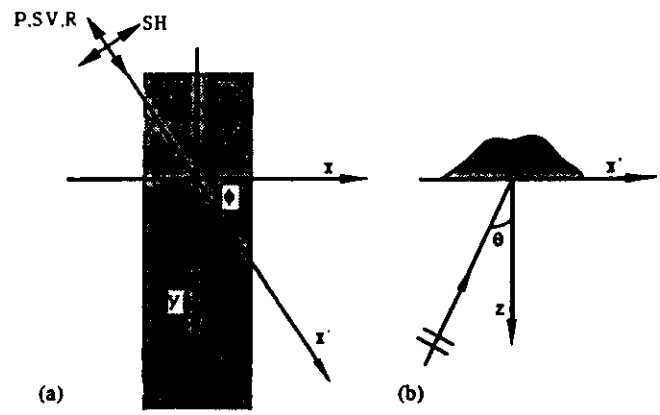

Figure 1. Geometry of the problem of scattering by two-dimensional topographies. (a) Horizontal plane; definition of azimuth ϕ. (b) Vertical plane; definition of incidence angle θ.

rection of the y axis is considered. The problem of three-dimensional scattering of plane waves by a two-dimensional structure is somewhat simpler than the full three-dimensional problem; at two cross sections perpendicular to the y axis the wave field will be identical but shifted in time. Point sources moving parallel to the y axis are therefore used to represent the diffracted field. This approach has also been used by Luco *et al.* (1990). The incoming wave arrives with an azimuth ϕ relative to the structure and an incidence θ to the vertical axis (see Fig. 1). It propagates with a velocity c. The wave has an apparent velocity c' along the y axis

$$c' = \frac{c}{\sin \phi \sin \theta} \tag{3}$$

The scattered wave field can be expressed by point sources that move parallel to the y axis with a constant velocity c' along the interfaces of the model. In the case of a topography, the point sources move along the free surface.

To derive compact expressions for traction and displacement Green's functions for these moving point sources, one can start by solving the same problem for an acoustic medium. The solution g' to the inhomogeneous scalar wave equation for a fixed point source at the origin is given by

$$g' = \exp(i\omega t) \frac{\exp(-ikr)}{r}, \tag{4}$$

where ω is the circular frequency, $k = \omega/V$ is the wavenumber, V is the acoustic wave propagation velocity, and r is the distance to the point source. This scalar Green's function can be expressed with a decomposition into plane waves (Weyl integral, see Aki and Richards, 1980)

$$g' = \exp(i\omega t) \frac{1}{2\pi} \cdot \int_{-\infty}^{\infty} \int_{-\infty}^{\infty} \frac{\exp(-ik_x x - ik_y y - \gamma|z|)}{\gamma} dk_x dk_y, \tag{5}$$

where k_x and k_y denote the x and y components of the wavenumber $\mathbf{k} = (k_x, k_y, i\gamma)^T$. The vertical wavenumber γ is defined as

$$\gamma = \sqrt{[k_x^2 + k_y^2 - (\omega/V)^2]} \quad \text{real}(\gamma) \geqq 0. \tag{6}$$

The Green's function g is searched for a moving point source. To obtain g, the influence of the source is integrated over all positions ϵ along the y axis, taking into account the position of the source:

$$g = \int_{-\infty}^{\infty} d\epsilon \exp\left(i\omega\left(t - \frac{\epsilon}{c'}\right)\right) \frac{1}{2\pi} \cdot \int_{-\infty}^{\infty} \int_{-\infty}^{\infty} \frac{\exp(-ik_x x - ik_y(y - \epsilon) - \gamma|z|)}{\gamma} dk_x dk_y. \tag{7}$$

Integration over the space variable ϵ and substitution of v as ω/c' gives

$$g = \int_{-\infty}^{\infty} \int_{-\infty}^{\infty} \delta(v - k_y) \cdot \exp(-ik_y y) \frac{\exp(-ik_x x - \gamma|z|)}{\gamma} dk_x dk_y, \tag{8}$$

ignoring the factor $\exp(i\omega t)$. Integration over k_y yields

$$g = \int_{-\infty}^{\infty} \frac{\exp[-ik_x x - iv y - \sqrt{k_x^2 + (\omega/c')^2 - (\omega/V)^2}|z|]}{\sqrt{k_x^2 + (\omega/c')^2 - (\omega/V)^2}} dk_x. \tag{9}$$

Rearrangement of equation (9) leads to

$$g = i \exp(-iv y) \cdot \int_{-\infty}^{\infty} \frac{\exp[-ik_x x - i\sqrt{(\omega/V)^2 - k_x^2 - v^2}|z|]}{\sqrt{(\omega/V)^2 - k_x^2 - v^2}} dk_x \tag{10}$$

with

$$Im[\sqrt{(\omega/V)^2 - k_x^2 - v^2}] \leqq 0.$$

This integral is the plane wave decomposition of the wave field radiated by a moving point source. It can be expressed using Lamb's (1904) representation for Hankel functions as

$$g = \pi i \exp(-iv y) H_0^{(1)}(\sqrt{k^2 - v^2} R) \tag{11}$$

with

$$R = \sqrt{(x - x')^2 + (z - z')^2}, \tag{12}$$

where (x', z') is the source location in the $(x - z)$ plane.

It is possible to express directly the equivalent of equation (11) for an elastic material with density ρ by (Morse and Feshbach, 1953; Pao and Varatharajulu, 1976)

$$G_{ij}(\mathbf{x}, \zeta) = \frac{1}{4\pi\rho\omega^2}\left\{k_s g_s(\mathbf{x}, \zeta)\delta_{ij} + \frac{\delta^2}{\delta x_i \delta x_j}[g_p(\mathbf{x}, \zeta) - g_s(\mathbf{x}, \zeta)]\right\}, \quad (13)$$

where indices s and p refer to shear and compressional waves, respectively.

The insertion of equation (12) in equation (13) gives the required displacement Green's functions. As discussed earlier, traction Green's functions can be obtained by applying Hooke's law. The compact expressions for the Green's functions are given in the Appendix.

These expressions were validated by comparison with well-known expressions of Green's functions in three dimensions. The spatial Fourier transform over y of the latter provides $G_{ij}(x, k_y, z, \omega)$ by replacing k_y by ω/c'.

Implementation of the Method

In implementing the method, the total wave field is assumed to be the superposition of the diffracted field and the "free field" u°; i.e., the field in the absence of the irregularity. The definition of the free field is addressed later in this section.

Under this assumption, equation (1) becomes

$$u_i(\mathbf{x}) = u_i^\circ(\mathbf{x}) + \int_s \psi_j(\zeta) G_{ij}(\mathbf{x}, \zeta)\, dS_\zeta. \quad (14)$$

At the free surface, tractions vanish. Denoting tractions of the free field t°, this condition gives

$$\frac{1}{2}\psi_i(\mathbf{x}) + \int_s \psi_j(\zeta) T_{ij}(\mathbf{x}, \zeta)\, dS_\zeta = -t_i^\circ(\mathbf{x}). \quad (15)$$

This continuous integral must be replaced by a discrete one for computer-based analysis. Again, the methodology of Sánchez-Sesma and Campillo (1991) was followed: the surface is discretized into N segments of equal length Δs. For each frequency, N is chosen so that Δs is much smaller than the wavelength of the shear waves. Consequently, the force density $\psi_i(\mathbf{x})$ is chosen to be constant on each of the segments. Testing of the discretization parameters showed that five segments per wavelength is sufficient to ensure accurate results. A finite portion of the surface is discretized. A discretization of five times the length L of the irregularity, as used in the results presented here, yielded results within a few percent of those obtained by discretizing $3L$ of the surface.

A discrete version of equation (15) can be used to find the surface force $\psi_i(\zeta_l)$ on each segment. The evaluation of the traction at the center of each segment leads to the system of linear equations

$$\sum_{l=1}^{N} \psi_j(\zeta_l) t_{ij}(\mathbf{x}_n, \zeta_l) = -t_i^\circ(\mathbf{x}_n) \quad n = 1, N \quad (16)$$

where

$$t_{ij}(\mathbf{x}_n, \zeta_l) = \frac{1}{2}\delta_{ij}\delta_{nl} + \int_{\zeta_l - \Delta s/2}^{\zeta_l + \Delta s/2} T_{ij}(\mathbf{x}_n, \zeta_l) dS_\zeta \quad (17)$$

The integral in equation (17) is evaluated by Gaussian integration, except when $n = l$. In this particular case, it is calculated analytically by using ascending series for Bessel functions (e.g., Abramowitz and Stegun, 1972).

Once $\psi_i(\zeta_l)$ has been found by resolution of the system of equations (16), the displacement at any point can be evaluated by the following discrete equivalent of equation (14):

$$u_i(\mathbf{x}) = u_i^\circ(\mathbf{x}) + \sum_{l=1}^{N} \psi_j(\zeta_l) g_{ij}(\mathbf{x}, \zeta_l), \quad (18)$$

where

$$g_{ij}(\mathbf{x}, \zeta_l) = \int_{\zeta_l - \Delta s/2}^{\zeta_l + \Delta s/2} G_{ij}(\mathbf{x}, \zeta_l) dS_\zeta. \quad (19)$$

If $\mathbf{x}$ is located on the surface, the integral is again evaluated by analytical expressions over the segment on which $\mathbf{x}$ is located. Gaussian integration is used on other segments.

This section is concluded by a short discussion of the definition of the free fields u° and t°. In the examples presented in the next sections, a free field is used that includes the reflection of the incoming wave on the free surface of the half-space. For ridges, this field is extended analytically to the points on the ridge that are located outside the reference half-space. This procedure has the advantage of reducing boundary effects due to the truncation of the model; the surface forces ψ_i will decrease in amplitude toward the limits of the model because the effect of the irregularity decreases. On the other hand, the analytically extended field is both nonphysical and noncausal. For strongly antisymmetrical ridges, we encounter problems in the form of noncausal arrivals when we use the half-space reference field. Use of the full space free field solves these problems but introduces artifacts in the form of reflections on the boundary of the model.

For canyons, analytical expressions for Rayleigh waves are used to define the free field. The problem of defining the free field for incoming Rayleigh waves on ridges is not addressed, as the exponential decrease with depth of the amplitude of Rayleigh waves leads to numerical problems for high frequencies when the analyt-

ical expression is extended upward. For the two-dimensional case, the Rayleigh waves can be simulated by a vertical point load applied far from the topographic relief (Sánchez-Sesma and Campillo, 1991).

Validation of the Method

The two-dimensional case is a limiting case of the method ($\phi = 0°$). In this case, the Green's functions listed in the Appendix are equivalent to well-known two-dimensional compact expressions for Green's functions (e.g., Sánchez-Sesma and Campillo, 1991). Our results agree with those of Sánchez-Sesma and Campillo (1991) for the two-dimensional case where the two methods are strictly equivalent. As Sánchez-Sesma and Campillo (1991) have compared their results to those of other authors, the two-dimensional case is not addressed further here, and the reader is referred to Sánchez-Sesma and Campillo (1991).

Literature on three-dimensional scattering by two-dimensional topographies is scarce. We compared our results with those of Luco *et al.* (1990) using the model depicted in Figure 2. The topographic irregularity is a semi-circular canyon of radius a in a homogeneous half-space. The half-space is characterized by a shear-wave velocity β and a compressional-wave velocity $\alpha = 2\beta$. Figure 3 shows the comparison with Luco *et al.* for an incident P wave arriving with an azimuth of 45° and an incidence angle of 45° for three normalized frequencies η where

$$\eta = \frac{\omega a}{\pi \beta}. \tag{20}$$

For $\eta = 1$, the shear wavelength equals the diameter of the canyon.

The agreement between our results and those of Luco *et al.* (1990) is generally good. Especially at low frequencies, the agreement is excellent, while small differences arise at higher frequencies. The level of amplification and deamplification are slightly different across the topography, while the general shape of the curves is similar.

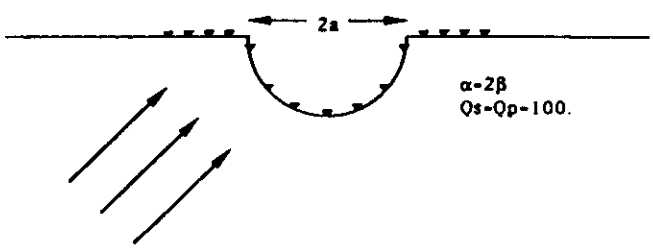

Figure 2. Model of the semi-circular canyon used in the simulations.

Numerical Results

Parameters for simulations of a wave field scattered by a two-dimensional topography include the geometry, the elastic parameters of the model, the type of the incident plane wave (P, SV, SH, Rayleigh), its azimuth ϕ, and incidence θ with respect to the z axis. Simulations were performed for incident P, SV, SH, and Rayleigh waves (except for Rayleigh waves incident on a ridge). Selected results are presented here for simulations with two simple geometries (semi-circular canyon, semi-circular ridge) and two types of incident waves (P and SV waves). Results will be presented in both the space-time (x, t) and in the space-frequency (x, η) domains for $-2 \leqq x/a \leqq 2$, where a is the radius of the canyon or the ridge. The normalized frequency η, defined previously, is used. Simulations were carried out between $\eta = 0$ and $\eta = 6.4$. Traces in time were obtained by convolution with a Ricker wavelet of central frequency $\eta = 2$, fol-

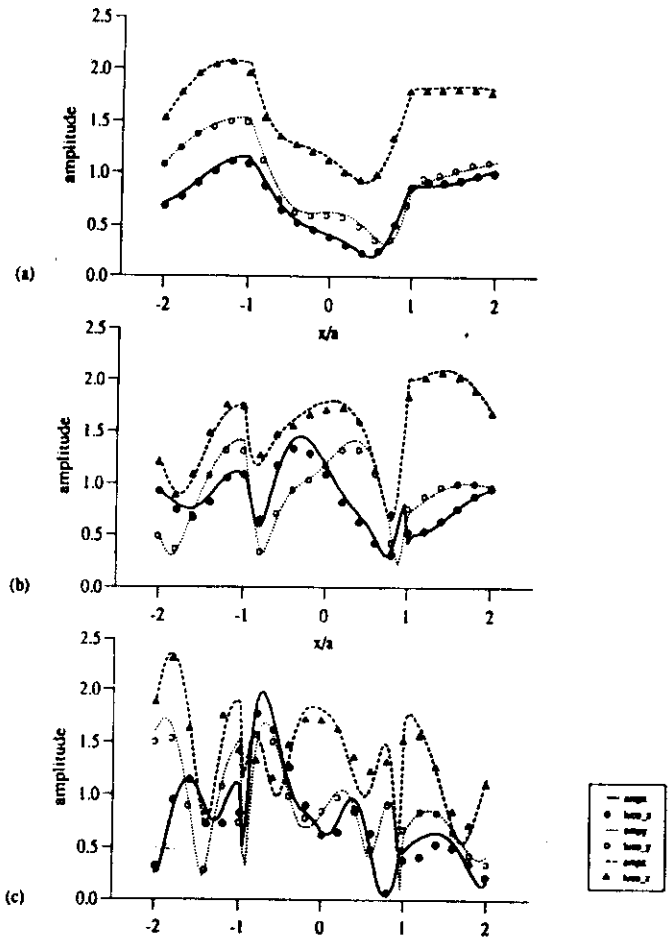

Figure 3. Example of comparison of obtained results with those of Luco *et al.* (1990). Continuous lines, dotted lines, and dashed lines; our results. Solid circles, open circles, and triangles; Luco *et al.* (1990). (a) $\eta = 0.5$, (b) $\eta = 1$, and (c) $\eta = 2$.

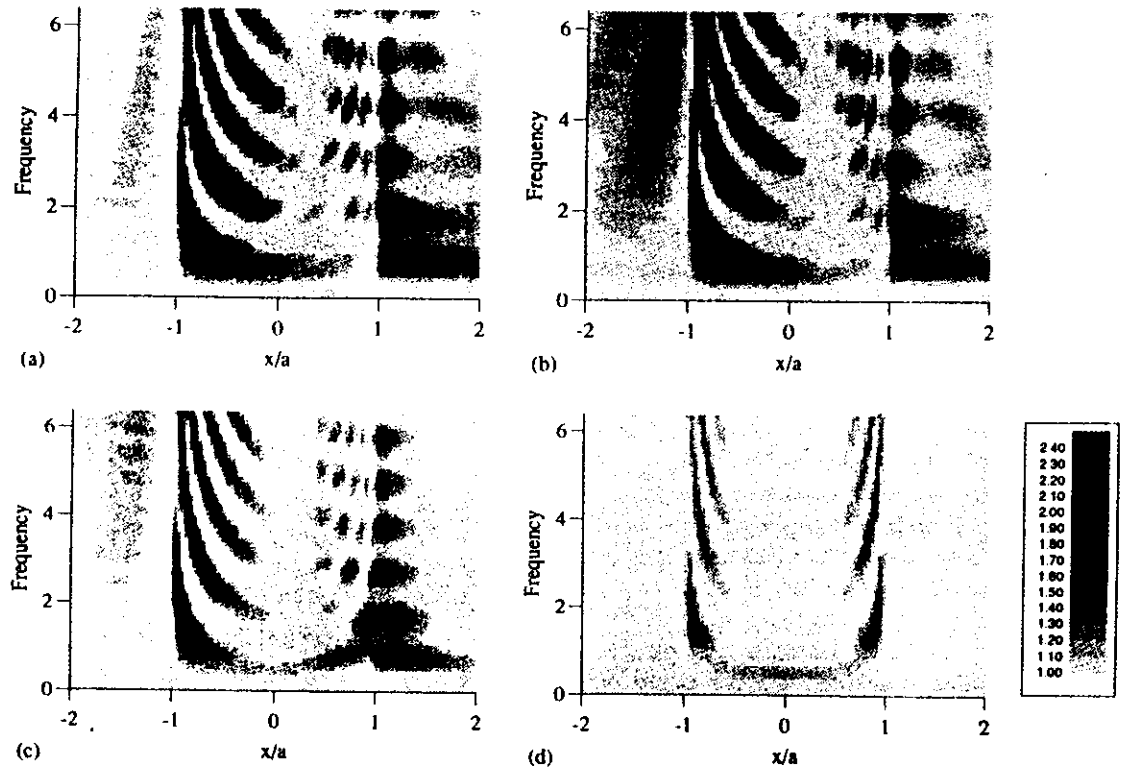

Figure 4. Spectral amplitude of total horizontal displacements across the semi-circular canyon. Incident wave field, *SV* wave with $\theta = 45°$. (a) $\phi = 0°$, (b) $\phi = 30°$, (c) $\phi = 60°$, and (d) $\phi = 90°$.

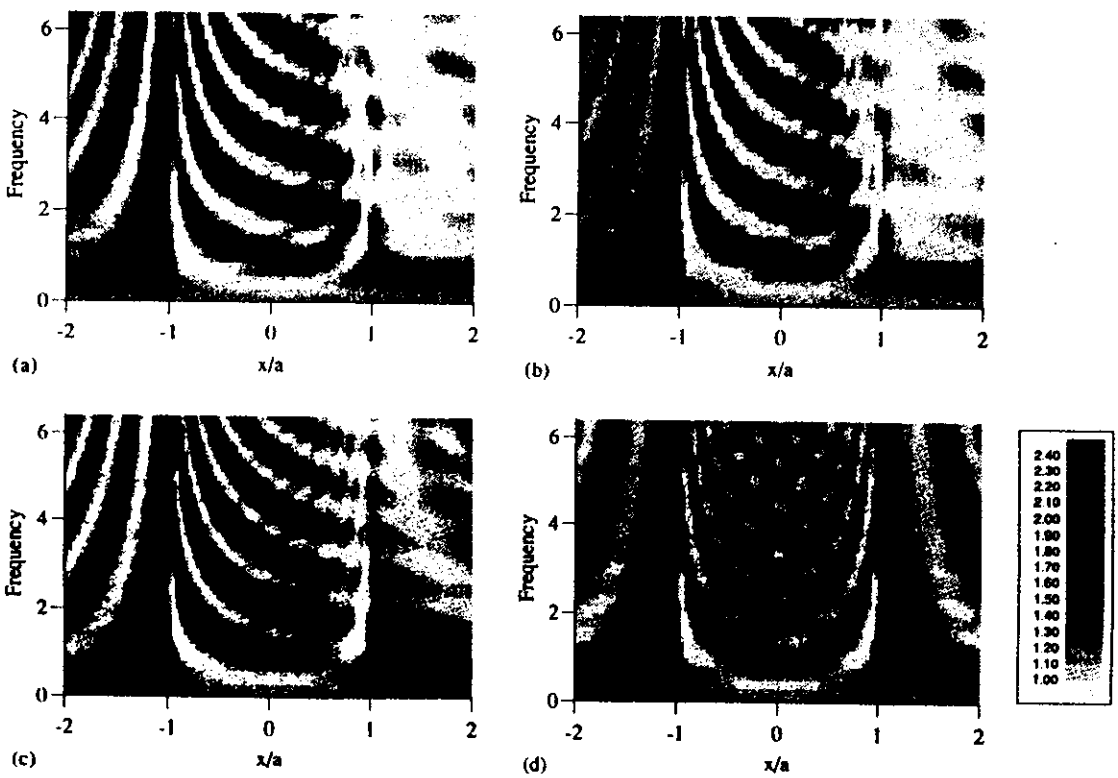

Figure 5. Same as Figure 4 for vertical displacements.

lowed by an inverse Fourier transform. The amplitude scale is the same in all synthetic seismograms shown in this article.

Semi-Circular Canyon

In the case of the semi-circular canyon, the model presented in Figure 2 was used with only one difference compared to the previous simulations: in the following, the quality factor for shear and compressional waves is 1000. Figures 4 and 5 show the (x, η) image of the wave field across the canyon for an incident SV wave with incidence $\theta = 45°$ and differing azimuths ($\phi = 0°$, 30°, 60°, and 90°). Figure 4 shows the total horizontal displacement and Figure 5 the vertical displacement.

As the azimuth increases, the amplitude of the scattering changes. Figures 4 and 5 show that for small and intermediate azimuths ($\phi \leqq 60°$), it is dominated by scattering generated by the edge of the canyon at $x/a = -1$. The vertical displacement for $\phi = 90°$ shows clearly how the scattered field across the canyon is the result of interference between scattered waves generated at the edges. Spectral amplitudes generally seem to decrease as the azimuth of the incident wave increases.

The synthetic seismograms for the four azimuths (Figs. 6 through 9) show that the scattered field is mainly composed of creeping waves across the canyon, while outside the canyon the scattered waves are mostly Rayleigh waves and waves reflected by the surface of the canyon. The general image seems to be the same for all azimuths, but the relative amplitudes and the apparent velocity of the diffracted waves are strongly dependent on the azimuth. Diffraction is less for an azimuth of 90°, but amplitudes can nevertheless be high at specific points because of the interference of waves. Even when the incident wave field has displacements only along the y and z axis, the scattered field has significant displacements on the x component.

The apparent velocity of the diffracted waves can be understood by considering the meaning of c', the apparent velocity along the y axis, in a simplified way using Huygen's principle. The c' can take any value between c_R and infinity, where c_R is the Rayleigh wave velocity in the half-space. The source emits S and P waves, with velocities c_β and c_α. If c' is greater than c_α, the field of the moving point source corresponds to supersonic waves. This situation is illustrated in Figure 10a. The resulting wave front moves with an angle ϕ' to the y axis, where

$$\cos \phi' = \frac{c_{\alpha,\beta}}{c'} = \frac{c_{\alpha,\beta}}{c} \sin \theta \sin \phi. \qquad (21)$$

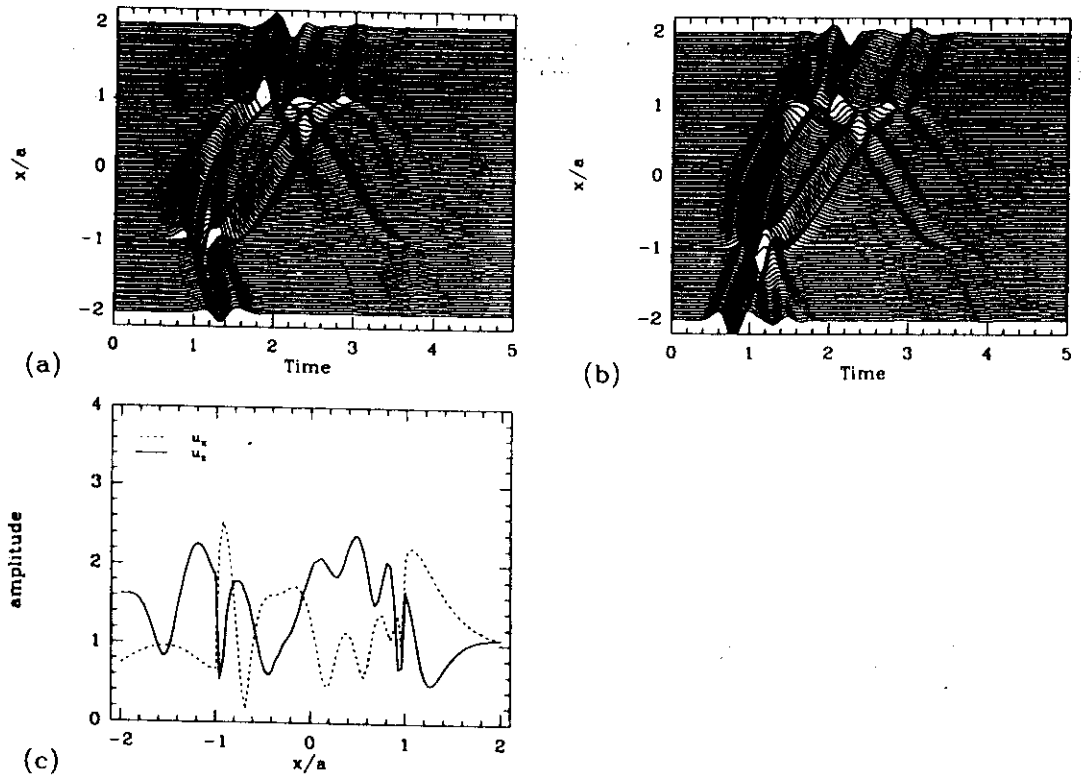

Figure 6. Displacement amplitudes across a semi-circular canyon. Incident wave field, SV wave with $\phi = 0°$ and $\theta = 45°$. (a) Synthetic seismograms, u_x, (b) synthetic seismograms, u_z, and (c) spectral amplitudes for $\eta = 2$.

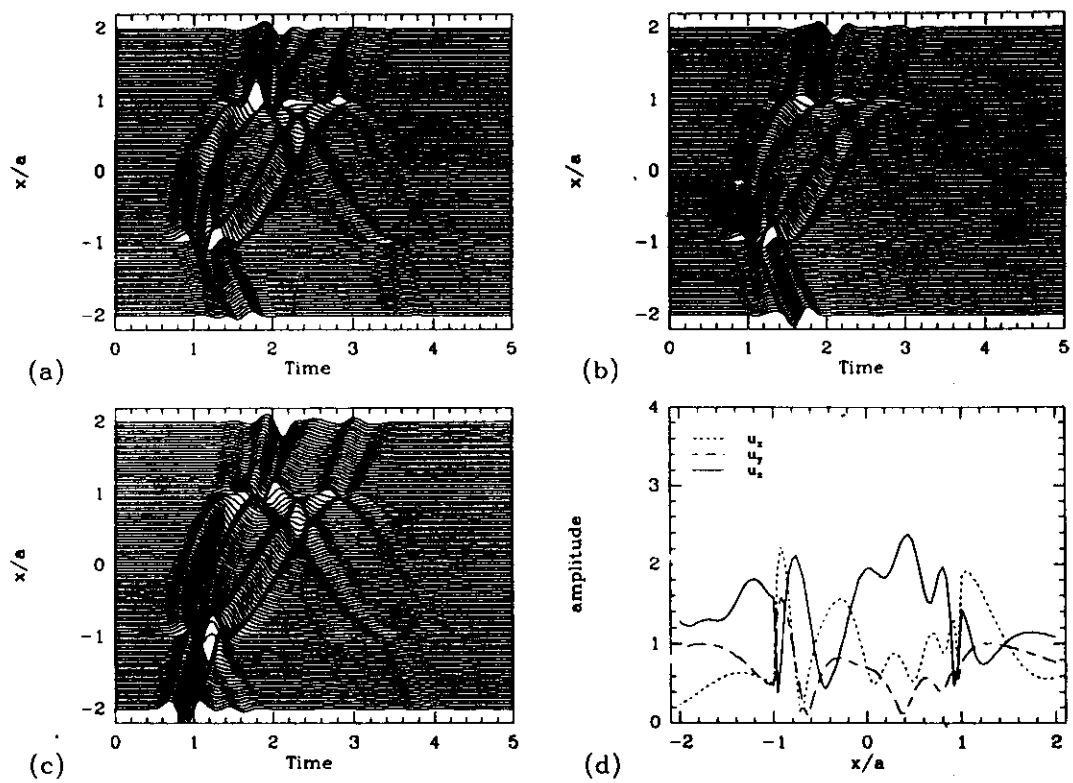

Figure 7. Same as Figure 6 with $\phi = 30°$. (a) Synthetic seismograms, u_x, (b) synthetic seismograms, u_y, (c) synthetic seismograms, u_z, and (d) spectral amplitudes for $\eta = 2$.

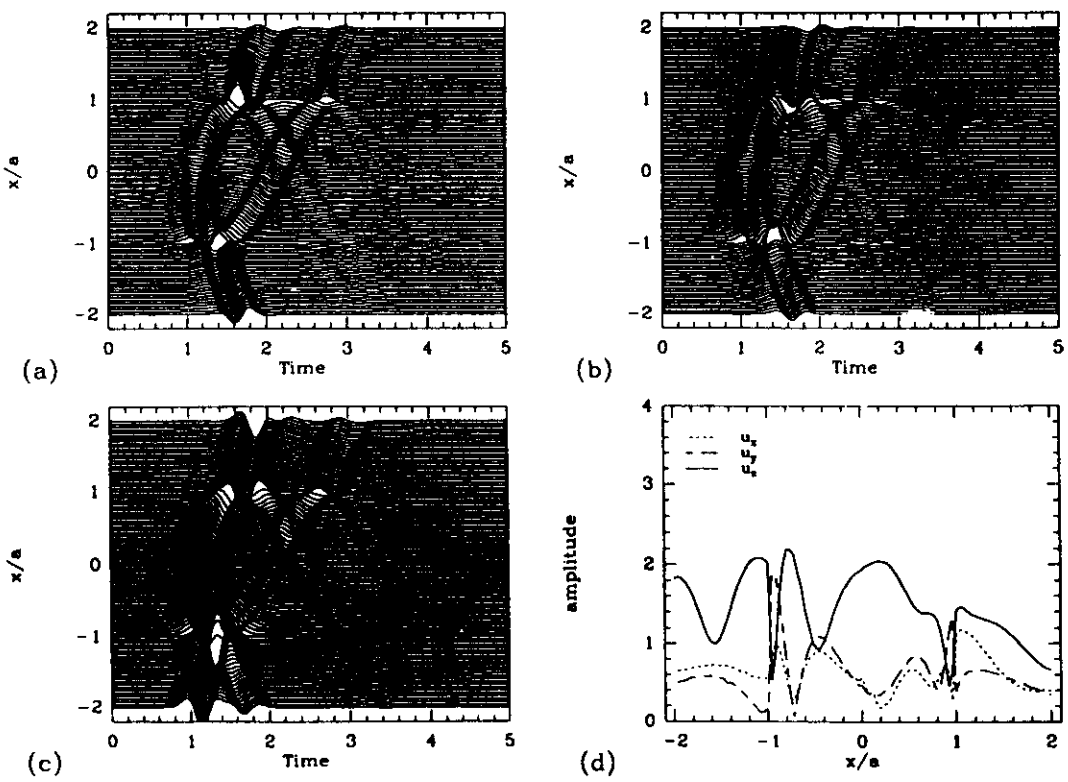

Figure 8. Same as Figure 7 with $\phi = 60°$.

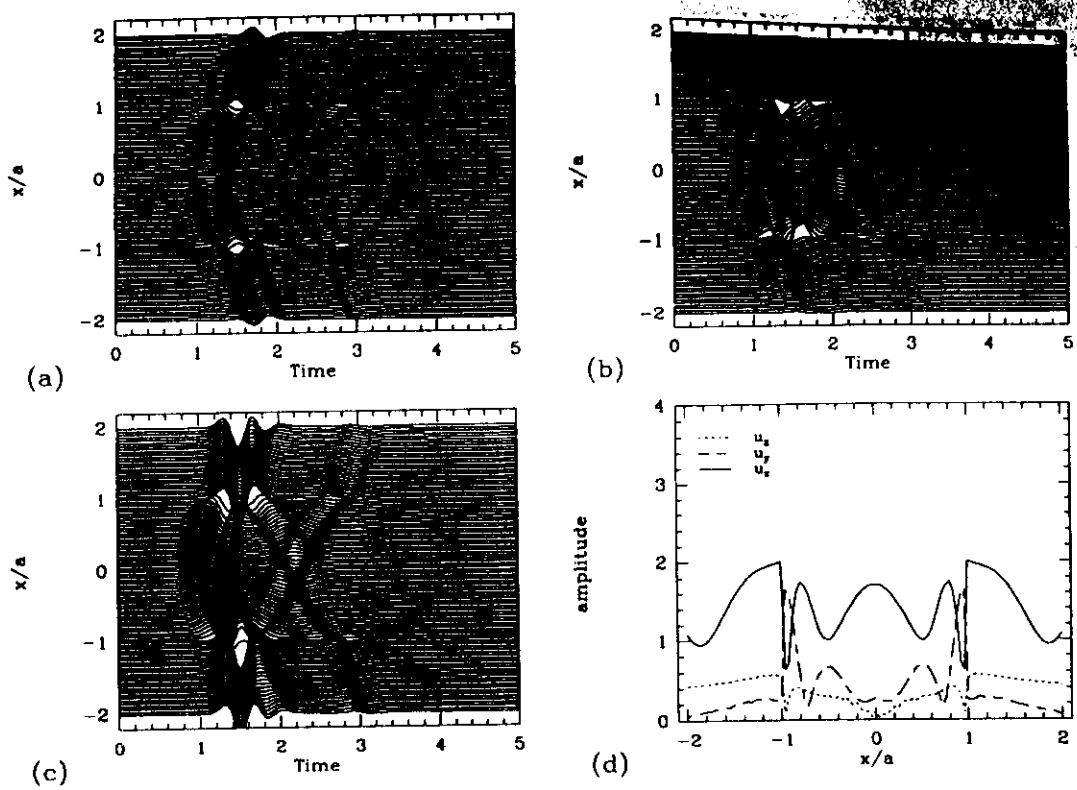

Figure 9. Same as Figure 7 with $\phi = 90°$.

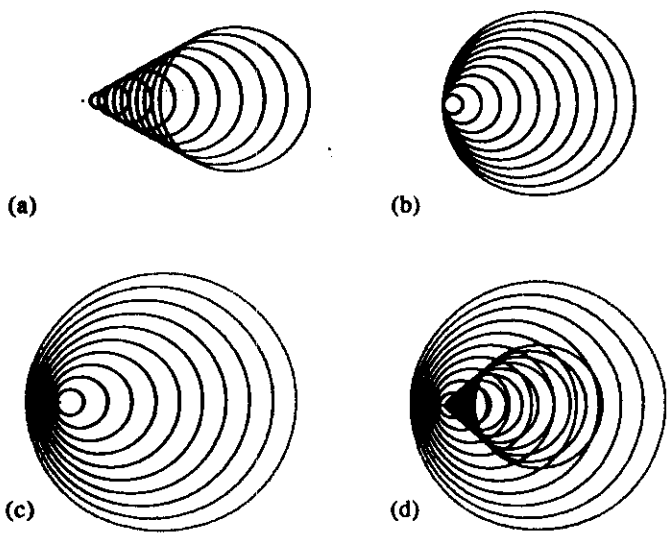

Figure 10. Simplified wave field radiated by a source moving with constant velocity c in medium of wave propagation velocities $V_{\alpha,\beta}$. (a) $c > V_{\alpha,\beta}$, (b) $c = V_{\alpha,\beta}$, (c) $c < V_{\alpha,\beta}$, and (d) $V_\beta < c < V_\alpha$.

The apparent velocity c_x along the x axis of this wave front is consequently

$$c_x = \frac{c_{\alpha,\beta}}{\sin \phi'}. \tag{22}$$

The use of these simple formulas to explain the apparent velocity of the diffracted waves was verified in several examples. They also explain why the scattered wave field almost equals the superposition of the two-dimensional in-plane and out-of-plane solutions (Pei and Papageorgiou, 1993a) when the incident waves arrive almost vertically (θ is small).

There is clearly a singularity when c' equals c_α or c_β. This is illustrated in Figure 10b. The singularity is, in fact, weak, as the Green's functions near the source can be integrated. Simulations with c' slightly smaller and greater than c_α and c_β confirmed that there is no particular effect to expect in practice in that particular situation. The wave field of the moving source when $c' < c_\beta$ is illustrated in Figure 10c. No plane wave is created and the wave field presents a "Doppler effect." The absence of a clearly defined wave front may explain why diffraction seems to decrease for large azimuths. When $c_\beta < c' < c_\alpha$, the situation is a mixture of the supersonic and the subsonic case, as illustrated in Figure 10d.

Semi-Circular Ridge

The various parameters of the model of a semi-circular ridge are identical to the model of the semi-circular canyon; the models differ only by the sign of the topography. In this section, we show examples of scattering

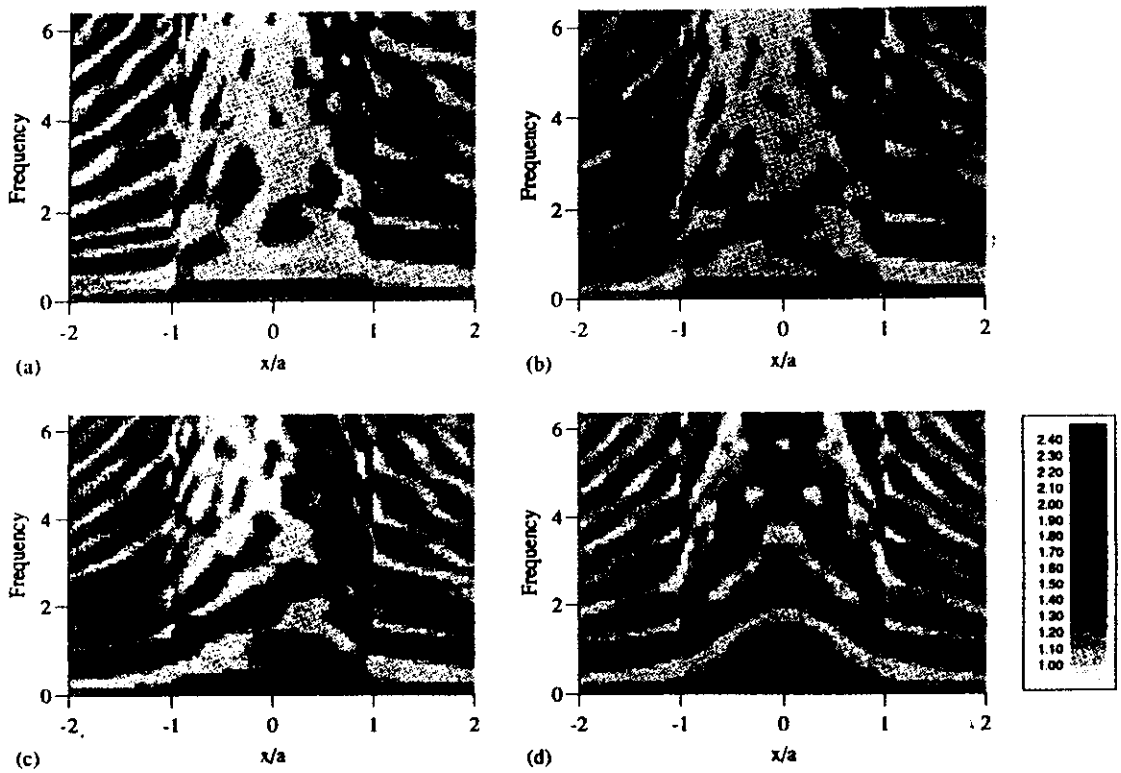

Figure 11. Spectral amplitude of horizontal displacements across a semi-circular ridge. Incident wave field, P wave with $\theta = 45°$. (a) $\phi = 0°$, (b) $\phi = 30°$, (c) $\phi = 60°$, and (d) $\phi = 90°$.

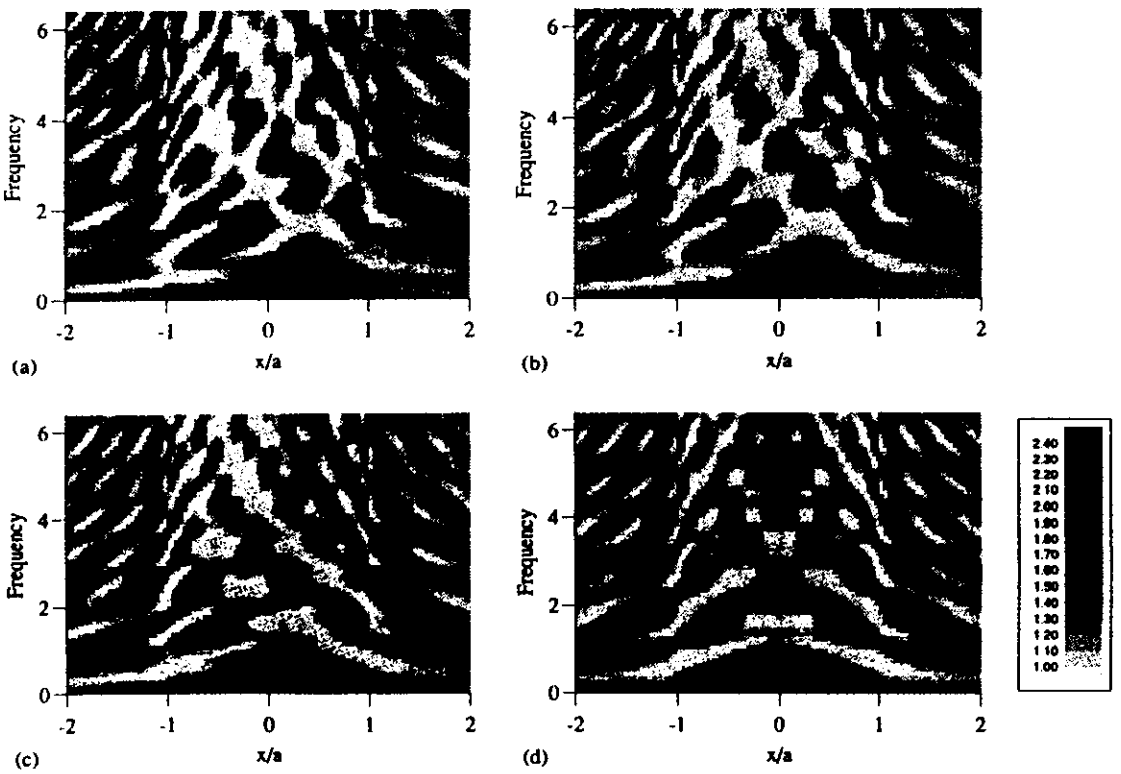

Figure 12. Same as Figure 11 for vertical displacements.

by the ridge of a plane P wave with an incidence θ of 45° to the z axis.

Figures 11 and 12 show results of these simulations for various azimuths of the incident P wave (ϕ = 0°, 30°, 60°, and 90°). Total horizontal displacement is shown in Figure 11 and vertical displacement in Figure 12. For all azimuths, the interference is significant. Apparently, scattered waves are created by both edges of the canyon and the interference pattern is very complicated. The amplitude of horizontal displacement is far from being symmetrical over the ridge when the azimuth is small; it is generally greatest near the far corner of the ridge (x/a = 1).

The synthetic seismograms for ϕ = 0° and 90° are shown in Figures 13 and 14, respectively. Analysis of the apparent velocities of the scattered waves indicate that creeping shear waves are generated at both edges of the ridge. The P waves are reflected away from the ridge at $x/a = -1$ and into the ridge near x/a = 1. The time duration of the signal is long because scattered waves bounce back and forth across the ridge.

Conclusions

An indirect boundary element method was presented for calculating the three-dimensional scattered wave field of plane waves incident on [illegible] phy. Results were presented in the frequency [illegible] domains for two topographies of simple geometry: a circular canyon and a semi-circular ridge. The signal to noise ratio of the synthetic seismograms was in general very low, so it was possible to interpret not only the amplification of the incident waves, but also the nature of the scattered wave field. The interpretations are based upon analysis of particle motions and apparent velocities of the waves. The total scattered wave field presents a complicated pattern of amplification and deamplification because it is the result of interference between different scattered waves: Rayleigh waves, reflected compressional and shear waves, and creeping waves. The complexity does not seem to change considerably when the incident plane waves arrive outside the symmetry axis of the topography. The points where amplification or deamplification occur change as a function of geometry, azimuth, incidence angle, and type of incident wave field, but the general level of amplification does not change significantly. Of all the simulations that we performed, the maximum spectral amplification of displacement was 4.9 (for Rayleigh waves, the reference value is the horizontal motion, which is assumed to be unitary). The simulations also showed that there is, in practice, no particular effect when the incident wave field is such that

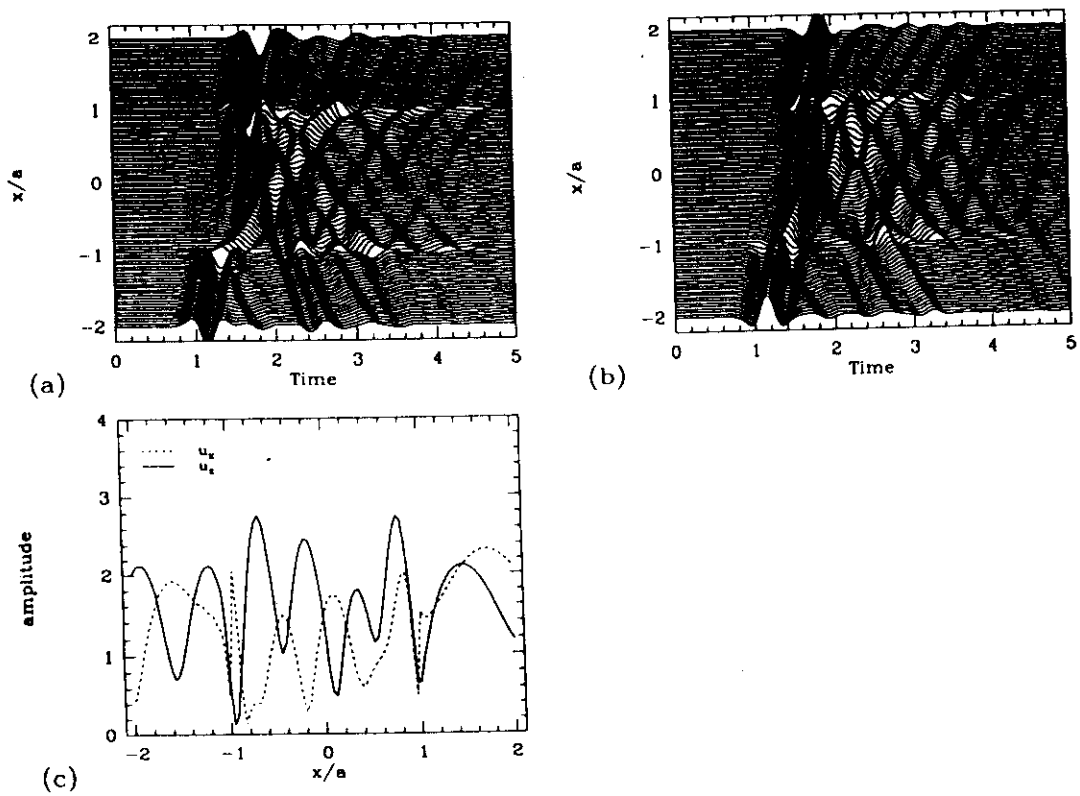

Figure 13. Displacement amplitudes across a semi-circular ridge. Incident wave field, P wave with ϕ = 0° and θ = 45°. (a) Synthetic seismograms, u_x, (b) synthetic seismograms, u_z, and (c) spectral amplitudes for η = 2.

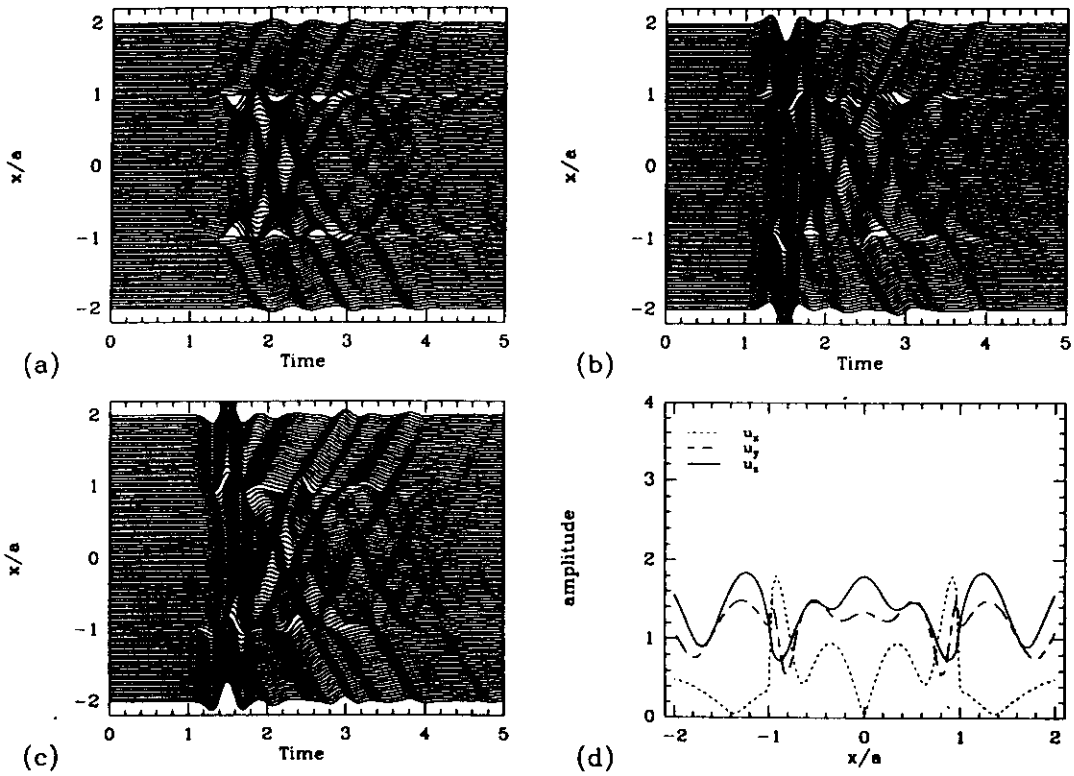

Figure 14. Same as Figure 13 with $\phi = 90°$. (a) Synthetic seismograms, u_x, (b) synthetic seismograms, u_y, (c) synthetic seismograms, u_z, and (d) spectral amplitudes for $\eta = 2$.

there is a singularity in the Green's function for a moving point source.

Our results indicate that in the three-dimensional case, as in the two-dimensional one, the wave field scattered by a topography is significant over large distances. Of course, the introduction of damping in the model will diminish this effect; nevertheless, it is not surprising to find extreme values of spectral ratios between the top and the base of mountains. Peaks in the spectral ratio are expected for frequencies where deamplification takes place at the reference station; there is no theoretical evidence, however, of broadband amplification at any location on the topography.

We needed to make only one approximation for the implementation of the method: we divided the topography into a number of segments, each with a constant force distribution. Tests showed that five segments per wavelength is sufficient to obtain a good accuracy of the results. In this way, performing each of the simulations presented here requires only a few hours CPU time on a medium-sized workstation (IBM Risc 6000, 9 Mflops). The low computation time means that the method can be extended to more complex problems, such as scattering of plane waves by alluvial valleys or propagation of crustal phases across large structures. Direct use of the method presented in this article could be parametric studies or modeling of observed topographic effects.

Acknowledgments

Thanks are given to Anne Paul and Rod Bark for useful discussions and critical reading of the manuscript. This work was partially supported by the European Community under Research Grant No. B/EPOC-913006 and under Contract No. C11*-CT92-0036 by Secretaría General de Obras of Departamento de Distrito Federal, Mexico, and by Consejo Nacional de Ciencia Y Tecnología, Mexico, under Grant No. P0523-T9109. The computations were performed at Centre de Calcul Intensif of Observatoire de Grenoble.

References

Abramowitz, M. and I. A. Stegun (1972). *Handbook of Mathematical Functions*, Dover, New York.

Aki, K. and K. L. Lamer (1970). Surface motion of a layered medium having an irregular interface due to incident plane SH waves, *J. Geophys. Res.* **75**, 1921–1941.

Aki, K. and P. G. Richards (1980). *Quantitative Seismology*, W. H. Freeman, San Francisco.

Bard, P.-Y. (1982). Diffracted waves and displacement field over two-dimensional elevated topographies, *Geophys. J. R. Astr. Soc.* **71**, 731–760.

Bard, P.-Y. and E. T. Tucker (1985). Underground and ridge site effects: a comparison of observation and theory, *Bull. Seism. Soc. Am.* **75**, 905–922.

Bouchon, M. (1973). Effect of topography on surface motion, *Bull. Seism. Soc. Am.* **63**, 615–632.

Bouchon, M. (1985). A simple, complete numerical solution to the problem of diffraction of SH waves by an irregular surface, *J. Acoust. Soc. Am.* **77**, 1–5.

Davis, L. L. and L. R. West (1973). Observed effects of topography on ground motion, *Bull. Seism. Soc. Am.* **63**, 283–298.

Geli, L., P.-Y. Bard, and B. Jullien (1988). The effect of topography on earthquake ground motion: a review and new results, *Bull. Seism. Soc. Am.* **78**, 42–63.

Griffiths, D. W. and G. A. Bollinger (1979). The effect of Appalachian mountain topography on seismic waves, *Bull. Seism. Soc. Am.* **69**, 1081–1105.

Kawase, H. (1988). Time-domain response of a semicircular canyon for incident SV, P, and Rayleigh waves calculated by the discrete wavenumber boundary element method, *Bull. Seism. Soc. Am.* **78**, 1415–1437.

Khair, K. R., S. K. Datta, and A. H. Shah (1989). Amplification of obliquely incident seismic waves by cylindrical alluvial valleys of arbitrary cross-sectional shape, Part I, Incident P and SV waves, *Bull. Seism. Soc. Am.* **79**, 610–630.

Khair, K. R., S. K. Datta, and A. H. Shah (1991). Amplification of obliquely incident seismic waves by cylindrical alluvial valleys of arbitrary cross-sectional shape, Part II, Incident SH and Rayleigh waves, *Bull. Seism. Soc. Am.* **81**, 346–357.

Kupradze, V. D. (1963). *Dynamical problems in elasticity*, in *Progress in Solid Mechanics*, Vol. 3, I. N. Sneddon and R. Hill (Editors), North-Holland, Amsterdam.

Lamb, H. (1904). On the propagation of tremors over the surface of an elastic solid, *Philos. Trans. R. Soc. London*, Ser. A **203**, 1–42.

Lee, V. W. and H. Cao (1989). Diffraction of SV waves by circular canyons of various depths, *J. Eng. Mech. Am. Soc. Civil. Eng.* **115**, 2035–2056.

Liu, S. W., S. K. Datta, and M. Bouden (1991). Scattering of obliquely incident seismic waves by a cylindrical valley in a layered half-space, *Int. J. Earthquake Eng. Struct. Dyn.* **20**, 859–870.

Luco, J. E., H. L. Wong, and F. C. P. De Barros (1990). Three-dimensional response of a cylindrical canyon in a layered half-space, *Int. J. Earthquake Eng. Struct. Dyn.* **19**, 799–817.

Morse, P. M. and H. Feshbach (1953). *Methods of Mathematical Physics, Part II*, McGraw-Hill, New York.

Pao, Y.-H. and V. Varatharajulu (1976). Huygens' principle, radiation conditions, and integral formulas for the scattering of elastic waves, *J. Acoust. Soc. Am.* **59**, 1361–1371.

Pei, D. and A. S. Papageorgiou (1993a). Three-dimensional response of an infinitely long cylindrical canyon to obliquely incident seismic waves (abstract), *Seism. Res. Lett.* **64**, 27.

Pei, D. and A. S. Papageorgiou (1993b). Study of the response of cylindrical alluvial valleys of arbitrary cross-section to obliquely incident seismic waves using the discrete wavenumber boundary element method, in *Soil Dynamics and Earthquake Engineering VI*, A. S. Cakmak and C. A. Brebbia (Editors), Comp. Mech. Publications—Elsevier Appl. Sc., Southampton–London, 149–161.

Sánchez-Sesma, F. J. and M. Campillo (1991). Diffraction of P, SV, and Rayleigh waves by topographical features: a boundary integral formulation, *Bull. Seism. Soc. Am.* **81**, 2234–2253.

Sánchez-Sesma, F. J. and M. Campillo (1993). Topographic effects for incident P, SV, and Rayleigh waves, *Tectonophysics*, **218**, 113–125.

Sánchez-Sesma, F. J. and E. Rosenblueth (1979). Ground motion on alluvial valleys under incident plane SH waves. *Int. J. Earthquake Eng. Struct. Dyn.* **7**, 441–450.

Todorovska, M. I. and V. W. Lee (1990). A note on response of shallow circular valleys to Rayleigh waves: analytical approach, *Earthquake Eng. Eng. Vibration* **10**, 21–34.

Todorovska, M. I. and V. W. Lee (1991). Surface motion of circular valleys of variable depth for incident plane SH waves, *Soil Dyn. Earthquake Eng.* **10**, 192–200.

Trifunac, M. D. (1973). Scattering of plane SH waves by a semi-cylindrical canyon, *Int. J. Earthquake Eng. Struct. Dyn.* **1**, 267–281.

Wong, H. L. (1982). Effect of surface topography on the diffraction of P, SV, and Rayleigh waves, *Bull. Seism. Soc. Am.* **72**, 1167–1183.

Wong, H. L. and P. C. Jennings (1975). Effect of canyon topographies on strong ground motion, *Bull. Seism. Soc. Am.* **65**, 1239–1257.

Zhang, L. and A. K. Chopra (1991). Three-dimensional analysis of spatially varying ground motions around a uniform canyon in a homogeneous half-space, *Int. J. Earthquake. Eng. Struct. Dyn.* **20**, 911–926.

Appendix

Green's Functions for a Moving Point Source in an Elastic Unbounded Medium

Consider a point source moving in a homogeneous isotropic elastic unbounded medium with density ρ, Lamé constants μ and λ, and shear- and compressional-wave velocities α and β, respectively. The point source moves with velocity c parallel to the x_2 axis along the line through $(x_1^0, 0, x_3^0)$. The observation point is situated at (x_1, x_2, x_3). The term $i^2 = -1$, t = time, ω = circular frequency, and $H_m^{(2)}$ is the Hankel functions of the second kind and order m. Other notations used are

$$R = \sqrt{(x_1 - x_1^0)^2 + (x_3 - x_3^0)^2},$$

$$\gamma_1 = \frac{x_1 - x_1^0}{R}, \quad \gamma_3 = \frac{x_3 - x_3^0}{R}$$

$$q = \frac{\omega}{\alpha}, \quad k = \frac{\omega}{\beta}, \quad \upsilon = \frac{\omega}{c}$$

$$Q = \sqrt{q^2 - \upsilon^2} = \omega \sqrt{\frac{1}{\alpha^2} - \frac{1}{c^2}},$$

$$K = \sqrt{k^2 - \upsilon^2} = \omega \sqrt{\frac{1}{\beta^2} - \frac{1}{c^2}}$$

with

$$\text{Imag}(Q) \leqq 0; \ \text{Imag}(K) \leqq 0$$

$$A = \left(\frac{1}{\alpha^2} - \frac{1}{c^2}\right) H_0^{(2)}(QR) + \left(\frac{1}{\beta^2} + \frac{1}{c^2}\right) H_0^{(2)}(KR)$$

$$B = \left(\frac{1}{\alpha^2} - \frac{1}{c^2}\right) H_2^{(2)}(QR) - \left(\frac{1}{\beta^2} - \frac{1}{c^2}\right) H_2^{(2)}(KR)$$

$$C = \sqrt{\frac{1}{\beta^2} - \frac{1}{c^2}}\, H_1^{(2)}(KR) - \sqrt{\frac{1}{\alpha^2} - \frac{1}{c^2}}\, H_1^{(2)}(QR)$$

$$E = \left(\frac{1}{\beta^2} - \frac{1}{c^2}\right) H_0^{(2)}(KR) - \left(\frac{1}{\alpha^2} - \frac{1}{c^2}\right) H_0^{(2)}(QR)$$

$$D(z) = zH_1^{(2)}(z).$$

The Green's functions for harmonic time dependence $\exp(i\omega t)$ of the moving point source can be expressed by the following compact forms:

$$G_{ij} = \frac{1}{8i\rho}[\delta_{ij}A - (2\gamma_i\gamma_j - \delta_{ij})B]\exp(-i\nu x_2), \quad i,j = 1, 3$$

$$G_{2j} = G_{j2} = \frac{1}{4\rho c}\left[\sqrt{\frac{1}{\beta^2} - \frac{1}{c^2}}\,H_1^{(2)}(KR) - \sqrt{\frac{1}{\alpha^2} - \frac{1}{c^2}}\,H_1^{(2)}(QR)\right]\gamma_j \exp(-i\nu x_2), \quad j = 1, 3$$

$$G_{22} = \frac{1}{4i\rho}\left[\left(\frac{1}{\beta^2} - \frac{1}{c^2}\right)H_0^{(2)}(KR) + \frac{1}{c^2}H_0^{(2)}(QR)\right] \cdot \exp(-i\nu x_2)$$

$$T_{11} = \lambda e_1 n_1 + \mu(\epsilon_{111}n_1 + \epsilon_{131}n_3)$$

$$T_{31} = \lambda e_1 n_3 + \mu(\epsilon_{131}n_1 + \epsilon_{331}n_3)$$

$$T_{13} = \lambda e_3 n_1 + \mu(\epsilon_{113}n_1 + \epsilon_{133}n_3)$$

$$T_{33} = \lambda e_3 n_3 + \mu(\epsilon_{133}n_1 + \epsilon_{333}n_3)$$

$$T_{12} = \lambda e_2 n_1 + \mu(\epsilon_{112}n_1 + \epsilon_{132}n_3)$$

$$T_{21} = \mu(\epsilon_{121}n_1 + \epsilon_{231}n_3)$$

$$T_{32} = \lambda e_2 n_3 + \mu(\epsilon_{132}n_1 + \epsilon_{332}n_3)$$

$$T_{23} = \mu(\epsilon_{123}n_1 + \epsilon_{233}n_3)$$

$$T_{22} = \mu(\epsilon_{122}n_1 + \epsilon_{232}n_3)$$

where

$$\epsilon_{ijk} = \frac{\delta G_{ik}}{\delta x_j} + \frac{\delta G_{jk}}{\delta x_i}$$

$$e_i = \frac{i}{4\rho R}\exp(-i\nu x_2)\,\gamma_i\frac{D(QR)}{\alpha^2}, \quad i = 1, 3$$

$$e_2 = -\frac{i}{4\rho}\exp(-i\nu x_2)\frac{\omega}{c\alpha^2}H_0^{(2)}(QR)$$

$$\epsilon_{111} = \exp(-i\nu x_2)\frac{i}{4\rho R}\gamma_1\left\{2\left(\frac{1}{\alpha^2} - \frac{1}{c^2}\right)\gamma_1^2 D(QR) + 2\left(\frac{1}{\beta^2} - \frac{1}{c^2}\right)\gamma_3^2 D(KR) + 2(3\gamma_3^2 - \gamma_1^2)B + \frac{2}{c^2}D(KR)\right\}$$

$$\epsilon_{131} = \exp(-i\nu x_2)\frac{i}{4\rho R}\gamma_3\left\{2\left(\frac{1}{\alpha^2} - \frac{1}{c^2}\right)\gamma_1^2 D(QR) + \left(\frac{1}{\beta^2} - \frac{1}{c^2}\right)(\gamma_3^2 - \gamma_1^2)\,D(KR) - 2(3\gamma_1^2 - \gamma_3^2)B + \frac{1}{c^2}D(KR)\right\}$$

$$\epsilon_{133} = \exp(-i\nu x_2)\frac{i}{4\rho R}\gamma_1\left\{2\left(\frac{1}{\alpha^2} - \frac{1}{c^2}\right)\gamma_3^2 D(QR) + \left(\frac{1}{\beta^2} - \frac{1}{c^2}\right)(\gamma_1^2 - \gamma_3^2)\,D(KR) - 2(3\gamma_3^2 - \gamma_1^2)B + \frac{1}{c^2}D(KR)\right\}$$

$$\epsilon_{333} = \exp(-i\nu x_2)\frac{i}{4\rho R}\gamma_3\left\{2\left(\frac{1}{\alpha^2} - \frac{1}{c^2}\right)\gamma_3^2 D(QR) + 2\left(\frac{1}{\beta^2} - \frac{1}{c^2}\right)\gamma_1^2\,D(KR) + 2(3\gamma_1^2 - \gamma_3^2)B + \frac{2}{c^2}D(KR)\right\}$$

$$\epsilon_{113} = \exp(-i\nu x_2)\frac{i}{4\rho R}\gamma_3\left\{2\left(\frac{1}{\alpha^2} - \frac{1}{c^2}\right)\gamma_1^2 D(QR) - 2\left(\frac{1}{\beta^2} - \frac{1}{c^2}\right)\gamma_1^2\,D(KR) - 2(3\gamma_1^2 - \gamma_3^2)B\right\}$$

$$\epsilon_{331} = \exp(-i\nu x_2)\frac{i}{4\rho R}\gamma_1\left\{2\left(\frac{1}{\alpha^2} - \frac{1}{c^2}\right)\gamma_3^2\,D(QR) - 2\left(\frac{1}{\beta^2} - \frac{1}{c^2}\right)\gamma_3^2\,D(KR) - 2(3\gamma_3^2 - \gamma_1^2)B\right\}$$

$$\epsilon_{121} = \exp(-i\nu x_2)\left[\frac{1}{4\rho cR}\{C(\gamma_3^2 - \gamma_1^2) + \omega ER\gamma_1^2\} - \frac{\omega}{8\rho c}\{A - B(2\gamma_1^2 - 1)\}\right]$$

$$\epsilon_{233} = \exp(-i\nu x_2)\left[\frac{1}{4\rho cR}\{C(\gamma_1^2 - \gamma_3^2) + \omega ER\gamma_3^2\} - \frac{\omega}{8\rho c}\{A - B(2\gamma_3^2 - 1)\}\right]$$

$$\epsilon_{112} = \exp(-i\nu x_2)\frac{1}{2\rho cR}\{C(\gamma_3^2 - \gamma_1^2) + \omega ER\gamma_1^2\}$$

$$\epsilon_{332} = \exp(-i\nu x_2)\frac{1}{2\rho cR}\{C(\gamma_1^2 - \gamma_3^2) + \omega ER\gamma_3^2\}$$

$$\epsilon_{122} = \exp(-i\nu x_2)\frac{i}{4\rho R}\cdot\left\{\left(\frac{1}{\beta^2} - \frac{2}{c^2}\right)D(KR) + \frac{2}{c^2}D(QR)\right\}\gamma_1$$

$$\epsilon_{232} = \exp(-i\nu x_2)\frac{i}{4\rho R}\cdot\left\{\left(\frac{1}{\beta^2} - \frac{2}{c^2}\right)D(KR) + \frac{2}{c^2}D(QR)\right\}\gamma_3$$

$$\epsilon_{123} = \exp(-i\nu x_2)\frac{\omega}{2\rho c}B\gamma_1\gamma_3$$

$$\epsilon_{231} = \exp(-i\nu x_2)\frac{\omega}{2\rho c}B\gamma_1\gamma_3$$

$$\epsilon_{132} = \exp(-i\nu x_2)\frac{\omega}{2\rho c}B\gamma_1\gamma_3$$

Laboratoire de Géophysique Interne et Tectonophysique
Université Joseph Fourier
F-38041 Grenoble Cedex
France
(H.A.P., M.C.)

Instituto de Ingenieria
UNAM
Cd Universitaria
Coyoacán 04510, México D.F.
Mexico
(F.J.S.)

Centro de Investigación Sísmica
Tlalpan 14200, México D.F.
Mexico
(F.J.S.)

Manuscript received 6 July 1993.

SEISMIC RESPONSE OF THREE-DIMENSIONAL ALLUVIAL VALLEYS FOR INCIDENT *P*, *S* AND RAYLEIGH WAVES

By

Francisco J. Sánchez-Sesma

Instituto de Ingeniería, UNAM, Cd. Universitaria, Apdo. 70-472 Coyoacán 04510, México D.F., Mexico, and
Centro de Investigación Sísmica, A.C.Carr. al Ajusco 203, Col. H. de Padierna. Tlalpan 14200 México D.F., Mexico

and

Francisco Luzón

Instituto Andaluz de Geofísica y Prevención de Desastres Sísmicos
Universidad de Granada, Apdo. 2145, 18080 Granada, Spain, and
Departamento de Física Aplicada
Universidad de Almería, 0471 Almería, Spain

Paper Submitted to the

Bulletin of the Seismological Society of America

Revised version

May, 1994

SEISMIC RESPONSE OF THREE-DIMENSIONAL ALLUVIAL VALLEYS FOR INCIDENT *P*, *S* AND RAYLEIGH WAVES

By

Francisco J. Sánchez-Sesma and Francisco Luzón

ABSTRACT

A simplified indirect boundary element method (BEM) is presented. It is used to compute the seismic response of three-dimensional alluvial valleys under incident *P*, *S* and Rayleigh waves. The method is based on the integral representations for scattered elastic waves using single layer boundary sources. This approach is called *indirect* BEM in the literature as the sources strengths should be obtained as an intermediate step. Scattered waves are constructed at the boundaries from which they radiate. Therefore, this method can be regarded as a numerical realization of Huygens' principle. Boundary conditions lead to a system of integral equations for boundary sources. A simplified discretization scheme is used. It is based on the approximate rectification of the surfaces involved using circles for the numerical and analytical integration of the exact Green's function for the unbounded elastic space. Various examples are given for three-dimensional problems of scattering and diffraction of elastic waves by soft elastic inclusion models of alluvial deposits in an elastic half-space. Results are displayed in both frequency and time domains. These results show the significant influence of locally generated surface waves in seismic response and evince three-dimensional effects.

INTRODUCTION

Since the pioneering studies of Aki and Larner (1970) and Trifunac (1971, 1973) a great deal of work has lead to a reasonable understanding of the physical basis of the site amplification problem. Most of the research effort has been concentrated on 2-D problems. This has allowed some explanation to observations. However, in order to improve the quantitative account of site response, modeling should consider the 3-D nature of the problem.

In fact, some strong motion records in Mexico City, recorded during the Michoacán earthquake of 1985, show clearly large amplifications beyond the level predicted using simple 1-D shear models (Sánchez-Sesma *et al.*, 1988; Kawase and Aki, 1989). This strongly suggests significant lateral effects of three-dimensional nature. On the other hand, the new accelerometric network of Mexico City Valley has recorded extensively seismic ground motion from coastal events. The spatial variability and polarization of observed ground motion have been interpreted as three-dimensional effects (Pérez-Rocha *et al.*, 1991; Sánchez-Sesma *et al.*, 1993b).

The seismic response of three-dimensional elastic features has been dealt with using 1) multipolar expansions of wave functions (*e.g.* Sánchez-Sesma, 1983; Lee, 1984; Eshragi and Dravinski, 1989; Sánchez-Sesma *et al.*, 1989; 1993b; Mossessian and Dravinski, 1990), 2) ray theory (Lee and Langston, 1983), 3) the Aki-Larner method (*e.g.* Horike *et al.*, 1990; Ohori *et al.*, 1990; Jiang *et al.*, 1993), 4) the finite element method (*e.g.* Toshinawa and Ohmachi, 1992; Li *et al.*, 1992; Rial *et al.*, 1992), 5) the finite difference method (*e.g.* Olsen and Schuster, 1991; Frankel and Vidale, 1992; Yomogida and Etgen, 1993; Frankel, 1993), 6) the boundary element method (*e.g.* Jiang and Kuribayashi, 1988; Luco *et al.*, 1990; Shinozaki and Yoshida, 1992; Kim and Papageorgiou, 1993; Kawano *et al.*, 1993; Pedersen *et al.*, 1993), 7) hybrid techniques (*e.g.* Khair *et al.*, 1989; Mossesian and Dravinski, 1992; Hisada *et al.*, 1993; Kato *et al.*, 1993), and 8) asymptotic methods (Rial, 1989).

The most realistic simulations to date are those of finite differences. The recent paper by Frankel (1993) on the response of the San Bernardino Valley, California, to nearby earthquakes illustrates well this fact. The other techniques have been used to understand basic effects and have been restricted to simple configurations, usually axisymmetric ones.

In the last two decades boundary methods have gained increasing popularity. In particular, the boundary integral equation approaches and their discretizations into boundary element methods (BEM) have produced successful solutions to various problems in dynamic elasticity. Recognized advantages over domain approaches are the dimensionality reduction, the relatively easy fulfillment of radiation conditions at infinity and the high

accuracy of results. Excellent surveys of the available literature on BEM in elastodynamics are those of Kobayashi (1987) and Manolis and Beskos (1988). Basically the BEM formulations can be *direct* and *indirect*. In the former, the unknowns are the sought values of displacements and tractions. This formulation arises from the discretization of reciprocal integral representation theorems. In contrast, the *indirect* BEM formulates the problems in terms of boundary densities which should be obtained as an intermediate step. Both formulations are related and it can be shown that they are mathematically equivalent (see *e.g.* Sánchez-Sesma and Campillo, 1991). However, we favor the indirect one as it leads to simple, intuitive visualization of problems.

Perhaps the first application of an integral formulation (a direct one) to study topography-related seismic amplificationis is due to Wong and Jennings (1975). They studied the seismic response of arbitrary canyon geometries under incident *SH* waves. A similar approach has been used by Zhang and Chopra (1991) to consider three-dimensional response of a canyon in an elastic half-space.

On the other hand, the combination of discrete wavenumber expansions for Green's functions (Bouchon and Aki, 1977; Bouchon, 1979) with boundary integral representations has been successful in various studies of elastic wave propagation. Bouchon (1985), Campillo and Bouchon (1985), Campillo (1987), Gaffet and Bouchon (1989), Bouchon *et al.* (1989) and Campillo *et al.* (1990) used source distributions on the boundaries whereas Kawase (1988), Kawase and Aki (1989) and Kim and Papageorgiou (1993) used Somigliana representation theorem. These are discrete wavenumber versions of BEM, indirect and direct, respectively. However, such procedures require considerable amount of computer resources. An alternative approach may be welcomed for many applications.

In this paper we present a simplified indirect boundary element method and apply it to simulate the seismic response of arbitrary shaped three-dimensional models of alluvial valleys. It is clear to us that some of the posibilities of both finite-differences and finite-elements to model complex configurations are not available yet in a BEM formulation. On the other hand, there is a wide class of problems for which the information on

geometry and properties have large uncertainties, so simplifying assumptions are in order. In such circumstances, a full fledged finite-difference analysis may be quite expensive as compared to a simple BEM study. This is the motivation for the present research.

Our method is based upon the integral representation of the scattered (diffracted, reflected and refracted) elastic waves in terms of single-layer boundary sources. Therefore, it can be classified as an indirect BEM. Scattered waves are thus constructed at the boundaries from which they radiate. Hence, it can be regarded as a numerical realization of Huygens' principle (in fact, this is true for any *indirect* method). This approach is in fact an improvement over a boundary method that has been used to deal with various problems of scattering and diffraction of elastic waves (see *e.g.* Sánchez-Sesma and Rosenblueth, 1979; Sánchez-Sesma and Esquivel, 1979; Wong, 1982; Dravinski, 1982; Dravinski and Mossessian, 1987; Luco *et al.* 1990). In its many variants, such technique is based upon the superposition of solutions for *sources* with their singularities placed *outside* the region of interest. However, this requires particular care and the trial and error process needed is difficult to apply, particularly when many frequencies are to be computed.

As the singularities of Green's functions are integrable (see *e.g.* Kobayashi, 1987; Manolis and Beskos, 1988) we can put the sources at the boundary and properly consider their effects. In this way, the uncertainty about the location of sources is eliminated and directly solve the linear system of equations that arises from the discretization. Therefore, our *indirect* BEM approach retains the physical insight of the sources method, with all the benefits of analytical integration of *exact* Green's functions.

A similar formulation applied to study three-dimensional soil-structure dynamic interaction has been recently proposed (Auersch and Schmid, 1990). In its 2-D version, the method has been applied by Sánchez-Sesma and Campillo (1991) to study the scattering and diffraction of *P*, *SV* and Rayleigh waves by topographical irregularities in an elastic half-space. Alluvial valleys were dealt with by Sánchez-Sesma *et al.* (1993a) and Luzón *et al.* (1993).

In what follows, the single layer boundary representation of elastic

wave fields is described and applied to compute the response of various models of alluvial deposits for incident elastic waves in a half-space. Comparisons are provided with other numerical solution for a soft hemispherical inclusion under incident *SH* waves. The responses of three-dimensional valleys are then computed in both frequency and time domains for incident *P*, *S* and Rayleigh waves.

INTEGRAL REPRESENTATION USING BOUNDARY SOURCES

Consider the three-dimensional Euclidian space and a continuous surface *S*, finite or infinite. If an elastic material occupies this 3-D domain, a harmonic displacement field can be written, neglecting body forces, by means of the *single-layer* boundary integral

$$u_i(\mathbf{x}) = \int_S \phi_j(\xi) G_{ij}(\mathbf{x},\xi) dS_\xi \qquad (1)$$

where $u_i(\mathbf{x})$ = ith component of displacement at point $\mathbf{x}$, $G_{ij}(\mathbf{x},\xi)$ = Green function of the whole space, i.e. the displacement in the direction i at point $\mathbf{x}$ due to the application of a unit force in the direction j at point ξ, $\phi_j(\xi)$=force density in the direction j. Therefore, $\phi_j(\xi)dS_\xi$ is clearly a force distribution at the surface *S*. Subscripts in the differential indicate the space variable over which the integration is performed. This *single-layer* integral, that can be obtained from Somigliana identity (Sánchez-Sesma and Campillo, 1991), has been studied by Kupradze (1963) from the point of view of potential theory. He showed that the displacement field is continuous across *S* if $\phi_j(\xi)$ is continuous *along* *S*.

This integral representation allows computation of tractions by direct application of Hooke's law except at boundary singularities, i.e. when $\mathbf{x}=\xi$ on surface *S*. By a limiting process based on equilibrium considerations around a neighborhood of the boundary it is possible to write, for $\mathbf{x}$ on *S*, that

$$t_i(\mathbf{x}) = c\,\phi_i(\mathbf{x}) + \int_S \phi_j(\xi) T_{ij}(\mathbf{x},\xi) dS_\xi \qquad (2)$$

where t_i= ith component of traction at a smooth boundary, c=0.5 if $\mathbf{x}$ tends to *S* from inside and c=-0.5 if $\mathbf{x}$ tends to *S* from outside, $T_{ij}(\mathbf{x},\xi)$= traction

Green function, i.e. the traction in the direction i at point $\mathbf{x}$ on the boundary with normal $\mathbf{n}(\mathbf{x})$ (assumed to be specified and pointing outside if $\mathbf{x}$ is at S) due to the application of a unit force in the direction j applied at ξ. The first term of the right hand side in equation 2 must be dropped if $\mathbf{x}$ is not at S. Equations 1 and 2 are the basis of our approach, which allows direct interpretation of the physical quantities involved.

3-D GREEN'S FUNCTIONS IN UNBOUNDED SPACE

In a homogeneous isotropic elastic unbounded medium, the Green functions for harmonic time dependence $\exp(i\omega t)$, where $i^2=-1$, ω=circular frequency and t=time, can be expressed in the following compact form

$$G_{ij}(\mathbf{x},\xi) = [f_2\delta_{ij} + (f_1-f_2)\,\gamma_i\gamma_j]/4\pi\mu r \qquad (3)$$

where $\gamma_j=(x_j-\xi_j)/r$, $r^2=(x_1-\xi_1)^2+(x_2-\xi_2)^2+(x_3-\xi_3)^2$. Here and in the sequel $\mu=\rho\beta^2$, $\lambda+2\mu = \rho\alpha^2$, λ,μ = Lamé's constants, ρ=mass density, δ_{ij}=Kronecker's delta, $k = \omega/\beta$ = S wavenumber, $q = \omega/\alpha$ = P wavenumber, β = S-wave velocity, and α = P-wave velocity. We define f_1 and f_2 as

$$f_1=(\beta^2/\alpha^2)[1-i2/(qr)-2/(qr)^2]\exp(-iqr)+[i2/(kr)+2/(kr)^2]\exp(-ikr) \qquad (4)$$

$$f_2=(\beta^2/\alpha^2)[i/(qr)+1/(qr)^2]\exp(-iqr)+[1-i/(kr)-1/(kr)^2]\exp(-ikr) \qquad (5)$$

which have the constants 1 and $(1+(\beta/\alpha)^2)/2$, respectively, as limits if ω or r tend to zero. The corresponding Green tractions are given by

$$T_{ij}=[(g_1-g_2-2g_3)\,\gamma_i\gamma_j\gamma_k n_k + g_3\,\gamma_i n_j + g_2\,\gamma_j n_i + g_3\,\gamma_k n_k\,\delta_{ij}]/4\pi r^2 \qquad (6)$$

with functions g_j, $j=1,2,3$, expressed as

$$g_j=[\,krA_{1j} + B_{1j} + C_{1j}/kr + D_{1j}/(kr)^2]\exp(-ikr) + [\,krA_{2j} + B_{2j} + C_{2j}/kr + D_{2j}/(kr)^2]\exp(-iqr). \qquad (7)$$

Coefficients of this expression are given in Table 1. In equations 3 and 6 the usual summation convention for subscripts is assumed. We may use in what follows the usual correspondence for axis' names: $x_1=x$, $x_2=y$ and $x_3=z$,

respectively. Also $u_1=u$, $u_2=v$ and $u_3=w$. Similar expressions for Green's functions have been presented by Auersch and Schmid (1990) using vector notation.

Equations 3 and 6 allow a direct view of the singularities at the point of application of the force. The singularity of displacements is $1/r$. This is clear from equation 3. Regarding the tractions the singularity is explicitely of the form $1/r^2$. In particular, when frequency tends to zero these equations lead to their static counterparts (see *e.g.* Love, 1944). These properties are used below in connection with our discretization scheme.

SCATTERING AND DIFFRACTION OF ELASTIC WAVES BY AN ELASTIC INCLUSION

Consider the elastic half-space, E, with an elastic inclusion, R, as shown in Figure 1 under incidence of elastic waves. The free-surface boundaries of regions E and R are denoted by $\partial_1 E$ and $\partial_1 R$, respectively. The interface $\partial_2 E = \partial_2 R$ is the common boundary between them. The ground motion in and around this irregular configuration comes from the interferences of incoming waves with scattered ones (reflected, diffracted and refracted). It is usual to say that the total motion in the half-space is the superposition of the free-field and the so called *scattered* or *diffracted* waves:

$$u_i^E = u_i^{(0)} + u_i^{(d)} \qquad (8)$$

where $u_i^{(0)}$=free-fied displacement, *i.e.* the solution in the elastic half-space in absence of the irregularity which for incident plane waves can be given analytically. The terms "scattering" and "diffraction" are used loosely as synonymous. The former is suitable to name waves "scattered" by an object (with an implicit high frequency meaning) whereas the later refers to the waves that smoothes out discontinuities of a geometrical description of wave field (which are stronger in low frequencies). An analysis of equation 8 may reveal that the free-field term includes "reflected" waves that never could be generated. Instead of leaving a hole in the free-field reflected wave term we choose a continuous description as we *know* that the effect of the irregularity decreases with increasing distance and the discontinuity of the reflected wave asymptotically disappears. Therefore, some waves are needed to locally *cancel* out some others and to smooth possible

discontinuities. We call them "scattered" or "diffracted" waves. The choice is a matter of taste. What we *really* have to care is to fulfill field equations and boundary conditions. The former are satisfied by construction as the Green's functions are solution of the equations of dynamic elasticity. Boundary conditions of continuity of displacements and tractions along the interface and those of traction null at the free surface must be enforced.

According to our previous discussion, the diffracted or scattered field is given by equation 1 which, with appropriate superscripts to indicate the region of validity, can be written as

$$u_i^{(d)}(\mathbf{x}) = \int_{\partial E} \phi_j^E(\xi) G_{ij}^E(\mathbf{x},\xi) dS_\xi. \tag{9}$$

Refracted elastic fields on the inclusion R can be written as

$$u_i^{(r)}(\mathbf{x}) = \int_{\partial R} \phi_j^R(\xi) G_{ij}^R(\mathbf{x},\xi) dS_\xi. \tag{10}$$

The traction-free boundary conditions imply that

$$t_i^{(0)} + t_i^{(d)} = 0 \qquad \text{on } \partial_1 E \tag{11}$$

and

$$t_i^{(r)} = 0 \qquad \text{on } \partial_1 R \tag{12}$$

then, from equation 2 such conditions can be expressed by means of

$$0.5\phi_i^E(\mathbf{x}) + \int_{\partial E} \phi_j^E(\xi) T_{ij}^E(\mathbf{x},\xi) dS_\xi = 0 \tag{13}$$

$$-0.5\phi_i^R(\mathbf{x}) + \int_{\partial R} \phi_j^R(\xi) T_{ij}^R(\mathbf{x},\xi) dS_\xi = 0. \tag{14}$$

In equation 13 it is considered that free field tractions on $\partial_1 E$ are null. On the interface $\partial_2 E = \partial_2 R$ continuity of displacements and tractions implies

$$u_i^{(0)} + u_i^{(d)} = u_i^{(r)} \qquad \text{on } \partial_2 E \tag{15}$$

$$t_i^{(0)} + t_i^{(d)} = t_i^{(r)} \qquad \text{on } \partial_2 E \tag{16}$$

and these conditions can be expressed as

$$\int_{\partial E} \phi_j^E(\xi) G_{ij}^E(\mathbf{x},\xi) dS_\xi - \int_{\partial R} \phi_j^R(\xi) G_{ij}^R(\mathbf{x},\xi) dS_\xi = -u_i^{(0)} \qquad (17)$$

$$0.5[\phi_i^E(\mathbf{x}) + \phi_i^E(\mathbf{x})] + \int_{\partial E} \phi_j^E(\xi) T_{ij}^E(\mathbf{x},\xi) dS_\xi - \int_{\partial R} \phi_j^R(\xi) T_{ij}^R(\mathbf{x},\xi) dS_\xi = -t_i^{(0)} \qquad (18)$$

equations 13, 14, 17 and 18 constitute a system of integral equations for boundary sources, i.e. those producing diffracted and refracted fields. These expressions are discretized along a finite portion of the boundary ∂E that includes the interface topography and part of the lateral flat free-surface and along ∂R, according to the definition of each integral. The extension of the discretized flat part in the applications reported herein typically have a width a which is the characteristic horizontal dimension (radius) of the elastic inclusion. Therefore, the discretization of free-surface is extended up to a radius of $2a$. The number of unknowns will be made clear in the next section.

DISCRETIZATION

In order to solve this system of integral equations we have to discretize them. The discretization of a surface is a well-known problem and several algorithms are already available (see *e.g.* George, 1991). In any event, the choice of the discretization scheme depends upon the problem and the mathematical formulation to be used. For instance, in many applications, triangular elements are used to discretize surfaces (*e.g.* Manolis and Beskos, 1988; Brebbia and Domínguez, 1992).

In this work we present a simplified scheme and discretize the surfaces using circles of various sizes that approximately cover the boundaries. This might be regarded as a crude choice. However, it allows keeping the formulation simple and relatively easy to implement by practicioners. This choice has been guided by the fact that the integrals of Green functions on circles can be easily obtained in a closed form. In order to partially overcome the effects of our approximate discretization we used at least four aligned boundary elements per shortest wavelength.

Let us assume the force densities $\phi_j(\xi)$ constant over each of the boundary circular elements, each with surface ΔS_l and centered at point ξ_l along the appropriate boundary. Let M, $2L$ and K be the number of elements of the discretized part of the flat surface, of the irregular interface and of the free surface of region R, as depicted in Figure 1. It is clear that the total number of equations is $3M+6L+3K$ which is the same as the number of unknowns. To clarify ideas, let us write the discretized versions of equations 1 and 2:

$$u_i(\mathbf{x}) = \sum_{l=1}^{N} \phi_j(\xi_l) g_{ij}(\mathbf{x},\xi_l) \tag{19}$$

where

$$g_{ij}(\mathbf{x}, \xi_l) = \int_{\Delta S_l} G_{ij}(\mathbf{x},\xi) dS_\xi . \tag{20}$$

and

$$t_i(\mathbf{x}_n) = \sum_{l=1}^{N} \phi_j(\xi_l) t_{ij}(\mathbf{x}_n,\xi_l) \tag{21}$$

where

$$t_{ij}(\mathbf{x}_n,\xi_l) = 0.5\delta_{ij}\delta_{nl} + \int_{\Delta S_l} T_{ij}(\mathbf{x},\xi) dS_\xi . \tag{22}$$

The integrals in equation 20 are computed numerically, except in the case when $\mathbf{x}$ is in the neighborhood of ξ_l, for which we obtained analytical expressions. In particular, for $\mathbf{x} = \xi_l$, *i.e.* at the center of a circle of radius R, it is possible to show that

$$\int_{\Delta S_l} G_{ij}(\mathbf{x},\xi) dS_\xi = [(F_2+F_1)\delta_{ij} + (F_2-F_1)n_i n_j] / 4\mu \tag{23}$$

where F_k, $k=1,2$, is simply the integral of f_k from 0 to R and n_i = ith component of the normal vector at the element. For $\mathbf{x}$ not at the center we performed analytical integration in polar local coordinates and considered the ascending power series of f_1 and f_2. Up to cubic terms were retained and

this is enough if the minimum wavelength is at least four diameters.

The integral in equation 22 is also computed numerically except when $x_n=\xi_i$. In this case, we have

$$t_{ij}(x_n,\xi_n) = 0.5\delta_{ij}, \qquad (24)$$

because the only contribution to the integral in that equation for $n=i$ comes from the Dirac's delta term. The contribution from the traction Green's tensor T_{ij} is null as long as the element is circular and flat, which is the case assumed here. In fact, from equations 6 to 7 it can be verified that, under this circumstance, such part of the integrand is a singular function on the element and its Cauchy's principal value is zero. The value for t_{ij} in equation 24 can be interpreted as half the applied unit point force and means that the force is distributed symmetrically for any two half-spaces containing the point of application of the load, regardless of its direction. This result also holds for the static solution.

Once the values of $\phi_j(\xi_i)$ are known, the scattered fields are computed by means of the appropriate discretization of equations 10 and 11.

TESTING OF THE METHOD

The accuracy of this approach is tested here for a problem that has been verified extensively. Sánchez-Sesma *et al.* (1989) used multipolar wave expansions in spherical coordinates and studied a hemispherical alluvial basin under oblique incidence of *SH* waves. Their results have been reproduced by Ohori *et al.* (1990), by Toshinawa and Ohmachi (1992), by Shinozaki and Yoshida (1992), among others. Therefore, we regard these results as trustworthy.

Comparisons are provided here for oblique incidence of plane *SH* waves. The model response is studied for a normalized frequency $\eta=1.0$, where $\eta=\omega a/\pi\beta_E$ and a=radius of valley. Material properties are set to be $\rho_R/\rho_E=1$ and $\beta_R/\beta_E=0.45$ for mass density and shear wave velocity ratios, respectively. Poisson coefficients were assumed $\nu_E=0.25$ and $\nu_R=0.30$. The discretization is extended horizontally up to a radius of $2a$. Figure 2 displays the surface

amplitudes for the three components due to a plane *SH* wave with an incidence angle γ=30 degrees, with respect to the vertical and azimuth zero (ϕ=0). Displacement amplitudes are plotted along the y=0 from x=-2a to x=+2a, and on line x=0 from y=-2a to y=+2a, where a is the radius of the hemispherical inclusion. Sánchez-Sesma *et al.*'s (1989) results are given by symbols and our solutions by dashed and solid lines. The overall agreement is good. There are small discrepancies which are probably due to our discretization scheme. We tested the discretization for the so-called "transparency test" in which the properties of the inclusion are set equal to those of the half-space. The maximum error in this case is smaller than 5 per cent the amplitude of particle displacement of the incoming wavefield. The same test was performed, and was satisfactory, for the examples that follow.

EXAMPLES

1. *Cylindrical soft deposit under incident* SV *waves*

In order to illustrate a complet set of results and analyze the 3-D effects we study the response of a cylindrical valley under oblique incidence of *SV* waves (as depicted in Figure 3) in both frequency and time domains. A radius of 4 km and depth of 1 km were assumed. Material properties are β_R=1 km/sec, B_E=2.5 km/sec, ν_R=ν_E=1/3 and ρ_R=ρ_E. A quality factor of 20 was considered for both *P* and *S* waves inside the valley. No attenuation was used for the half-space. An angle of incidence γ=30 degrees was assumed. Given the Poisson ratio of the half-space, this incidence is "critical". This means that, in order to satisfy free boundary conditions for the half-space, a horizontally propagating plane *P* wave must be assumed in addition to the reflected *SV* wave (see *e.g.* Aki and Richards, 1980). Critical incidence in this case produces at the surface an amplification of 2$\sqrt{3}$ for the horizontal displacement whereas the vertical motion is null.

Figures 4 and 5 show the contours of displacement amplitudes u and w for surface receivers along the x-axis, between x=-8 km and x=8 km, against frequency. These f-x diagrams display the transfer funcion (relative to the amplitude of incident waves) for all receivers and provide a good description of the frequency behavior of the valley. The plots also evince lateral resonances, which sometimes are clear when a series of peaks are more or less

evenly distributed in space for a given frequency. This is true for two-dimensional configurations (see *e.g.* Sánchez-Sesma *et al.* 1993). However, in three-dimensional problems space resonant patterns tend to be more complicated. The recent papers by Rial (1989) and Rial *et al.* (1992) point out this fact. In any event, the maximum amplitudes appear in the "rear" side of valley, *i.e.* the side oposite to the incidence, at least for the lower resonant frequencies. The refracted waves along the x-axis, although complicated, have a good portion of Rayleigh waves generated at the edge.

For other slice, the one along the y-axis, Figures 6, 7 and 8 present the corresponding contours for u, v and w. As expected, they are symmetrical (v is asymmetric but the plot is for amplitude) and show complex interactions of the refracted fields inside the softer material. For instance, a significant amount of horizontal component u along the y-axis is composed by Love waves. This is due to the tangential motion induced by the incident field at the valley's extremes in x=0. In this case the spatial resonant patterns that appear at frequencies of about 0.3 and 0.4 Hz can be explained in terms of Love waves.

The maximum amplification of u is of about 15 for a frequency of about 0.28 Hz, which is slightly larger than 0.25 Hz, the 1-D shear resonant frecuency for a flat layer (see Jiang and Kuribayashi, 1988). The large amplification is associated to the incoming plane *SV* wave. However, this amplification relative to the horizontal free-field surface displacement is of about 4.33, nearly twice the impedance ratio. The shifting of the fundamental resonant frequency and the localized increase of amplification are lateral effects.

From frequency domain results we computed synthetic seismograms using the FFT algorithm for a Ricker wavelet with central frequency f_p=0.33 Hz thus the characteristic period of the Ricker pulse is t_p = 3 sec. In Figure 9 such time series are plotted for 48 receivers equally spaced between x=-1.82a and x=1.74a. The amplification effect seen in the frequency domain is also clear in the synthetics.

2. Irregular valley under incident P, SH, SV and Rayleigh waves

We present here some results for a closed irregular alluvial valley. The soft material is, horizontally, within a region for which the conditions $r<a$ and $R>b$ hold, where $r^2 = x^2 + y^2$ and $R^2 = (x-a)^2 + y^2$. In other words, the valley zone is limited by two circumferences of radii a and b, where $a>b$, as depicted in Figure 10a. In this region the geometry of the interface between the sediment and the half-space is given by

$$f(x,y) = h(b^2-R^2)[1-2a(a-x)/R^2] \qquad (25)$$

where h is a parameter that controls the valley depth. The choice of this analytical expression is arbitrary (it is inspired by the Weber's solution for the Saint-Venant stress function for the torsion of a bar of circular cross section of radius a with a circular groove of radius b). We selected $b=0.7a$ and $h=0.4/a$; thus the maximum depth is of about $0.25a$. Figure 10b displays the level contours of the interface whereas Figure 11 shows a perspective of this profile. The free surface of both the alluvial deposit and the half-space is assumed flat. The discretization is extended up to a radius of $2a$. The value for a is set to be 4 km. Material properties are β_R=1 km/sec, B_E=2 km/sec, ν_R=0.35, ν_E=0.25 and $\rho_R=0.8\rho_E$. A quality factor of 100 was assumed for both P and S waves inside the valley. Again, the half-space has no internal attenuation.

We consider the incidence of plane waves of the *P*, *SH*, *SV* and Rayleigh types, all with an azimuth $\phi=0$. An incidence angle $\gamma=30$ degrees with respect to the vertical is assumed for body waves (for the *SH* incidence results for $\gamma=60$ degrees are also presented). We computed synthetic seismograms and assumed for the incoming wave a Ricker wavelet with a characteristic period t_p=3 sec. Results are portrayed in Figures 12 to 16 where the non zero components are shown along the x or y axes, respectively. These results present very interesting patterns of interference of the refracted waves inside the basin and, in some cases, significant emission of waves is observed. In fact, the incidences of *P*, *SV* and Rayleigh waves produce forward and backward scattering of Rayleigh waves by late emission after refracted waves bounce back and forth in the sediment. Some emission of difracted *SH* energy (for instance u along the y-axis) can be observed but the geometrical

attenuation is very strong.

The cases of *SH* incidence show significant late emission of scattered *SH* pulses. In particular, for γ=60 degrees the forward difraction has an amplitude comparable to the input motion as shown in Figure 16. This is a consequence of the irregular shape of our valley in which refracted waves of Love and Rayleigh types are generated continuously at the edge in such a way that they are focused near the "bump". This focusing also give rise to spectacular amplification inside the basin.

DISCUSSION

Our choice of the Green's function for the unbounded space lead us to explicitly consider the half-space free surface boundary condition of null tractions. We deal with the problem aproximately by treating only a finite portion around the inclusion. The discretization is extended up to a radius of $2a$. Therefore, we must expect some spurious waves coming from the model's edge. However, our synthetics appear to be free of such an effect. This is partially due to our choice to include the free-field. In our formulation, such part of the solution satisfies the free surface boundary condition by construction. We did several tests. For instance, if we cancel the reflected waves and let the excitation with only incident waves, the edge effects can be very strong. Moreover, some extensive numerical tests in 2-D problems showed that scattered waves in the lateral strips of models were esentially *outgoing* waves explaining the small edge effects (Sánchez-Sesma and Campillo, 1991). Owing to a stronger geometrical attenuation, we can see that in 3-D problems such edge effects are smaller.

The approach presented herein is general. It can be extended to deal, for example, with a layered half-space. Of course, in such a case both the free-field and the scattered waves should be constructed using the appropriate Green's functions.

CONCLUSIONS

A simplified indirect boundary element method has been presented and applied to study the seismic response of three-dimensional alluvial valleys of arbitrary shape for incident *P*, *S* and Rayleigh waves. The method is based upon the integral representation of scattered and diffracted elastic waves in terms of single layer boundary sources. Such waves are constructed at the boundaries from which they radiate. This method can be regarded as a numerical realization of Huygens' principle. From boundary conditions a system of integral equations for boundary sources is obtained. An approximate discretization scheme based on the numerical and analytical integration of exact Green's functions for displacements and tractions is used.

Various examples are given for three-dimensional problems of scattering and diffraction of elastic waves by soft elastic inclusion models of alluvial deposits in an elastic half-space. We found significant effects of three-dimensional nature in our models. Complicated patterns arise for surface displacements even in simple axisymmetric cases. In some cases the generation of Love and Rayleigh surface waves can easily be seen.

Synthetics for the irregular valley evince a variety of complex patterns. Focusing of energy, at least for the central frequency selected for the Ricker pulse, generally takes place at the deeper parts. Very large amplification was found for incident *SH* waves. Significant forward scattering was observed and it is interpreted as due to the geometry of our alluvial basin and the constructive interference of various refracted waves.

Although azimuthal variations were not studied, our results show that they can have important effects. Impedance contrast and basin geometry are among the issues that require attention. It is too early to give more precise conclusions. Meanwhile, this method can be used and extended to deal with practical situations and to calibrate more powerful procedures.

ACKNOWLEDGEMENTS

This work is dedicated to the memory of E. Rosenblueth (1926-1994). His encouragement, advice and example along the years are among the multifarious legacy of this great man. Thanks are given to F.J. Chávez-García, G. Ekström,

L.E. Pérez-Rocha, J.L. Rodríguez-Zúñiga and J. Tromp for the critical reading of the manuscript and many useful suggestions; to M. Suárez and R. Olvera for their kind assistance. The comments of an unknown reviewer helped to improve this paper. Part of the computations were done at the CRAY-YMP of UNAM, Mexico. This work was partially supported by Secretaría General de Obras del Departamento del Distrito Federal, México, by Consejo Nacional de Ciencia y Tecnología, México, under Grant P0523-T9109, by Dirección General de Asuntos del Personal Académico of UNAM, under Grant IN104792, by the European Economic Community under Grant CI1-CT92-0036, by DIGICYT, Spain, under Grant GEO90-1017, by VI y VII Convenios Específicos de la Junta de Andalucía-Universidad de Granada, Spain, and by Grupo de Investigación No. 4057 de la Junta de Andalucía, Spain.

REFERENCES

Aki, K. and K.L. Larner (1970). Surface motion of a layered medium having an irregular interface due to incident plane SH waves, *J. Geophys. Res.* **75**, 1921-1941.

Aki, K. and P.G. Richards (1980). *Quantitative Seismology. Theory and Methods*. W. H. Freeman and Company. San Francisco.

Auersch, L. and G. Schmid (1990). A simple boundary element formulation and its application to wavefield excited soil-structure interaction, *Int. J. Earthq. Eng. Struct. Dyn.* **19**, 931-947.

Bard, P-Y and M. Bouchon (1980a). The seismic response of sediment-filled valleys. Part 1. The case of incident *SH* waves, *Bull. Seism. Soc. Am.* **70**, 1263-1286.

Bard, P-Y and M. Bouchon (1980b). The seismic response of sediment-filled valleys. Part 2. The case of incident *P* and *SV* waves, *Bull. Seism. Soc. Am.* **70**, 1921-1941.

Brebbia, C.A. and J. Domínguez (1992). *Boundary elements an introductory course*, 2nd ed., Comp. Mec. Publ., Southampton & Mc Graw-Hill Book Co., New York.

Bouchon, M. (1979). Discrete wave number representation of elastic wave fields in three-space dimensions, *J. Geophys. Res.* **84**, *B7*, 3609-3614.

Bouchon, M. (1985). A simple, complete numerical solution to the problem of diffraction of SH waves by an irregular surface, *J. Acoust Soc Am* **77**, 1-5.

Bouchon, M. and K. Aki (1977). Discrete wave-number representation of seismic-source wave fields, *Bull. Seism. Soc. Am.* **67**, 259-277.

Bouchon, M., M. Campillo and S. Gaffet (1989). A boundary integral equation-discrete wavenumber representation method to study wave propagation in multilayered media having irregular interfaces, *Geophysics* **54**, 1134-1140.

Campillo, M. (1987). Modeling of SH wave propagation in an irregularly layered medium. Application to seismic profiles near a dome, *Geophys. Prospecting* **35**, 236-249.

Campillo, M. and M. Bouchon (1985). Synthetic SH seismograms in a laterally varying medium by the discrete wavenumber method, *Geophys. J. R. astr. Soc.* **83**, 307-317.

Campillo, M., F.J. Sánchez-Sesma and K. Aki (1990). Influence of small lateral variations of a soft surficial layer on seismic ground motion, *Int. J. Soil Dyn. Earthquake Eng.* **9**, 284-287.

Dravinski, M. (1982). Influence of interface depth upon strong ground motion, *Bull. Seism. Soc. Am.* **72**, 597-614.

Dravinski, M. and T.K. Mossessian (1987). Scattering of plane harmonic P, SV and Rayleigh waves by dipping layers of arbitrary shape, *Bull. Seism. Soc. Am.* **77**, 212-235.

Eshraghi, H. and M. Dravinski (1989). Scattering of elastic waves by non axisymmetric three-dimensional dipping layer, *J. Num. Methods for Partial Differential Equations* **5**, 327-345.

Frankel, A. (1993). Three-dimensional simulations of ground motion in the San Bernardino Valley, California, for hypothetical earthquakes on the San Andreas fault, *Bull. Seism. Soc. Am.* **83**, 1020-1041.

Frankel, A. and J. Vidale (1992). A three-dimensional simulation of seismic waves in the Santa Clara Valley, California, from a Loma Prieta aftershock, *Bull. Seism. Soc. Am.* **82**, 2045-2074.

Gaffet, S. and M. Bouchon (1989). Effects of two-dimensional topographies using the discrete wavenumber-boundary integral equation method in P-SV cases, *J. Acoust. Soc. Am.* **85**, 2277-2283.

George, P.L. (1991). *Automatic mesh generation: application to finite element methods*, John Wiley & Sons, N.Y.

Hisada, Y., K. Aki and T-L Teng (1993). 3-D simulations of surface wave propagation in the Kanto sedimentary basin, Japan. Part 2: Application of the surface wave BEM, submitted to *Bull. Seism. Soc. Am.*

Horike, M., Uebayashi H. and Takeuchi Y. (1990), Seismic response in three-dimensional sedimentary basin due to plan S wave incidence, *J. Phys. Earth* **38**, 261-284.

Jiang, T. and E. Kuribayashi (1988). The three-dimensional resonance of axisymmetric sediment-filled valleys, *Soils and Foundations* **28**, 130-146.

Jiang, T., S. Nishioka, H. Nagasaka and E. Kuribayashi (1993). Three-dimensional reflectivity method for complicated irregular formations, *Soil Dyn. and Earthquake Engrg.* **12**, 173-182.

Kato, K., K. Aki and T-L Teng (1993). 3-D simulations of surface wave propagation in the Kanto sedimentary basin, Japan. Part 1: Application of the surface wave Gaussian beam method, submitted to *Bull. Seism. Soc. Am.*

Kawano, M., S. Matsuda, K. Toyoda and J. Yamada (1993). Seismic response of three-dimensional alluvial deposit with irregularities for incident wave motion from a point source, submitted to *Bull. Seism. Soc. Am.*

Kawase, H. (1988). Time-domain response of a semicircular canyon for incident SV, P, and Rayleigh waves calculated by the discrete wavenumber boundary element method, *Bull. Seism. Soc. Am.* **78**, 1415-1437.

Kawase, H. and K. Aki (1989). A study on the response of a soft basin for incident S, P and Rayleigh waves with special reference to the long duration observed in Mexico City, *Bull. Seism. Soc. Am.* **79**, 1361-1382.

Khair, K.R., S.K. Datta and A.H. Shah (1989). Amplification of obliquely incident seismic waves by cylindrical alluvial valleys of arbitrary cross-sectional shape. Part I. Incident P and SV waves, *Bull. Seism. Soc. Am.* **79**, 610-630.

Kim, J. and A. Papageorgiou (1993). Discrete wavenumber boundary-element method for 3D scattering problems, *J. Engrg. Mech. ASCE* **119**, 603-624.

Kobayashi, S. (1987). Elastodynamics, in *Boundary element methods in mechanics* D.E. Beskos (Ed.) North-Holland, Amsterdam.

Kupradze, V.D. (1963). *Dynamical problems in elasticity*, in *Progress in solid mechanics Vol.*III, I.N. Sneddon and R. Hill (Eds.), North Holland Publ. Co., Amsterdam.

Lee, V.W. (1984). Three-dimensional diffraction of plane P, SV & SH waves by a hemispherical alluvial valley, *Soil Dyn. Earthquake Eng.* **3**, 133-144.

Lee, J.J. and C.A. Langston (1983). Wave propagation in a three-dimensional circular basin, *Bull. Seism. Soc. Am.* **73**, 1637-1655.

Li, X., J. Bielak and O. Ghattas (1992). Three-dimensional earthquake response on a CM-2, *Proc. 10th World Conf. Earthquake Engnrg.* **2**, 959-964, Madrid, Spain.

Love, A.E.H. (1944). *A treatise on the mathematical theory of elasticity*, Dover Publications, New York.

Luco, J.E., H.L. Wong, and F.C.P. de Barros (1990). Three-dimensional response of a cylindrical canyon in a layered half-space, *Earthq. Engrg. Structl. Dyn.* **19**, 799-817.

Luzón, F., S. Aoi, D. Fäh and F. J. Sánchez-Sesma (1993). Realistic seismic response of a 2D sedimentary basin, Submitted to *Bull. Seism. Soc. Am.*

Manolis, G.D. and D.E. Beskos (1988). *Boundary Element Methods in Elastodynamics*, Unwin Hyman Ltd, London.

Mossessian, T.K. and M. Dravinski (1990). Amplification of elastic waves by a threedimensional valley. Part 1: Steady state response. *Earthq. Engrg. and Structl. Dyn.* **19**, 667-680.

Mossessian, T.K. and M. Dravinski (1992). A hybrid approach for scattering of elastic waves by three-dimensional irregularities of arbitrary shape. *J. Phys. Earth.* **40**, 241-261.

Ohori, M., K. Koketsu and T. Minami (1992). Seismic responses of three-dimensional sediment filled valleys due to incident plane waves, *J. Phys. Earth* **40**, 209-222.

Olsen, K.B. and G.T. Schuster (1991). Seismic hazard analysis in Salt Lake Valley by finite difference simulation of three-dimensional elastic wave propagation. *IBM Supercomputing Contest*, 135-165.

Pedersen, H.A., F.J. Sánchez-Sesma and M. Campillo (1993). Three-dimensional scattering by two-dimensional topographies, submitted to *Bull Seism Soc Am*

Pérez-Rocha, L.E.,F.J. Sánchez-Sesma and E. Reinoso (1991). Three-dimensional site effects in Mexico City: evidence from accelerometric network observations and theoretical results, in *Proc. 4th Int. Conf. Seismic Zonation*, Stanford, California, Aug 26-29, Earthq Eng Res Inst 2, 327-334.

Rial, J.A. (1989). Seismic wave resonances in 3D sedimentary basins, *Geophys. J. Intl.* **99**, 81-90.

Rial, J.A., N.G. Saltzman and H. Ling (1992). Earthquake-induced resonance in sedimentary basins, *American Scientist* **80**, 566-578.

Sánchez-Sesma, F.J. (1983). Diffraction of elastic waves by three-dimensional surface irregularities, *Bull. Seism. Soc. Am.* **73**, 1621-1636.

Sánchez-Sesma F.J. and M. Campillo (1991). Diffraction of *P*, *SV* and Rayleigh waves by topographic features: a boundary integral formulation, *Bull. Seism. Soc. Am.* **81**, 2234-2253.

Sánchez-Sesma, F.J. and J. Esquivel (1979). Ground motion on alluvial valleys under incident plane *SH* waves, *Bull. Seism. Soc. Am.* **69**, 1107-1120.

Sánchez-Sesma, F.J. and E. Rosenblueth (1979). Ground motion at canyons of arbitrary shape under incident SH waves, *Int. J. Earthq. Eng. Struct. Dyn.* **7**, 441-450.

Sánchez-Sesma, F.J., L.E. Pérez-Rocha and S. Chávez-Pérez (1989). Diffraction of elastic waves by three-dimensional surface irregularities. Part II. *Bull. Seism. Soc. Am.* **79**, 101-112.

Sánchez-Sesma, F.J., J. Ramos-Martínez and M. Campillo (1993a). An indirect boundary element method applied to simulate the seismic response of alluvial

valleys for incident P, S and Rayleigh Waves, *Earthq. Engrg. Structl. Dyn.* **22**, 279-295.

Sánchez-Sesma, F.J., L.E. Pérez-Rocha and E. Reinoso (1993b). Ground motion in Mexico City during the April 25, 1989, Guerrero earthquake, *Tectonophysics* **218**, 127-140.

Shinozaki, Y. and K. Yoshida (1992). Seismic ground motion in three-dimensional sedimentary basin, *Special Seminar on Seismic Ground Motion in sedimentary Basin*, Nov. 1992, Disaster Prevention Research Institute, Kyoto University, Kyoto, Japan.

Toshinawa, T. and T. Ohmachi (1992). Love wave propagation in a three-dimensional sedimentary basin, *Bull. Seism. Soc. Am.* **82**, 1661-1667.

Trifunac, M.D. (1971). Surface motion of a semi-cylindrical alluvial valley for incident plane SH waves, *Bull. Seism. Soc. Am.* **61**, 1755-1770.

Trifunac, M.D. (1973). Scattering of plane SH waves by a semi-cylindrical canyon, *Int. J. Earthquake Eng. Struct. Dyn.* **1**, 267-281.

Wong, H.L. (1982). Effect of surface topography on the diffraction of P, SV and Rayleigh waves, *Bull. Seism. Soc. Am.* **72**, 1167-1183.

Wong, H.L. and P.C. Jennings (1975). Effect of canyon topographies on strong ground motion, *Bull. Seism. Soc. Am.* **65**, 1239-1257.

Yomogida, K. and J. T. Etgen (1993). 3-D wave propagation in the Los Angeles Basin for the Whittier-Narrows earthquake, *Bull. Seism. Soc. Am.* **83**, 1325-1344.

Zhang, L and A.K. Chopra (1991). Three-dimensional analysis of spatially varying ground motions around a uniform canyon in a homogeneous half-space, *Int. J. Earthq. Eng. Struct. Dyn.* **20**, 911-926.

Instituto de Ingeniería, UNAM
Cd. Universitaria, Apdo. 70-472
Coyoacán 04510 México D.F., Mexico
and
Centro de Investigación Sísmica, A.C.
Carr. al Ajusco 203, Col. H. de Padierna
Tlalpan 14200 México D.F.,Mexico
(F.J.S.-S.)

Instituto Andaluz de Geofísica y
Prevención de Desastres Sísmicos
Universidad de Granada, Apdo. 2145
18080 Granada, Spain
and
Departamento de Física Aplicada
Universidad de Almería
0471 Almería, Spain
(F. L.)

Table 1 Coefficients of Equation 7

	j		
	1	2	3
A_{1j}	0	0	$-i$
A_{2j}	$-i\beta/\alpha$	$i(2\beta^3/\alpha^3-\beta/\alpha)$	0
B_{1j}	4	-2	-3
B_{2j}	$-4\beta^2/\alpha^2-1$	$4\beta^2/\alpha^2-1$	$2\beta^2/\alpha^2$
C_{1j}	$-i12$	$i6$	$i6$
C_{2j}	$i12\beta/\alpha$	$-i6\beta/\alpha$	$-i6\beta/\alpha$
D_{1j}	-12	6	6
D_{2j}	12	-6	-6

FIGURE CAPTIONS

FIGURE 1. Half-space, E, with a three-dimensional elastic inclusion, R, and incidence of *P*, *S* and Rayleigh waves. (a) Plan view that shows the regions, the contour lines of the interface $\partial_2 E$ and an incident plane *SH* wave from the depth along the x'-axis with azimuth ϕ. (b) Cross section along x' that illustrates the incidence of *P*, *SV* and Rayleigh waves. For the first two types of waves the incidence angle γ is depicted. The discretization along the interface $\partial_2 R = \partial_2 E$, the free surface of inclusion $\partial_1 R$ and a portion of the flat surface of the half-space $\partial_1 E$ gives $2L$, K and M elements, respectively.

FIGURE 2. Amplitudes of displacements u, v and w at the surface of a hemispherical alluvial valley for oblique incidence (γ=30°) of harmonic *SH* waves. Normalized frequency η=1 .Material properties are given in the text. The amplitudes for u,v and w of the present study are given with dash, solid and dotted lines, respectively, while open symbols (squares, circles and triangles, respectively) are from Sánchez-Sesma *et al.* (1989).

FIGURE 3. Cylindrical alluvial valley under oblique incident *SV* waves. The radius of 4 km and depth of 1 km were assumed. Material properties are given in the text. The angle γ=30 degrees corresponds to the "critical" incidence, given the Poisson ratio of the half-space.

FIGURE 4. Contours of horizontal displacement amplitude u for surface receivers along the x-axis against frequency. Cylindrical valley under incidence of *SV* waves at the critical angle.

FIGURE 5. Contours of vertical displacement amplitude w for surface receivers along the x-axis against frequency. Cylindrical valley under incidence of *SV* waves at the critical angle.

FIGURE 6. Contours of horizontal displacement amplitude u for surface receivers along the y-axis against frequency. Cylindrical valley under incidence of *SV* waves at the critical angle.

FIGURE 7. Contours of horizontal displacement amplitude v for surface receivers along the y-axis against frequency. Cylindrical valley under incidence of *SV* waves at the critical angle.

FIGURE 8. Contours of vertical horizontal displacement amplitude w for surface receivers along the y-axis against frequency. Cylindrical valley under incidence of *SV* waves at the critical angle.

FIGURE 9. Synthetic seismograms for u, v and w at 48 receivers equally spaced along the x or y axes. The range of x or y is between $-1.82a$ and $1.74a$, where a = 4 km. Cylindrical valley under incidence of *SV* waves at the critical angle. The incident waveform is a Ricker wavelet with characteristic period t_p = 3 sec.

FIGURE 10. Irregular three-dimensional alluvial valley. (a) The softer material is limited by two circumferences of radii a and b, where $a > b$ and is represented by the shaded area. Here $b = 0.7a$ and a = 4 km. (b) Topographic contour levels of the valley's basement.

FIGURE 11. Perspective view of the irregular valley's basement. Incidence of plane *P*, *SH*, *SV* and Rayleigh waves, all with an azimuth ϕ=0. Incidence angle γ with respect to the vertical for body waves.

FIGURE 12. Synthetic seismograms for u, v and w at 48 receivers equally spaced along the x or y axes. The range of x or y is between $-1.82a$ and $1.74a$, where a = 4 km. Irregular valley under incidence of *P* waves at γ=30 degrees. The incident waveform is a Ricker wavelet with characteristic period of t_p = 3 sec.

FIGURE 13. Same as Figure 12 but incidence of *SV* waves at γ=30 degrees.

FIGURE 14. Same as Figure 12 but incidence of Rayleigh waves.

FIGURE 15. Same as Figure 12 but incidence of *SH* waves at γ=30 degrees.

FIGURE 16. Same as Figure 12 but incidence of *SH* waves at γ=60 degrees.

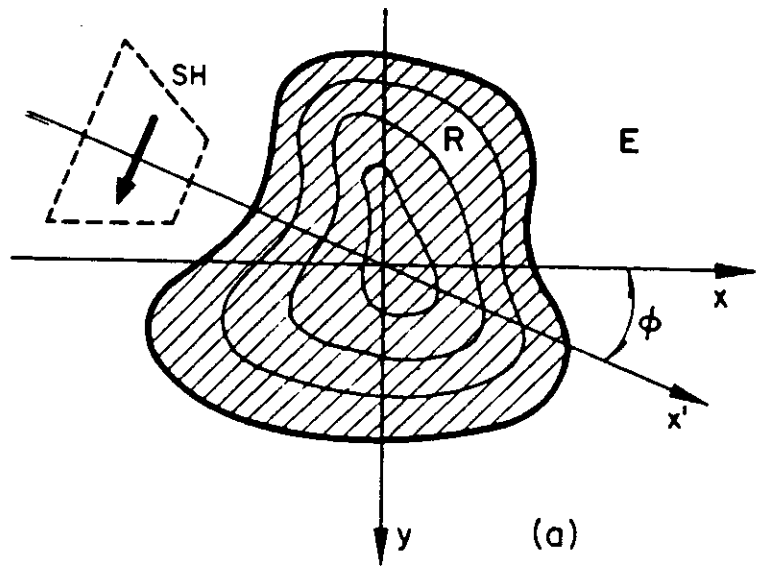
SH
R
E
x
ϕ
x'
y
(a)

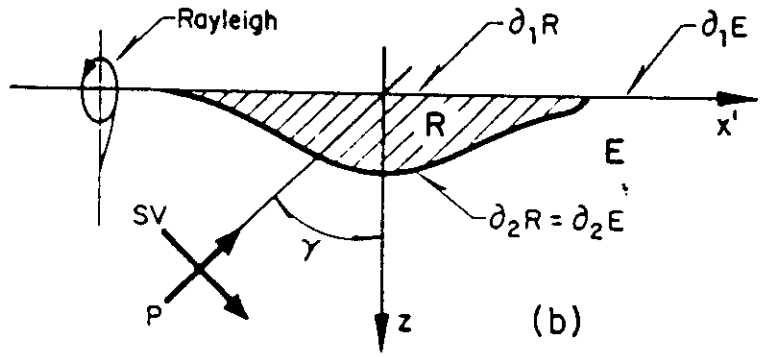
Rayleigh
$\partial_1 R$
$\partial_1 E$
R
x'
E
SV
γ
$\partial_2 R = \partial_2 E$
P
z
(b)

Fig 1

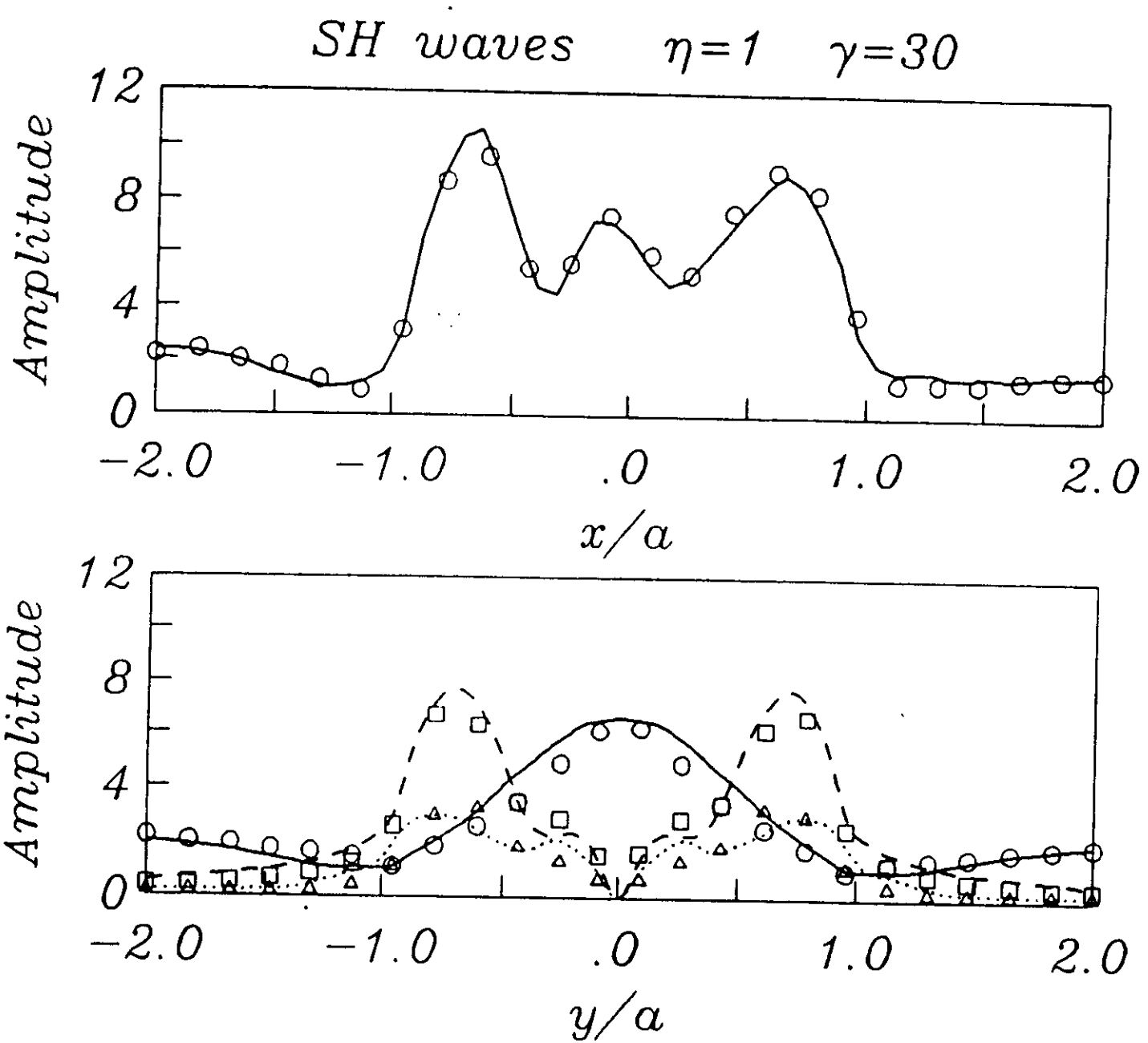
SH waves η=1 γ=30
Amplitude
12
8
4
0
−2.0
−1.0
.0
1.0
2.0
x/a
Amplitude
12
8
4
0
−2.0
−1.0
.0
1.0
2.0
y/a

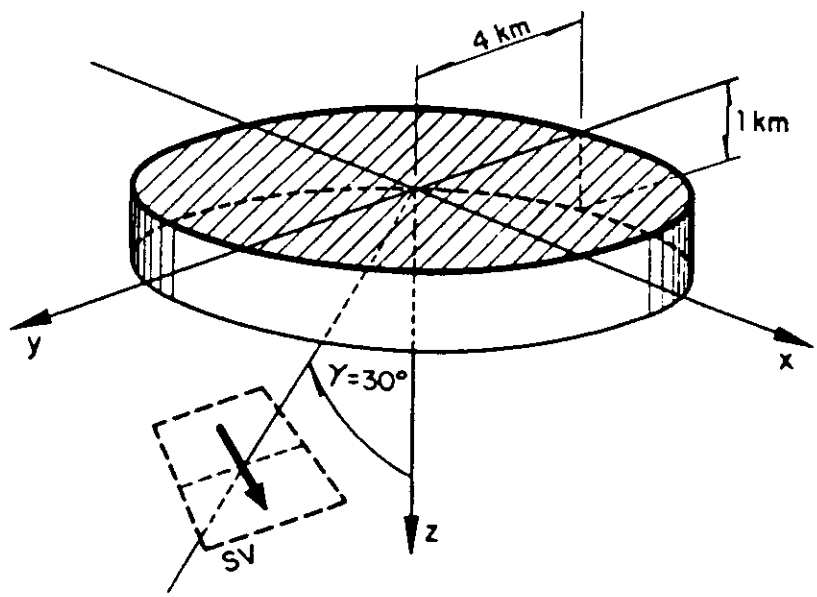

Fig 3

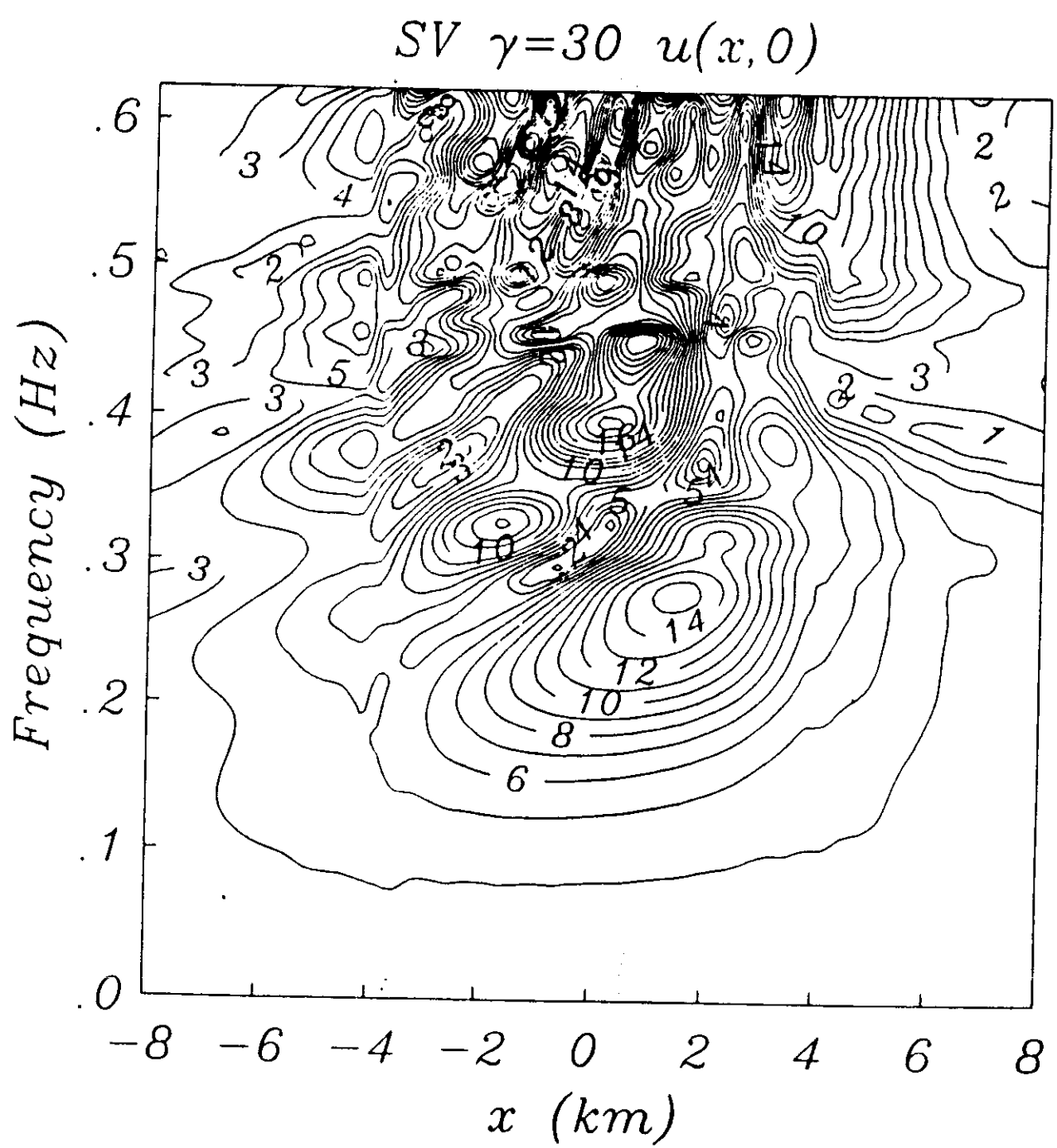
SV γ=30 u(x,0)
Frequency (Hz)
.6
.5
.4
.3
.2
.1
.0
−8 −6 −4 −2 0 2 4 6 8
x (km)

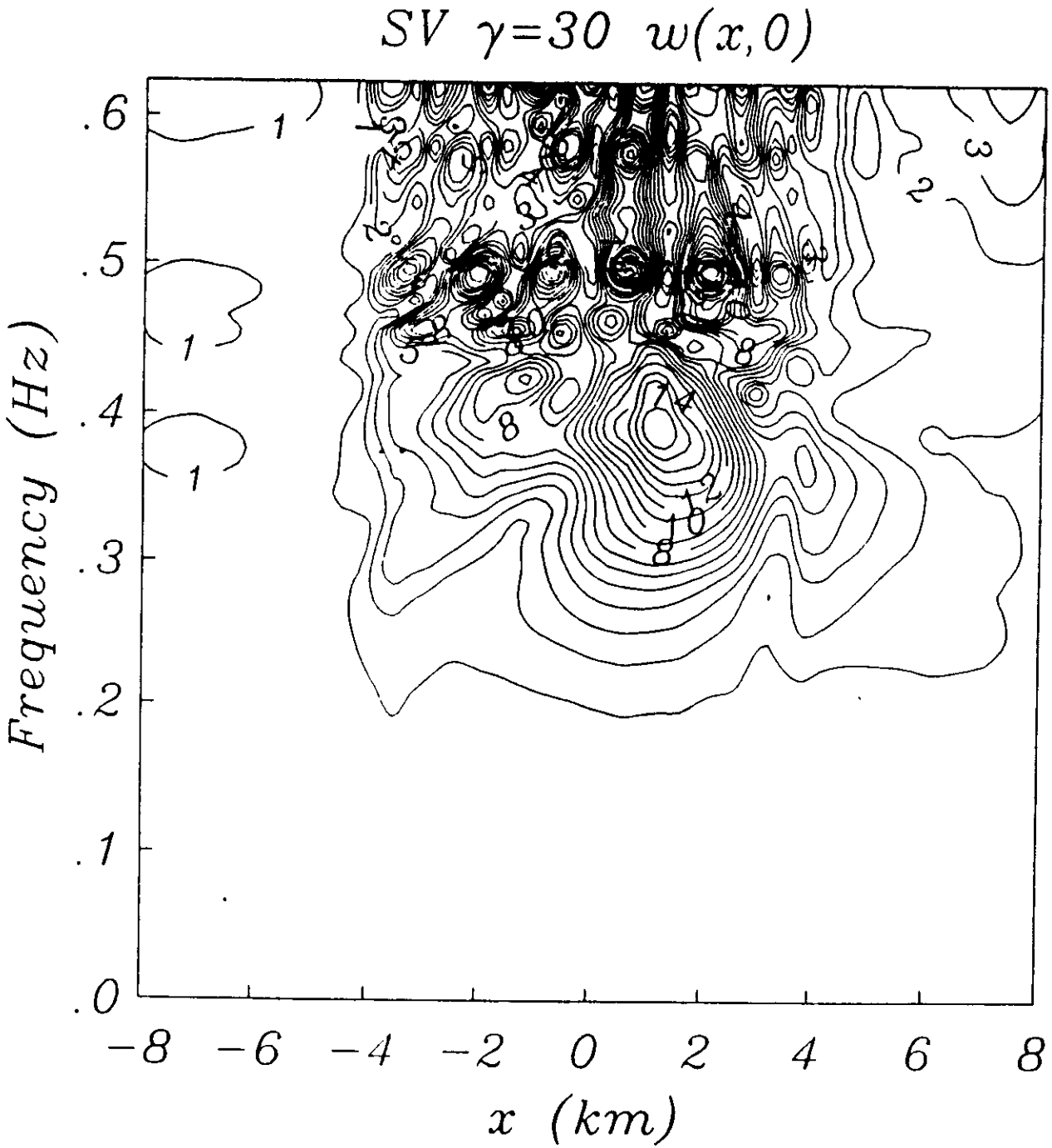
SV γ=30 w(x,0)
Frequency (Hz)
.6
.5
.4
.3
.2
.1
.0
−8 −6 −4 −2 0 2 4 6 8
x (km)

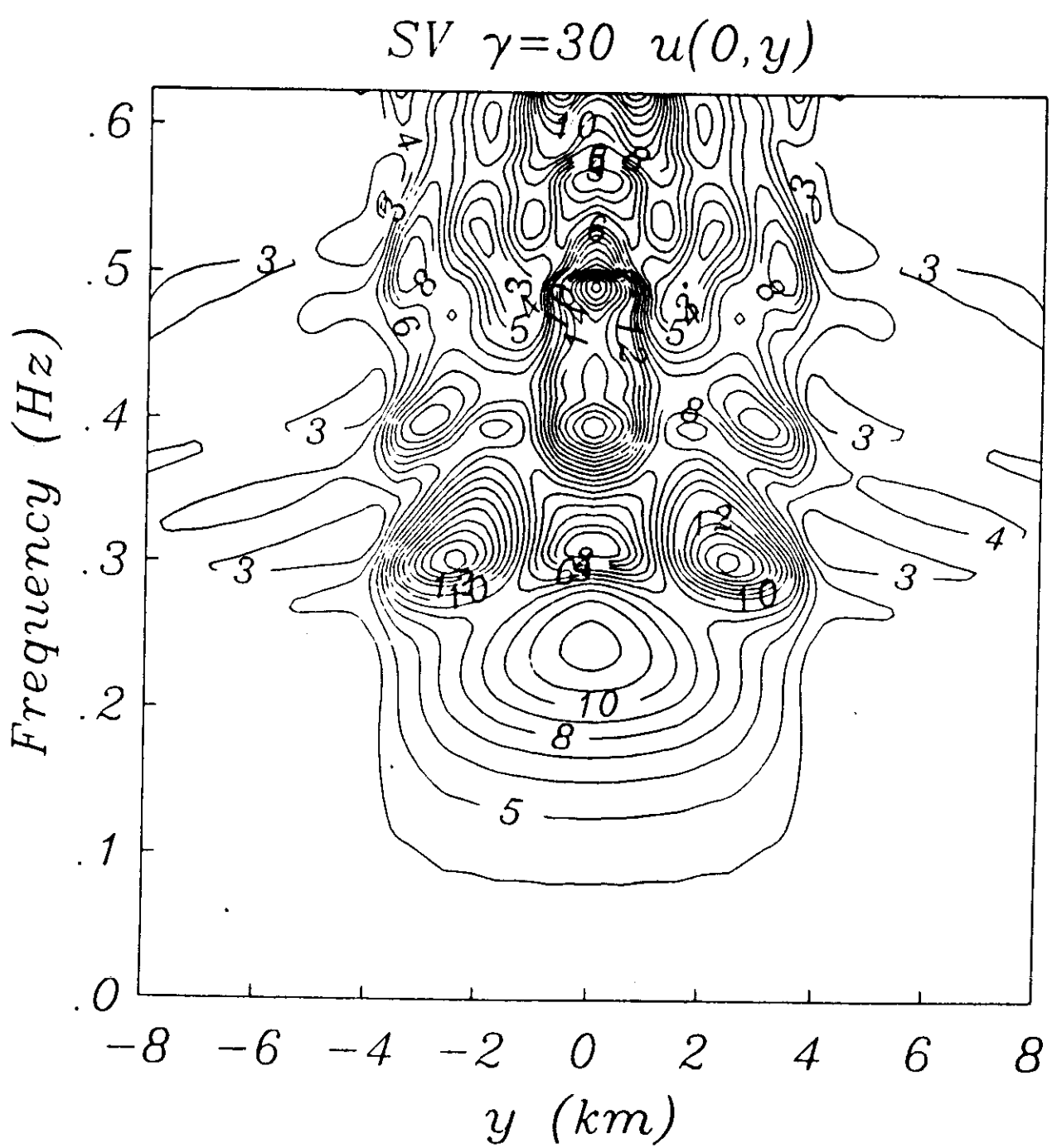
SV γ=30 u(0,y)
Frequency (Hz)
.6
.5
.4
.3
.2
.1
.0
−8 −6 −4 −2 0 2 4 6 8
y (km)

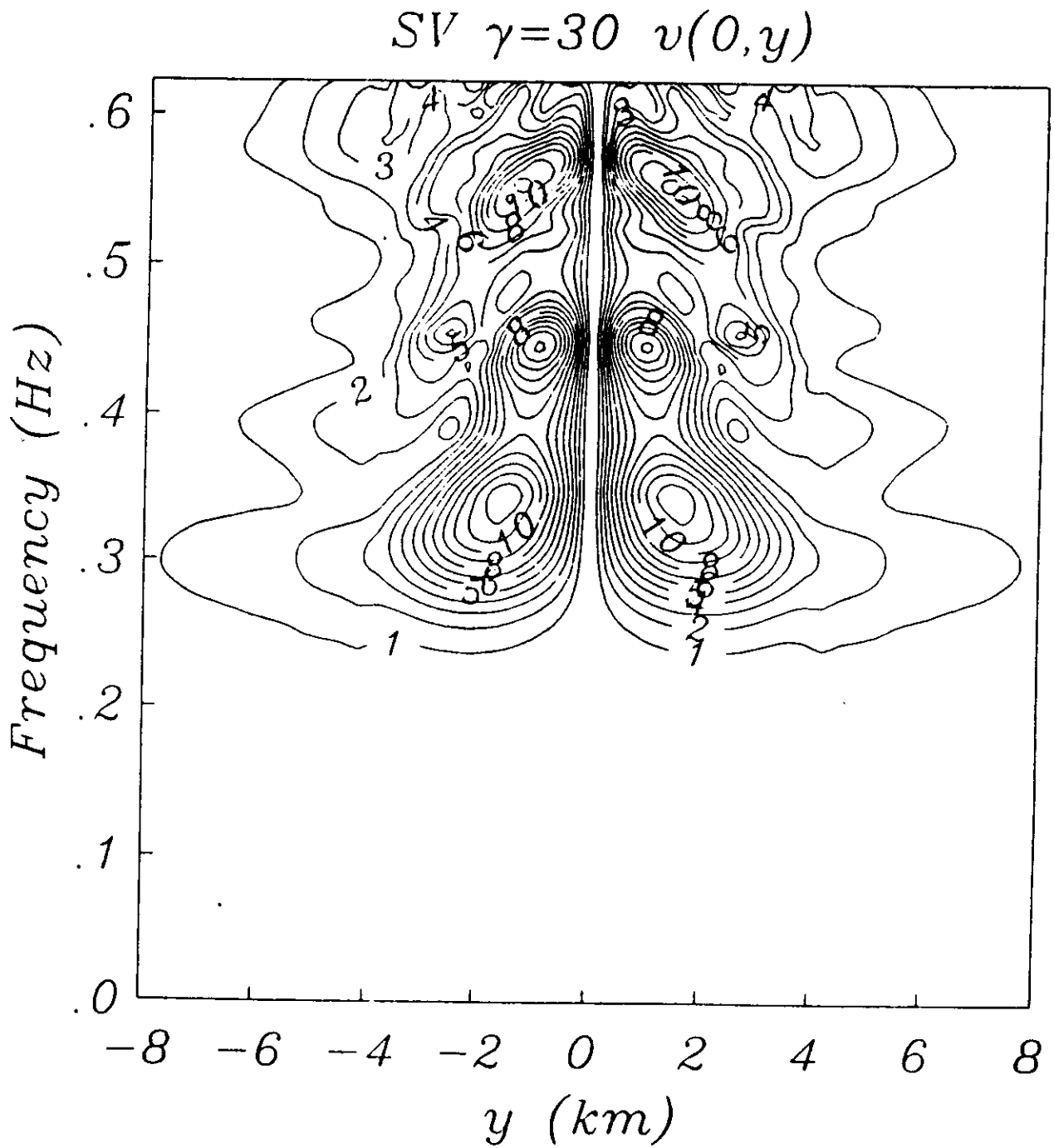
SV γ=30 v(0,y)
Frequency (Hz)
.6
.5
.4
.3
.2
.1
.0
−8 −6 −4 −2 0 2 4 6 8
y (km)

Frequency (Hz)
0
.1
.2
.3
.4
.5
.6
-8
-6
-4
-2
0
2
4
6
8
y (km)
S1, γ=30 w(0,y)

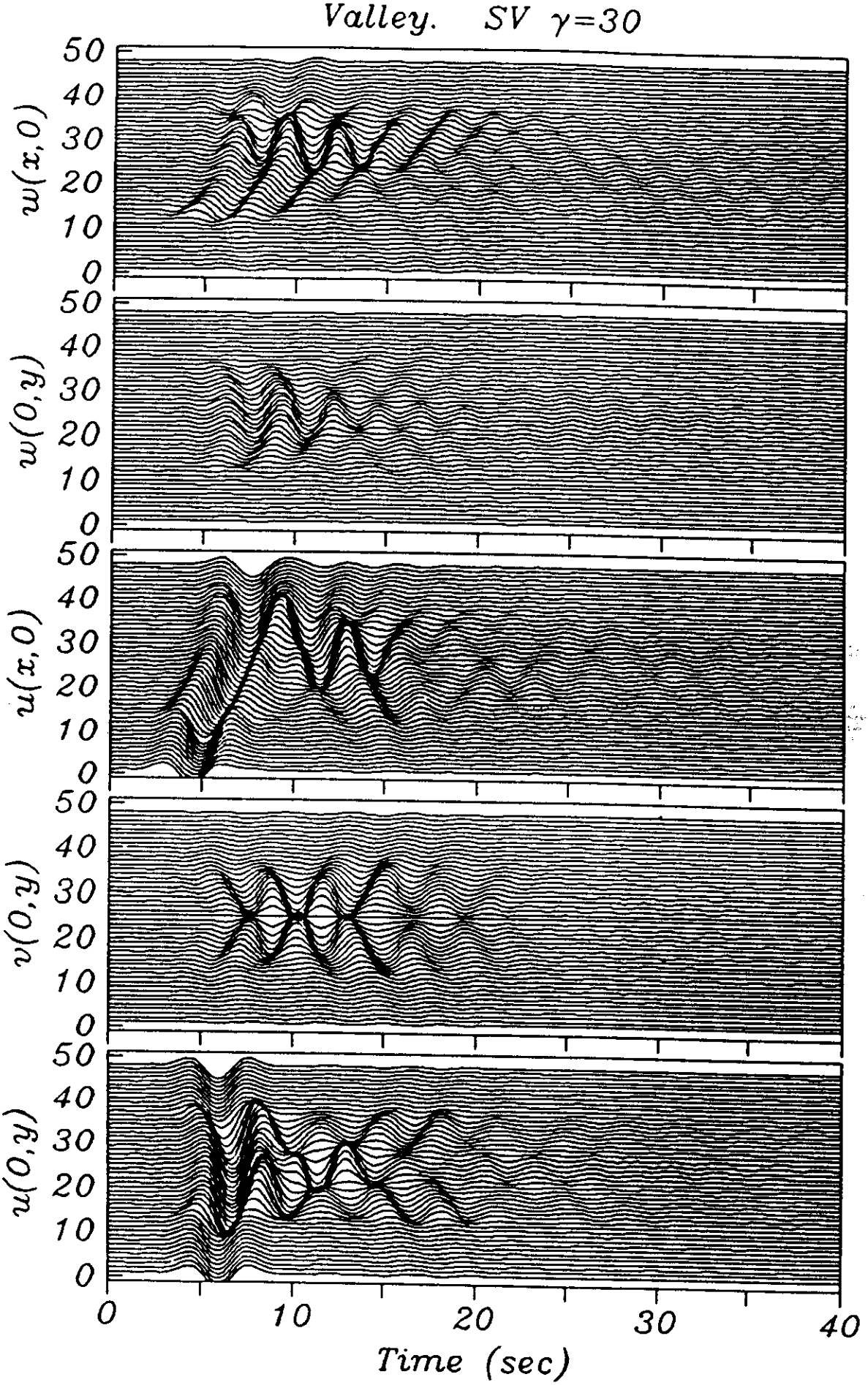

Fig 9

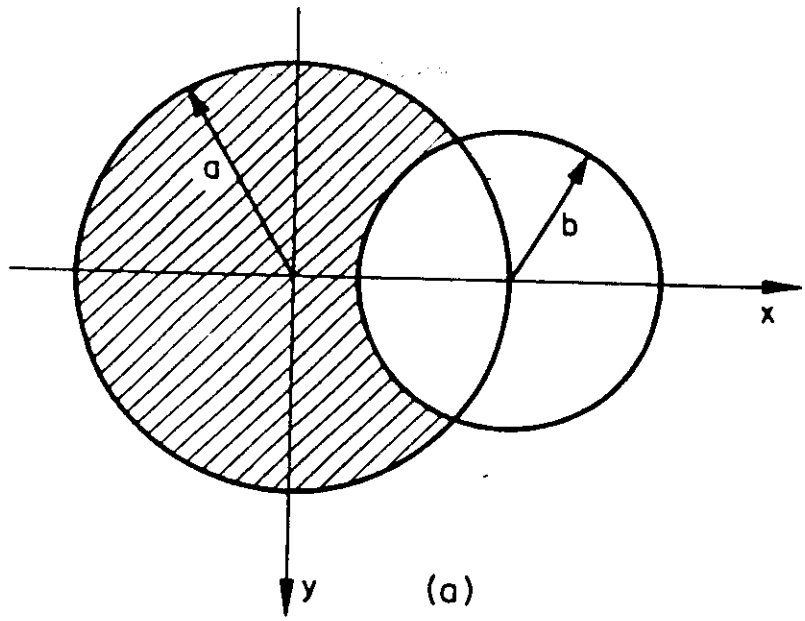

(a)

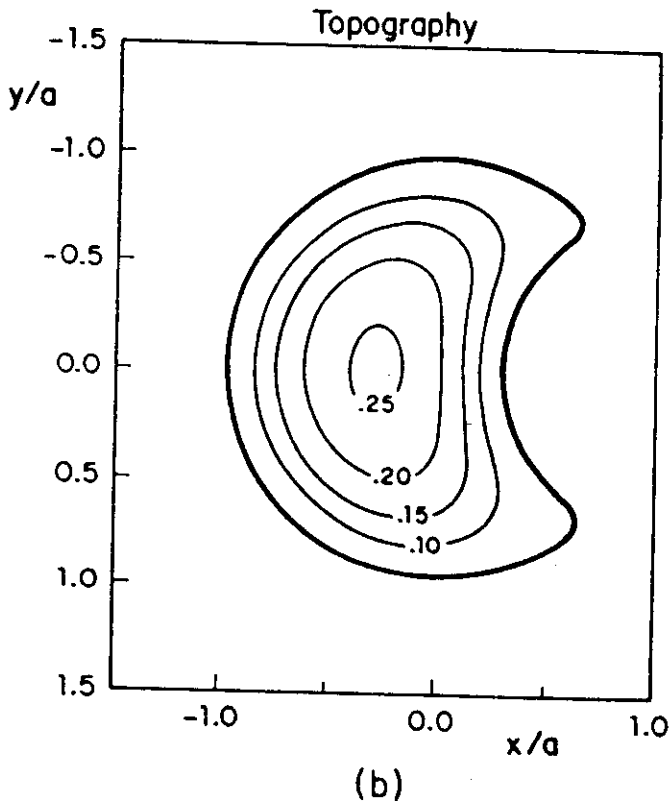

(b)

Fig 10

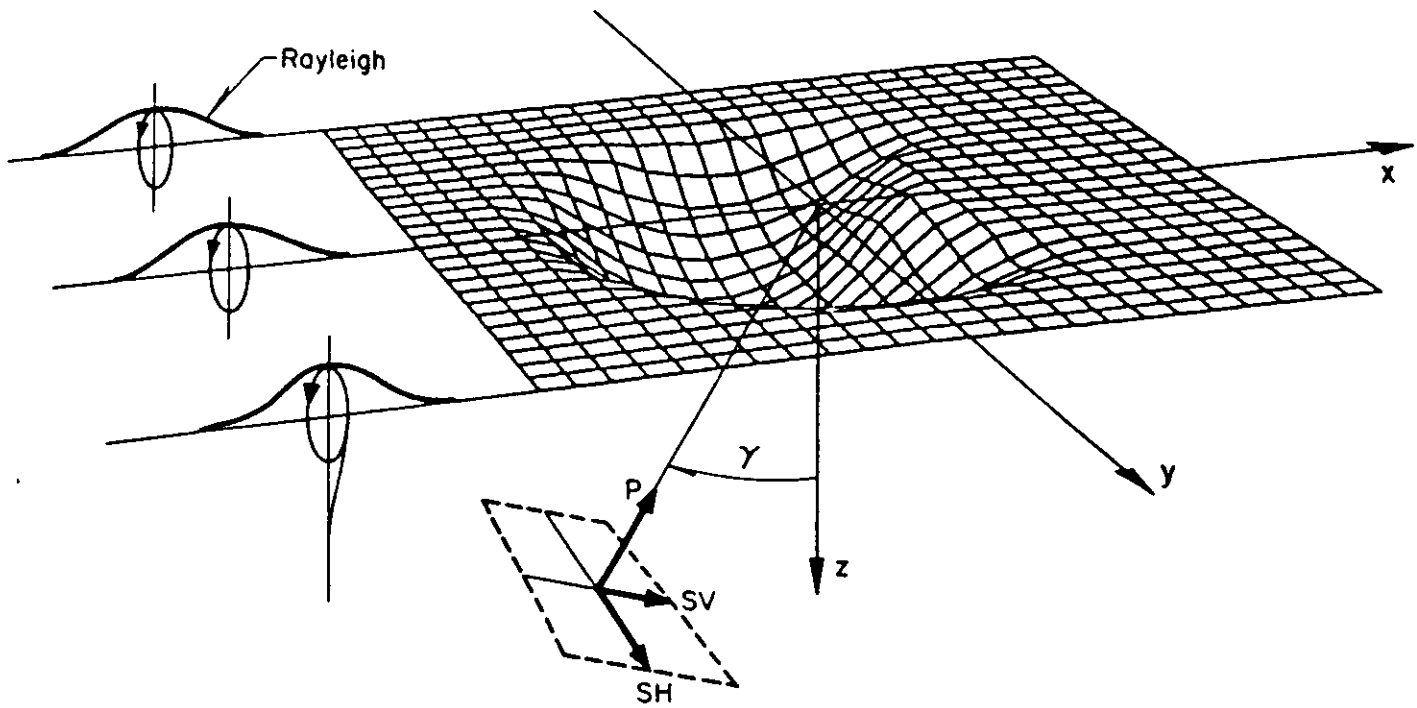

Fig 11

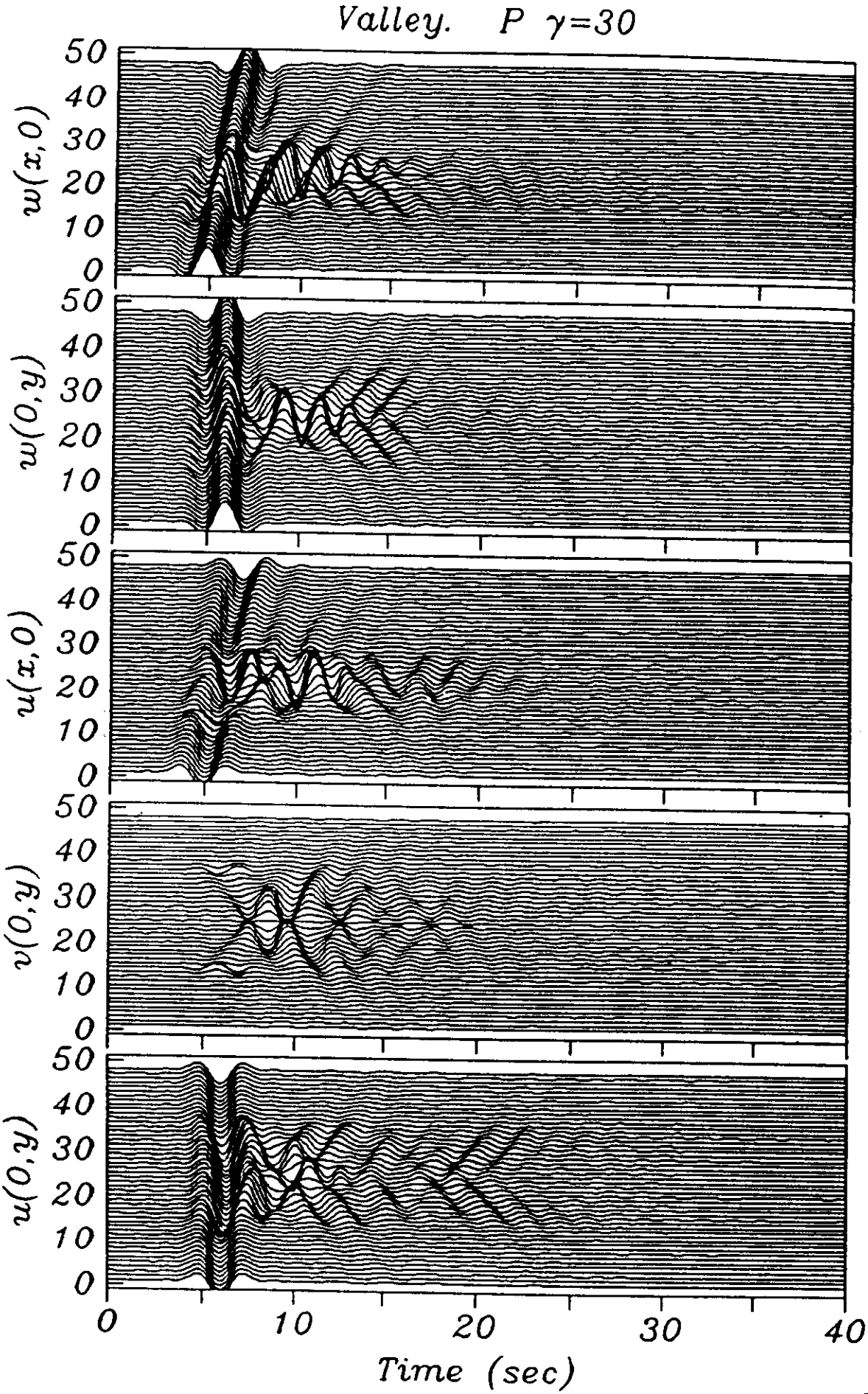
Valley. P γ=30
w(x,0)
w(0,y)
u(x,0)
v(0,y)
u(0,y)
50
40
30
20
10
0
0
10
20
30
40
Time (sec)

Fig 12

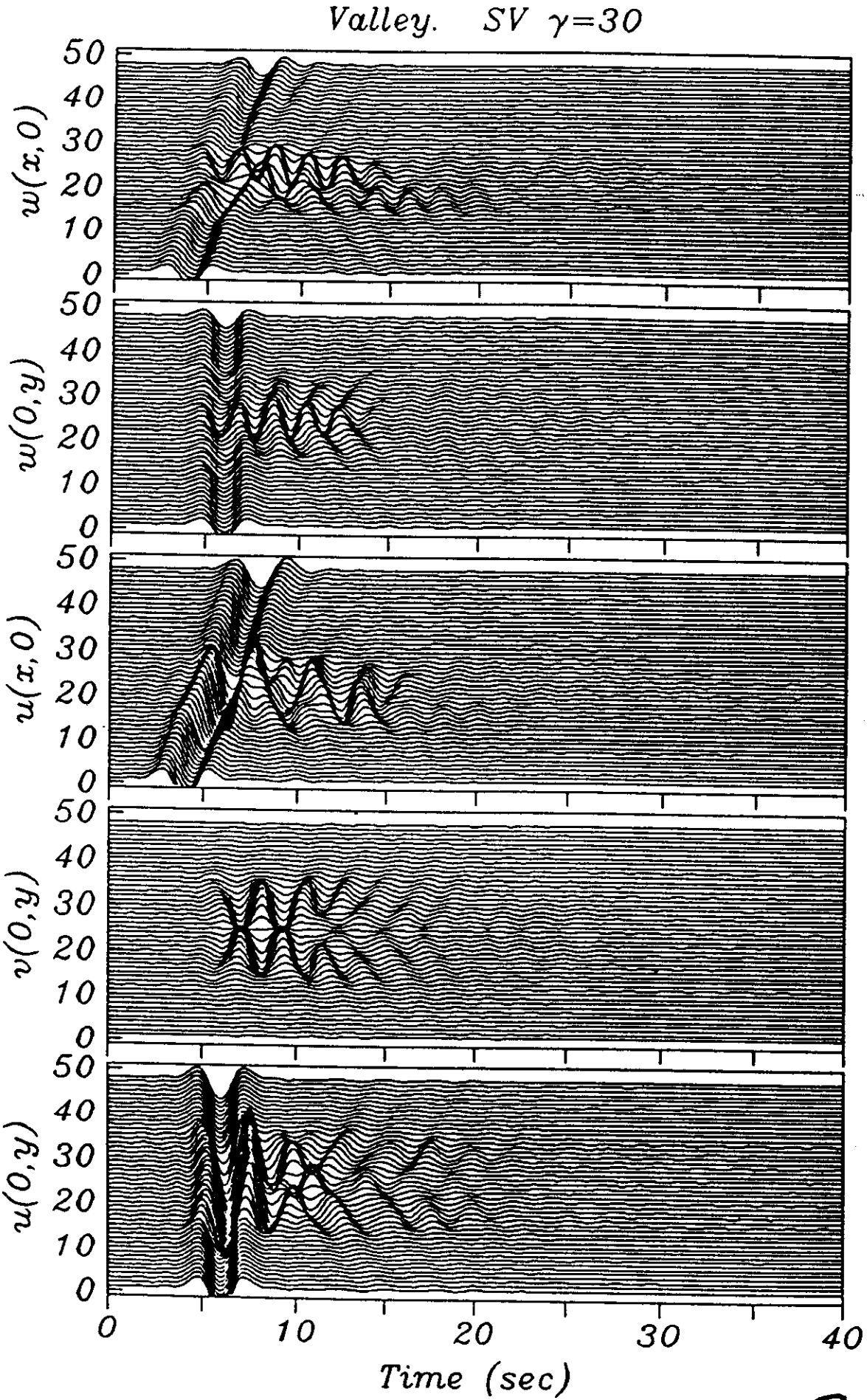
Valley. SV γ=30
w(x,0)
w(0,y)
u(x,0)
v(0,y)
u(0,y)
50
40
30
20
10
0
0
10
20
30
40
Time (sec)

Fig 13

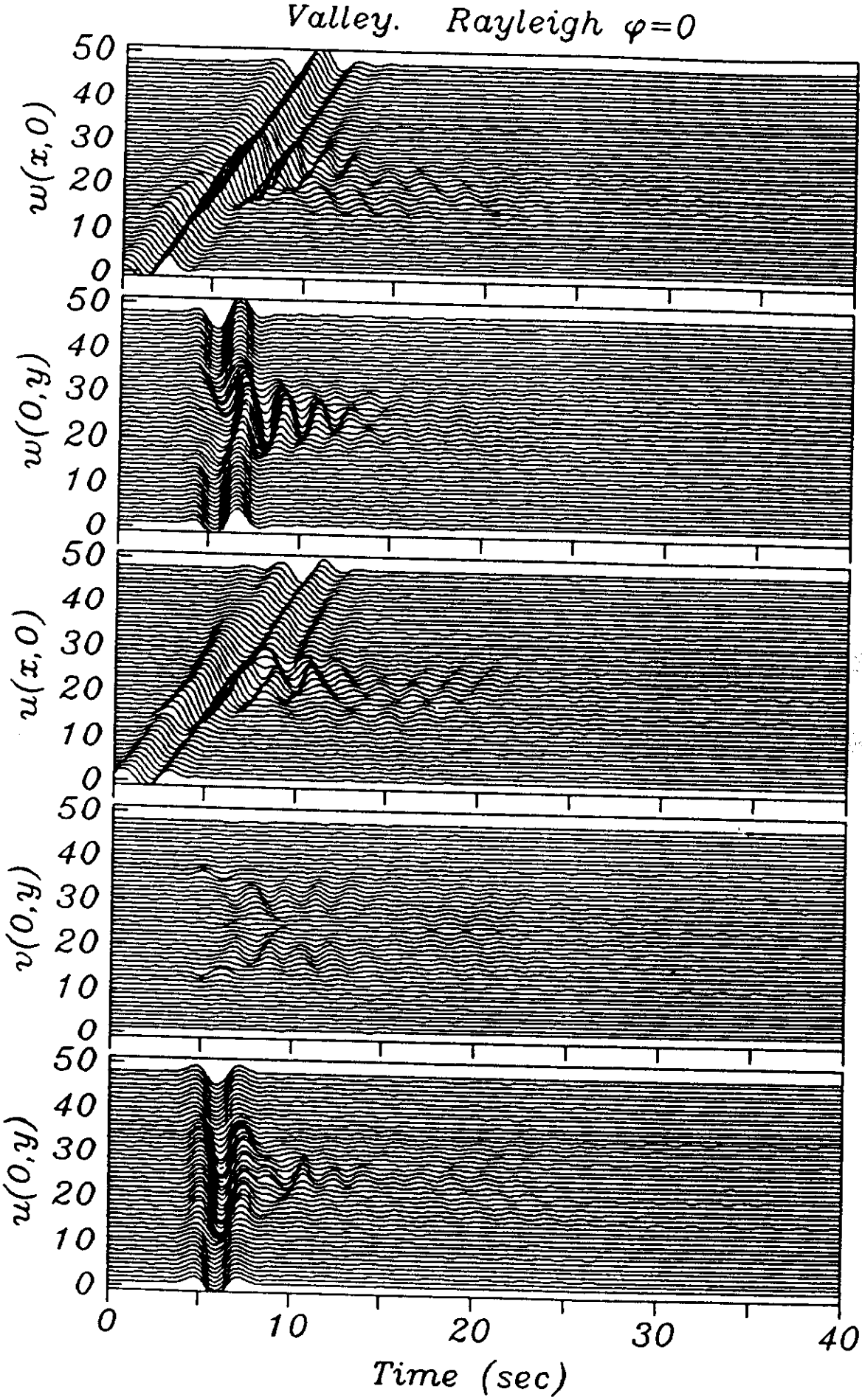

Fig 14

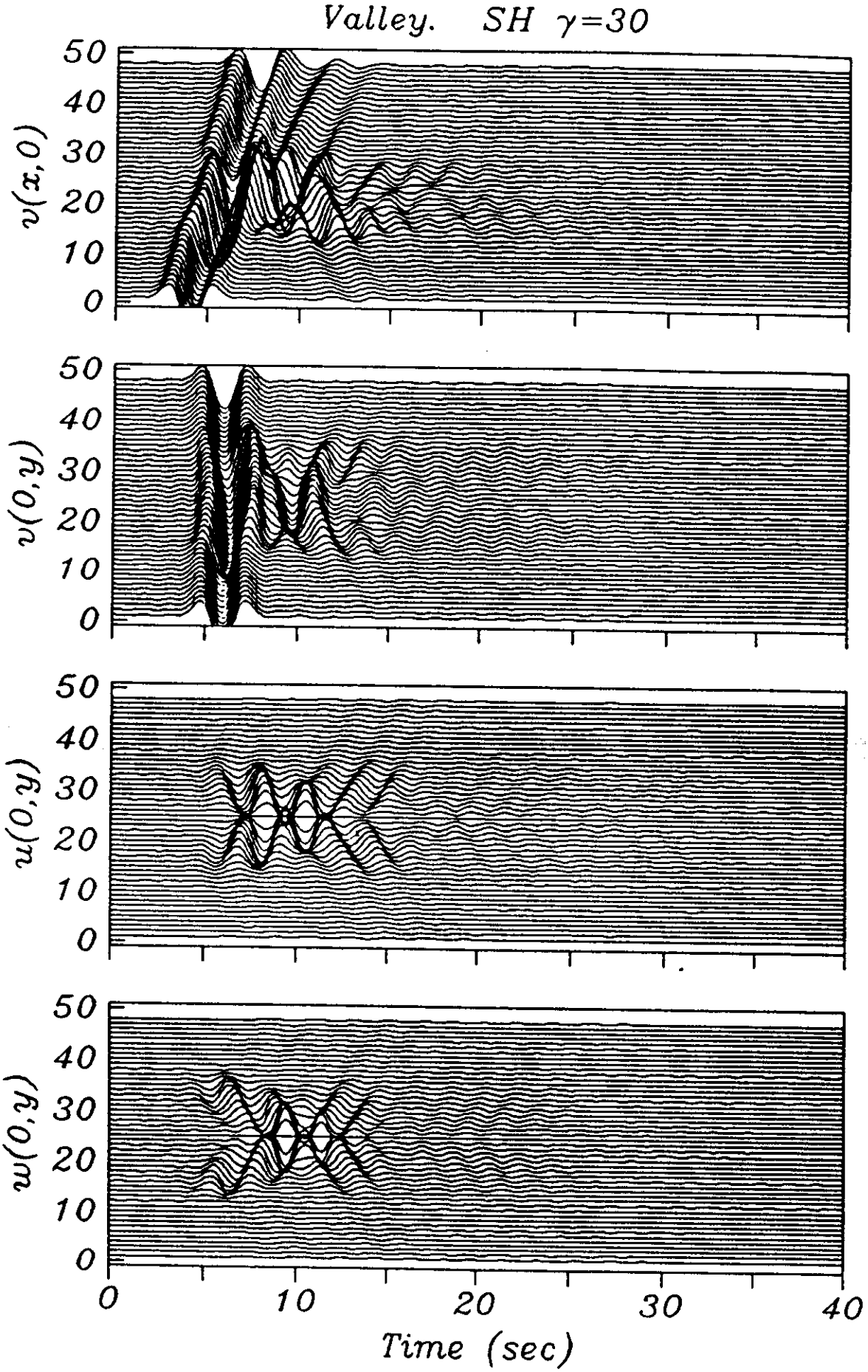
Valley. SH γ=30
v(x,0)
v(0,y)
u(0,y)
w(0,y)
50
40
30
20
10
0
0
10
20
30
40
Time (sec)

Fig 15

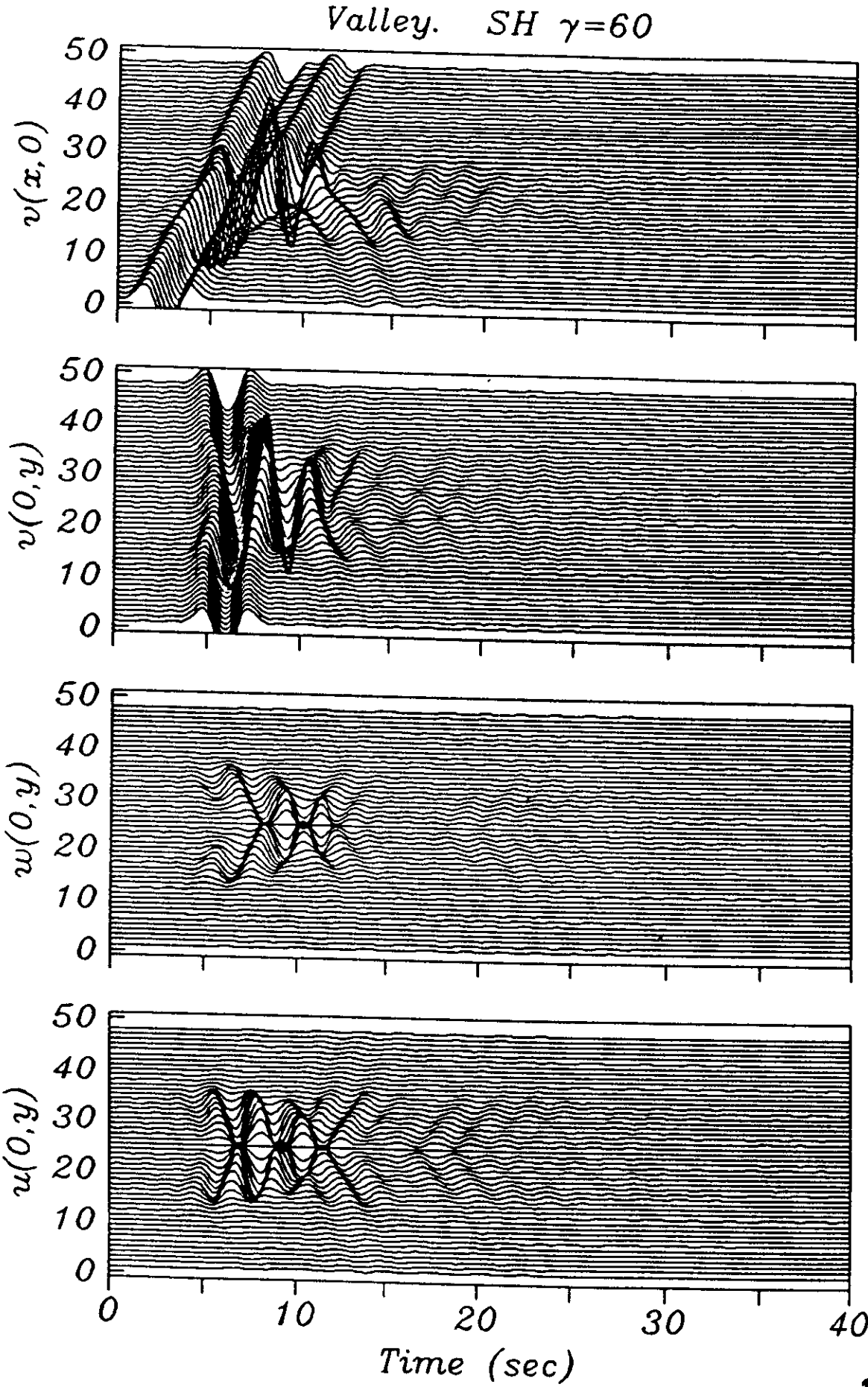
Valley. SH γ=60
v(x,0)
v(0,y)
w(0,y)
u(0,y)
50
40
30
20
10
0
0
10
20
30
40
Time (sec)

Fig 16